DEVELOPMENT OF RYERSON'S HYPERLOOP POD SYSTEMS USING A MODULAR AND SYSTEMATIC APPROACH

By

Mohammed Mohiuddin Khan (Mohi Khan)
Bachelor of Engineering, Ryerson University (2016)

A thesis
presented to Ryerson University
in partial fulfillment of the
requirements for the degree of
Master of Applied Science
in the program of
Aerospace Engineering

Toronto, Ontario, Canada, 2019

AUTHOR'S DECLARATION FOR ELECTRONIC SUBMISSION OF A THESIS

I hereby declare that I am the sole author of this thesis. This is a true copy of the thesis, including any required final revisions, as accepted by my examiners.

I authorize Ryerson University to lend this thesis to other institutions or individuals for the purpose of scholarly research.

I further authorize Ryerson University to reproduce this thesis by photocopying or by other means, in total or in part, at the request of other institutions or individuals for the purpose of scholarly research.

I understand that my thesis may be made electronically available to the public.

ABSTRACT

Development Of Ryerson's Hyperloop Pod Systems Using A Modular And Systematic Approach

Mohammed Mohiuddin Khan (Mohi Khan)

Master of Applied Science, Aerospace Engineering, Ryerson University, Toronto (2019)

Ryerson International Hyperloop is a special projects team with the intent of developing a fully functioning Hyperloop Pod. The team believes in driving revolutionary change within the transportation industry, with the greater cause of saving time, and to help make Canadian cities more accessible. The Pod was designed using a systematic approach with modularity and reliability as major foci. Its design featured an innovative, student researched and developed linear induction based MagDrive, and MagLev systems for propulsion and levitation. The braking system featured a fail-safe pneumatic deployment system to facilitate braking at high speeds as well as a wireless "Keep Alive" command. The onboard hyperionics is entirely composed of student researched and developed components which provides an expansive communication range and the ability to transmit real time data back to the mission control through all states and stages of the Pod's run.

ACKNOWLEDGEMENTS

The author would like to express his sincerest appreciation to his supervisor, *Dr. Seyed M. Hashemi,* who is an exceptional mentor to his students. Besides being remarkably knowledgeable, Dr. Hashemi also has great skill in explaining complex topics with great clarity and simplicity. His genuine attitude towards all his students has made him an extremely approachable person. Without his guidance and support, the Development of Ryerson's Hyperloop Pod would not have been possible.

The author would like to acknowledge members of Ryerson International Hyperloop for their endless contributions towards the development of the fifth mode of transportation. It was an honor working amongst such brilliant minds.

The author would like to recognize Ryerson International Hyperloop's cherished and generous supporters: *Ryerson University*, *Office of the President*, *The Department of Aerospace Engineering*, *ANSYS Inc.*, *MSC Software,* and *MiSUMi*. Their unwavering support, whether monetary, material, or through words of advice, afforded the team the opportunity to see this design to its full potential.

The author feels extremely fortunate and grateful to the faculty advisors (*Dr. Seyed M. Hashemi*, *Dr. Paul Walsh*, *Dr. Hamid Ghaemi*, *Dr. Kazem Fayazbakhsh*, *Cliff Chan*, *Peter Bradley*, *Jerry Karpynczyk*, *Francine Belnavis*, *Kim Gallo*, *Leah Rogan*, *Gerald Bootes*, *Zohair Khan*, and *Rose Ghamari*) and industry advisors (*Ron Bakowski*, *Rob Paterson*, *Gordon Cook*, and *Moeid Elahi*) for their hard work throughout the year, and their dedication in making this design the best it could be.

The author would also like to thank *SpaceX*, *The Boring Company*, and *Tesla* for hosting the Hyperloop Pod Competitions, and providing teams the opportunity to showcase their skills.

Lastly, the author feels indebted to his parents and sister for their endless love, words of encouragement, and support over the years.

Without the support of all these people and organizations, the Development of Ryerson's First Hyperloop Pod would have remained an idea yet to be realized.

TABLE OF CONTENTS

LIST OF TABLES

LIST OF FIGURES

LIST OF APPENDICES

LIST OF SYMBOLS, CONSTANTS, AND ABBREVIATIONS

Symbols

γ	Isentropic Expansion Coefficient
λ	Wavelength
μ_0	Permeability of Free Space
$\mu_{k,\ Track}$	Coefficient of Kinetic Friction
ρ	Density
ρ_r	Volume Resistivity
σ	Bending Stress
τ	Pole Distance
f	Frequency
a	Edge Length
a	Pod Acceleration/Deceleration Under Time Step
A	Ampere
A_{Bypass}	Cross-Sectional Area of the Pod Bypass
A_{Piston}	Piston Head Cross-Section Area
A_{Pod}	Cross-Sectional Area of the Pod
A_{Tube}	Cross-Sectional Area of the Tube
CG	Center of Gravity
d	Diameter of Winding
dA	Infinitesimally Small Area
F_B	Newton's Second Law
F_{Brake}	Piston Braking Force
$F_{Brake,Req}$	Required Piston Braking Force
F_{LIM}	Generated LIM Thrust
F_s	Stator Thrust Force
G	Goodness Factor
g_e	Airgap Effectiveness
g_{Earth}	Force of Gravity (Earth)
I	Area Moment of Inertia
I_1	Stator Phase Current
L_s	Stator Core Length
M	Moment
M	Mach Number
M_{Bypass}	Pod Bypass Mach Number

M_{Pod}	Pod Mach Number
m_{Pod}	Pod Mass
N_{Pod}	Pod Normal Force
P	Number of Poles
P_o	LIM Output Power
P_{Piston}	Internal Piston Pressure
q	Shear Flow
R	Stator Radius
R_2	Rotor Resistance
r_i	Inner Radius
r_o	Outer Radius
s	Pod Distance Under Particular Time Step
S	Slip
S	Soric
t	Time
u	Initial Pod Velocity
v	Final Pod Velocity
V	Voltage
V_∞	Shear Force
V_c	Rotor Linear Speed
V_{DC}	Voltage DC
V_{DC}	Voltage AC
V_f	Pod Final Velocity
V_i	Pod Initial Velocity
V_{Ref}	Landing Reference Speed
V_s	Synchronous LIM Velocity
W	Watt
y	Vertical Distance (From The Neutral Axis)

Constants

γ	1.4
μ_0	4π x 10^{-7}
π	3.14159
ρ_w	19.27 x 10^{-9}
g	9.81 m/s^2 or 32.17 ft/s^2

Abbreviations

BRK	Braking System
CDR	Critical Design Review
CFD	Computational Fluid Dynamics
CG	Center of Gravity
COTS	Commercial-Off-The-Shelf
DAFT	Dual Axis Force Transducer
DCV	Directional Control Valve
DOT	Department of Transportation
ECU	Electronic Control Unit
EPG	Electronic Pressure Gauge
EPR	Electronic Pressure Regulator
FEAS	Faculty of Engineering and Architectural Science
FEM	Finite Element Method
FoS	Factor of Safety
GNC	Guidance, Navigation & Control
GS	Ground Station
HPA	High Pressure Air
HQ	Headquarters
ICASSE	International Conference on Aerospace System Science and Engineering
LCM	Longitudinal Chassis Member
LIM	Linear Induction Motor
MTR	Modular Test Rig
NASA	National Aeronautics and Space Administration
OPS	Operations
PDR	Preliminary Design Review
PRP	Propulsion
PWM	Pulse Width Modulation
RH	Ryerson International Hyperloop
RIM	Rotary Induction Motor
ROI	Return On Investment
SF	Safety Factor
SLF	Steady Level Flight
SRAD	Student Researched and Developed
STEM	Science, Technology, Engineering, and Mathematics
STR	Structures
TC	Transport Canada
VRR	Vehicle Readiness Review
VSM	Vehicle Stability Module

1 INTRODUCTION

This document outlines the design, manufacturing, and testing plans of Ryerson International Hyperloop and Ryerson's first Hyperloop Pod for SpaceX's Hyperloop Pod Competition in Hawthorne, California.

1.1 Academic Program

Ryerson International Hyperloop (RH) is a special projects team for the Office of the President at Ryerson University, led by the author. The Department of Aerospace Engineering made numerous key resources accessible to RH which would otherwise have been impossible to obtain. These supportive services included: University recognition, University backing, funding, financial management, and countless University and departmental facilities. Although the University provides a portion of the funding through a yearly budget request, the team was responsible for securing its own funds and thus, the rest of the financial support came in the form of sponsorships, awards, and grants.

As the research team is primarily composed of engineering students, RH benefits from many of the departments within the Faculty of Engineering and Architectural Science (FEAS) to design, manufacture, and test the systems. The team has access to various facilities including, a subsonic wind tunnel, supersonic wind tunnel, stress and fatigue laboratories, additive manufacturing zones, as well as machine shops.

The team is primarily composed of Aerospace (85%), Mechanical (5%), and Electrical (5%) Engineering students. However, the team encourages the contribution from varied academic disciplines with the expectation that a diverse organization will inspire the development of more sophisticated systems while offering a more realistic (and accurate) depiction of an industry environment.

During 2019, the team successfully recruited high school students to foster growth within Science, Technology, Engineering, and Mathematics (STEM) fields. In doing this, the team offers younger students the opportunity to develop their technical and communication skills early in their academic career. The team's long-term goal is to build an avenue where members apply their academic knowledge to real world situations and gain valuable experience preparing for their future careers in the industry.

1.2 Team Structure

In order to delegate tasks efficiently, Ryerson Hyperloop was split into four major sub-teams — Operations (OPS), Structures (STR), Guidance, Navigation & Control (GNC), and Propulsion (PRP) with each sub-team researching to produce an innovative, modular, and reliable design.

The sub-teams undertook a number of design projects while the administration, management, and operations were handled by the OPS sub-team. During the initial phase of the design, several workshops were conducted to identify areas of interest and to stimulate innovative system designs.

To ensure effective communication, RH utilized varied modes of communication, such as digital, oral, and written. The primary method of communication was through Slack, a virtual space that facilitated project discussions and decisions, collaborations, and conversations centered around the day-to-day operation of the team. In addition to the general team wide channels, each sub-team was assigned an exclusive channel that was dedicated to troubleshooting sub-team related issues and for promoting specific discussions.

The large amount of documentation generated by the team was sorted, stored, and shared on a working Team Drive through the university based Google Drive account. Google Drive is a cloud based file storage and synchronization service provided by Google. It allows users to upload, synchronize, and share their files to a working directory. Being the chief document storage directory, Google Drive served as one of the most vital resources in our effort to ensure smooth team operations.

In order to ensure progress and the transfer of information to new members, each sub-team met on a weekly basis. At these meetings, members presented their accomplishments as well as setbacks. Additionally, tasks that needed to be tackled in the upcoming weeks along with any pertinent information that required attention was discussed. To hold all members accountable, several systems of checks were established. In addition to weekly meetings, the team held three formal reviews: Preliminary Design Review (PDR), Critical Design Review (CDR), and Vehicle Readiness Review (VRR); all members were required to be in attendance at these reviews. The stakeholders such as the faculty advisors, industry advisors, and sponsors, who were invited to these reviews ensured sound technical decisions were made through all stages of development. At these meetings, the designs, analyses, manufacturing methods, and certification plans were presented. This ensured that the systems authorized to proceed to fabrication and testing met a predefined performance standard. Furthermore, it allowed for a clear understanding of the work completed and the establishment of interfacing requirements between the various available systems. The panel also included industry professionals who were able to provide feedback and constructive criticism exposing oversights, errors, and incorrect assumptions.

This document was intended to be a detailed guide that contained all information pertinent to the design, build, and testing of Ryerson's first Hyperloop Pod. It also contained reasoning behind design decisions, analyses performed on designs, results from testing of individual components, and findings from full system testing. This document was also intended to serve as a reference for the subsequent team when making design or managerial decisions. The goal was to produce a document so robust such that the new team can operate independently with minimal input from the former team captain.

This system of organization was established in an attempt to ensure the deficiencies faced by other teams do not potentially affect RH and its operations. It was also done to curb any bad habits from cultivating during the design year. It also offers a foundation upon which to further improve the management of the team.

1.3 Key Objectives and Contributions

The objective of this thesis was to design, develop, and validate various Hyperloop Pod systems systematically and with modularity at the forefront. This was done by establishing the requirements defined within Elon Musk's Hyperloop Alpha document as the baseline set of requirements [1]. Aerospace methodologies and standards were heavily relied upon in the design and testing of the Hyperloop Pod systems. In addition, key engineering disciplines such as finite elements, stress analysis, outgassing of materials, space grade soldering techniques, optimization for weight and cost, were applied during the entire design process of the Hyperloop Pod systems. A of the key objectives that were considered during the design of the Hyperloop Pod systems were:

- Investigation of the requirements set by the Hyperloop concept.
- Establishment of the constraints, objectives, and requirements necessary for the development of the Hyperloop Pod systems.
- Development of the Pod architecture for the Hyperloop concept.
- Address technical and system testing challenges imposed when operating within the Hyperloop environment.
- Provide the design details of the Hyperloop Pod architecture to SpaceX for the SpaceX Hyperloop Pod Competitions.
- Present key tests performed on the developed Hyperloop systems and highlight future opportunities for research.

The author's contribution throughout the development of the Hyperloop Pod systems allowed the author to present their research at Hexagon's Technologies In Action Conference, HxGN | LIVE in Las Vegas, Nevada, USA and at the International Conference on Aerospace System Science and Engineering (ICASSE) 2019 in Toronto, Ontario, Canada were the papers were also accepted for publication [2] and [3].

2 HYPERLOOP

2.1 The Hyperloop Concept

Currently, the four modes of transportation can be classified into the following categories: Road, Rail, Water, and Air. These modes of transportation tend to be slow, expensive, or a combination thereof. The Hyperloop is the next mode of transportation that aims to shift this notion by being fast and inexpensive after being commercialized.

Ever since the release of the Hyperloop Alpha document, great strides have been undertaken within the Hyperloop sphere [1]. This has been made possible by the research and developmental efforts being carried out by universities, and the industry. The newest mode of transportation is being developed to be safer, faster, economical, convenient, resilient to weather changes, and sustainable.

Current modes of transportation include — Air, Water, Rail, and Road where each of them are greatly impeded by air or water resistance at sea level. This prevents them from achieving high travel speeds. For example, an aircraft's Steady Level Flight (SLF) is at altitudes greater than 9,144 m (30,000 ft), resulting in a considerably lower aerodynamic drag. With aerodynamic or hydrodynamic drag increasing with the square of speed, a significantly large power input is required to go faster. This can be seen as power requirements need to be met with the cube of speed. The Hyperloop concept aims to circumvent this issue by placing a vehicle, in this case a Pod within a low pressure environment. This coupled with the implementation of contactless propulsion systems will aid in high speed travel that would otherwise have been extremely difficult to achieve at the ground level.

Furthermore, Elon Musk proposed that Hyperloop Pods could utilize air bearings or magnetic levitation for support, and could either be propelled via traditional motor and wheeled systems or via magnetic linear motors. Initial studies by SpaceX on the Hyperloop system extensively studied the route between its headquarters in Hawthorne (Los Angeles), California to San Francisco, California. From their research, a one-way trip should approximately take 35 minutes with a Pod departing each station every two minutes on average [1].

2.1.1 The Toronto-Montreal Corridor

After a global proposal to narrow down possible cities where the Hyperloop could be implemented, the Toronto-Montreal corridor was chosen to be one of the top contenders for the implementation of the fifth mode of transportation [4]. According to research, connecting these two Canadian cities together would create a supercluster of cities providing businesses with easy access to approximately 4.437 million Canadian for trade purposes as shown below [5].

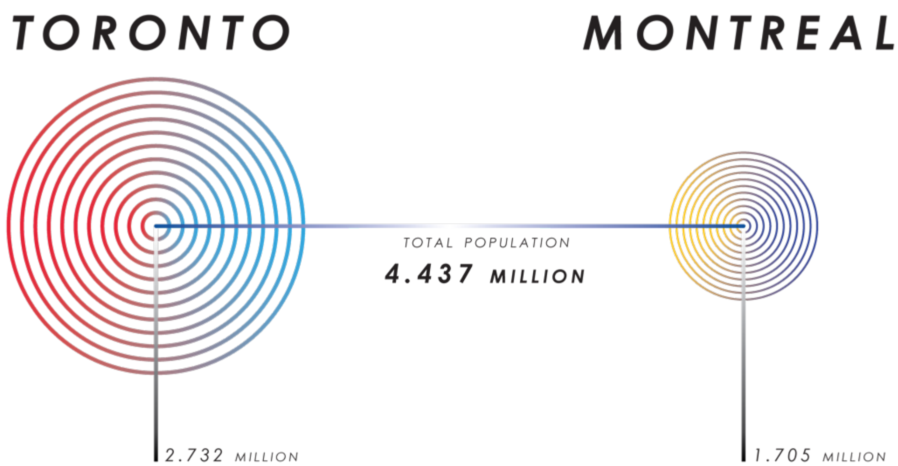

Figure 1. Toronto-Montreal population estimates [5].

Once the system is implemented, passengers on the Hyperloop can expect to travel between Toronto-Montreal in 35 minutes, leading to a dramatic reduction in commute times compared to the other modes of transportation as illustrated in Figure 2 [6].

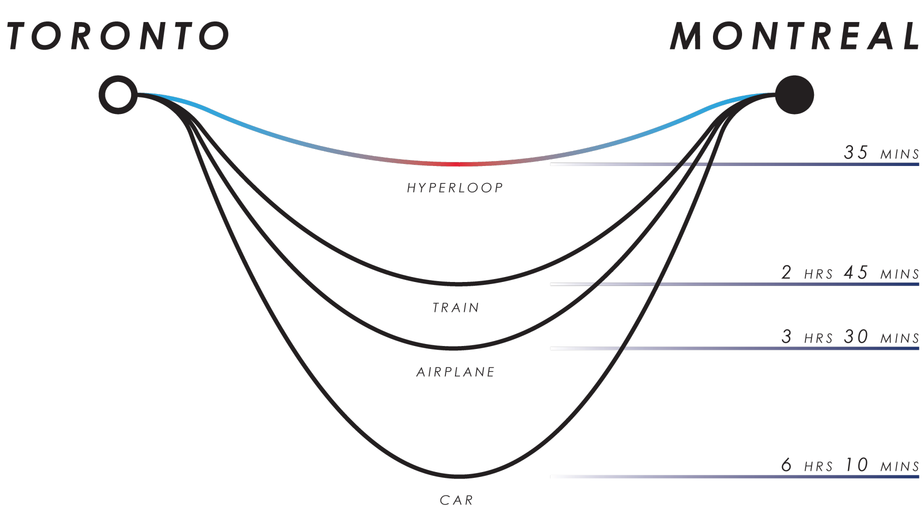

Figure 2. Commute times for the Toronto-Montreal corridor [6].

Figure 3 shows the energy consumption for a journey of about 600 km (373 miles) for the different modes of transportation such as Toronto-Montreal or Los Angeles-San Francisco. Furthermore, the energy costs of implementing either a passenger + cargo Hyperloop Pod or a passenger only Hyperloop Pod were significantly lower than the other modes of transportation in existence as shown in Figure 3 [1] and [7].

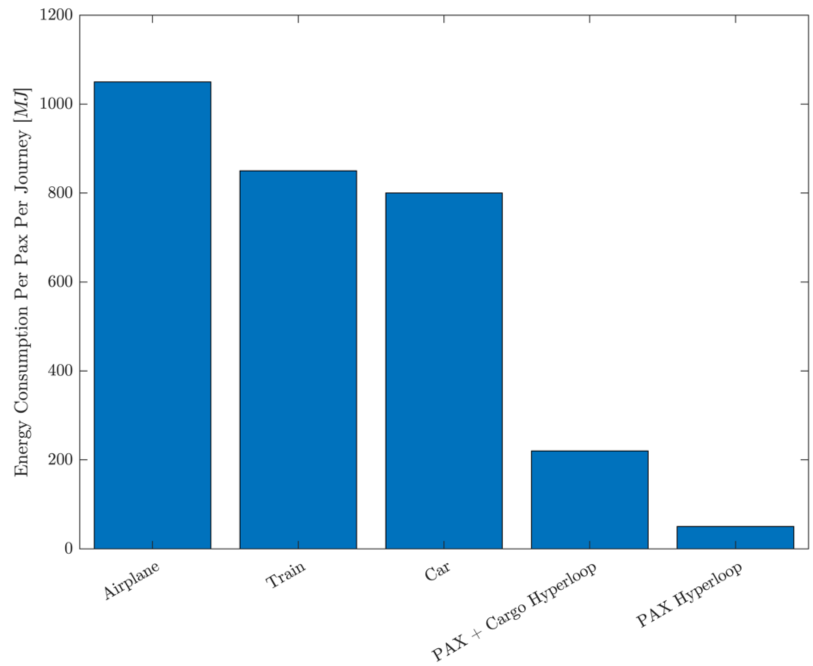

Figure 3. Energy consumption per passenger for various modes of transportation [1].

2.2 The Hyperloop Pod

Pods are currently being designed by the industry to accommodate between 28 to 40 people or a similar load in cargo [8]. With a Pod departing from its station every two minutes, commercial Pods are being designed to withstand cyclic and fatigue loads due to the continuous depressurization and pressurization of the environment within.

2.2.1 Hyperloop Pod Sub-Systems

Development of the passenger Hyperloop Pods has been attempted by various companies, and each has their own take on its design. A general Pod architecture as envisioned by Elon Musk within the White Paper has been illustrated in Figure 4.

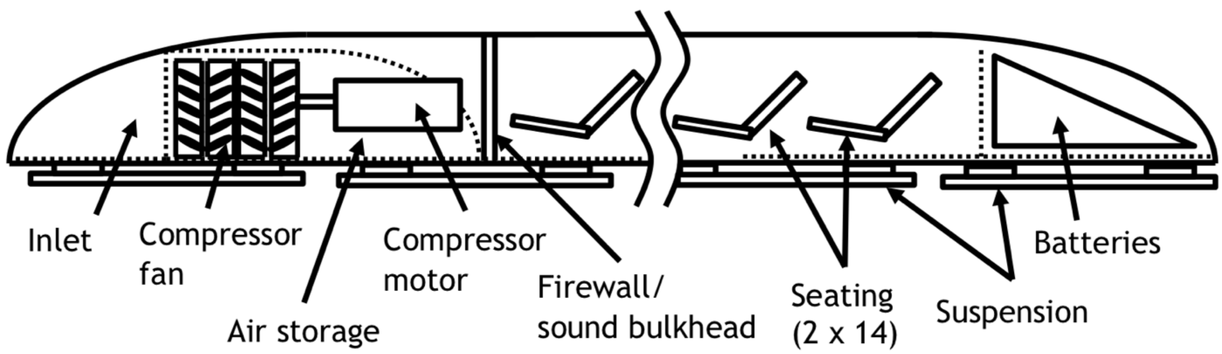

Figure 4. Concept architecture of a Hyperloop Pod as illustrated in the White Paper.

As illustrated above, the initial concept of the Hyperloop Pod included the following systems (from left-to-right):

1. Propulsion System: In order to be driven at the proposed speeds, the Pod requires the implementation of advanced linear motors. The moving element, also known as the rotor, will be located on the Pod itself. On the other hand, the stator or the stationary portion of the linear motor will be located on the tube. The implementation of such a system would allow for the Pod to accelerate up to 1,220 kmph or 760 mph [1]. In order to ensure the comfort of the passengers at all times, acceleration and braking is expected to be kept below 1 g during nominal operations.

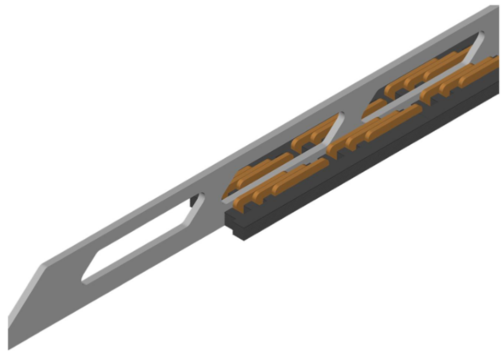

Figure 5. The Hyperloop's propulsion system showcasing the rotor and stator [1].

2. Compressor System: Initial designs included an onboard compressor for two reasons. It allowed for the Pod to travel with minimal gap between the tube and itself without the choking the flow around it. Current designs utilize a perforated leading edge of the Pod to channel the surrounding air around it. Additionally, if air bearings were being implemented to levitate the Pod, it served as inlet.

3. Passenger Support System: As the Hyperloop operates within a low pressure environment, a passenger support system is required onboard the Pod to circulate pressurized air. This support system needs to circulate, collect, filter, and recirculate clean air back into the cabin. This needs to be done all the while regulating and maintaining the Pod at a comfortable temperature.

4. Suspension System: In order to levitate or suspend a Pod at a predetermined height, various methods had been proposed. The three key methods include: traditional wheel and axle system, air bearings, and magnetic levitation system. For high speed travel, conventional wheel and axle systems tend to become impractical due to stability problems and frictional issues. On the other hand, air bearings or magnetic levitation tend to be more viable in this circumstance due to its extremely low drag stability advantages.

5. Power System: With the Hyperloop Pod not being powered by a ground power during its run, onboard batteries are required to keep its systems operational. This includes powering the passenger support systems, propulsion, telemetry, braking, and any other auxiliary systems.

6. Braking System: The implementation of permanent magnets as the primary braking system is being thoroughly researched. Such a system would tremendously reduce wear-and-tear as no contacting parts are being used. For the purpose of redundancy, traditional contact braking methods need to also be implemented in the event additional braking force is required.

2.3 The Hyperloop Tube

The Hyperloop concept utilizes a low pressure environment where the system is proposed to be a closed loop connecting two cities together. The drawing of a hard vacuum has been avoided due to the difficulties that would potentially arise in maintaining them. In addition, operating in a low pressure environment would allow for the implementation of Commercial-Off-The-Shelf (COTS) pumping systems. With the development of a few large scale Hyperloop tubes across the globe, research indicated that the dimensions of the tube are predominantly based on the route they will be covering. As a result, a prespecified final size for the Hyperloop tube has not been put out [9].

2.3.1 The SpaceX Hyperloop Tube

To accelerate the development of the Hyperloop concept, SpaceX independently developed the design and built a kilometer long Hyperloop test track located outside their HQ in Hawthorne, California.

The Hyperloop tube has been manufactured from steel due to its availability, low cost, strength, and weldability. The tube contains an Aluminum (Al) test track, and a sub-track that is mounted to a concrete base.

Table 1. SpaceX Hyperloop tube material specifications.

Hyperloop Tube Parameters	**Value**
Hyperloop Tube	*ASTM A1018 Grade 36*
Test Track	*Aluminum 6061-T6*
Sub-Track	*Aluminum 6101-T61*
Mounting Base	*Concrete*

As per SpaceX's design, their Hyperloop Tube is said to be approximately a half-scale version of the full-scale production concept [10]. As a result, Ryerson's first Hyperloop Pod had been designed to meet the dimensional requirements of SpaceX's Hyperloop tube. Some of the key dimensions that were adhered during the entire design process have been outlined in Table 2.

Table 2. SpaceX Hyperloop tube major dimensional specifications.

Hyperloop Tube Parameters	Value
Tube Length	*4150 ft (1.25 km)*
Outer Diameter	*72 in*
Inner Diameter	*70.6 in*
Radius of Curvature	*> 15 miles (24 km)*

2.4 The SpaceX Hyperloop Operating Environment

2.4.1 Low Pressure Environment

When operating within the Hyperloop environment, the Pods are subjected to a cyclic pressure loading due to the continuous depressurization and pressurization. This results in the structure experiencing fatigue stresses. The SpaceX Hyperloop operates at a minimum ambient pressure of 0.125 psi [10]. This is done to support the various propulsion systems that were developed.

Table 3. SpaceX Hyperloop operating pressures.

Hyperloop Tube Parameters	Value
Number of Vacuum Pumps	*4*
Minimum Operating Pressure	*0.125 psi (862 Pa)*
Maximum Operating Pressure	*14.7 psi (0.102 MPa)*
Pump Down Period	*45 minutes*
Pump Up Period	*25 minutes*

With the test track being located in Hawthorne, California, the operating pressure within the tube is highly dependent on the season, weather conditions, and time of day. With four vacuum pumps, the pump down time was approximately 45 minutes to reach an operating pressure 862 Pa, while the pump up period took around 25 minutes.

2.4.2 Tube Thermal Management

The SpaceX Hyperloop Tube does not contain any thermal management control system. As a result, the tube's internal temperature is solely dictated by the season, weather conditions, and the time of day the test was scheduled for. Majority of the testing occurred during the weeks of July and the corresponding METAR data for the SpaceX facility has been tabulated in Table 4 [11].

Table 4. Temperature range for SpaceX during the testing period.

Parameter	Value
General Testing Period	*10^{th} – 21^{st} July*
Maximum Temperature (High)	*23°C*
Maximum Temperature (Average)	*21°C*
Maximum Temperature (Low)	*18°C*
Minimum Temperature (High)	*22°C*
Minimum Temperature (Average)	*20°C*
Minimum Temperature (Low)	*17°C*

Since the tube temperature ranged from 35°C to 45°C, Pod designs needed to account for degradation in the cooling by convection resulting from the low pressure environment. The loss in heat dissipation coupled with the frequency of Pod deployment in the full-scale version could result in thermal hotspots that needed to be accounted for in the Pod's thermal management system.

3 SpaceX HYPERLOOP POD COMPETITION

In order to accelerate the development of the Hyperloop concept, SpaceX announced a Hyperloop Pod Competition utilizing their newly built mile long test track outside their HQ in Hawthorne, California. This was done to encourage innovation, research and development, and testing of the concept by student teams from across the United States and the globe.

Following the release of the White Paper in 2013, SpaceX announced the very first Hyperloop Competition in 2015 to accelerate the development of the Hyperloop concept. Universities from all across the world were tasked to design high speed Pods and to present it in January 2016. Top teams from all entries were selected to advance and build their prototypes.

Teams who were successful in manufacturing a prototype Pod were allowed to compete at the first ever Hyperloop Pod Competition 2017 where they raced their Pods on SpaceX's Hyperloop test track. After receiving a number of high quality submissions, the organizers subsequently held four more Hyperloop Pod Competitions.

3.1 2019 Hyperloop Pod Competition

As with the previous iterations of the competition, the 2019 Hyperloop Pod Competition was judged solely on the Pod's top speed [1]. In addition to speed as a criterion, the designed Pod was required to propel or crawl itself to within 30 m of the exit airlock doors of the Hyperloop tube. During the entire 2019 Competition, Ryerson achieved the following.

- **Being from the top 10%** out of the 1,500 entries after being selected to proceed to the second round of the Hyperloop Pod Competition.
- Successfully passed the second round and got approved to proceed to the third round.
- **Being from the top 8%** after being selected for various technical interviews by the competition organizers.
- Received special invitations from SpaceX to attend both the 2018 and the 2019 Hyperloop Pod Competition in Hawthorne, California.

3.1.1 Technical Documentation

After completion of all necessary legal and governance documentation, the team submitted a comprehensive design proposal to the competition officials. This document provided the judges with an overview of design and a means to perform a sanity check. This ensured the team was proceeding in the correct direction. In order to manage the number of teams, the organizers had the ability to down select teams at this stage.

After all the necessary approvals were received, a technical document was completed for the judges highlighting the design, analysis, and manufacturing plans for the Hyperloop Pod. Teams that fulfilled all the integral prerequisites set by the organizers were approved to proceed to the technical presentations portion of the competition.

3.1.2 Technical Presentation

Based on all the deliverables received by the competition judges, select teams were asked to present their designs via video conferencing technology to a judging panel consisting of engineers, technicians, safety officers, business personnel from SpaceX, The Boring Company, Tesla, and so forth. This format allowed the organizers and judges to better understand the Pod and provided the panel an opportunity to gain clarity (on technical issues). Furthermore, the team received valuable feedback on the designed Pod.

3.2 2020 Hyperloop Pod Competition

The 2020 Hyperloop Pod Competition is planned to run within a 10 km Hyperloop tube rather than the kilometer long test track currently being used in Hawthorne, California. To help advance this emerging technology even further, the new track is no longer expected to be linear. It is proposed to have a curve of an unknown radius. Furthermore, this new track is proposed to have the same level of vacuum combability as the shorter Hyperloop tube [12].

4 RYERSON'S HYPERLOOP POD ARCHITECTURE

4.1 Pod Overview

Ryerson's Hyperloop Pod consisted of three major systems – Structures (STR), Guidance, Navigation & Control (GNC), and Propulsion (PRP). Figure 6 illustrated the breakdown of the aforementioned systems into their characteristic sub-systems.

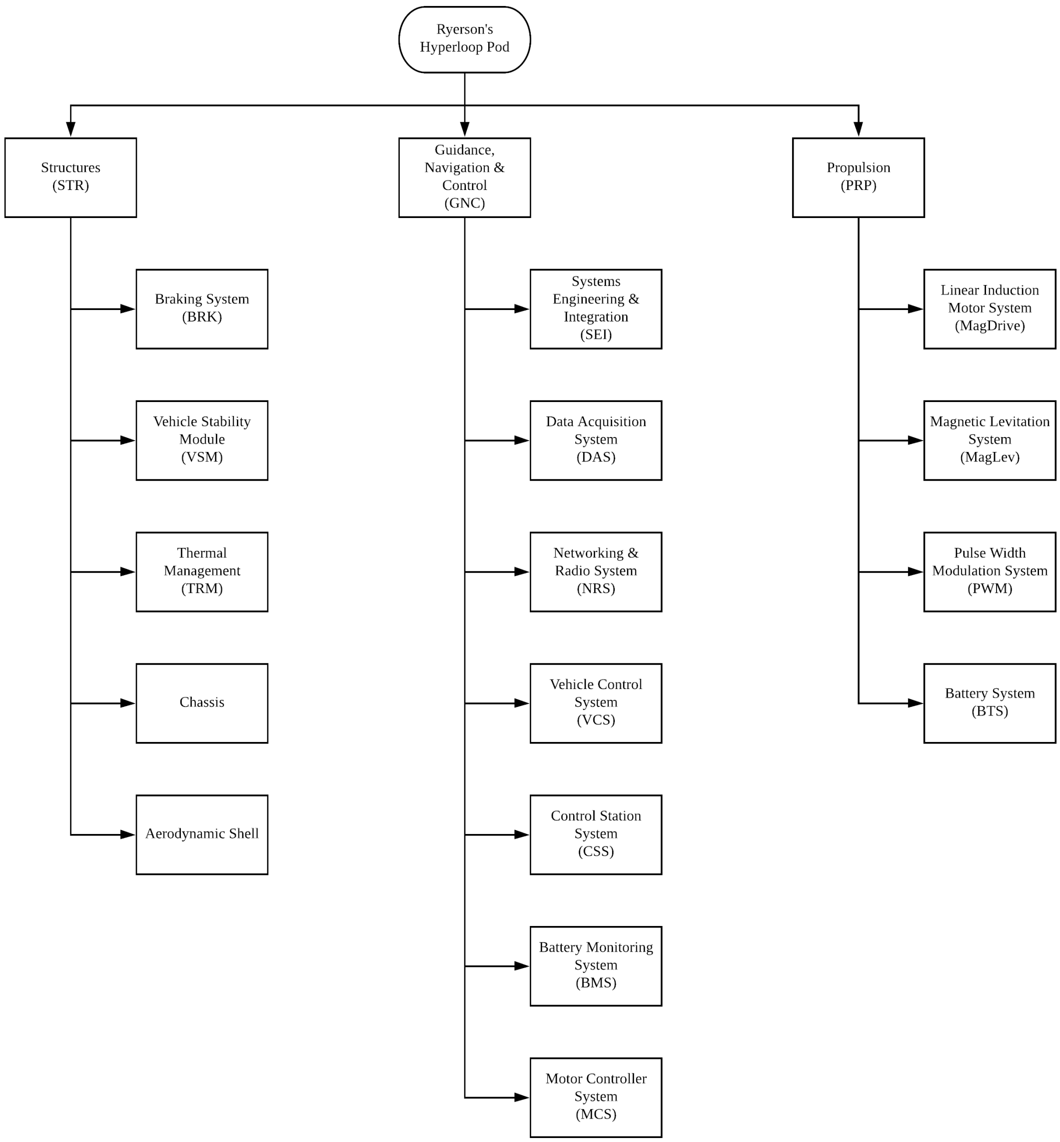

Figure 6. Ryerson International Hyperloop's pod architecture.

4.1.1 Pod Design

Figure 7 and Figure 8 showcase the isometric view of Ryerson's Hyperloop Pod consisting of all its systems. The Pod designed for the Hyperloop Pod Competition measures in at 2.3 m in length, 0.5 m in width, 0.3 m in height, and a loaded weight of 140 kg. The Pod's aforementioned systems have been shown and labelled in Figure 9, while its major specifications have been tabulated in Table 5.

Table 5. Ryerson's Hyperloop Pod specifications.

Overall Pod Parameters	Value
Pod Length	*2.3 m*
Width	*0.5 m*
Height	*0.3 m*
Structures Weight	*29 kg*
Propulsion Weight	*73 kg*
Guidance, Navigation and Control Weight	*15 kg*
Pod Weight (With Safety Margin)	*140 kg*

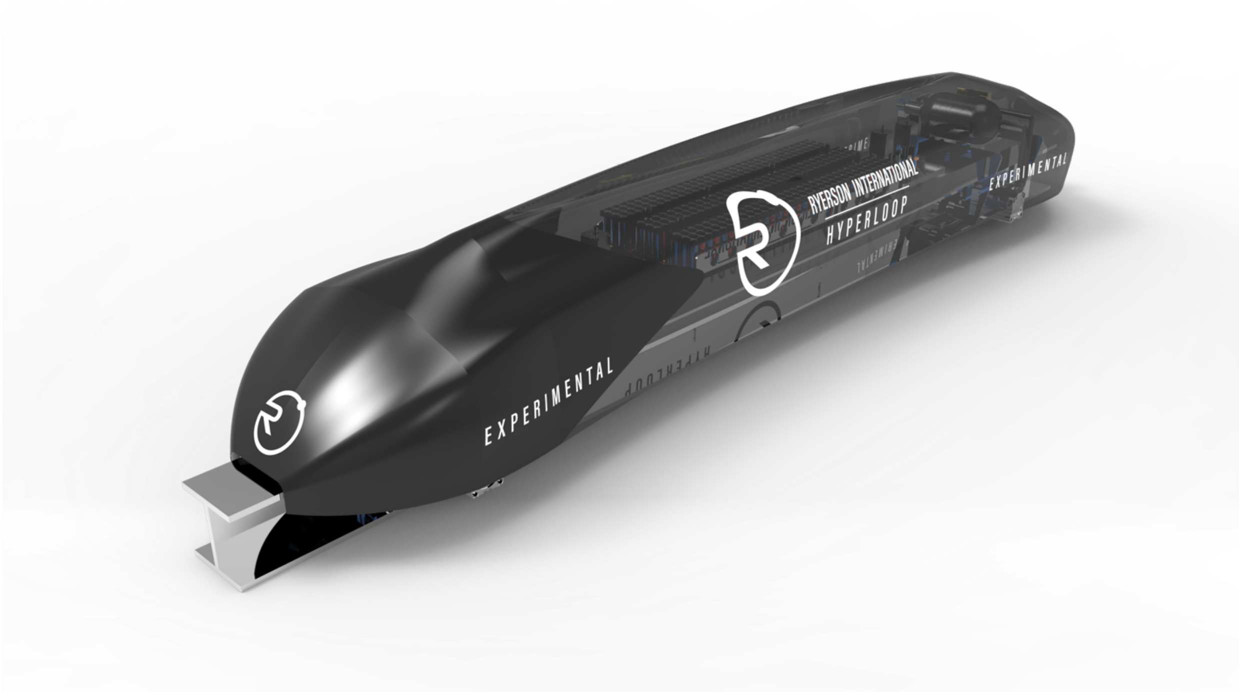

Figure 7. Ryerson's Hyperloop Pod design with an aerodynamic shell.

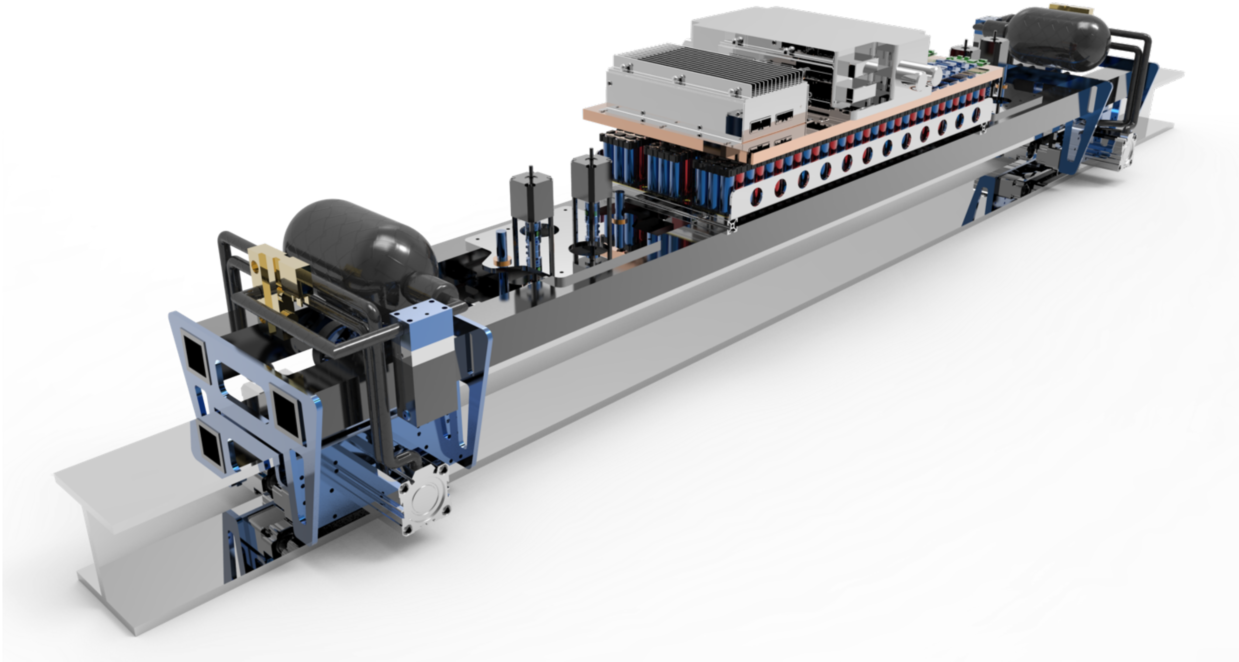

Figure 8. Ryerson's Hyperloop Pod design showcasing its internal systems.

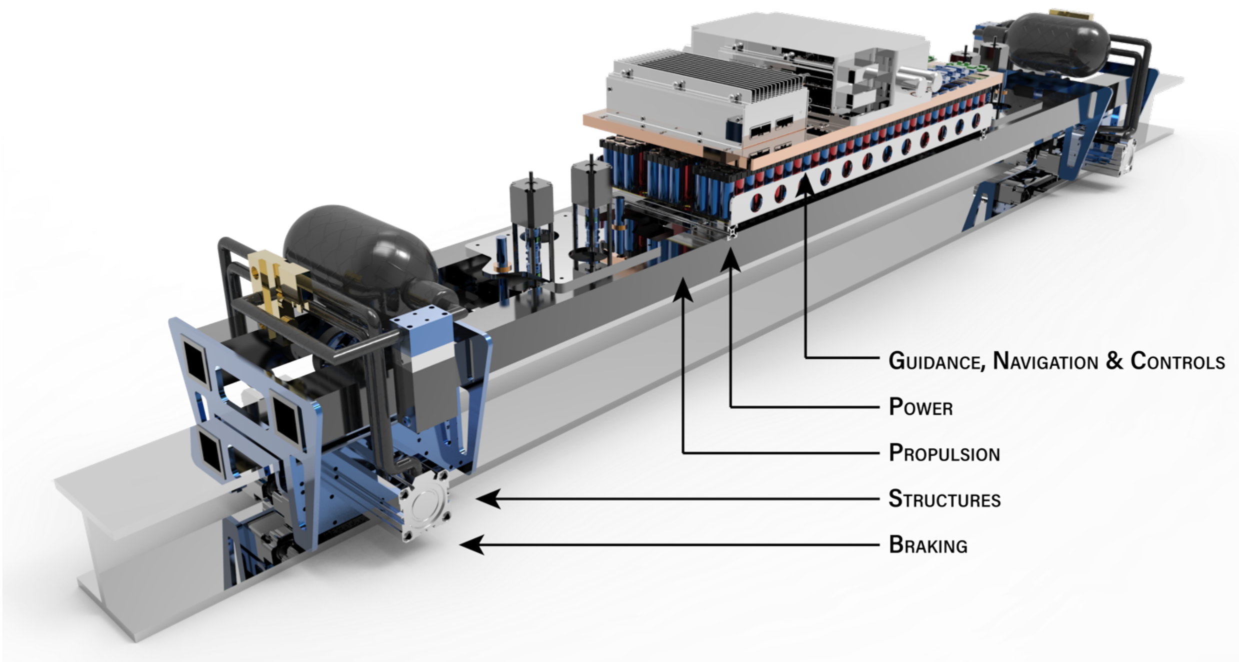

Figure 9. Ryerson's Hyperloop Pod with its internal systems labelled.

4.1.2 Structures Overview

The Hyperloop Pod included two independent pneumatic braking systems that consist of two independent pairs of braking pistons as shown in Table 6. The systems have been arranged in a forward, and aft configuration of the Hyperloop Pod. Both systems have their own pneumatic tank, control systems, control valves, and pneumatic tubing. This was done to prevent a cascading failure in the event a system failure was to occur.

Table 6. Pod's braking system overview.

Braking System Parameters	Value
Number of Independent Systems	*2*
Number of Pistons	*4*
System Weight	*14 kg*
Nominal Braking Force	*900 N*
Maximum Braking Force	*1800 N*

When designing the chassis of the Pod, critical cases needed to be examined. These were the acceleration, levitation, and braking phases. System weights along with the phase particular loads were accounted for. In such load cases as the Center of Gravity (CG) position changed, it was also needed to be accounted for in the design.

The Pod's chassis consists of a forward and an aft bulkhead connected together by two longitudinal Aluminum extrusions referred to as Longitudinal Chassis Members (LCM). Aluminum extrusions were chosen for modularity and to aid the placement of all the Pod systems on it.

Although an aerodynamic shell was unnecessary due to the Pod operating in a low pressure environment, as per the competition requirements, completing a run with a shell simply added to the Pod's overall aesthetic and mass resulting in a lower top speed. Even though runs can be completed without a shell, one was still designed in order to place all the sponsor logos on the Pod.

4.1.3 Guidance, Navigation & Control Overview

As the Pod powers up, it automatically defaults to a “Safe To Approach” state. This is done only when the Pod is stationary, in good working condition without any major faults, and is safe for humans to approach it. Upon the completion of the necessary checks within the tube, the Pod will then have the potential of entering into the remaining states as shown in Table 7.

Table 7. A few of the Pod states controlled by GNC.

Pod State	Description
Safe To Approach	Indicates that the Pod is stationary, in good working condition without any major faults, and is safe for humans to approach it.
Ready To Launch	Performs final checks, and readies key systems for launch.
Fault	A non-nominal, unknow or unsafe event or a parameter falls outside is envelope is detected, and Pod automatically comes to a stop.

In addition to performing all of the state transitions, GNC receives data from the Pod including its location within the tube, velocity data, acceleration data, temperatures and pressure, Pod health, and so on. This vital telemetry data is transmitted in real time to the mission control (ground station) for Pod status and analysis.

Although control decisions are taken autonomously onboard the Pod, the Pod has been designed in such a way that all the commands to initiate movement (from standstill) were required to be sent from the mission control. This built-in safety feature ensured that the Pod would consistently obey the incoming commands from the ground station. If for some reason the signal was lost, the Pod automatically defaults to the fault state and comes to a safe halt.

4.1.4 Prolusion Overview

For propulsion, the Pod is propelled and levitated by a true contactless system as envisioned by Musk [1]. Propulsion is achieved by the MagDrive along the track through the means of electromagnetic induction via a Linear Induction Motor (LIM). The motor utilized an alternating current that is passed through its coils wound around a stator. By doing so, it created a changing magnetic field which in turn produced a force that propels the Pod forward.

In order to achieve the highest possible thrust, i.e. velocity, a three LIM propulsion system was initially designed. However, after further analysis, it was found that this sort of configuration would have diminishing returns. By performing a Return On Investment (ROI) analysis, the overall weight increase incurred as a result of the Pod being heavier would reduce the overall effectiveness of the levitation system. As a result, a single LIM configuration was opted for.

Magnetic levitation system was used to support the Pod at a predetermined height. The system consists of permanent N42 Neodymium magnets configured in a Halbach array to create a repulsive magnetic field to suspend the Pod. This resulted in a drag reduction when compared to wheeled systems at high speeds.

4.2 Pod Structures

The breakdown of the Hyperloop Structures system has been illustrated in Figure 10, where the design of the Pod's chassis, and braking system were considered the topmost priority. This design approach allowed for the development of the overall Pod chassis required to mount all the other Pod systems to it.

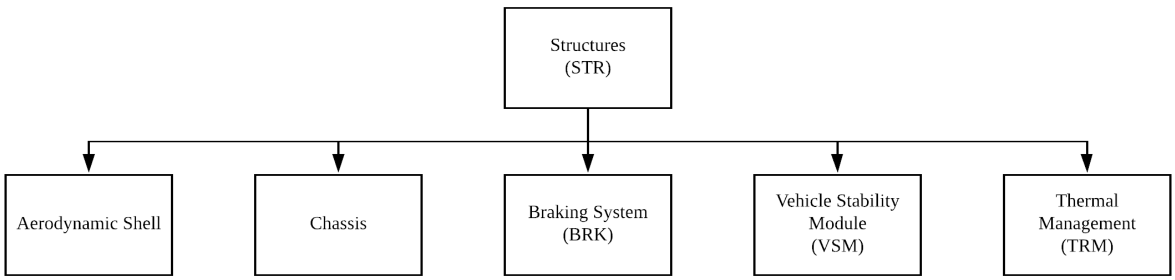

Figure 10. Pod structures breakdown.

Two major components for the Pod structure included the design, and development of the bulkheads, and the Longitudinal Chassis Members (LCM). The two aforementioned components form the Pod's chassis where a forward, and aft bulkheads are connected together via two LCMs. When designing these components, the principal design loads that were considered were the weight of the PRP system, GNC, and BRK systems.

4.2.1 Pod Longitudinal Chassis Members (LCM)

One of the design objectives was to ensure all the aforementioned systems had a mounting location on the LCM, while maintaining structural rigidity. Analysis conducted on the propulsion system required the optimal gap height between the LIM, and the track to be at 2 mm. With the LCM holding the LIM in place, a design constraint allowed for a maximum deflection of the LCM to be lower than 1 mm.

Table 8. Potential cross-sectional areas for the LCM.

LCM	Cross-Section
Design 1	*Circular*
Design 2	*Tubular*
Design 3	*Square Tubing*
Design 4	*Hexagonal*
Design 5	*Extrusion*
Design 6	*C Channels*
Design 7	*L slots*

Table 9 highlights the various criteria that were selected when designing the LCM after their individualistic priorities were established. Meanwhile, Table 8 showcases the different cross-sectional areas that were considered during its design [13].

Table 9. Important criteria for the design of the LCM.

	Ease of Use	Surface Area	Manufacturability	Cost
Ease of Use	N/A	0	1	1
Surface Area	1	N/A	1	1
Manufacturability	0	0	N/A	0
Cost	0	0	1	N/A

One of the scenarios that was analyzed is if the MagLev system does not perform as intended. If such a failure were to occur, it would result in the total Pod mass to be rested on the LCMs, and the bulkheads. The worst case scenario would occur if the rear braking system were to become inoperative. During such an event, the Pod's braking force would cause the front end to lock up while the aft portion to continue to move forward leading to the buckling of the LCMs. As a result, the Pod needed to fulfill any and all safety requirements during all its phases. And to do so, the various load cases that were analyzed have been tabulated below.

Table 10. LCM loading scenarios based on Pod state.

Case	Pod State
Loading Case I	*Pod Staging*
Loading Case II	*Launch Phase*
Loading Case III	*Levitation Phase*
Loading Case IV	*Braking Phase*

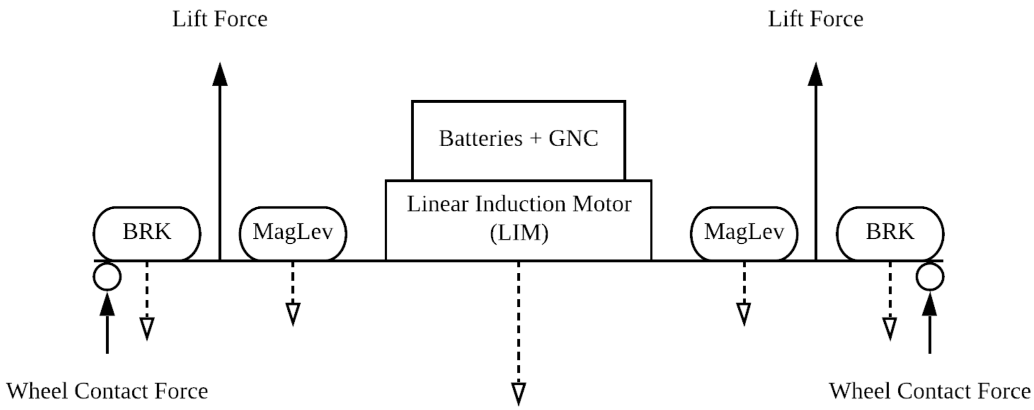

Figure 11. Pod staging load case for the LCM.

Figure 11 illustrates the schematic of the loading of the LCM as the Pod is lifted to be placed on the Hyperloop staging area. The dotted lines represent the weight of the respective systems on the LCM, while the solid lines represent a force being applied to the system. In this case, a contact force is applied by the stability modules, and the lift force that occurs when the Pod is lifted.

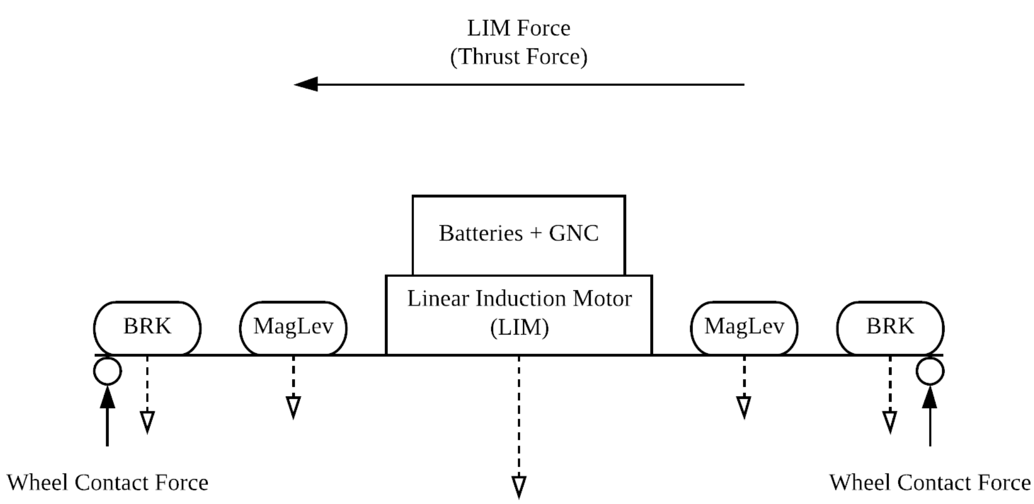

Figure 12. Pod launching load case for the LCM.

As the Pod enters the launch phase and begins its run, it generates thrust via the LIM. In addition to the system weights acting on the structure, the stability module (wheel contact force) would still be in contact with the test track as the Pod would not have gained sufficient speed for the MagLev system to levitate the Pod at this point.

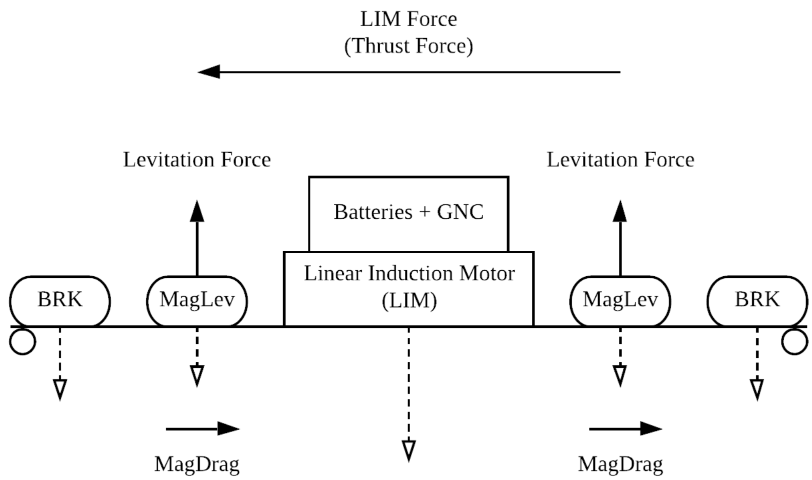

Figure 13. Pod levitation loading scenario for the LCM.

The above schematic represented the forces acting on the LCM as the Pod began its run, and levitates. As illustrated, the Pod experiences a thrust force generated by the LIM. In addition, once the MagLev system is deployed, a drag force is generated known as MagDrag.

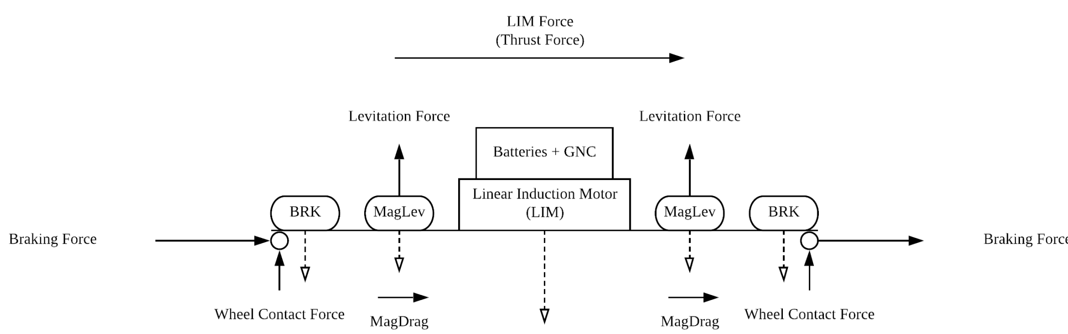

Figure 14. Pod braking loading scenario for the LIM.

As the Pod's braking sequence initiated, the braking force applied slows it down. To improve the Pod's braking profile, reversing the polarity (current) flowing to the LIM will subsequently cause it to generate thrust in the opposite direction to motion as shown in Figure 14. The final bit of braking power can be extracted from the Pod by deploying and bottoming out the MagLev system. In doing so, it will cause the generation of MagDrag, resulting in a much better braking profile.

Under the aforementioned load cases, the objective was to find a suitable cross-section where the stresses, and deformation were minimized while maintaining a sufficient working area to mount the Pod systems. To do so, the area moment of inertia was maximized for the cross-sections outlined in Table 8, and the following equations were used.

Circular Cross-Section:

$$I = \frac{\pi}{4} {r_o}^4 \tag{1}$$

Tubular Cross-Section:

$$I = \frac{\pi}{4} ({r_o}^4 - {r_i}^4) \tag{2}$$

Square Cross-Section:

$$I = \frac{a^4}{12} \tag{3}$$

Hexagonal Cross-Section:

$$I = \frac{5\sqrt{3}}{16} a^4 \tag{4}$$

where for all the cross-sections, the area moment of inertia is denoted by I. For the circular, and tubular designs, the r_o is its outer radius and r_i is the inner radius. Whereas for the square, and hexagonal cross-sections, a represented the length of its side.

The materials for the LCM were proposed to be either manufactured out of carbon fiber composite, steel or aluminum. Steel LCMs were ruled out due to the large weight penalty that would be incurred when used for the structure. On the other hand, the carbon fiber LCMs would provide the necessary strength while being lightweight. However, it was ruled out due the difficulties associated in manufacturing the long LCM pieces while maintaining a high tolerance. In the end, Aluminum 6061-T6 was selected for its optimal balance between its strength, and weight while being a material that is easy to be worked upon. The material specifications for the Aluminum have been tabulated in Table 11 [14], [15], and [16].

Table 11. Aluminum 6061-T6 material specification for the LCM.

Parameter	Value
Material	*Aluminum*
Specification	*6061*
Hardening	*T6*
Density	*2700* kg/m^3
Modulus of Elasticity	*68.9 GPa*
Poissons Ratio	*0.33*
Ultimate Tensile Strength	*310 MPa*
Yield Tensile Strength	*276 MPa*

With the material specifications on hand, the properties for the LCM was calculated. Observing Table 12, a tubular LCM would be of an ideal weight while having a high enough area moment of inertia. However, with a circular and tubular cross-section, mounting other systems on the LCM would be difficult as it does not allow for the presence of a flat mounting surface. On the other hand, a hexagonal LCM would provide sufficient surface area for system mounting at the expense of the added weight.

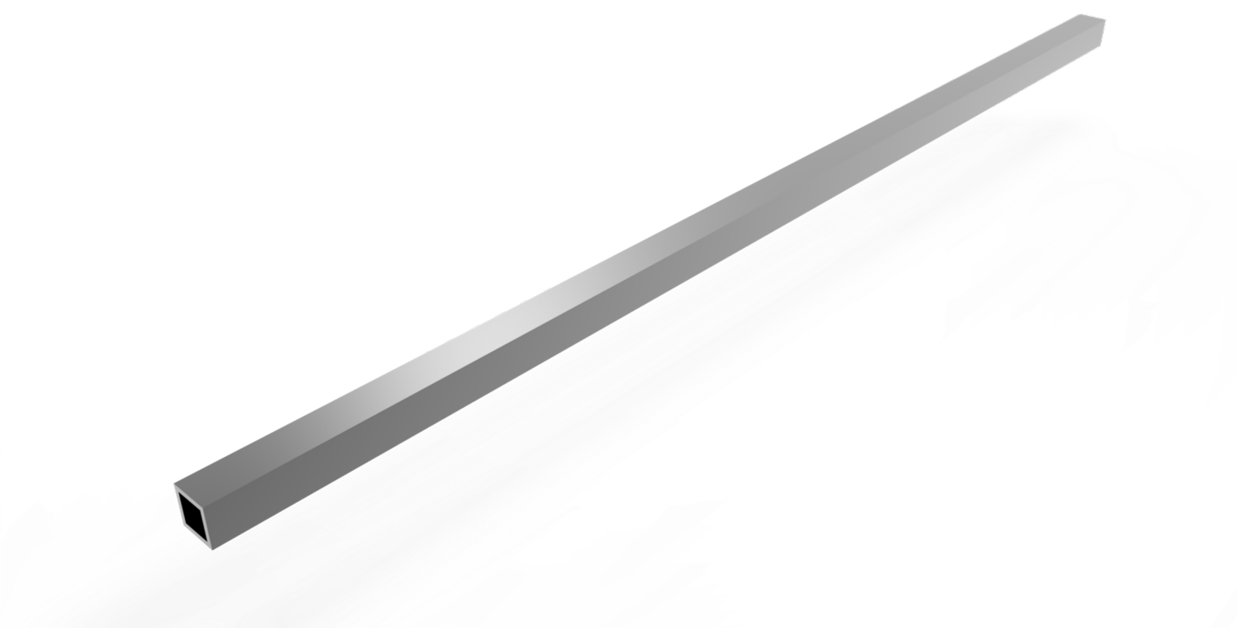

Figure 15. Pod's LCM manufactured using anodized black Aluminum 6061-T6.

Aluminum extrusions were initially considered to be the best solution due to its high strength, area moment of inertia all the while having a low enough mass as shown in Table 12. In addition, the presence of T-slots would allow for the incorporation of a modular mounting method. During tests, it was found that placing systems on the exact mounting coordinates to be extremely difficult as a result of the slots. And replicating their location after a component swap was almost impossible. As a result, the extrusion was swapped out for traditional square tubing manufactured out of Aluminum 6061-T6 [17].

Table 12. Property calculation of the various LCM designs.

LCM Design	Volume	Mass	Area Moment of Inertia
Circular	*0.004 m^3*	*10.945 kg*	*3.65 kgm^2*
Tubular	*0.002 m^3*	*4.788 kg*	*1.597 kgm^2*
Square Tubing	*0.002 m^3*	*6.097 kg*	*2.034 kgm^2*
Hexagonal	*0.004 m^3*	*11.314 kg*	*3.786 kgm^2*
Extrusion	*0.002 m^3*	*4.498 kg*	*1.501 kgm^2*

4.2.1.1 LCM Analysis

To ensure the LCM met the structural requirements, the aforementioned cross-section (square tubing) was analyzed within ANSYS. Furthermore, to successfully design and validate the LCM, the braking phase was considered to be the most load bearing case on the Pod. As a result, its corresponding boundary conditions where the one ends of the LCM become locked up (clamped). This was in addition to the principal system loads occurring on the structure within ANSYS. Figure 16 highlighted the workflow setup for the various Pod loading scenarios within ANSYS Workbench.

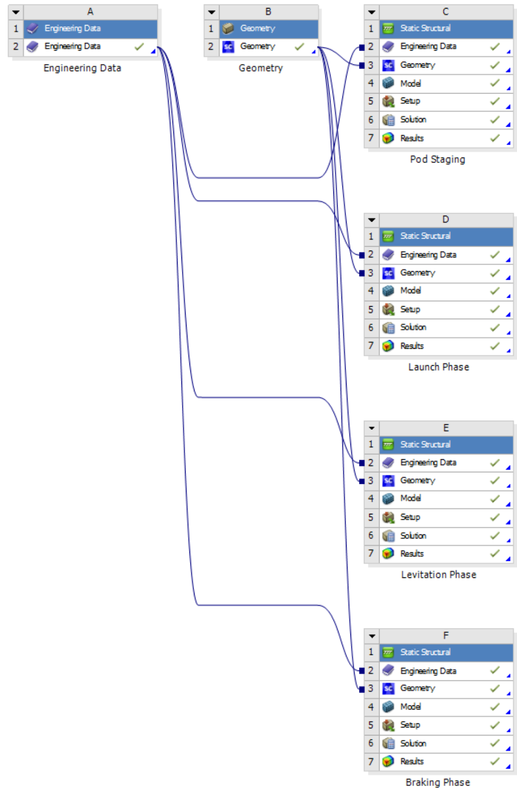

Figure 16. ANSYS workflow setup for the Pod's LCM.

4.2.1.1.1 Loading Case I (Pod Staging)

During the staging phase, the Pod is lifted via a forklift from the chassis. This resulted in the Pod to experience a lift force, and a reactionary force from the stability wheels on the LCM. In addition, the analysis accounted for the weights of all the Pod systems as illustrated in Figure 11.

Table 13. LCM loading case for Pod staging.

LCM Loading Parameters	Value
Braking System (Per System)	*74 N*
MagLev System (Per System)	*84 N*
LIM, Batteries & GNC Systems	*403 N*
Pod Staging Lift Load (Per System)	*687 N*

Within the Pod staging load scenario as highlighted in Table 13, a maximum deformation of 0.55 mm was to be expected at the centroid of the LCM with a maximum stress value of 165.71 MPa as illustrated in Figure 17 and Figure 18 respectively.

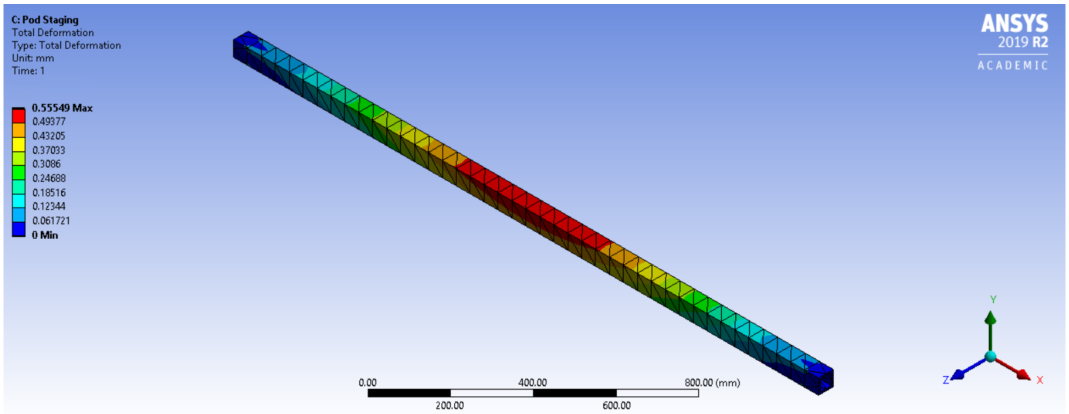

Figure 17. LCM deformation during Pod staging scenario.

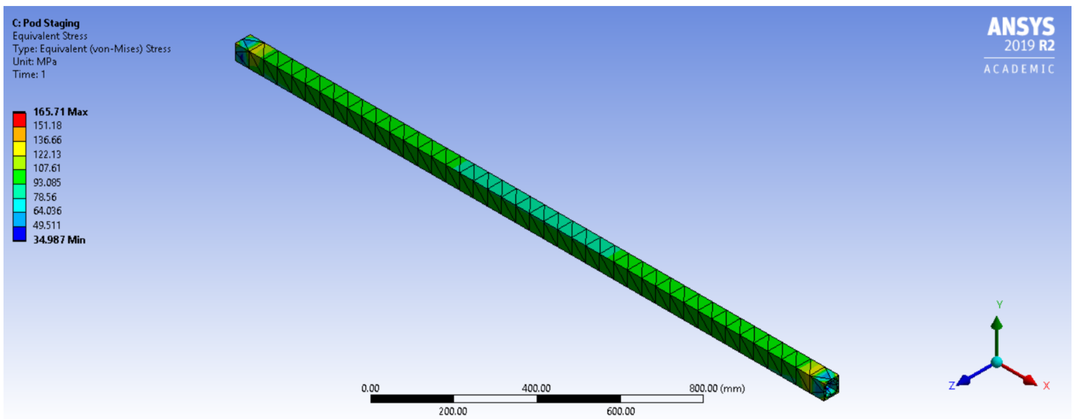

Figure 18. LCM stress during Pod staging.

4.2.1.1.2 Loading Case II (Launch Phase)

Once the Pod is placed on the test track, and launch clearance is obtained from SpaceX, only then will the Pod have the ability to go into the launch phase. As the Pod is launched, it experiences the thrust generated by the LIM. In addition to all the system weights acting on the chassis, the stability wheels would still apply a reactionary force on the Pod as a result of the low speed the Pod would be traveling at during this segment of its run.

Table 14. LCM loading case for launching phase.

LCM Loading Parameters	Value
Braking System (Per System)	*74 N*
MagLev System (Per System)	*84 N*
LIM, Batteries & GNC Systems	*403 N*
Vehicle Stability Module (Per System)	*687 N*

With the loading scenario highlighted in Table 14, a maximum deformation of 0.55 mm was observed at its center due to the weight of the LIM, batteries and the GNC system. Whereas, a maximum stress value of 165.71 MPa was observed within the LCM. The deformations and stresses have been illustrated in Figure 19 and Figure 20 respectively.

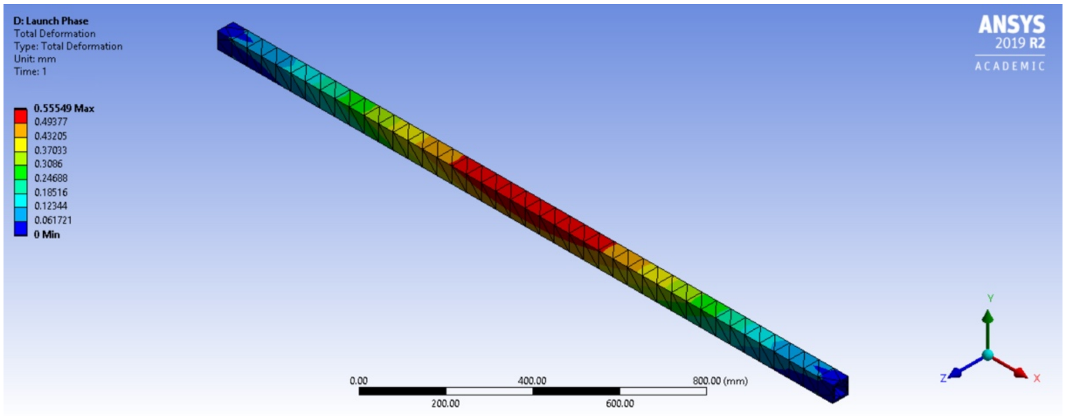

Figure 19. LCM deformation during Pod's launching phase.

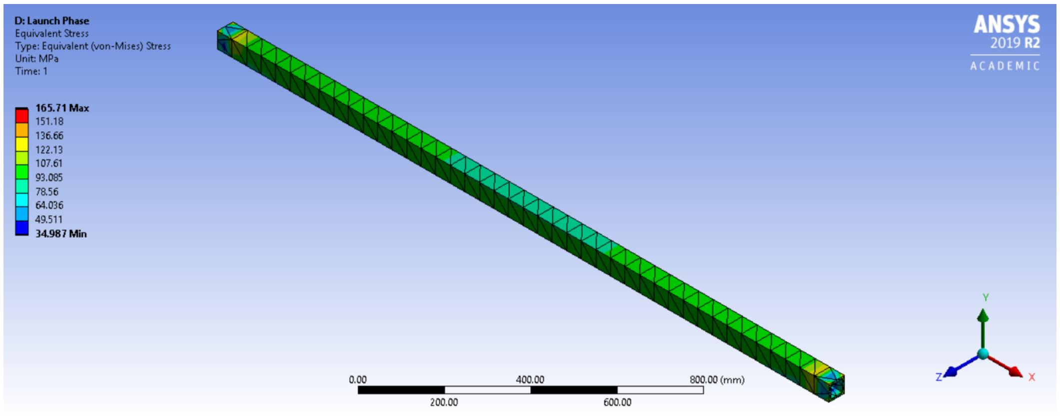

Figure 20. LCM stress during Pod's launching phase.

4.2.1.1.3 Loading Case III (Levitation Phase)

Further into the run, the Pod would have gathered enough speed allowing for the MagLev system to take over, and to support the Pod. During this phase, the aforementioned forces such as the thrust, system weights would continue to act on the structure. However, with the MagLev being initiated, the drag force generated by it will begin to have an effect on the Pod. With the Pod fully levitating, the contact force from the vehicle stability modules no longer act on it.

Table 15. LCM loading case for the Pod's levitation phase.

LCM Loading Parameters	Value
Braking System (Per System)	*74 N*
MagLev System (Per System)	*687 N*
LIM, Batteries & GNC Systems	*403 N*

Table 15 showcased the major system loads acting on the LCM during the levitation phase. As majority of the load is exerted upwards by the MagLev on the LCM, a maximum deflection of 0.68 mm and a stress value 165.09 MPa was obtained. Figure 21 and Figure 22 showcase the contour plots for the new loading scenario.

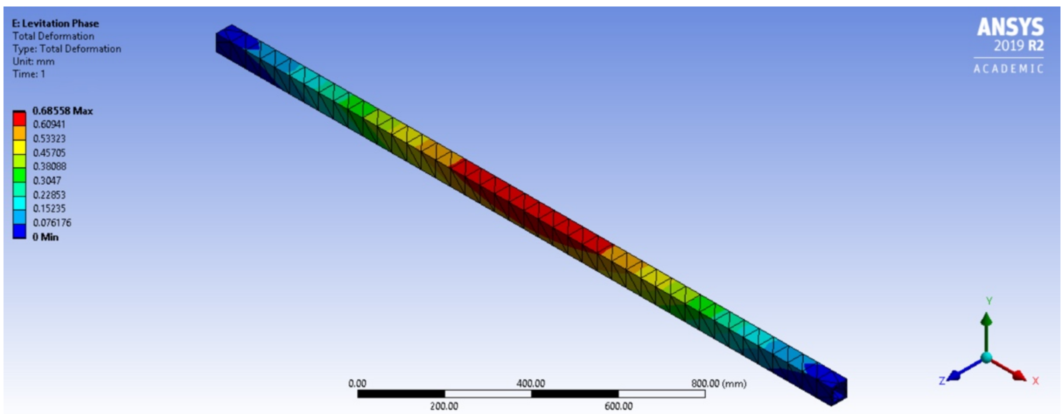

Figure 21. LCM deformation during Pod levitation.

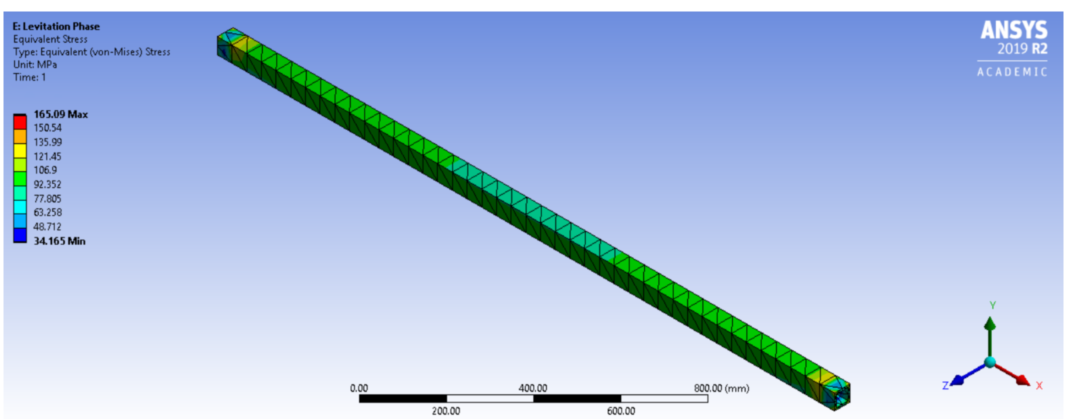

Figure 22. LCM stress during Pod levitation.

4.2.1.1.4 Loading Case IV (Braking Phase)

When the Pod's braking sequence is initiated, the first major event that would occur is the deployment of the braking system. To take advantage of the onboard systems, additional braking power could be generated by reversing the polarity of the LIM. By doing so, the LIM would generate thrust in the opposite direction to motion, slowing the Pod down drastically. The final method of obtaining more braking power is through the deployment of the MagLev system. This would result in generation of MagDrag where even more braking power can be extracted from the system.

Table 16. LCM loading case for braking phase.

LCM Loading Parameters	Value
Braking System (Per System)	*74 N*
MagLev System (Per System)	*687 N*
LIM, Batteries & GNC Systems	*403 N*
Vehicle Stability Module (Per System)	*687 N*
Braking Lock-Up Force (Per System)	*1374 N*

For the load case highlighted in Table 16, a maximum deformation of 0.55 mm was obtained as show in Figure 23. While its stress was found to be approximately 165.71 MPa as illustrated in Figure 24.

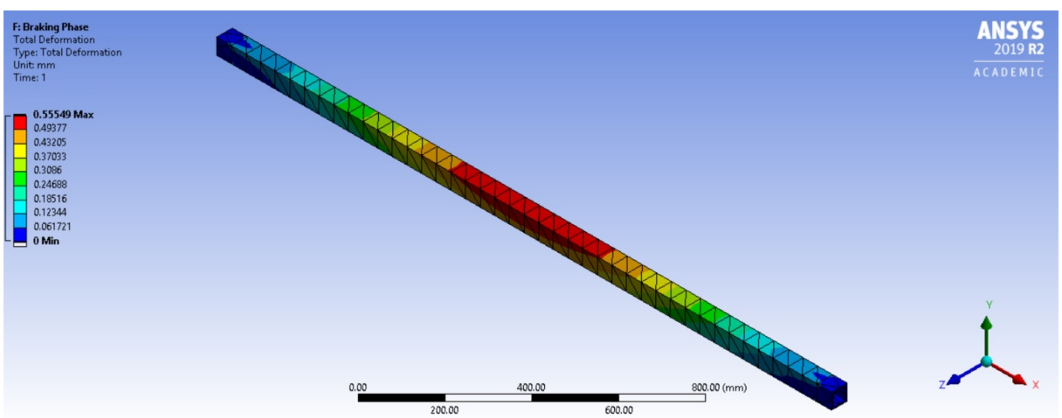

Figure 23. LCM Deformation During The Pod's Braking Phase.

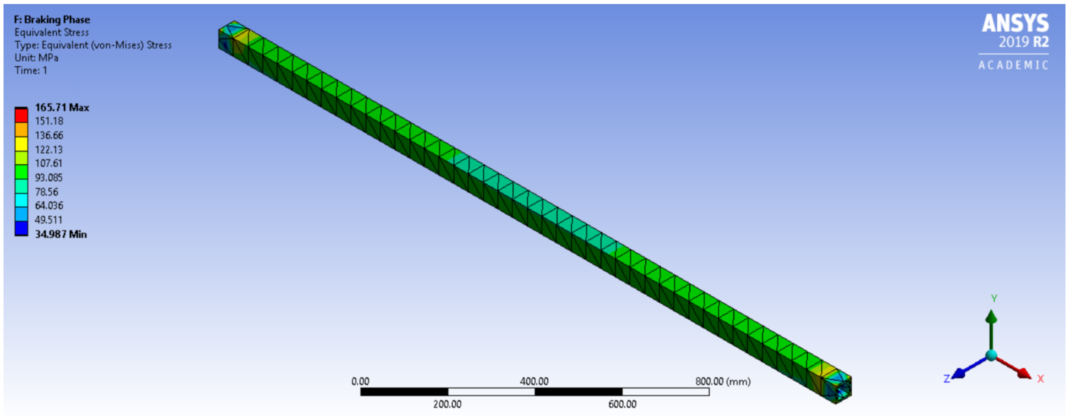

Figure 24. LCM Stress For The Pod's Braking Phase.

4.2.2 Pod Bulkhead

The bulkheads are a critical feature of the Pod's design. Being highly integrated within the Pod, they are used to transfer concentrated loads to the remainder of the Pod's structure [18]. In addition to the transfer of loads, they also provide support to the LCMs. The design of the bulkheads revolved around ensuring the Pod's structural rigidity was increased, and to ensure critical dimensions would be maintained during the Pod's braking phase.

The first step in the design of the bulkhead was to obtain the loads that acted on it. With the Pod being symmetrical about the vertical centerline, it resulted in a symmetrical load application as well. The Pod's bending stresses, and shear flow were obtained by the flexure formula.

$$\sigma = \frac{My}{I} \tag{5}$$

where the σ is the bending stresses undergone by the Pod due to a moment M located at a y distance from the neutral axis. Where the area moment of inertia for the component being analyzed was represented by I.

$$q = \frac{V_\infty}{I} \int y dA \tag{6}$$

where the shear flow for the bulkhead is denoted by q, V_∞ is the shear force, I is the area moment of inertia located at a y distance from the neutral axis, and dA is an infinitesimally small area under examination.

With the LCMs being manufactured out of Aluminum, the bulkhead material was also chosen to be Aluminum 6061-T6 with its material specification being tabulated in Table 17 [17]. This was done as the forward, and rear bulkheads needed connected to the LCMs to form one superstructure.

Table 17. Aluminum 6061-T6 material specification for the bulkhead.

Parameter	Value
Material	*Aluminum*
Specification	*6061*
Hardening	*T6*
Density	*2700 kg/m³*
Modulus of Elasticity	*68.9 GPa*
Poissons Ratio	*0.33*
Ultimate Tensile Strength	*310 MPa*
Yield Tensile Strength	*276 MPa*

Following the design principles used in the aerospace industry for aircraft wings, the bulkhead design utilized a rib-frame method. This was done to reduce the torsion that was generated as the braking system was engaged. In order to optimize the design while dealing with the stress, initially the bulkheads were made without any cutouts. Using an iterative design approach, the design was optimized to include cutouts where excess material was not required in order to cut down on weight as shown in Figure 25 and Table 18.

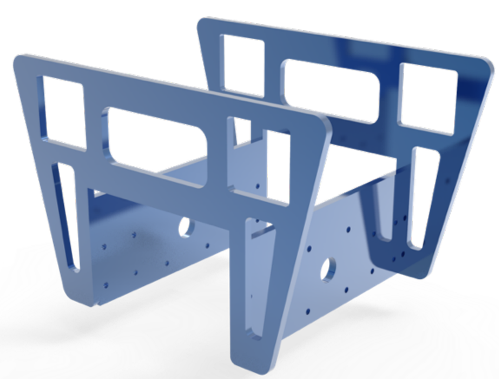

Figure 25. Pod's bulkhead manufactured using anodized blue Aluminum 6061-T6.

Table 18. Dimensional specifications for the Pod Bulkhead.

Bulkhead Parameter	Value
Length	*17.27 cm*
Width	*25.11 cm*
Height	*18.16 cm*

4.2.2.1 Bulkhead Analysis

Analysis on the bulkhead was performed for its worst case scenario which would occur during the Pod's braking phase where the two pneumatic pistons were expected to apply a braking force of 1,957 N. Therefore, the bulkhead design was validated to withstand this load application.

Under the aforementioned load condition, a maximum deformation of 1.01 mm was to be expected as illustrated in Figure 26. In addition, this deformation occurred in the region where the two pneumatic pistons would be affixed to it. This occurs as a reactionary force is transmitted to the bulkhead during the braking sequence application. Additionally, maximum stress of 193.69 MPa was observed in the Aluminum 6061-T6 bulkhead as shown in Figure 27. This was well below the yield and shear strengths.

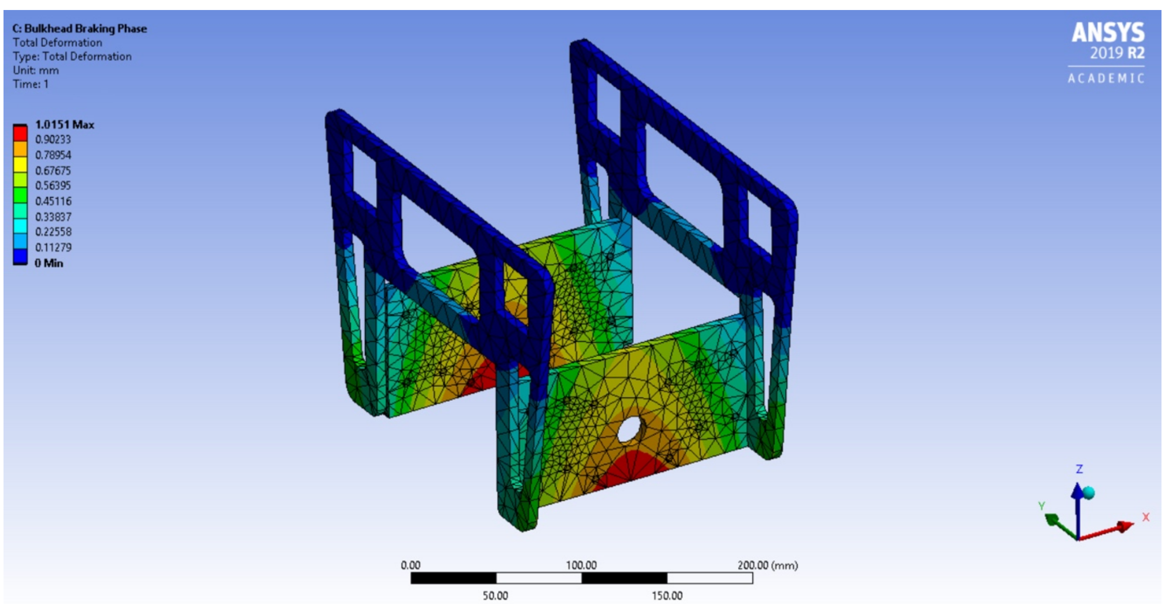

Figure 26. Pod bulkhead's deformation during Pod braking.

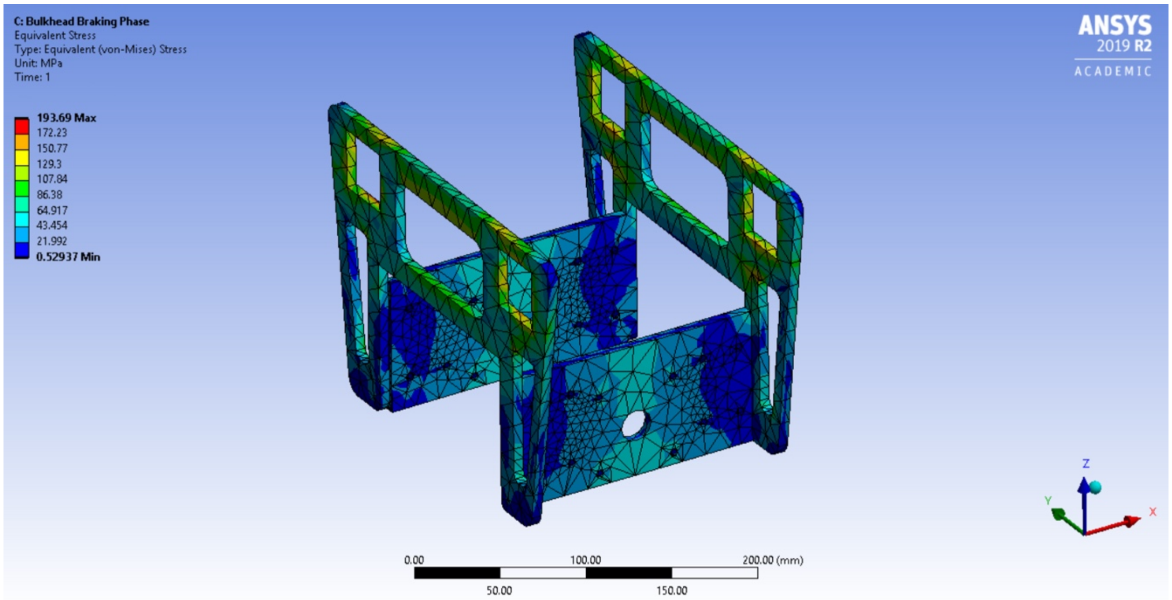

Figure 27. Pod bulkhead's stresses during Pod braking.

4.2.3 Pod Chassis

The forward and rear bulkhead connected the two LCMs together to create the Pod's chassis as illustrated in Figure 28. The LCM ran from one bulkhead to the other. As mentioned before, based on the application of the bulkheads and the LCMs within the Pod, both were selected to be manufactured out of Aluminum 6061-T6. It was done primarily due to its density, ultimate and yield strength, stiffness, temperature limits, producibility, repairability, cost, and availability.

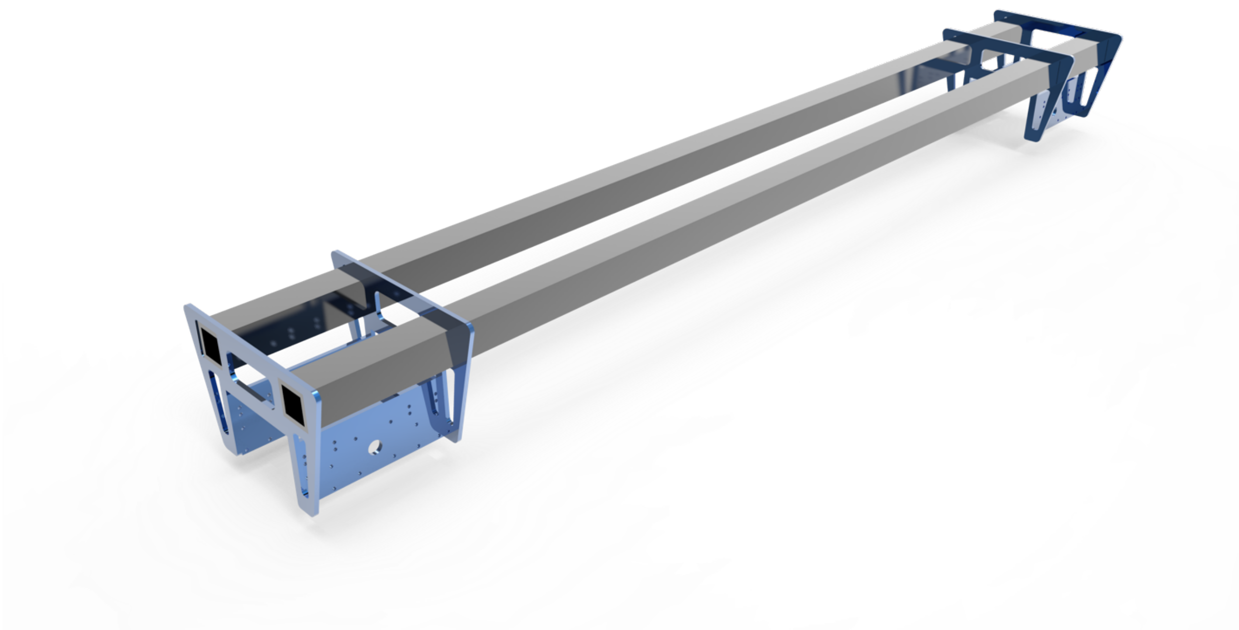

Figure 28. Assembled Hyperloop Pod chassis with the LCMs and bulkheads.

The Pod's chassis is subjected to a repeated cyclic loading, and the structure is expected to experience fatigue stress. Although this may be the case, the formation and propagation of cracks has been unaccounted for due to the low cycle count of this particular structure. For the Pod, one cyclic load is when the environment goes from ambient pressure to near vacuum, and back to ambient pressure [19]. The final Pod chassis conducting the run will have approximately ten cycles on it as outlined in the table below.

Table 19. Total cycle count for the Pod's chassis.

Cycle	Number of Cycles
Post Manufacturing Check	*2*
Test Vacuum Certification	*2*
Final Vacuum Certification	*2*
Hyperloop Tube Test	*3*
Hyperloop Tube Run	*1*

4.2.3.1 Chassis Analysis

Analysis was performed for this superstructure using the loadings that would be seen during the Pod's worst case scenario, being the braking phase. As buckling of the Pod chassis was a concern, it was analyzed through the assumption that this would occur in the event a braking system was inoperable while the other system applied maximum braking force cause one end of the Pod to lock up. This was done in addition to all the system loads being applied to it as tabulated within Table 20.

Table 20. Pod chassis loading during single operating braking system.

Chassis Loading Parameters	Value
Braking System (Per System)	*74 N*
MagLev System (Per System)	*687 N*
LIM, Batteries & GNC Systems	*403 N*
Vehicle Stability Module (Per System)	*687 N*
Braking Lock-Up Force (Per System)	*1374 N*

Under the aforementioned worst case loading scenario where only one braking system functioned, a total of 14.162 mm of deformation was to be expected from the free end as shown in Figure 29. Although the chassis does not fail, this linear deformation could result in the other Pod systems to fail prematurely. With one braking system still operational, it would apply maximum force on the face of bulkhead that resulted in a stress value of 354.03 MPa as illustrated in Figure 30.

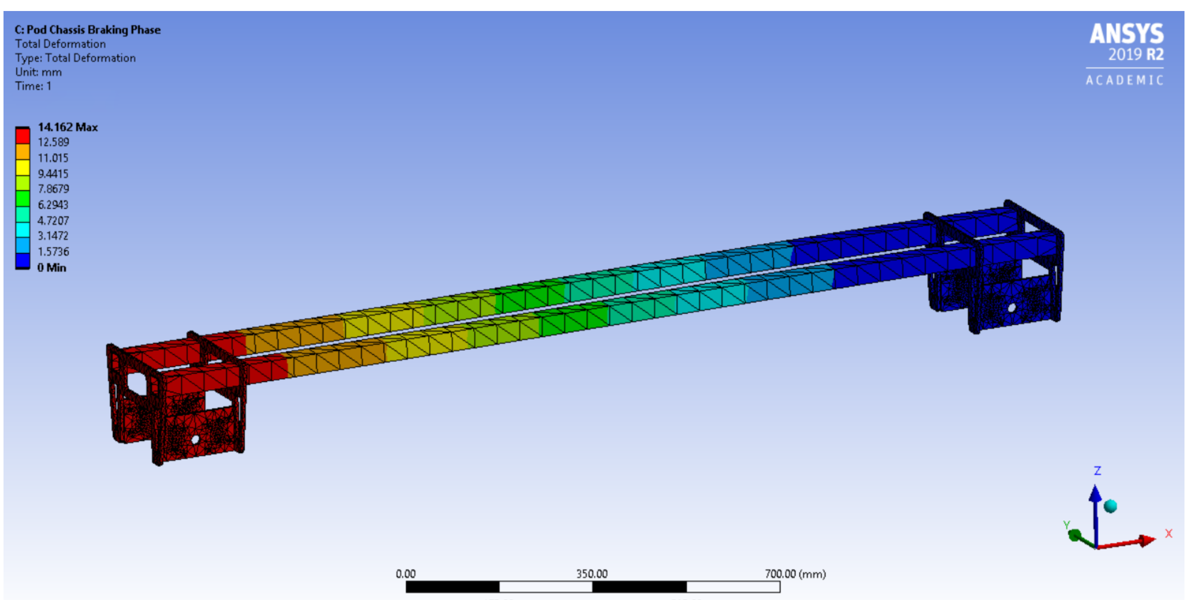

Figure 29. Pod chassis deformation with one inoperable braking system.

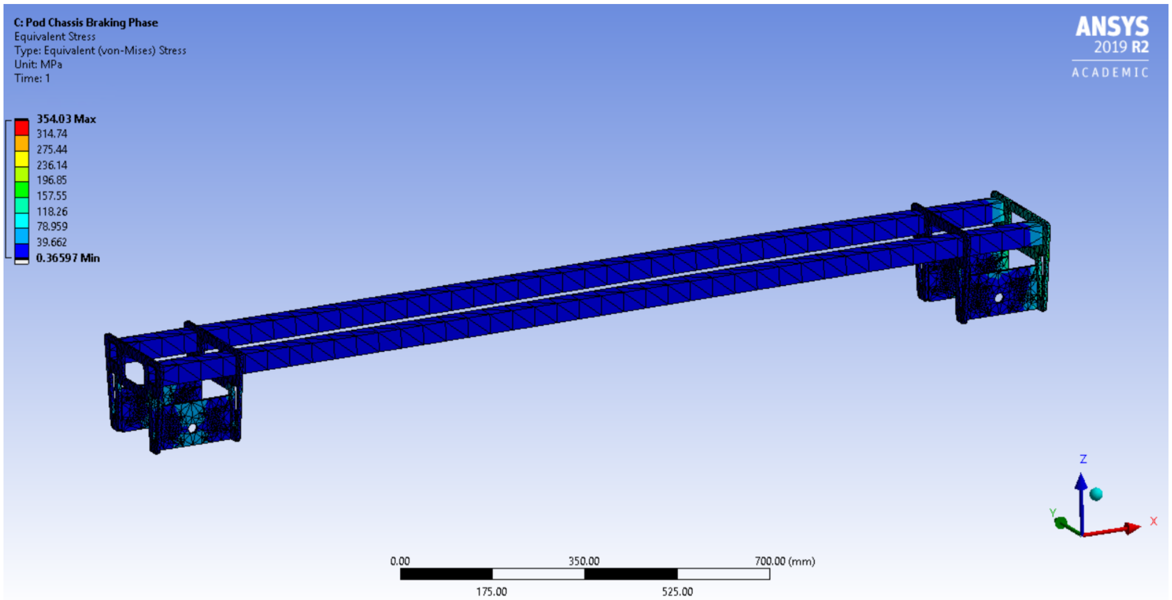

Figure 30. Pod chassis stress with one inoperable braking system.

4.2.4 Pod Shell

Operating in a low pressure or a near vacuum environment, a Pod shell is not a must have component. Although this may be the case, a shell was still designed for the Pod. In order to optimize speed and performance, the Pod's frontal area was minimized, and a streamlined shell was designed to reduce drag. In addition, the shell was designed to ensure whatever air that remained within the tube continuously flowed around the Pod. This was done to ensure the Kantrowitz limit was not reached during the high speed run [20].

As the Pod's speed is further increased, not all of the air can flow around the Pod resulting in it being stagnated at the front. This stems when the tube walls are too close to the Pod's shell resulting in a syringe effect forcing the Pod to push this entire column of air built up in front of it [21]. The drag force originating from the pressure differential in front of and behind the Pod increases exponentially, and independently of the Hyperloop tube pressure. This following equation has been modified for the Hyperloop concept [22].

$$\frac{A_{Bypass}}{A_{Tube}} = \left[\frac{\gamma-1}{\gamma+1}\right]^{\frac{1}{2}} \left[\frac{2\gamma}{\gamma+1}\right]^{\frac{1}{\gamma-1}} \left[1+\frac{2}{\gamma-1}\frac{1}{M^2}\right]^{\frac{1}{2}} \left[1-\frac{\gamma-1}{2\gamma}\frac{1}{M^2}\right]^{\frac{1}{\gamma-1}} \tag{7}$$

Where A_{Bypass} is the cross-sectional area free of the Pod, and A_{Tube} is the total inner cross-sectional area of the Hyperloop tube. The isentropic expansion coefficient is given by γ, and M denotes the Mach number of the Pod.

To better understand this coupling, we can assume that if the air around the Pod is moving at a relative Mach number, M_{Pod}. As the air moves, it needed to squeeze from the larger cross-sectional area of the tube to the smaller available area around the Pod, A_{Bypass}. Based on the isentropic flow equations, the relationship between the M_{Pod} and M_{Bypass} can be further simplified using the aforementioned area equation.

$$\frac{A_{Bypass}}{A_{Tube}} = \frac{M_{Pod}}{M_{Bypass}} \left(\frac{1 + \frac{\gamma - 1}{2} {M_{Bypass}}^2}{1 + \frac{\gamma - 1}{2} {M_{Pod}}^2} \right)^{\frac{\gamma+1}{2(1-\gamma)}} \tag{8}$$

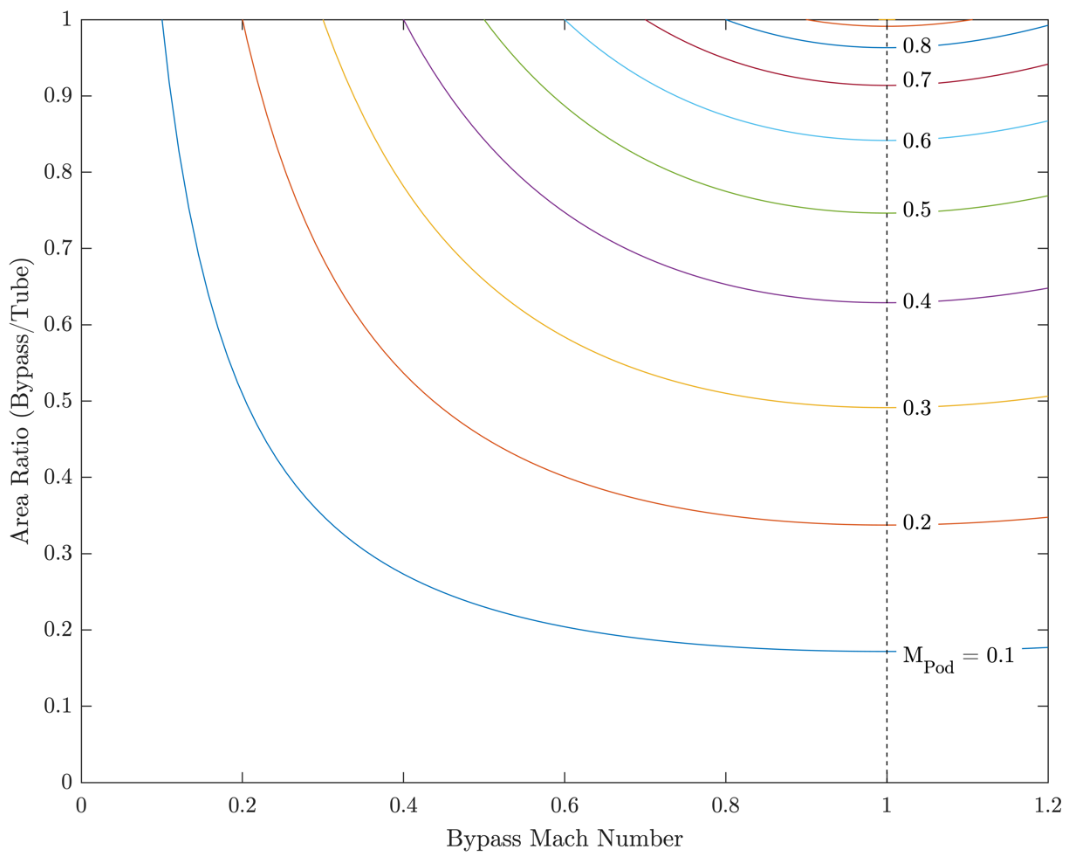

Figure 31. Area ratio vs bypass Mach number plot for varying Mach numbers.

Figure 31 shows the family of curves for a ranging M_{Pod} and M_{Bypass}. For all the values of M_{Pod}, the minimum required area ratio occurs at a M_{Bypass} of one. In other words, as this value equates to one it would result in the smallest possible value for the A_{Bypass} or A_{Tube} when the M_{Pod} and A_{Pod} are known. If the area of the tube is smaller than its minimum value, it would result in the mass flow rate to not flow freely around the Pod.

As the Pod reaches transonic speeds, the small volume of air present within the tube will begin to choke. There are certain sections around the Pod where the flow will be sonic. This so called sonic condition is known as the Kantrowitz limit where the mass flow rate around the Pod has reached it maximum value. In addition to the Pod's velocity, there is a minimum tube to Pod area ratio below which the flow will also be choked. As illustrated in Figure 31, if the Pod were required to travel faster, a larger A_{Bypass} was needed and must be relative to the tube's area. For an M_{Pod} of one, the area ratio almost equals one forcing the A_{Pod} to be almost zero [9].

Figure 32. An isometric view of the Pod shell.

In order to optimize speed and performance without the incorporation of a front end compressor, the Pod's frontal area was minimized, and a streamlined shell was designed to reduce aerodynamic drag. In addition, the shell was designed to ensure whatever air is remaining within the tube continuously flows around the Pod without reaching the Kantrowitz limit.

The completion of Finite Element Method (FEM) and Computational Fluid Dynamic (CFD) resulted the design shell as shown in Figure 32. To maintain a minimal cross-sectional area, the design incorporated a dog bone shape as illustrated in Figure 33. This was also done to ensure sufficient mass flow during the high speed run. A carbon composite laminate shell using a resin and hardener combination was selected to produce a lightweight component while enclosing all the Pod's systems.

4.2.4.1 Shell Analysis

The shell is a carbon fiber laminate with a Soric core. The laminate was designed to be quasi-isotropic with the following laminate, where *S* describes the Soric core: $[\,[\,90\ 45\ 90\,]_s\ S\,[\,90\ 45\ 90\,]\,]$. For the laminate, HexTow AS4C 3K carbon fiber was used as it was a continuous, high strength, and high strain material. This laminate was surface treated by the supplier to improve the its handling characteristics, structural and mechanical properties as tabulated in Table 21 [23].

Table 21. HexTow AS4C 3K material specification for the Pod shell.

Parameter	Value
Manufacturer	*Hexcel Corporation*
Specification	*HexTow AS4C 3K*
Filament Count Tows	*3,000*
Tow Cross-Sectional Area	*0.11 mm^2*
Filament Diameter	*6.9 microns*
Carbon Percentage	*94.0%*
Density	*1780 kg/m^3*
Modulus of Elasticity	*231 GPa*
Tensile Strength	*4.723 GPa*
Yield Strength	*5.00 m/g*
Strain	*1.8%*

To account for the thermal heating of the shell, the composite shell utilized Aeropoxy's PR2032 and PH3665. This particular resin-hardener combination provided a curing time of approximately two hours while being rated to a temperature of 93°C. This provided ample amount of working time while ensuring the shell can withstand the California heat, and the heat generated by the systems during a full power run. The Aeropoxy's material specifications have been tabulated in Table 22 [24]. In addition, the shell will be locked onto the chassis using internal friction fit dowel locking system eliminating the need for drag inducing screws.

Table 22. Aeropoxy PR2032 and PH3665 material specification for the shell.

Parameter	Value
Manufacturer	*Aeropoxy*
Resin	*PR2032*
Hardener	*PH3665*
Density	$1134.94\ kg/m^3$
Tensile Strength	*316.26 MPa*
Modulus of Elasticity	*21.02 GPa*
Pot Life	*2 hours*
Mix Ratio	*100:27*
Rated Temperature	*93* °C

Figure 33. A top down view of the Pod shell.

4.2.5 Pod Braking

The Pod is required to have its own onboard braking system to slow it down as it approaches the end of the Hyperloop tube. Braking can be done in a variety of ways, with frictional braking being performed on the Hyperloop tube, concrete base, the Aluminum sub-track, or the test track itself.

When the BRK system was designed, major consideration was put on ensuring that any surfaces used for braking does not get damaged as a result of it. This was done by selecting a braking material with a lower hardness value than the track. In addition, BRK was designed to wear rather than to exhibit sticking characteristics. Furthermore, analysis and reliability tests were conducted for the Pod's worst case scenarios. For example, having the one of the braking systems to become locked up resulted in the Pod to come an immediate stop. This was done in conjunction with the largest steps and variations in the Hyperloop tube. These considerations ensured the Pod's braking system behaved nominally and would not result in a system failure.

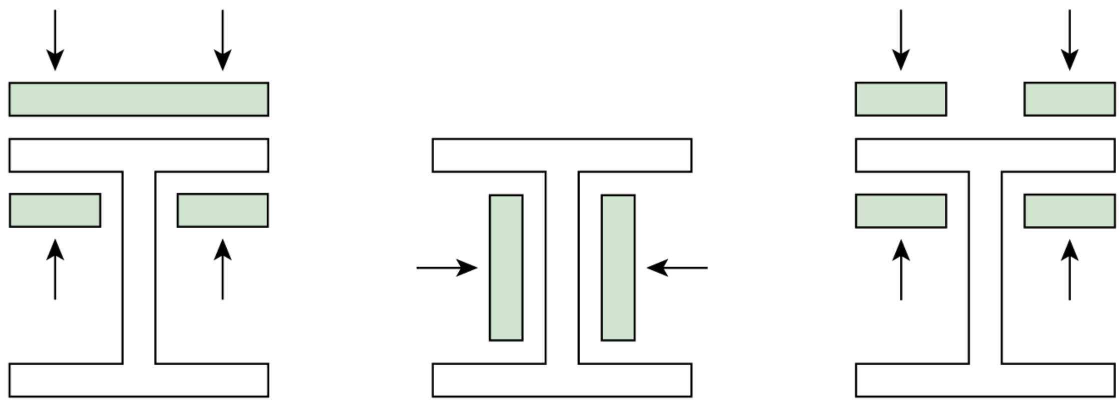

Figure 34. Acceptable Pod braking scenarios on the test track.

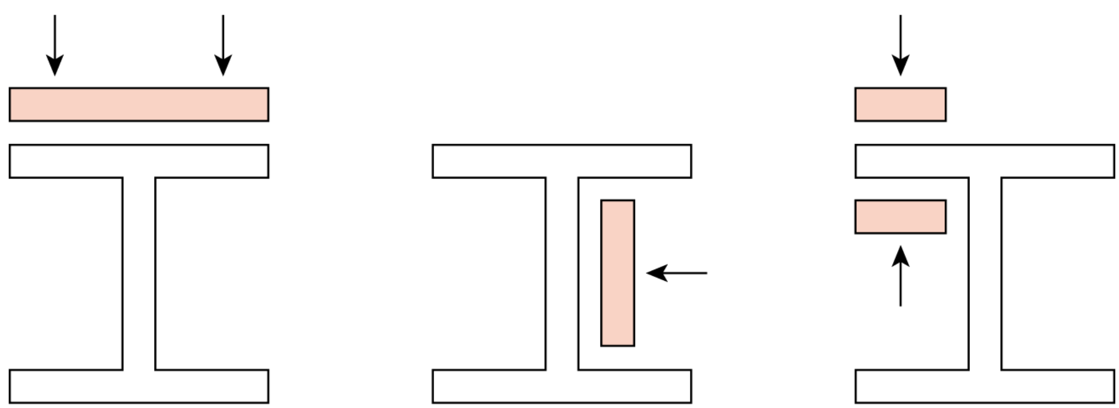

Figure 35. Unacceptable Pod braking scenarios on the test track.

As the Pod utilized the test track to perform its braking operations, it was made to be self-reacting and symmetric about the vertical axis of the track. In other words, the braking operation was made to clamp down on the test track as illustrated in Figure 34, rather than to push on it as shown in Figure 35.

4.2.5.1 Braking Configuration

For effective and high braking performance, the system has been arranged in a forward, and aft configuration within the Hyperloop Pod. To ensure braking capabilities during all phases, BRK has two independent systems. Both the braking systems have its own pneumatic pressure vessels, control systems, control valves, and pneumatic tubing as highlighted in Table 23. This is done to prevent cascading failure in the event a system failure was to occur.

Table 23. Pod braking system component list.

Braking System Parameters	Quantity
Number of Independent Systems	*2*
Pneumatic Braking Pistons	*4*
Pressure Vessels	*2*
Pressure Regulators	*2*
Shut-Off Valves	*3*
Directional Control Valves (DCV)	*2*
Electronic Control Unit (ECU)	*GNC*
Power Source	*Pod Batteries*

The four pneumatic braking pistons placed on either side of the Pod have been designed to utilize the web of the test track during braking operations. To ensure the CG was located at its optimal point, all of the BRK components are placed on the top of the test track except for the pneumatic pistons.

For high performance braking, the pneumatic braking pistons supply a total of 1,957 N of braking power when a 10 bar internal supply pressure was maintained as shown in Table 25. Furthermore, as the Pod was expected to perform a number of braking cycles as highlighted in Table 24, a closed loop double acting piston was used. Such a piston allows for the extension and retraction without venting internal pressure during the various phases of the Pod as shown in Figure 36 [25].

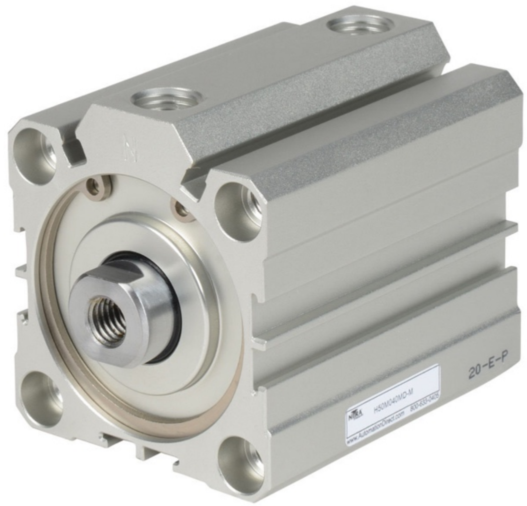

Figure 36. Double acting pneumatic braking piston for the braking system [25].

Table 24. Braking cycle count for pre and post Hyperloop run.

Braking Cycle	Cycle Count
Pre-Tube Brake Check	*2*
Test Track Brake Check	*1*
Airlock Closure Brake Check	*1*
Low Pressure Brake Check	*2*
Pre-Launch Brake Check	*2*
Pod Braking Phase	*1*
Pre-Crawl Braking Check	*1*
Crawl Braking Phase	*1*

This piston was chosen for its performance when compared with to mass. To ensure acceptable results, the worst case scenario was once again analyzed, where one braking system was considered to be inoperable. With the expected output force over the span of the braking time, enough braking force was generated to bring the Pod to a safe halt with a Factor of Safety (FoS) of two.

Table 25. Pneumatic braking piston specifications.

Braking Piston	Value
Bore Size	*50 mm*
Stroke Size	*40 mm*
Mass	*0.73 kg*
Maximum Braking Force	*1957 N*
Minimum Supply Pressure	*10 Bar*
Tank Supply Pressure	*17.2 Bar*

To ensure safe operation of the braking system during any phase of the run, a minimum of 10 bar was required to be maintained within the system. Furthermore, to account for any leaks that that may occur as a of the system being manufactured in house, a pressure vessel capable of safely being pressurized up to 17.2 bar was selected. This was done through the usage of a High Pressure Air (HPA) carbon composite pressure vessel. In addition to being lightweight, and compact, the carbon fiber tanks have been certified by the Department of Transportation (DOT), and Transport Canada (TC) as illustrated in Figure 37 [26].

Figure 37. Carbon composite HPA pressure vessel for the braking system [26].

The selected pressure vessel has a volume of 0.0438 cm^2 which is capable of supplying enough to the BRK system with a sizable Safety Factor (SF). For the Pod, it was pressurized to 17.2 bar. The inclusion of a four way, two position Directional Control Valve (DCV) within the system allowed for one supply pressure vessel to control two pistons simultaneously. With an electric switch, the DCV was supplied with 24 V that switched the position of the solenoid valve that directed the airflow allow for the piston to extend or retract the brakes [27].

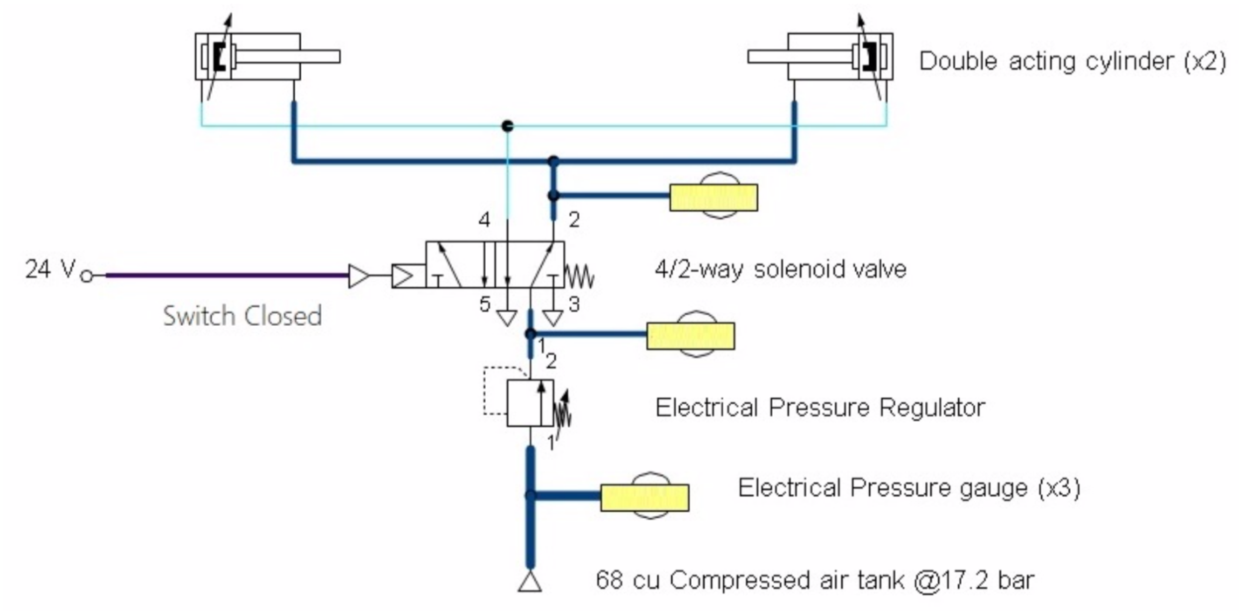

Figure 38. Retracted pneumatic braking schematic for one piston set.

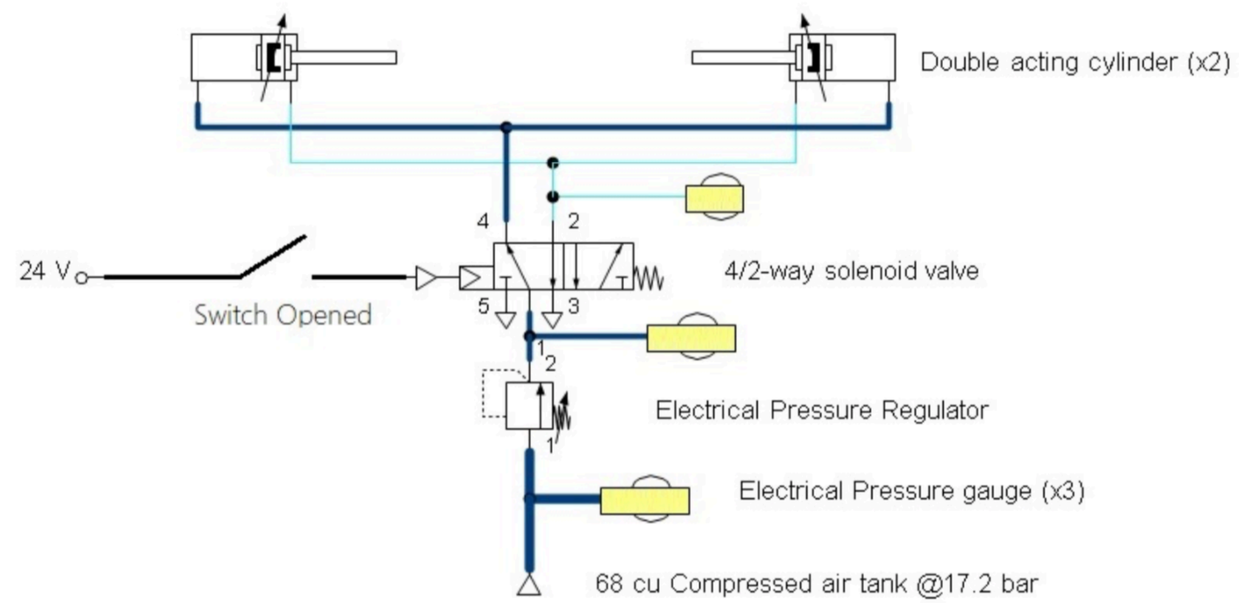

Figure 39. Extended pneumatic braking schematic for one piston set.

As the forward and aft braking systems were identical, Figure 38 was the schematic for a single pneumatic braking system. For the safety of the Pod, the Hyperloop tube, and all the involved personnel, the BRK system was designed with its default position being open.

Figure 40. Directional control valve with two solenoid valve coils [27].

In the event of a power loss to any critical system, the braking system has been designed to automatically deploy as its design feature as illustrated in Figure 39. This ensured the Pod always comes to a safe halt. This was made possible as this particular DVC has a fast response time which dramatically reduced the amount of coasting time between when the polarity is reversed of MagDrive, and to when the brakes kick-in. However, during nominal system operations the power requirements for some of the BRK components such as the Electronic Pressure Regulator (EPR) and Electronic Pressure Gauge (EPG) have been outlined in Table 26.

Table 26. Power requirements for a few braking components.

Power Requirements	Value
DCV Voltage	*24 V*
DCV Current	*0.3 A*
DCV Power	*6.9 W*
EPR Voltage	*24 V*
EPR Current	*0.18 A*
EPR Power	*4.32 W*
EPG Voltage	*24 V*
EPG Current	*0.0002 mA*
EPG Power	*0.48 W*

4.2.5.2 Braking Analysis

The Hyperloop Pod's braking system was designed to decelerate it from its maximum speed at the furthest possible braking engagement distance. This in combination with the assumption that only one BRK system was operating ensured that the shortest allowable braking distance was used. In order to compute the basic braking parameters, the following equation was used.

$$v^2 = u^2 + 2as \tag{9}$$

where v, and u is the initial and final velocities of the Pod, a is the Pod's acceleration or deceleration over the time period under consideration, and s denotes the distance being covered by the Pod under this particular time period. The aforementioned equation can be further simplified as the Pod was required to come to a safe halt, i.e. the final velocity needed to be zero.

$$a = \frac{-v^2}{2s} \tag{10}$$

During the worst case scenario, the assumption made that only one braking system works nominally. Under this assumption, the braking force that needed to be applied by the piston to bring the Pod to a safe halt was calculated through the following equation.

$$F_B = m_{Pod}a \tag{11}$$

where F_B in the aforementioned equation is derived from the Newton's Second Law, m_{Pod} and a_{Pod} are the mass and acceleration of the Pod.

$$F_{Brake,Req} = \frac{F_B}{\mu_{k,Track}N_{Pod}} \tag{12}$$

where $F_{Brake,Req}$ is the braking force required to be delivered from the pneumatic piston to safely stop the Pod, F_B is the Newton's Second Law that was calculated from the Pod's mass, and deceleration rate. The coefficient of kinetic friction is denoted by $\mu_{k,Track}$, and N is the normal force generated from the Pod as it decelerated.

$$F_{Brake} = P_{Piston}A_{Piston} \tag{13}$$

where F_{Brake} is the output force supplied by the pneumatic piston, P_{Piston} is the internal pressure acting within the double acting piston and A_{Piston} is its cross-sectional area.

$$F_{Brake} > F_{Brake,Req} \tag{14}$$

To ensure the Pod always has the ability to safely stop, the braking force produced by the pneumatic pistons need to always be greater than the braking force required to stop the Pod. Using this criterion, the Pod was designed to have a SF of two when the brakes are engaged from its maximum possible speed. The nominal and off-nominal Pod braking distances required for it to come to a complete stop have been tabulated in Table 27.

Table 27. Performance specification for nominal and off-nominal braking.

Braking Parameter	Value
Nominal Braking and Optimal Brake Performance	*58.62 m*
Nominal Braking and Lower Brake Performance	*63.77 m*
Off-Nominal Braking and Optimal Brake Performance	*117.24 m*
Off-Nominal Braking and Lower Brake Performance	*127.55 m*

4.3 Pod Propulsion

To effectively develop the Hyperloop Pod's Propulsion (PRP) system, it was broken down into its sub-systems as shown in Figure 41. The Linear Induction Motor (LIM), and the Magnetic Levitation System (MagLev) constituted a large part of the PRP system.

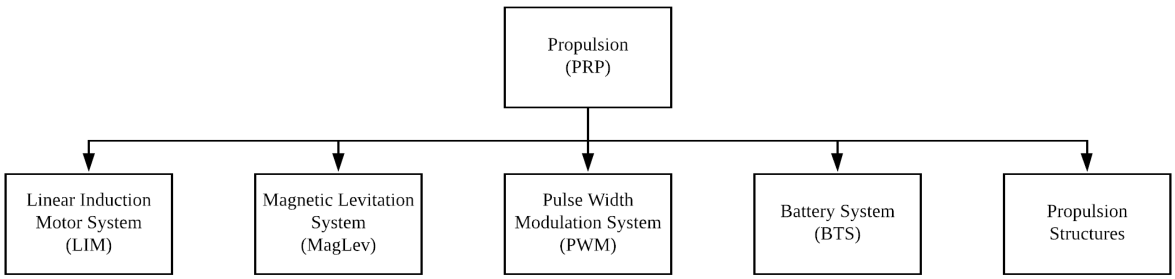

Figure 41. Pod propulsion breakdown.

In addition, as the Linear Induction Motor (LIM) and the Magnetic Levitation (MagLev) systems were the only onboard propulsion systems, it was considered to be the main focus of the PRP. The Pulse Width Modulation (PWM) system, and the batteries were considered to be auxiliary to the LIM and MagLev as they were COTS systems.

4.3.1 Linear Induction Motor

The basis of operation of a LIM is very similar to that of a Rotary Induction Motor (RIM). In a way, when a rotary motor is opened up, and flattened out, a LIM is obtained. This cutting process to form a LIM from a RIM has been illustrated in Figure 42 [28]. This in allows for the production of a linear force instead of a rotary torque that would otherwise be generated from a RIM. Based on the winding pattern, input current and voltage, and the supply input, the generated linear force from the LIM could be varied.

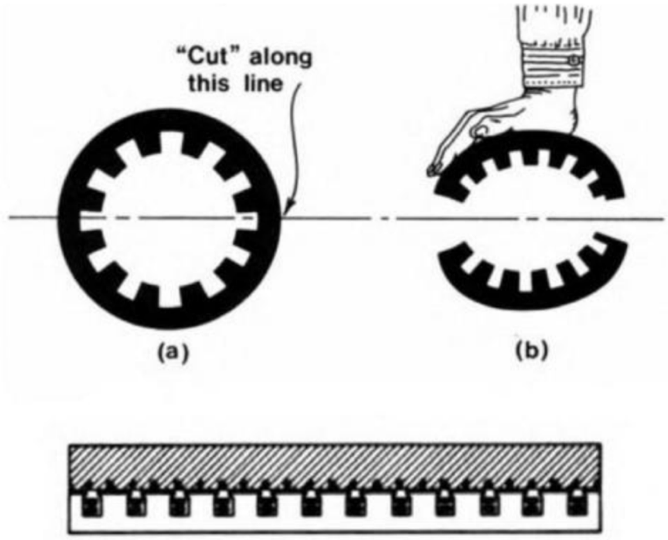

Figure 42. The formation of a LIM from a RIM by I. Boldea [28].

With the absence of mechanical gears, and transmission systems, a LIM results in higher efficiency, higher dynamic performance, and improved overall stability. These advantages in combination with its simple structure and low cost made it an ideal candidate for the Hyperloop [29].

A conventional RIM consists of a stator, and a rotor that form the main basis to produce the rotary torque. The stator consists of windings that are uniformly and sequentially placed within its slots. This configuration generated a sinusoidally distributed magnetic field. However, in the case of a LIM, instead of producing a rotating flux, the windings now created a flux in a linear direction [30].

In order for a voltage to be induced within, there needed to be relative motion between the conductor and the magnetic fields. As a result, this can be computed through the following equation.

$$V_s = 2f\tau \tag{15}$$

where V_s is the LIM's synchronous velocity, f is the input frequency, and τ is the distance between two poles on the circumference of the stator. This parameter is also known as the pole's pitch which can be further defined as follows.

$$\tau = \frac{2\pi R}{P} \tag{16}$$

where $2\pi R$ represents the circumference of a non-flattened out stator, and P is the number of poles present in the motor. However, with the analysis being conducted for a LIM, the aforementioned equation can be modified as follows.

$$\tau = \frac{L_s}{P} \tag{17}$$

where the $2\pi R$ can be equated to be the length of the LIM's stator core [31].

4.3.1.1 LIM Forces

As the LIM was supplied with power, three main forces that are generated are thrust, lateral and normal forces as illustrated in Figure 43. In the case of the Hyperloop Pod, the thrust acts along the longitudinal axis which is along the direction of the proposed motion. The lateral forces are the undesirable forces that tend to throw the stability of the Pod off axis as these were highly dependent on the stator orientation. While the normal force was perpendicular to the stator itself [28].

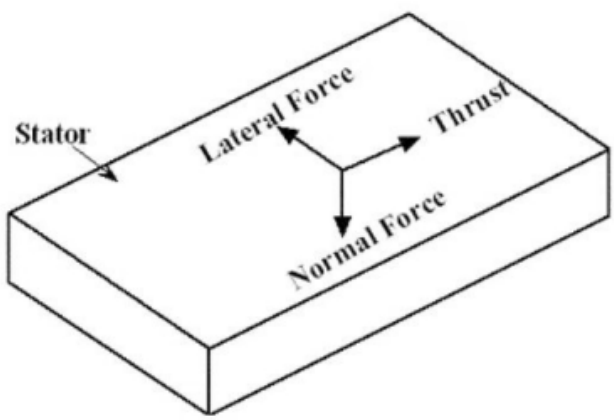

Figure 43. LIM forces adopted from S. P. Bhamidi [32].

4.3.1.1.1 Thrust Force

Under nominal Pod operations, the LIM should develop its thrust force proportional to the square of the supplied voltage. This application tends to reduce slip similar to that of an induction motor with high resistance. This thrust force could be computed through the following equation.

$$F_s = \frac{P_o}{V_c} \tag{18}$$

where F_s is the amount of thrust produced by the LIM, P_o is the output power of the LIM, and V_c is the linear speed of the rotor.

4.3.1.1.2 Lateral Force

The lateral forces generated from the LIM tend to throw off the stability of the Pod. These occur as a result of the asymmetric position of the stator within the LIM. These forces tend to be small in magnitude resulting in a negligible displacement away from the nominal CG configuration. Furthermore, simply through the incorporation of the Vehicle Stability Module (VSM), which were a small set of mechanical wheels meant to help guide the Pod corrected any instability issues that stemmed from this force.

4.3.1.1.3 Normal Forces

The implementation of a single sided LIM within the Pod generated a large normal force due to its asymmetry in topology resulting from a single stator. At the LIM's synchronous speed, the force generated was attractive and got reduced as Pod speed was decreased. In certain cases, especially during high frequency operations, and at certain speeds, this force tends to be repulsive.

However, if the LIM was configured to be double sided, a reaction plate would have been placed between the two stators instead of a single stator. This would result in a normal force to be generated between one stator, and the reaction plate which would ideally be equal and opposite to that of the second stator. This would result in a net force of zero. This would only result when this plate is located asymmetrically between the two stators.

4.3.1.2 LIM Winding Configuration

In order to produce an effective and efficient LIM, its windings were done in a variety of different of configurations. The prominent ones included a single, double, and the triple layer configurations. For the single layer configuration, the number of coils was one half the number of slots available as shown in Figure 44. This resulted in each slot contains only one coil side with such a configuration. With the convenience it provided during the coil assembly, and the need to not have coil-coil insulation that resulted from a single winding layer made it ideal. This configuration is generally used within a single phase motor.

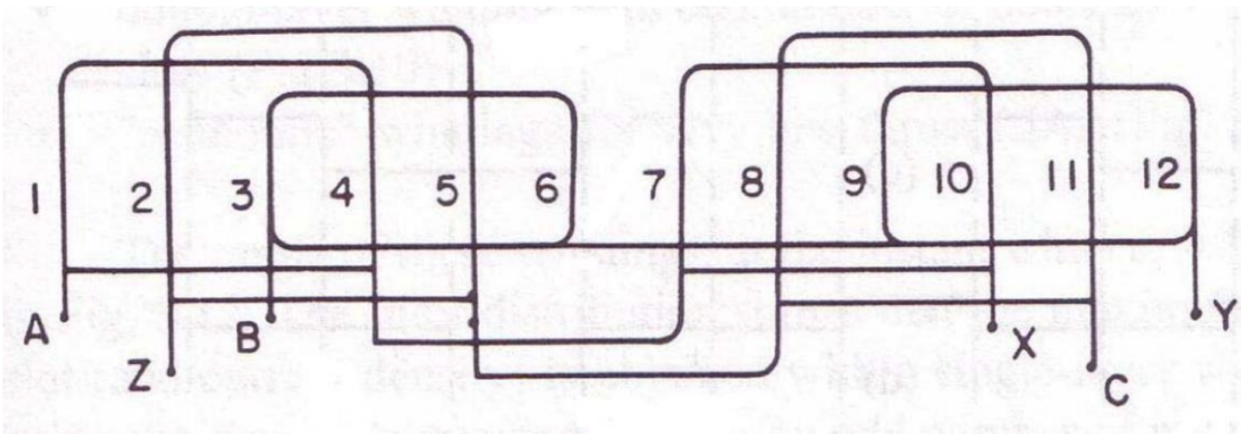

Figure 44. Single layer winding configuration adopted from S. P. Bhamidi [32].

However, most induction motors above a few kilowatts utilize double layer windings. Within this configuration, there were two set of windings of different phases placed within the same slot, except at the end slots as shown in Figure 45. Each coil had two sides to ensures that the windings were placed identically resulting in a balanced arrangement with all the three phases.

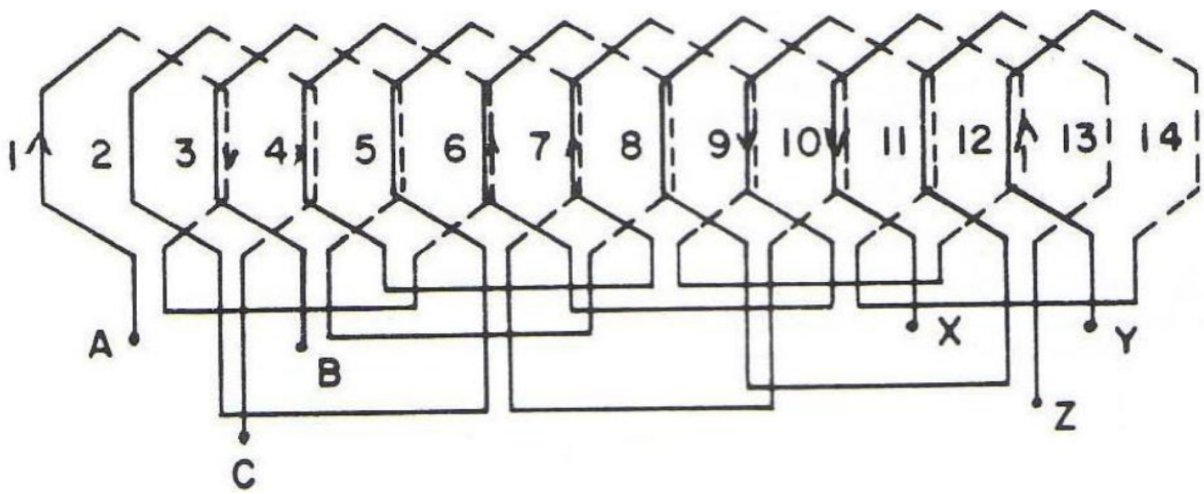

Figure 45. Double layer winding configuration adopted from S. P. Bhamidi [32].

To ensure the same amount of current flowed in each layer, the number of windings and the parallel arrangement depended on the size of each slot. Assuming the permeability of free space (μ_0) was $4\pi \times 10^{-7}$, and the copper's volume resistivity (ρ_r) was 19.27×10^{-9}, the following equation was used.

$$g_e = \frac{2\mu_0 f \tau^2}{\pi \left(\frac{\rho_r}{d}\right) G} \tag{19}$$

where g_e is the effectiveness of the airgap, f is the electrical frequency, ρ_r is the conductor's volume resistivity, d is its diameter, and G is the Goodness factor. The resulting thrust required to be generated by the LIM could be calculated as follows.

$$F_{LIM} = \frac{m{I_1}^2 R_2}{\left[\frac{1}{(SG)^2} + 1\right] V_s S} \tag{20}$$

With overall trajectory of the Pod being dictated by the thrust output from the MagDrive system, i.e. the LIM. In order for the Pod to move at approximately 45 m/s, the power specifications have been outlined in Table 28 while the schematic for the propulsion system is shown in Figure 46.

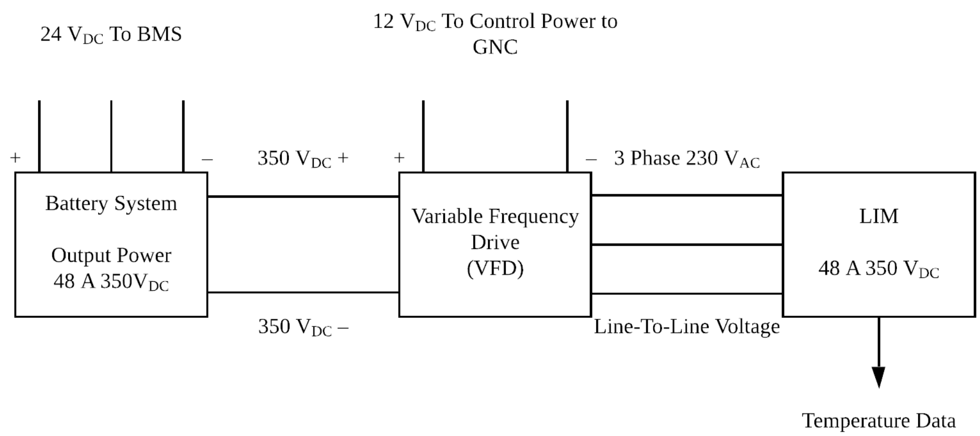

Figure 46. Electrical power schematic for the propulsion system.

Table 28. Basic power breakdown for the Pod.

Parameter	Value
Battery System Current Output To VFD	*48 A*
Battery System Voltage Output To VFD	*350* V_{DC}
Battery System Voltage Output To BMS	*24* V_{DC}
VFD Current Output To LIM	*48 A*
VFD Voltage Output To LIM	*350* V_{DC}
VFD Voltage Output To GNC	*12* V_{DC}

4.3.2 Magnetic Levitation System

To improve the Pod's efficiency and to reduce the contact friction generated from a wheeled system, the Pod utilized a passive Magnetic Levitation (MagLev) system at high speeds as shown in Figure 47. The MagLev system consisted of the MagLev Actuator, and MagSkis. The inclusion of the MagLev Actuator allowed for the MagSkis to move along the normal direction. By doing so, the magnetic levitation force could be precisely controlled to ensure the Pod was maintained at constant height above the test track. Furthermore, through testing and optimization, it was found that the LIM should be maintained at a height of approximately 3 mm above the track to generate the largest amount of thrust while minimizing MagDrag.

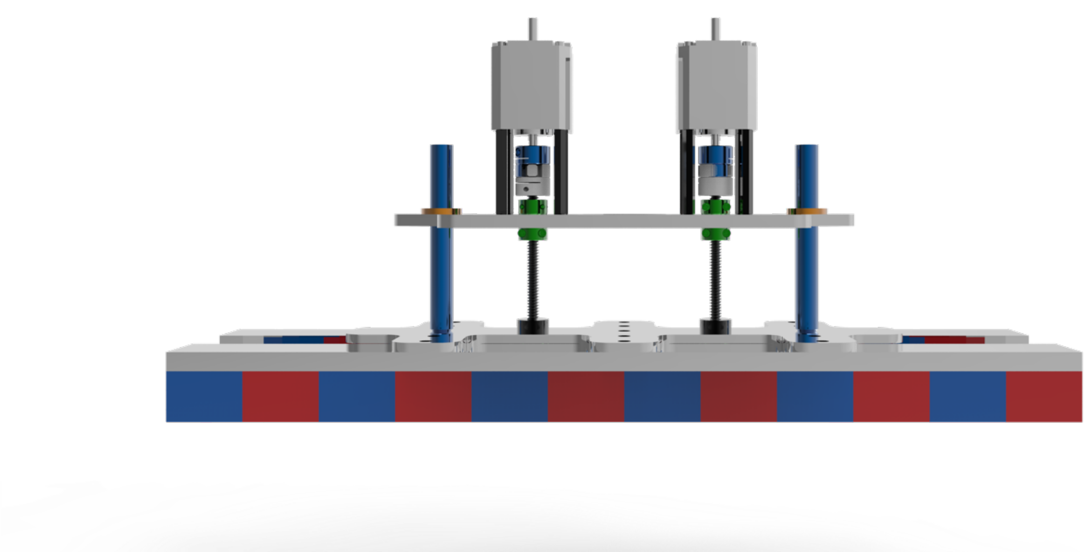

Figure 47. Assembled Hyperloop Pod MagLev system.

To levitate the Pod while maintaining the LIM at the predetermined height, a total of 24 permanent magnets were attached to the steel backing plate. The magnetic force generated from the magnets will induce both a levitating force, and a magnetic drag force (MagDrag). As a result, the magnets and the steel backing plate made up the highest percentage of the total system mass. This was done to ensure the system produced the necessary levitating force. Furthermore, this was done as they were the only components that created, and channeled the magnetic fields within the MagLev system.

Using a coefficient of dynamic friction of 0.15, the torque needed to move the MagLev system up and down was found to be 0.305762 N and 0.091579 N respectively as shown in Table 29. As a result, the total torque required to actuate the mechanical system was low. Therefore, the motor was selected based upon its rated force to effectively actuate the system upwards and downwards. In addition, this was done with a FoS of 1.3 to ensure system reliability at all times.

Table 29. Mechanical load computations on MagLev actuators.

Parameter	Value
Coefficient of Dynamic Friction	*0.15*
System Raise Required Torque	*0.305762 Nm*
System Lower Required Torque	*0.091579 Nm*
Lead Screw Calculation	*1.5875 mm*
Thread Count	*16 Threads/in*
Pitch Diameter	*6.35 mm*
Factor of Safety	*2*

Due to the MagLev generating a levitation force and MagDrag acting on the system, axial, bending, and shear loadings would be induced on the linear guides. As a result, the guides were designed to withstand the forces along these directions.

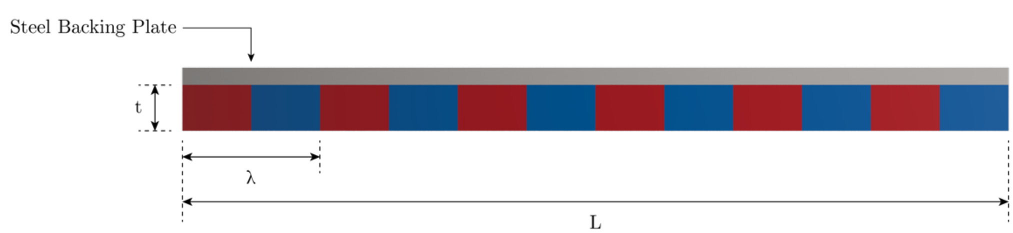

Figure 48. Magnet Dimensional Parameters.

With the goal being to create an optimized MagLev, an appropriate grade of magnet needed to be selected. With a variety of magnetic field strengths being available, analysis showed that grades above N52 experienced a noticeable increase in its demagnetization effects as shown in Figure 49. This graph provided information on its strength and demagnetization properties based on operating temperatures. As a result, a magnet grade of N42 was selected, and its properties have been tabulated in Table 30 [33].

Table 30. Magnet grade specifications for N42 Magnets.

Parameter	Value
Magnet Grade	*N42*
Weight	*0.2766 kg*
Length	*38.1 mm*
Width	*38.1 mm*
Thickness	*25.4 mm*
Rated Pull Force	*688 N*
Maximum Operating Temperature	*80°C*
Br Max	*13,200 Gauss*
B-H Max	*42 MGOe*

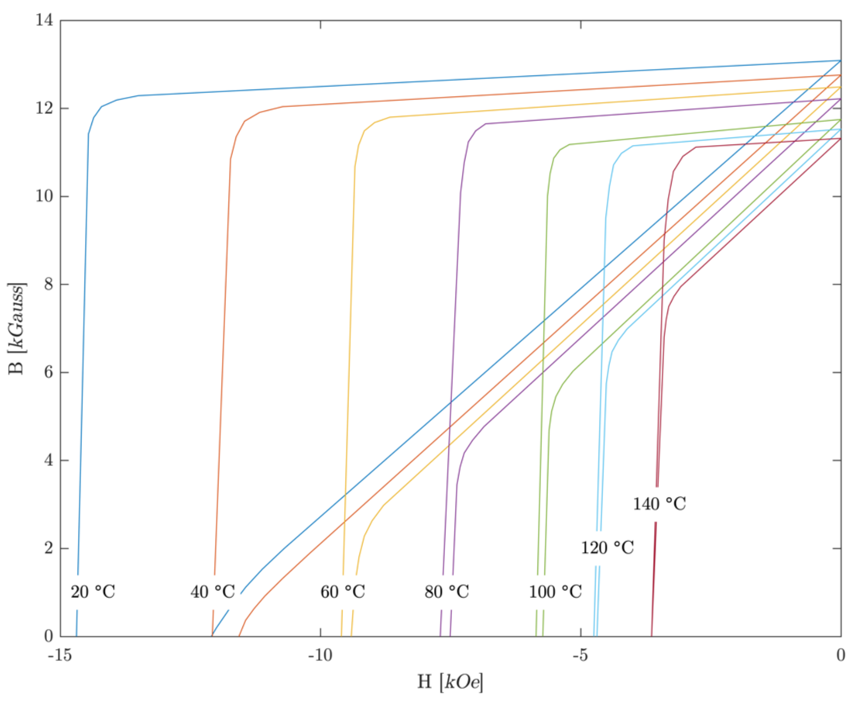

Figure 49. Demagnetization B-H curve for N42 Neodymium magnet [33].

Table 31. Magnet and backing plate specifications for Pod MagSkis.

Parameter	Value
Wavelength (λ)	*76.2 mm*
Length (L)	*457.2 mm*
Width (w)	*38.1 mm*
Magnet Thickness (t_{Mag})	*25.4 mm*
Backing Plate Thickness (t_{plate})	*9.525 mm*
Total Number of Periods	*24*

4.4 Pod Guidance, Navigation and Control

Figure 50 illustrates the Pod's trajectory for the entire duration of the Hyperloop run. As seen from the graph, the run had been classified into four distinct categories – Launch, Levitation, Braking, and Crawling phases. Each of which engaged certain systems. This graph provided an operating envelope for the Pod during nominal and an off-nominal Hyperloop runs.

The plot included two distinct acceleration curves representing the Pod's maximum (2.55 m/s^2), and minimum (1.25 m/s^2) acceleration profiles based on the LIM's expected performance data. Once levitation velocity of 45 m/s is attained, the MagLev system is activated. Whereby, acceleration is expected to decrease by a slight amount due to MagDrag being generated by the MagLev. At the conclusion of the levitation phase, the braking sequence is initiated.

All the profiles including the two acceleration, levitation, and braking phases were computed by equating their slopes to be solved for the distance they intersected at. Knowing that the MagLev system took approximately 0.5 s to extend or retract, the point at which the system began to have an effect on the run was calculated through basic dynamic equation as follows.

$$V_f = V_i + at \tag{21}$$

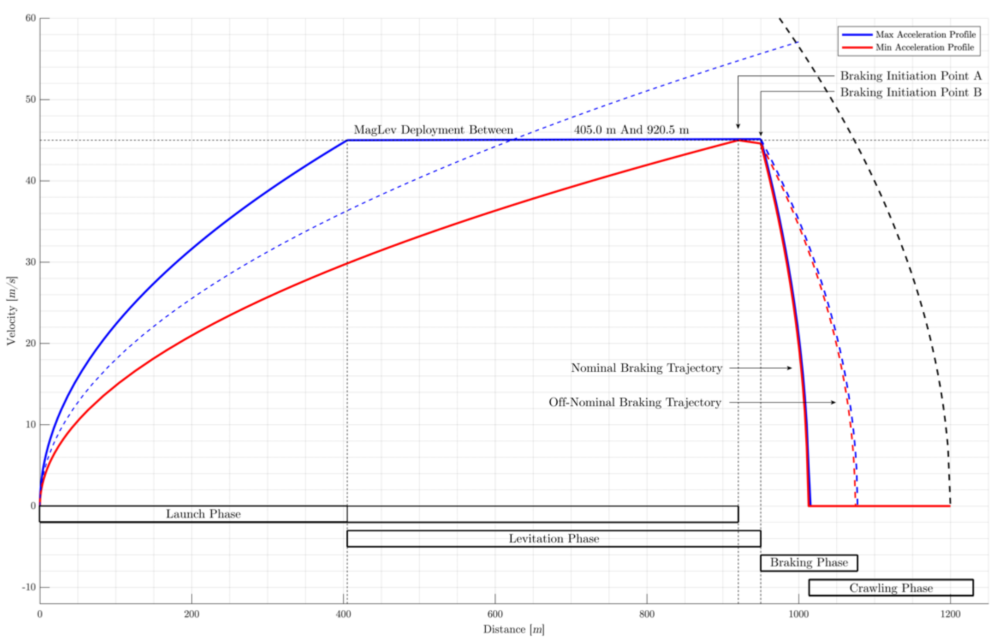

Figure 50. Pod trajectory profile.

In addition to the acceleration and levitation profiles, the Pod's nominal and off-nominal braking scenarios were accounted for. This was done to highlight the effects of braking when one braking system became inoperable. With a delay of about 0.5 s needed for the pneumatic braking lines to be fully pressurized, the braking sequence was made to be activated at the 927 m mark. By doing so, it allowed for Pod to be at full power and to begin braking at full force as it reached the 950 m marker within the Hyperloop tube.

With braking being the most critical phase within the entire run, the activation of its sequence was made to be dynamically computed. This was particularly crucial as testing within the Hyperloop tube had not been conducted before. By doing so, if the Pod experienced higher acceleration and the Pod velocity exceeded its target velocity, the braking sequence would be initiated earlier. This was done to ensure enough braking was available to bring the Pod to a safe halt. However, if the Pod performs with a lower acceleration, the braking sequence would be activated at a much later point.

Once the Pod comes to a safe halt and if it underwent nominal operations, the crawling phase could be activated. This would allow it to move forward at a low speed of 1 m/s until the forward range sensor detects the end of the Hyperloop tube approximately 20 m away. With the controllers running at a frequency of 20 Hz, 50 ms per loop, a lag in position of approximately 3 m was to be expected and was accounted for in the telemetry data.

4.4.1 Pod States

As Hyperloop Pods are expected to travel at high speeds, the designed Pod was made to be fully autonomous with a constant stream of data transmitted to the Ground Station (GS). The Pod has a total of seven states that assist it in completing its mission. Once powered up, it automatically defaults to a "Safe To Approach" state. This is done only when the Pod is stationary, in good working condition without any major faults, and is safe for humans to approach it. Upon the completion of the necessary checks within the tube, the Pod then has the capability to go into the remaining states as shown in Table 32.

After receiving necessary approvals from the launch authorities, the Pod is entered into the Ready To Launch state, where final braking checks are performed. The Pod also verifies all temperature readings to be within their operational limits. During this phase, the laser sensor required to measure its location within the tube is verified to be receiving nominal data. Upon the successful completion of all requirements, the Pod is accelerated to its predefined target velocity of 45 m/s. As levitation speed is attained, the MagLev system is deployed whereby, the Pod is lifted off its wheels greatly reducing drag, and improving its linear acceleration.

To ensure safety of Hyperloop tube, the Pod, and all the personnel involved, regardless of the MagLev functionality, the Pod is entered into the braking state 0.5 s before reaching the 950 m mark. This ensured both the forward, and aft braking system's pressure lines are fully charged and ready to be engaged at the 950 m milestone. For added safety in the event the Pod fails to identity the 950 m navigational marker, a second redundant braking trigger point was built into the system once the final 76 m are remaining. The ensured the Pod automatically deployed its brakes as it arrived at the redundant trigger point.

At any point during the run, if the Pod encounters an anomaly, a critical system failure, system error, or a loss in communication with the GS, the Pod automatically transitioned into the fault state. This transition activates the braking system whereby it is brought to a safe halt no matter the earlier state of the Pod.

Table 32. Pod states controlled by the GNC system.

Pod State	Description
Safe To Approach	Indicated that the Pod is stationary, in good working condition without any major faults, and is safe for humans to approach it.
Ready To Launch	Performed final checks, and readies key systems for launch.
Launch	The Pod is accelerated to the predefined target velocity.
Levitation	During a nominal Pod launch, and upon reaching a predefined velocity, the MagLev system is deployed to achieve levitation.
Braking	Brings the Pod to a safe halt.
Crawl	Moves the Pod at a very low speed using manual control from the GS.
Fault	A non-nominal, unknow or unsafe event or a parameter fell outside its operating envelope was detected, and Pod automatically comes to a stop.

4.4.2 Mission Concept of Operations

Figure 51 provides a detailed overview of the nominal mission concept of operations of the Pod. Within this breakdown, the mission was categorized into three distinct phases — Pre-Launch, Launch, and Post-Launch. Each of these categories consist of various system interactions with real time Pod telemetry being transmitted back to the GS for viewing and analysis.

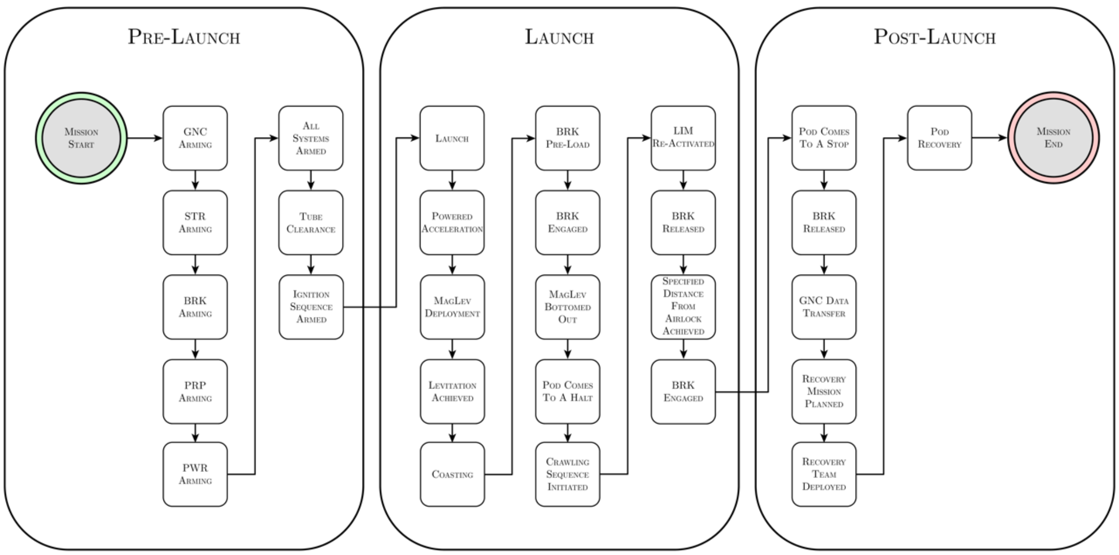

Figure 51. Ryerson International Hyperloop's mission concept of operations.

4.5 Testing Challenge

With the Hyperloop tube being located in Hawthorne, California, the Hyperloop Pod needed to be tested to ensure all its systems met certain standards. This was very critical as the Pod needed to operate within a low pressure environment, using the predefined track specifications at a varying temperature rage.

As a university team, the possibility of travelling to Hawthorne, California more than once a year was out of question mainly due to logistical and economic difficulties. To overcome this, a possible solution that was looked into was to design and build an exact replica of the test track used within the Hyperloop tube. In doing so, testing could be conducted without the need to make multiple trips to Hawthorne. In addition, such a development would open the doors to an iterative design process where even minor modifications in the design could be tested, and validated at a very rapid pace.

In order to replicate the test track, approximately 45 m was needed to have substantial linear length in order to gather meaningful results. As the Pod utilized a LIM and MagLev systems, the test track was required to be manufactured out of a similar material in order to ensure results obtained from the replica track would still be comparable with the test track in Hawthorne, California. The breakdown for such a test track has been tabulated in Table 33.

Table 33. Replica testing and development track specifications.

Parameter	Value
Test Track	*Replica Testing & Development Track*
Material	*Aluminum*
Designation	*5051-T6 / 6061-T6*
Stock Profile	*Flat Plate*
Finished Profile	*I-Beam*
Linear Length	*45 m*
Total Length	*135 m*
Width	*127 mm*
Height	*127 mm*
Thickness	*10.46 mm*
Cost	*CAD$ 84.65 per m*

Being a downtown university, square footage is a sought after, and an expensive commodity. As a result, the possibility of acquiring the necessary square footage to lay down a track along with its accompanying safety measures was next to impossible. Therefore, alternative methods of testing, and validating the systems were looked into.

4.6 Modular Test Rig

With aircraft structures subjected to high level of forces and shocks, ensuring such components passed all the necessary aviation standards is critical step within its design process. [34] The aerospace industry performs a series of quality control tests during the components lifecycle including during its design, manufacturing, and service life.

For example, the landing of an aircraft exposes the landing gear to significantly high forces when compared to all other phases. As a result, aircraft brake dynamometer testing is used to simulate real life operating conditions including take-off, taxi, and landing. During testing, its wheels are accelerated to its landing reference speed (V_{Ref}) [35]. Upon reaching V_{Ref}, the gear is dropped to simulate similar loads experienced by aircraft during a real landing. Such a process allowed for the determination of all the loads accurately while observing its behavior and response. By having rigorous testing and validation standards, today's aircraft structures are designed with sufficient margins to account for any loads it may see throughout its lifespan.

With the aerospace and the landing gear industry using such tools for its tests, an innovative approach was taken to design an in-house Hyperloop systems test rig. The modular test rig that was developed was made to accommodate tests from STR, GNC, and PRP. Furthermore, it allowed for the validation of said systems individually, or while being integrated in combination and in conjunction with each other. Figure 52 showcases the Modular Test Rig (MTR) designed to test and validate the various Hyperloop systems. Internally, this test rig is also referred to as "The Doughnut".

Figure 52. The Hyperloop modular test rig.

Furthermore, the need to lay down the guide rail as outlined in Table 33 was completely eliminated after the MTR was made to rotate about the axis. By doing so, instead of having a 45 m test track, an infinite track was achieved. Through this approach the MTR occupied minimal square footage of approximately 1.4 m^2. Rather than the 93 m^2 that would have otherwise been needed to lay down the 45 m of the required test track.

Observing Figure 52 and going from bottom to top of the MTR, it could be broken down into its support frame, system mounting frame, track, and the motor itself. This breakdown has been illustrated below.

Table 34. Breakdown of the Modular Test Rig.

Component	Purpose
Support Frame	Supported the MTR and allowed for it to be bolted to the ground.
System Mounting Frame	Allowed for the integration of the track to the MTR and provided a modular method to test various Hyperloop systems.
Track	Allowed for the characterization of system behaviors such as STR, GNC, and PRP.
Motor	Provided a means to rotate the track at a specified RPM.

The development and manufacturing of the MTR utilized a similar material to that of the actual Hyperloop test track. This allowed for the characterization of the Hyperloop systems, and ensured similar behavior would be observed had the same tests been conducted in Hawthorne, California. This was critical to generate the necessary test data required to validate the various Hyperloop systems. Furthermore, the performance of MagLev, MagDrive, Eddie Current Braking, and GNC tests were critical as they were highly dependent on the material properties of the track being used.

The material breakdown for the major MTR components have been defined in Table 35. Whereas, Figure 53 highlights the motor's performance. Observing its speed and torque characteristics, continuous operation of the MTR was possible when its operated within the continuous duty region. Whereas, the limited duty region was primarily reserved to aid in the acceleration of the MTR [36].

Table 35. Material selection breakdown for the Modular Test Rig.

Component	Material Selection
Support Frame	*High Strength Steel*
System Mounting Frame	*Aluminum Al 6105-T6*
Track	*Guide Rail Replication*
Motor	*120 W (1/6 HP) Brushless DC Motor*

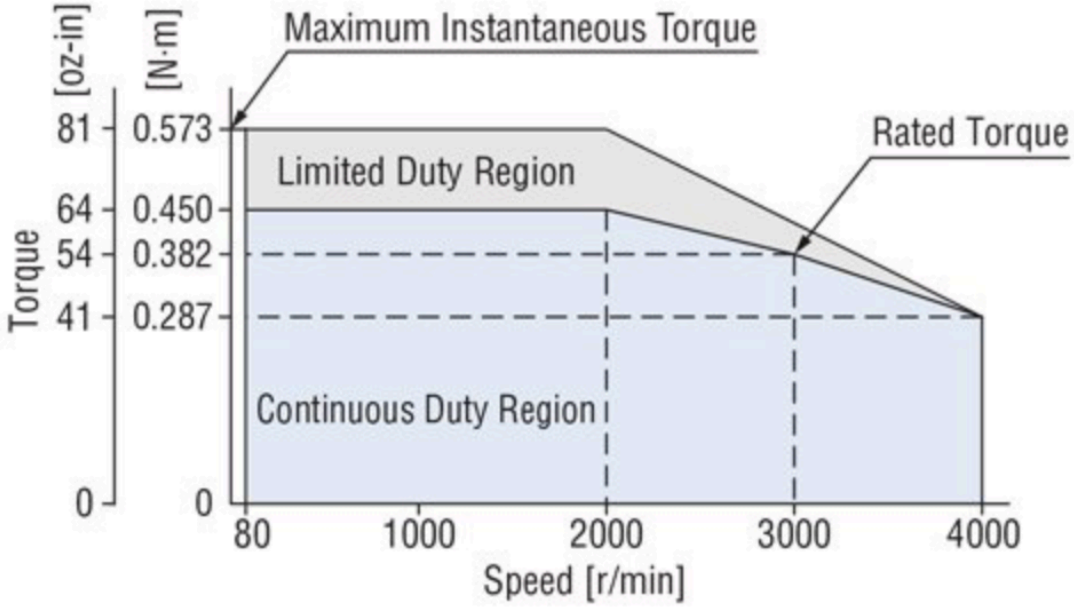

Figure 53. Motor performance plot for the MTR adapted from Oriental Motors [36].

4.6.1 Modular Test Rig Analysis

Before the MTR could be used for the Hyperloop systems tests, the test track and its supporting shaft were analyzed to ensure it met the necessary safety standards. During the analysis, it was subjected two worst case scenarios.

4.6.1.1 Load Case I (MTR Lock-Up)

The first being, the shaft would inadvertently locked-up which in turn would cause the track to experience a lock-up as well causing it to come to an abrupt stop. Under this load condition, the shaft is expected to have a deformation of 0.0925 mm, while it experienced a stress value of 26.615 MPa as shown in Figure 54 and Figure 55 respectively.

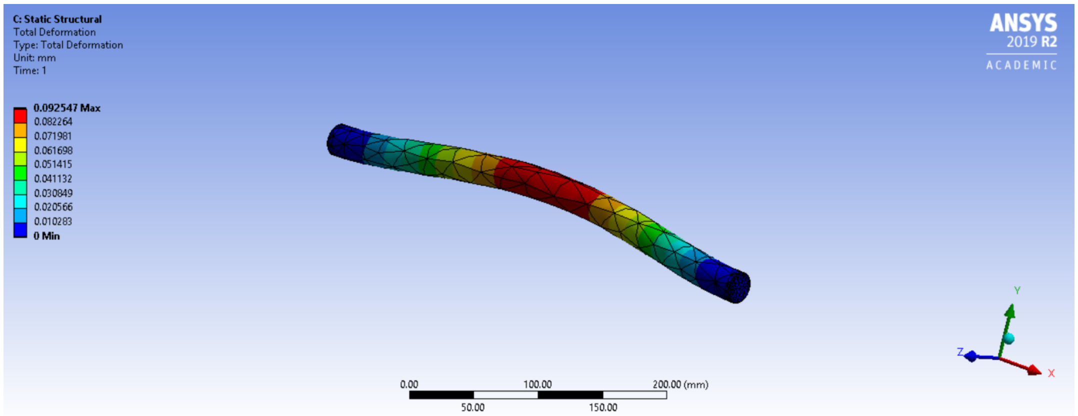

Figure 54. Shaft deformation during MTR lock up.

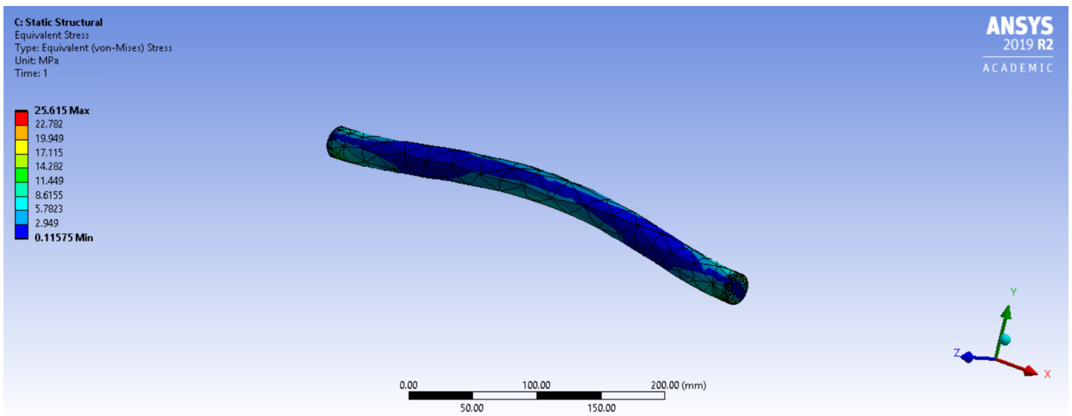

Figure 55. Shaft stresses during MTR lock up.

Meanwhile, under this same loading condition, the track experienced a deformation of 0.00208 mm outwards as illustrated in Figure 56. Whereas Figure 57 displays the track stress that was computed to be 1.978 MPa.

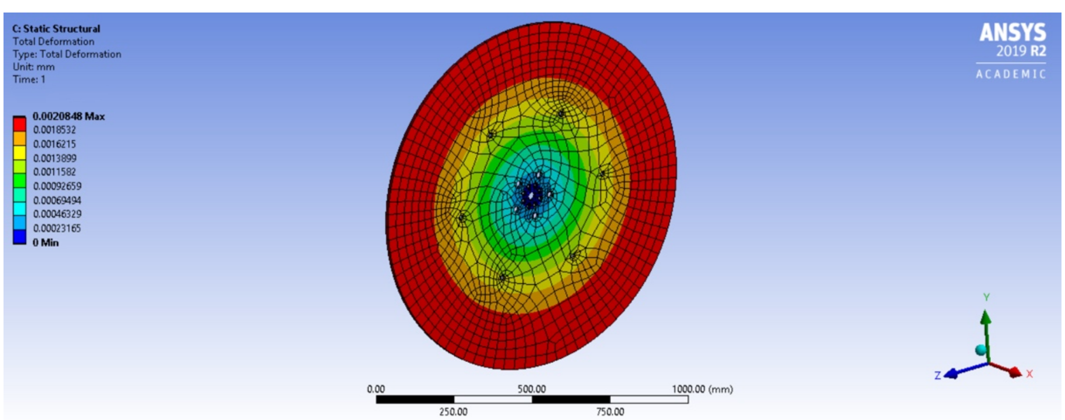

Figure 56. Track deformation during MTR lock up.

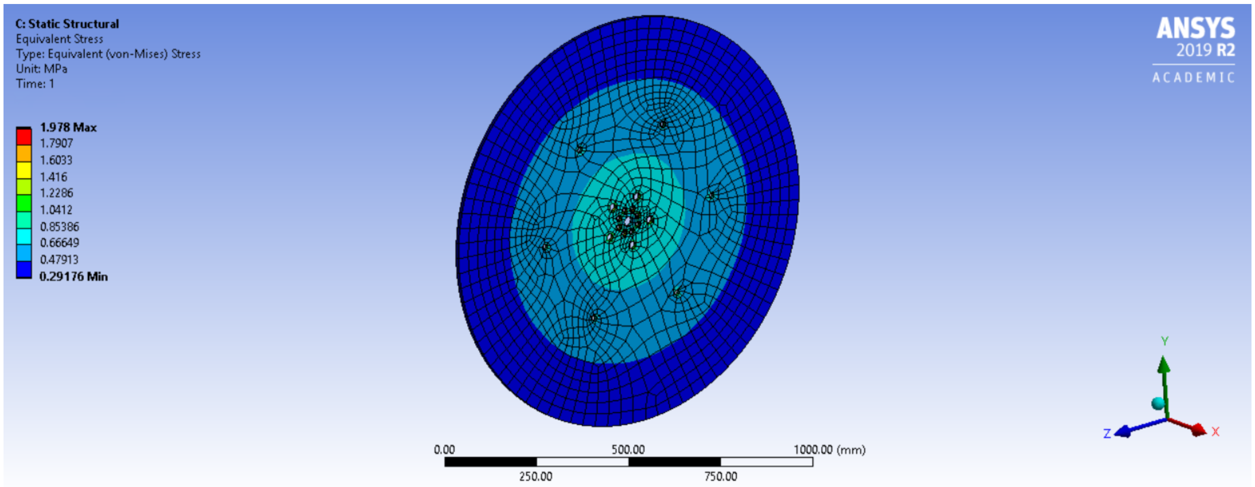

Figure 57. Track stress during MTR lock up.

4.6.1.2 Load Case II (MTR Overspeed)

Under this loading scenario, it was assumed that the overspeed limit built into the MTR malfunctioned. This caused the track to increase its angular acceleration up to a high rated velocity of 50 rad/s. Under this load case, a deformation of 0.00208 mm was to be expected as illustrated in Figure 58. Whereas, an internal stress of 1.978 MPa was generated within it as shown in Figure 59.

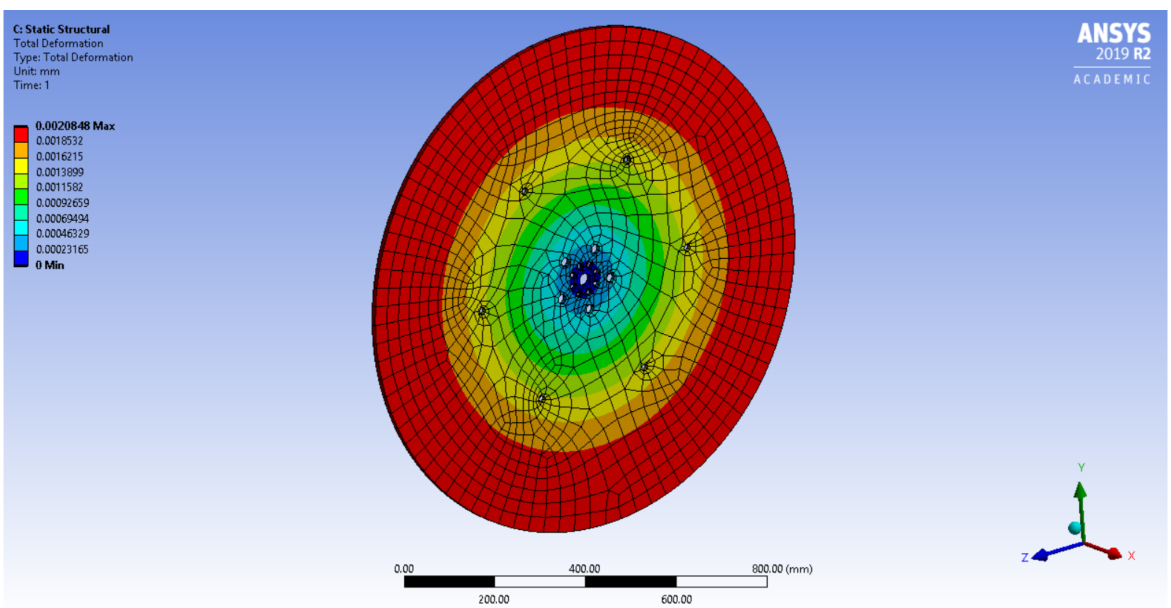

Figure 58. Track deformation during MTR overspeed.

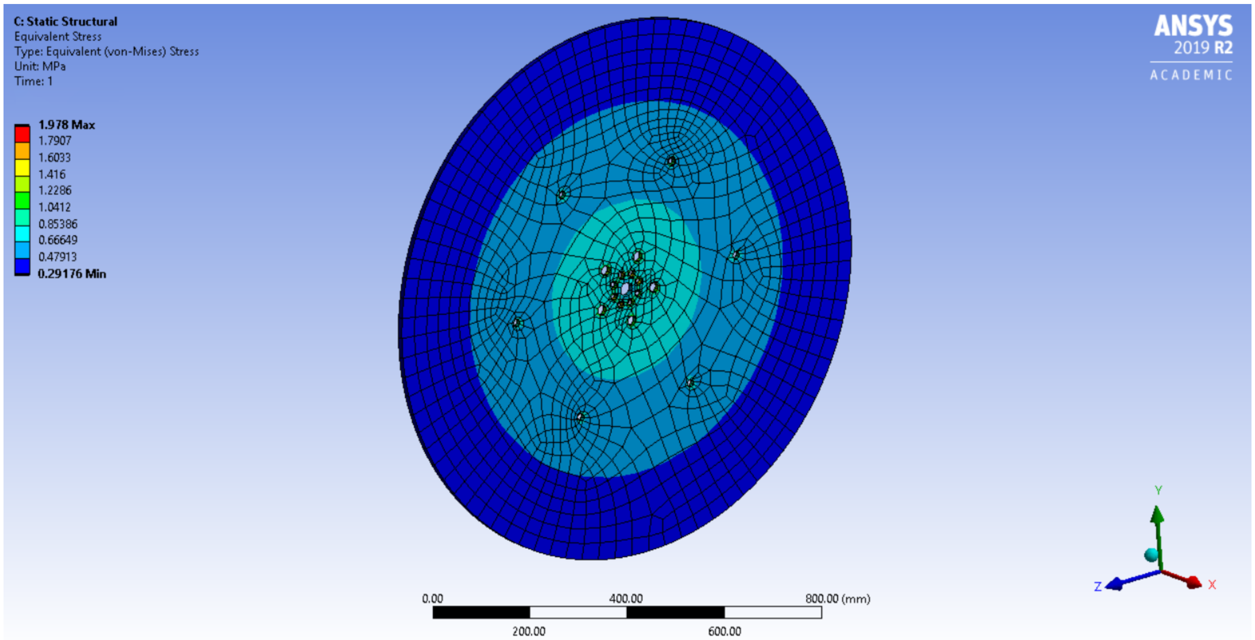

Figure 59. Track stress during MTR overspeed.

4.6.2 Guidance, Navigation and Control Tests

Although the Pod operates autonomously, a constant stream of data flows between the Pod and the Ground Station (GS). With data continuously transmitted some of the parameters monitored by the Pod and sent to the GS were its position, velocity and acceleration, Pod health, temperatures and pressures, and so on.

With the Hyperloop Pod operating in a low pressure environment, initial GNC tests were performed in a pressurized environment. Although this was the case, final Pod electronics needed to be vacuum certified, and thermally rated. This included the use of space grade solder while being in a controlled environment, and x-ray imaging of all the joints to guarantee performance when operated in a low pressure environment. All soldering and electrical work was conducted by following National Aeronautics and Space Administration (NASA) technical standards to ensure the highest levels of performance [37].

The Hyperloop tube has a reflective circumferential tape placed at regular intervals for navigation purposes [10]. In order to make use of this tube feature, GNC's navigation mechanism consisted of a stripe counting sensor that provided the absolute position of the Pod within the Hyperloop tube. Testing of the stripe counter was conducted on the MTR to ensure the Pod's navigation mechanism performed as intended. It also allowed for the necessary fine tuning in order to compensate for the reflectivity of the test track's material, which was Aluminum. This was important as a laser beam needed to be reflected off it.

Furthermore, the fluorescent lighting setup within the tube could be replicated, and accounted for in order to generate accurate results. With the accuracy of the stripe counter being critical to the Pod, the drift occurring as the position and velocity errors over time needed to be quantified in order to demonstrate its accuracies.

4.6.3 Structures Tests

During the design of the braking system, key considerations included the distance required to stop, braking effectiveness, system reliability, resulting temperature change, and so on. As the Pod underwent various state changes, multiple tests were conducted using the MTR to characterize them.

As the Pod contained two independent pneumatic braking systems, each system had the ability to deploy two brake pistons simultaneously. As outlined previously, to ensure stability of the Pod during all braking phases, the systems were placed at the forward, and aft locations of the Pod. To validate this setup, a simplification was made where only one of the two systems was mounted on the MTR. By doing so, the braking tests in a way were performed for the worst case scenario, i.e. one system was considered to be inoperative. This particular setup can be observed in Figure 60 where the two pneumatic pistons were mounted to the mounting frame on either side of the MTR.

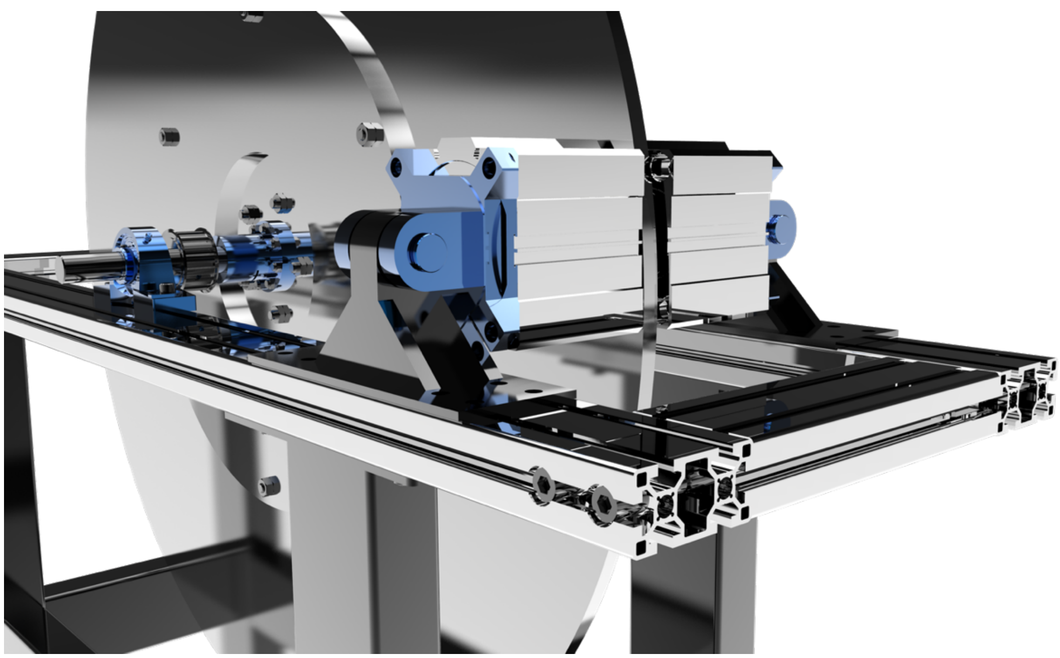

Figure 60. The Integrated Pneumatic Braking System on the MTR.

With the MTR being manufactured out of nearly the same material as the Hyperloop test track, the MTR could also be used to obtain the braking systems thermal characteristics under the worst case scenario. With one system inoperative, results showed that a temperature change of 11.895°C would occur. As a result of heat being dissipated between the braking system and the track itself. Without having the ability to install the entire MTR in a pressure chamber, such tests could only be performed in a pressurized environment. As such, the only source of heat dissipation would be conduction. With convection not cooling the braking system, a higher temperature change was expected, and was accounted for within the design.

Furthermore, to ensure all the pistons outputted an equal amount of braking force, they were also tested and validated on the MTR. During these tests, internal piston pressure was capped at 0.42 MPa to ensure the safety of all the personnel involved. The results obtained from the MTR piston tests have been tabulated in Table 36.

Table 36. MTR Piston input and output braking force test.

Piston Test Parameter	Input Pressure / Output Braking Force
Piston Test 1	*0.10 MPa / 800 N*
Piston Test 2	*0.14 MPa / 956 N*
Piston Test 3	*0.18 MPa / 1,272 N*
Piston Test 4	*0.21 MPa / 1,504 N*
Piston Test 5	*0.28 MPa / 2,077 N*
Piston Test 6	*0.35 MPa / 2,602 N*
Piston Test 7	*0.42 MPa / 3,158 N*

Figure 61 showcases the data points obtained from the MTR testing of the pneumatic braking pistons. Observing the theoretical and experimental plots, a deviation of 11.70% occurred between the pneumatic pistons [38]. This slight deviation was to be expected as testing was conducted using an analogue pressure gauge to dial in the piston's internal pressure. However, having the gauge replaced with a digital one should resolve this issue.

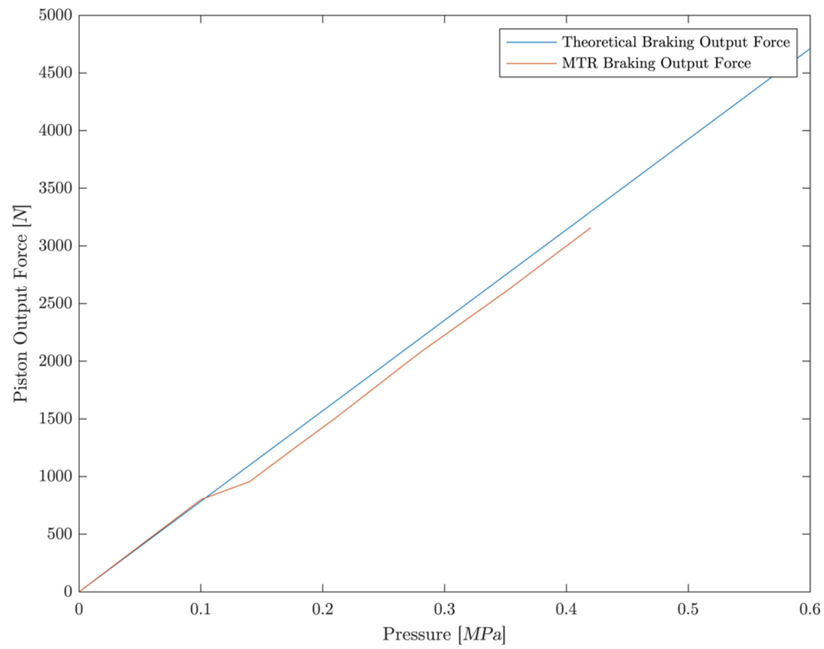

Figure 61. Brake output force data for MTR pistons.

4.6.4 Propulsion Tests

With the propulsion system capable of propelling and levitating the Pod through a true contactless system, the systems were developed from the ground up to cater to the specific requirements of the Hyperloop Pod. As a result, the Student Researched And Developed (SRAD) systems such as MagLev and MagDrive needed to be validated using the MTR.

MagLev is derived from the magnetic levitation system that is used to support the Pod along the normal axis at high speeds [39]. It uses a Halbach array to induce a repulsive magnetic field to suspend the Pod at a predefined altitude or height. With the system being SRAD, it needed to be validated thoroughly on the MTR to show that a sufficient force or lift was developed in order to levitate the Pod. To do so on the MTR, a Dual Axis Force Transducer (DAFT) was developed for the MTR as shown in Figure 62.

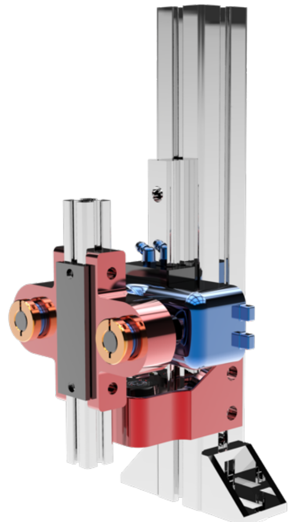

Figure 62. Assembled Dual Axis Force Transducer for MagLev testing.

The DAFT was capable of measuring the lift and drag forces, or the levitation force and MagDrag generated by MagLev when deployed. In addition, it was made to sense these forces as a function of the MTR's rotational velocity.

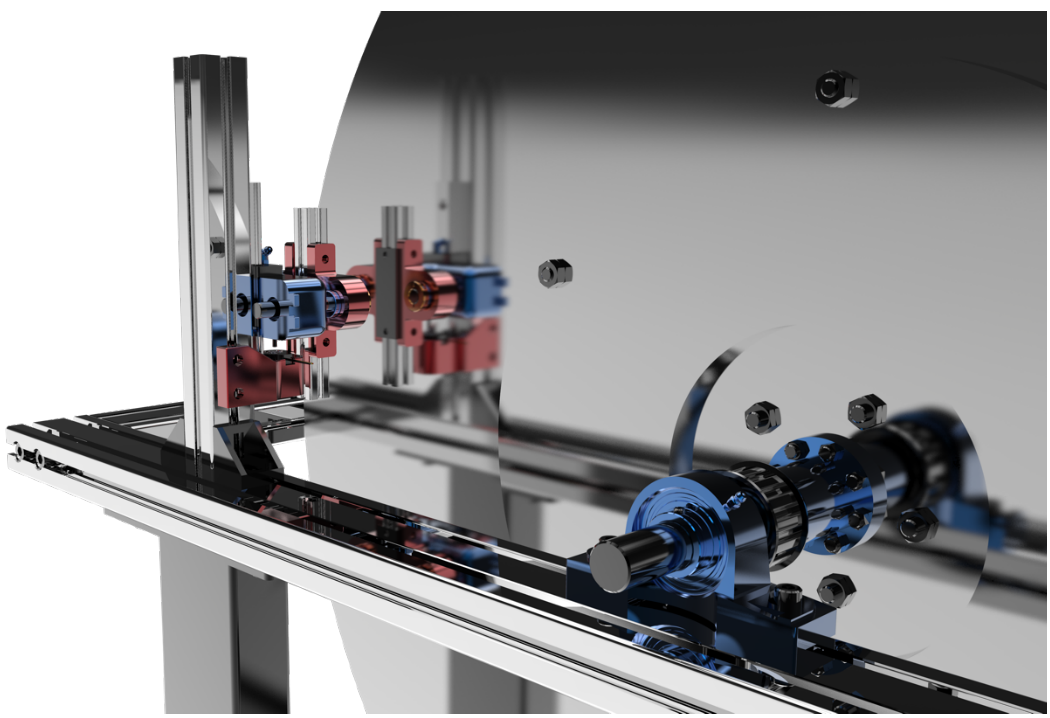

Figure 63. MTR showcasing the mounted DAFT.

Tests were performed utilizing the DAFT on the MTR with a singular North-South (N-S) period configuration of N42 magnets measuring 25.4 mm by 25.4 mm by 12.7 mm in dimension.

The results obtained from MTR tests were used to generate a theoretical profile of the MagLev's behavior. The creation of this profile allowed for the characterization of the MagLev system's performance. The MTR was able to run up to a peak velocity of 15 m/s while holding the rotations at a constant speed reliably. In Figure 64, the reading taken between zero and 5×10^4 clearly demonstrate the ramp up in the MTR's speed as it was powered up. As peak velocity was achieved around the 5.5×10^4 reading mark, the lift to drag, or levitation force to MagDrag was observed to be almost one, and can be seen in Figure 64 as well.

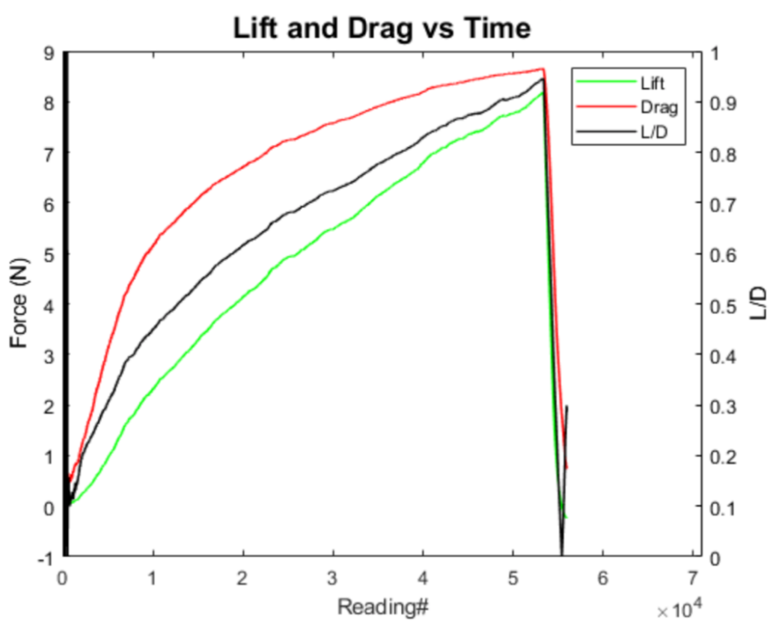

Figure 64. MagLev test results for singular North-South period configuration.

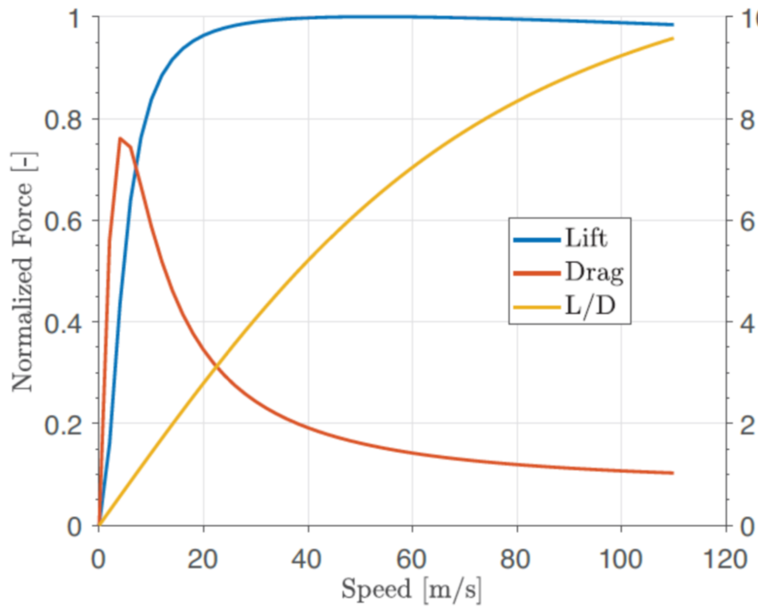

Figure 65. Simulated behavior of lift and drag with an extended velocity profile [40].

With the results obtained, the theoretical profile was generated to show MagLev's behavior had the speed been increased further to the speeds seen by the Hyperloop Pod [40]. Some significant observations that could be made from Figure 65 included the discernibility of the crossover point. This is where MagDrag began to depreciate considerably as the lift or levitation force continued to increase. This occurred up to a certain speed, in this case 70 m/s after which both the parameters began to plateau.

The development of the theoretical profile aided in better understanding of the system if it is modified through a change its array, number of periods, magnet strength, and so on as tabulated below [40].

Table 37. Parametric performance effects on MagLev.

Design Parameter	Effect on Lift	Effect of L/D	Effect on Weight
Array Wavelength	*Slight Decrease*	*Square Root Increase*	*Increase*
Number of Periods	*Linear Increase*	*No Effect*	*Increase*
Array Width	*Linear Increase*	*No Effect*	*Increase*
Array Thickness	*Squared Increase*	*Negligible*	*Increase*
Magnet Grade	*Increase*	*No Effect*	*No Effect*
Back Plate Thickness	*Slight Increase*	*Negligible*	*Increase*
Nominal Gap Height	*Inverse Square Decrease*	*No Effect*	*No Effect*

5 CONCLUSION

The objective of the research work was to design Ryerson's first Hyperloop Pod for the fifth mode of transportation, the Hyperloop. With this new mode of transportation still in its infancy, the challenge was to design and develop its systems and to have them tested in a university environment. In doing so, new requirements, constraints, guidelines, objectives, and standards were developed and explored for the Hyperloop. Any issues and unknowns were solved by applying aerospace engineering knowledge and its principles.

Furthermore, key ideas from the aerospace industry led to the development of the modular test rig that proved to be a very reliable and unique testing rig for the developed Hyperloop systems. The employment of a multidisciplinary approach coupled with various engineering management resources enabled the team to define the problem at its most basic level. This simplified approach permitted various designs, components, and systems to be tested utilizing the MTR to its full potential. This was extremely important in the development of the Hyperloop systems.

The design of Ryerson's Pod for the Hyperloop Pod Competition contributed towards the advancement of Ryerson University and the Department of Aerospace Engineering within the Hyperloop industry. Furthermore, the developed design achieved success at various stages of the Hyperloop Pod Competition.

Based on Ryerson International Hyperloop's performance, the team received a special invitation from SpaceX to attend the 2019 Hyperloop Pod Competition in Hawthorne, California after having previously also attended the 2018 Hyperloop Pod Competition.

6 FUTURE WORK

Although tremendous strides were made within the development of the Hyperloop, various areas of deficiencies have been identified in team organization, documentation, analysis, and testing procedures. New methods are continuously being introduced to address issues both in coordination and communication between the various systems. With the integration of these new methods, time spent on the assembly and systems engineering is greatly reduced as components would interface seamlessly.

Since development of the Hyperloop is ongoing, the following are some potential points of research:

- Optimization of the thermal management solutions required to dissipate heat generated from the LIM, BRK, and GNC systems.
- Braking system characterization when operating within low pressure or near vacuum environments.
- Characterization of permanent magnet's behavior within low pressure or near vacuum environments.
- Development of a fatigue model for Pod structures to better understand Hyperloop's cyclical loading that occurs every 35 minutes.
- Composite testing to observe the laminates' behavior as it undergoes constant depressurization and pressurization.
- Optimization of the MagLev system to better support a higher Pod mass during the levitation phase.
- Characterization of the MagDrag to aid in extracting additional braking power from the MagLev system.
- Optimization of the MagDrive system to reduce its overall mass while improving its thrust capabilities within a low pressure environment.
- Manufacturing of a larger modular test rig capable of conducting high speed tests for full scale Hyperloop systems.
- Development of standardized and certified Hyperloop components and systems that could easily be implemented within Hyperloop Pods. (Similar to standardized aerospace components).
- Development of a legal framework for the Hyperloop, including constraints, guidelines, certification standards, and testing procedures.

APPENDICES

Appendix A.1 Final Pod Prototype


RYERSON INTERNATIONAL
HYPERLOOP
EXPERIMENTAL
EXPERIMENTAL


RYERSON INTERNATIONAL
HYPERLOOP
EXPERIMENTAL
EXPERIMENTAL


RYERSON INTERNATIONAL
HYPERLOOP
EXPERIMENTAL
EXPERIMENTAL

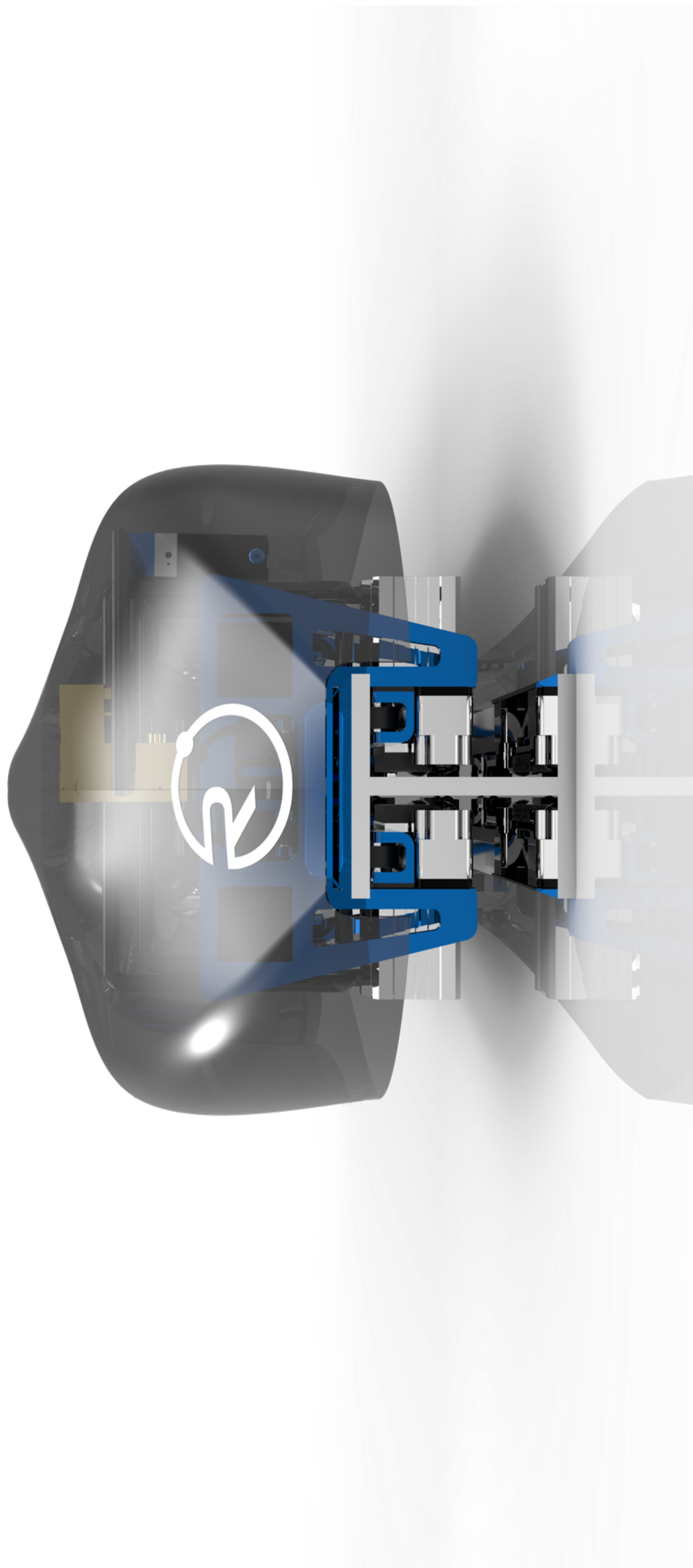

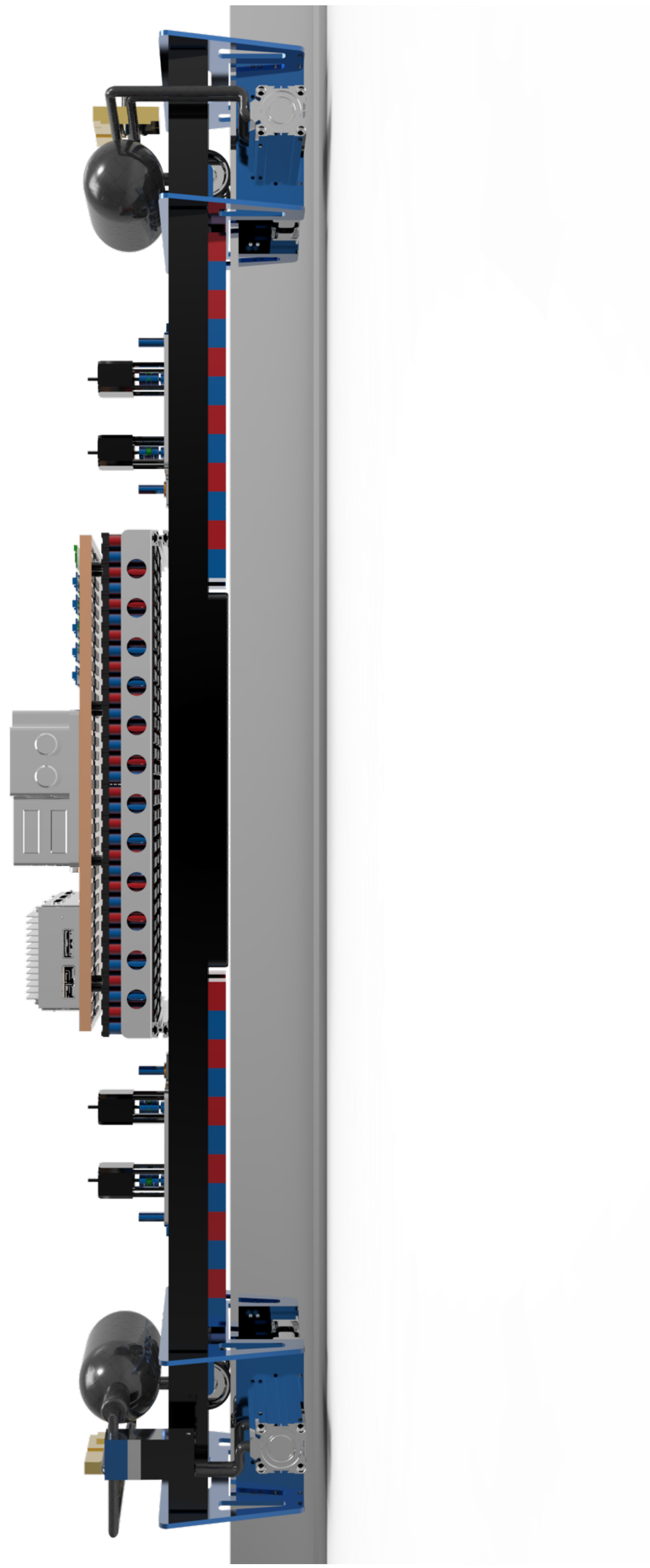

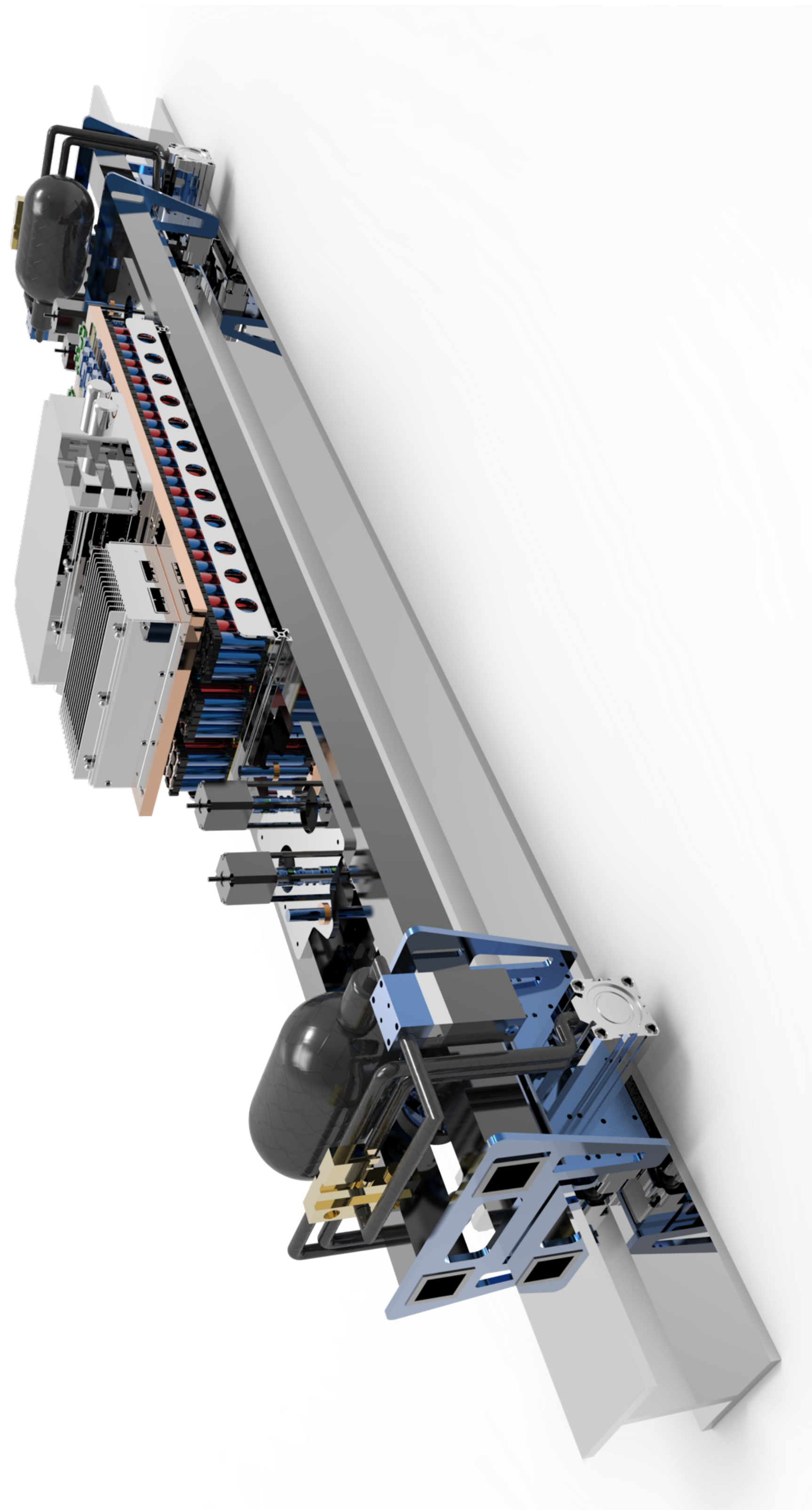

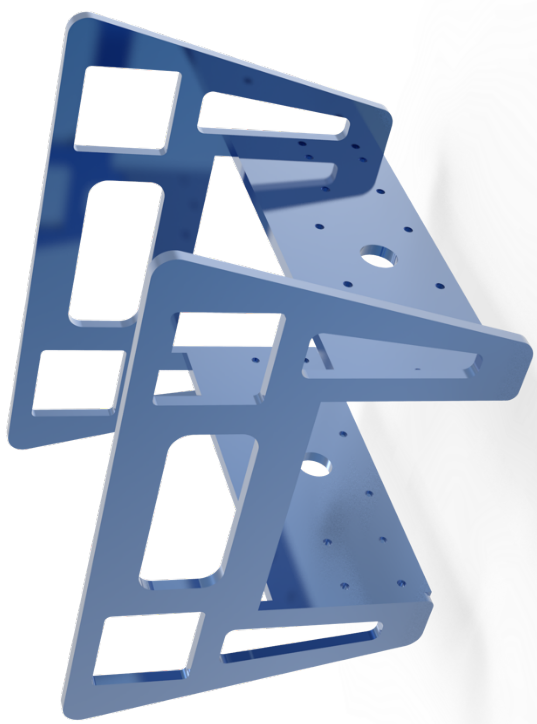

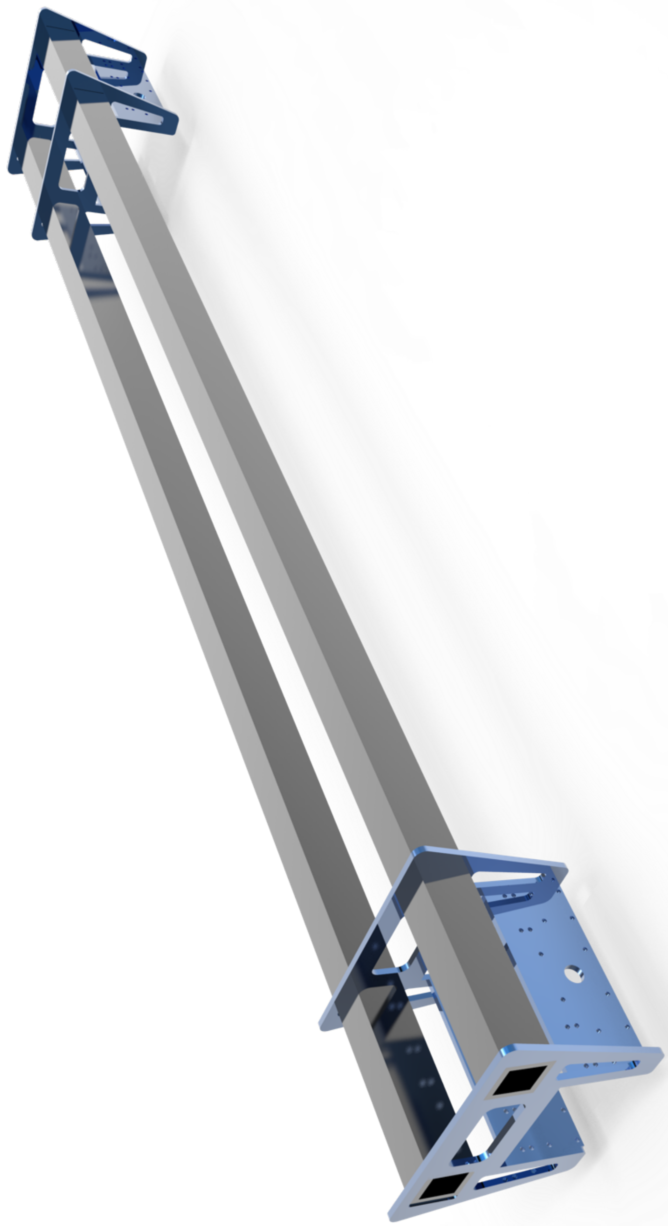

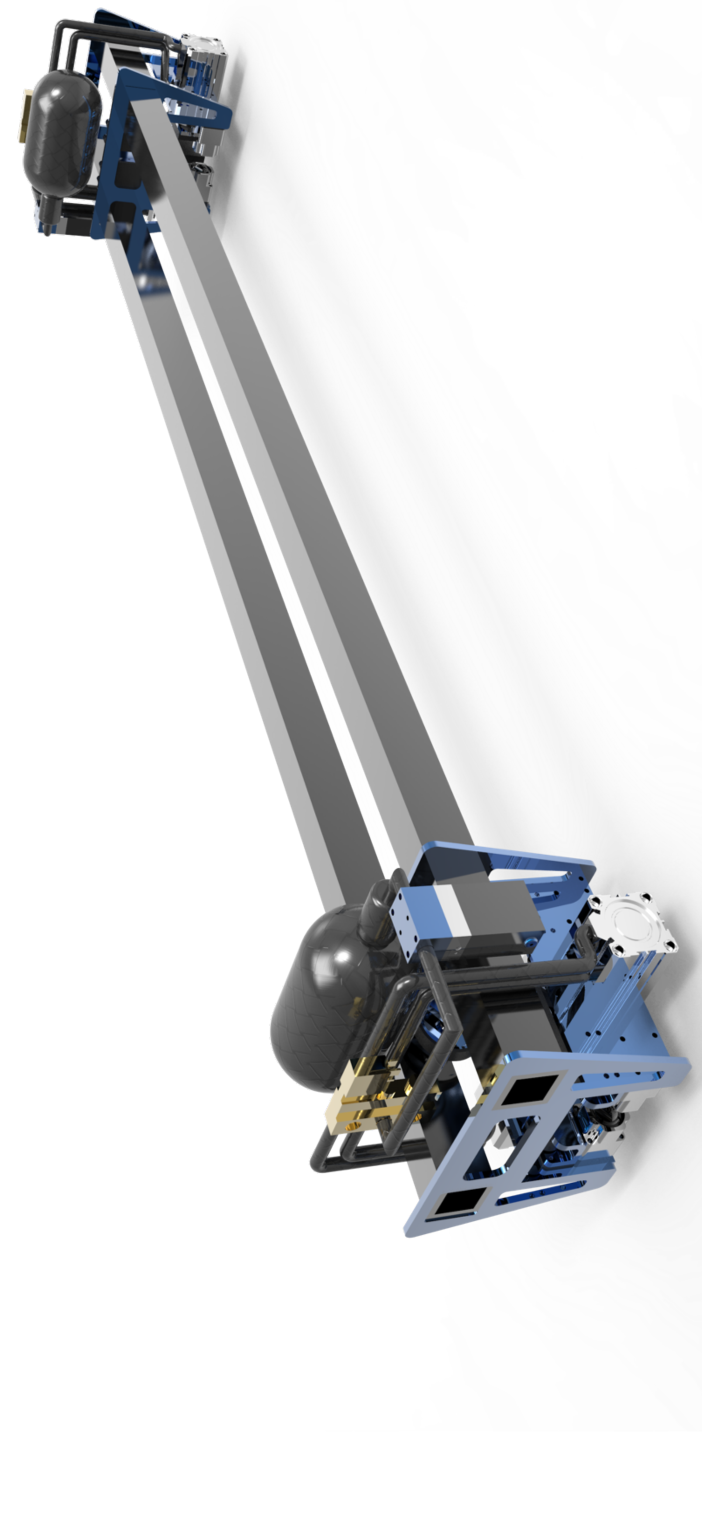

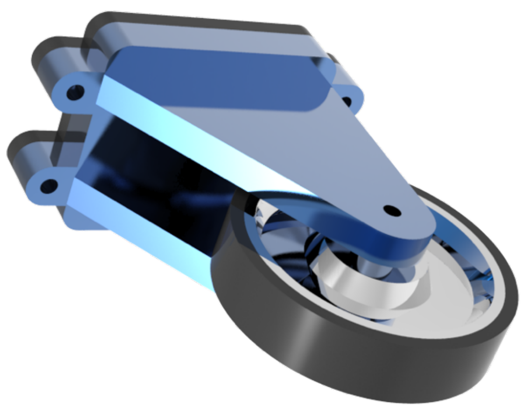

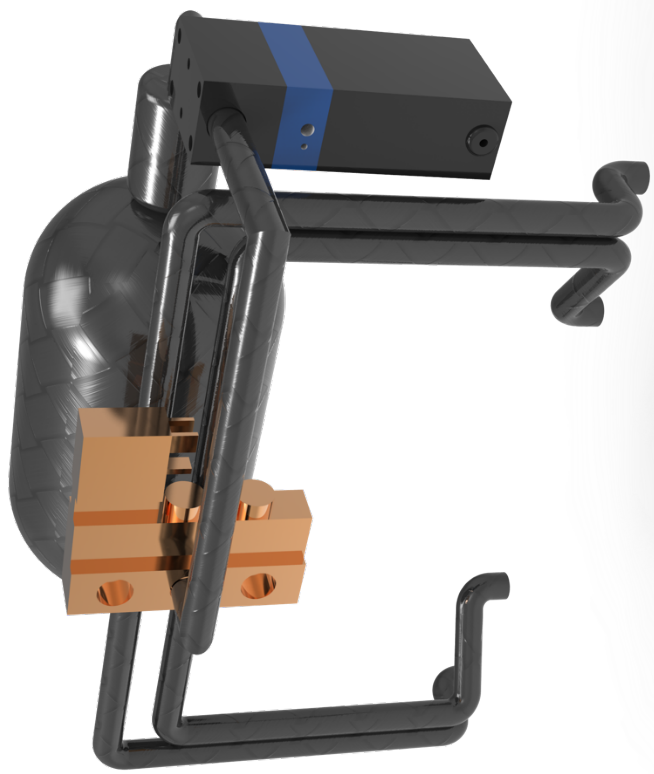

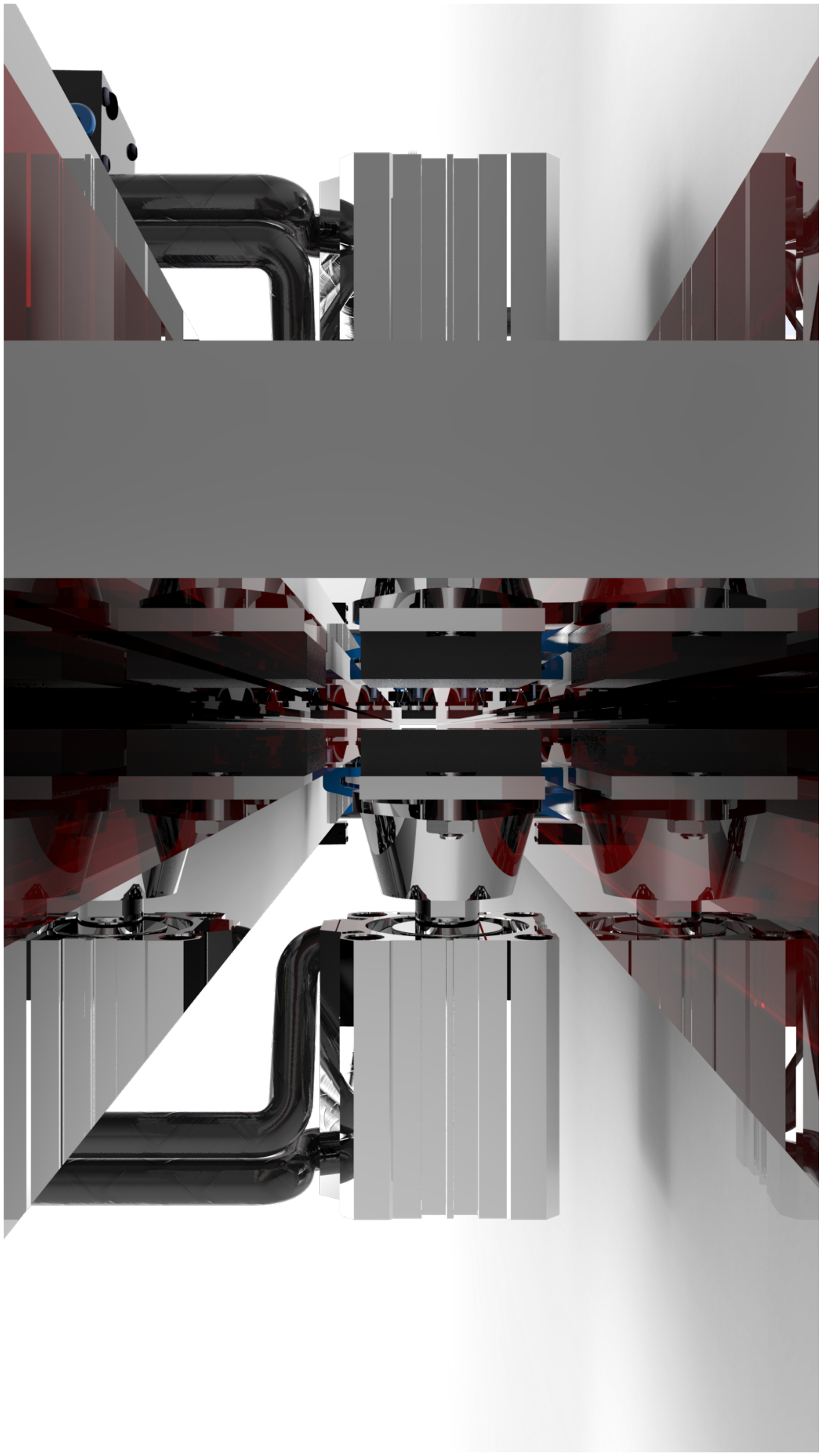

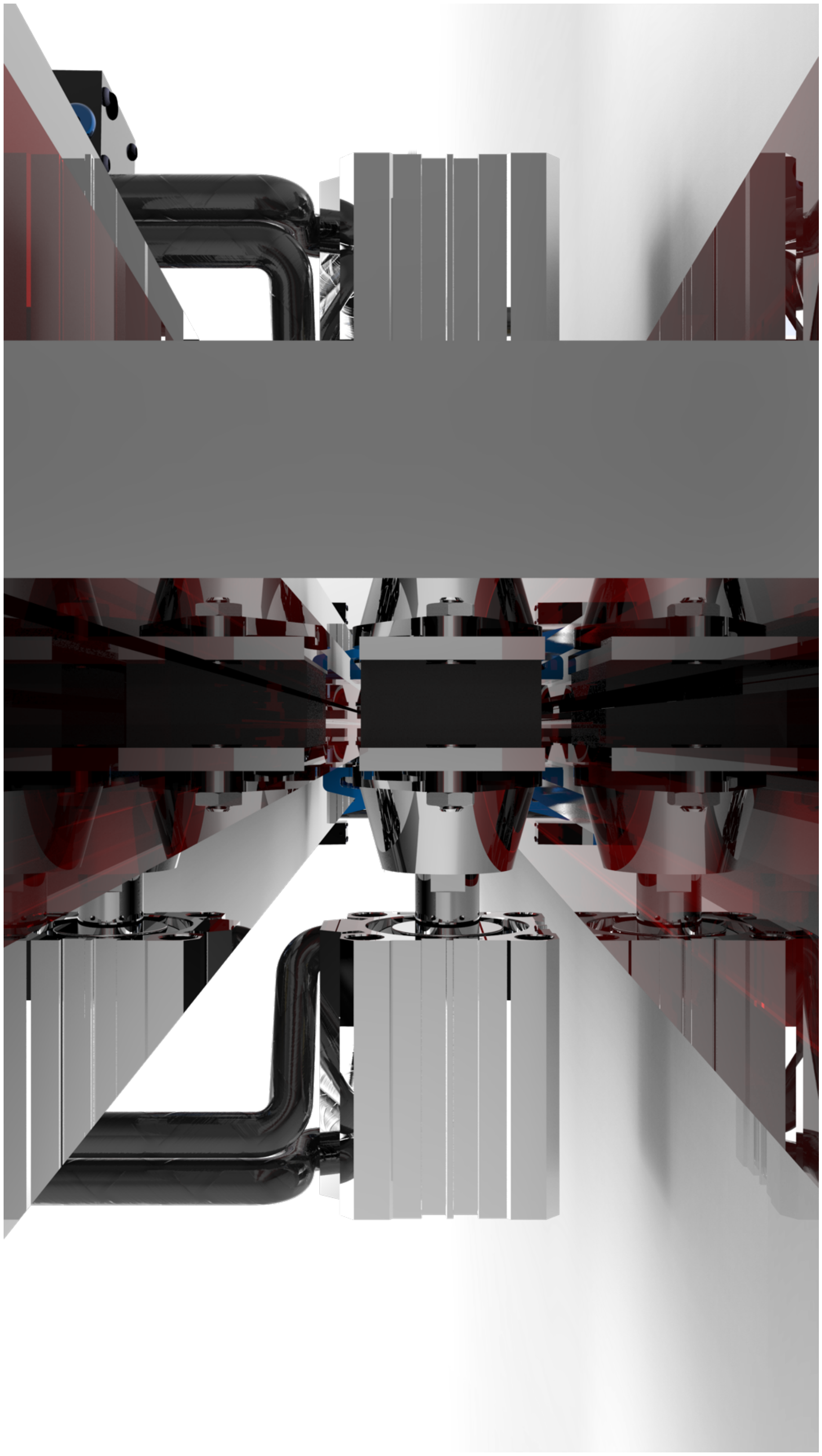

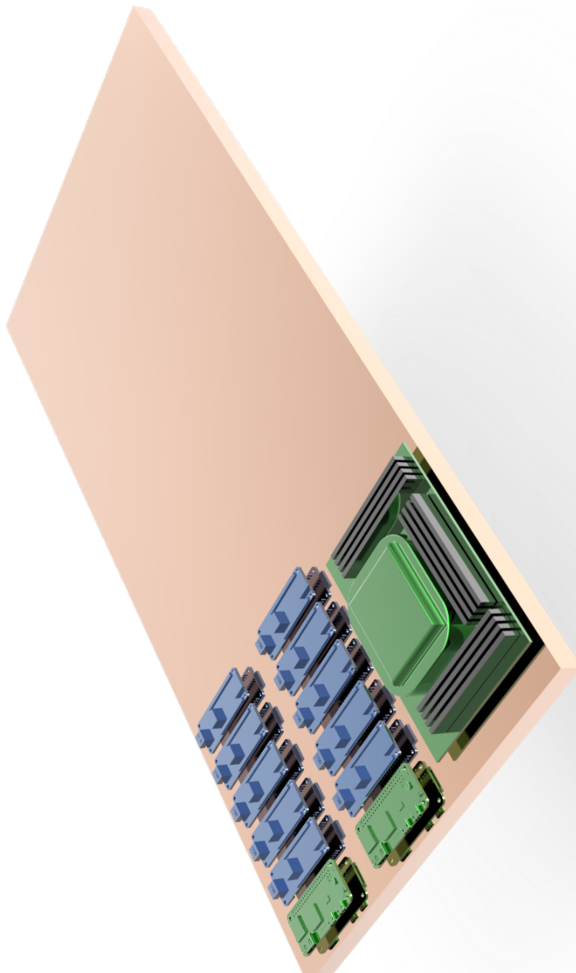

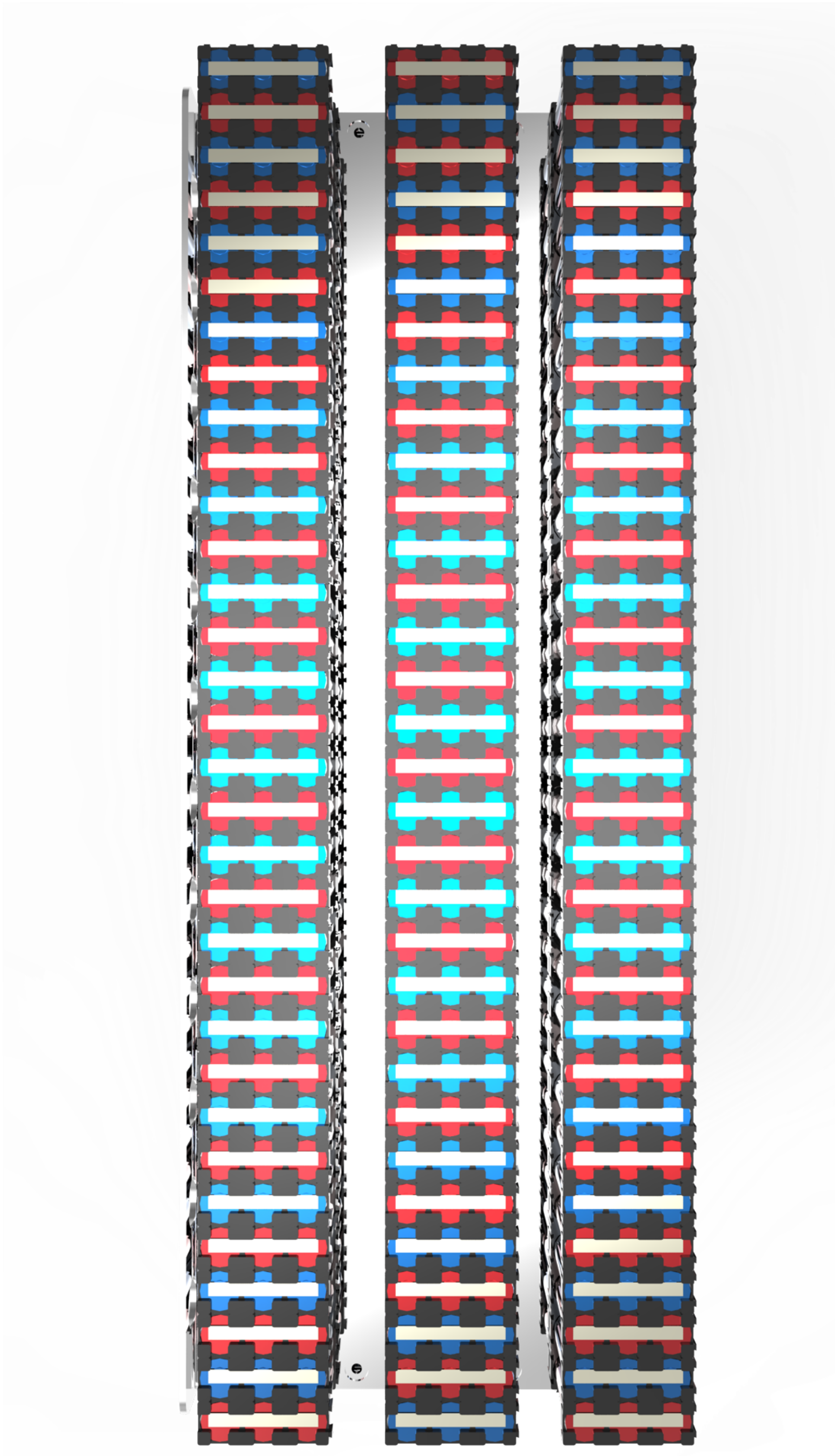

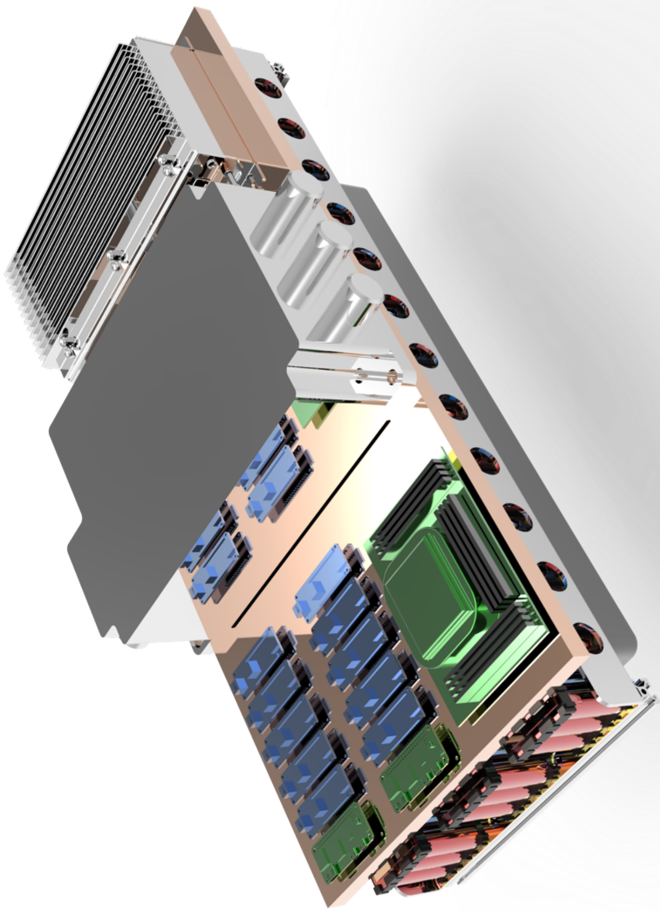

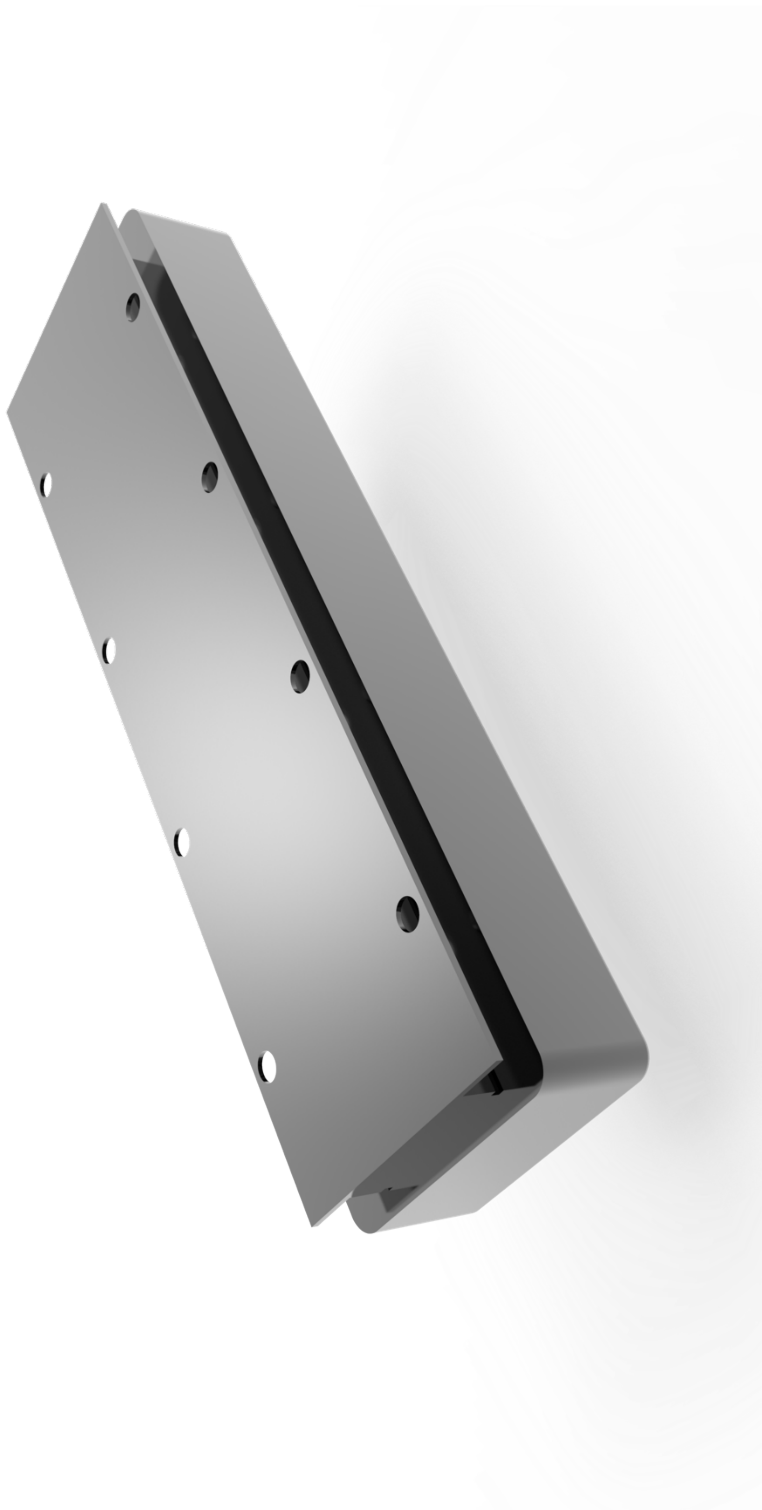

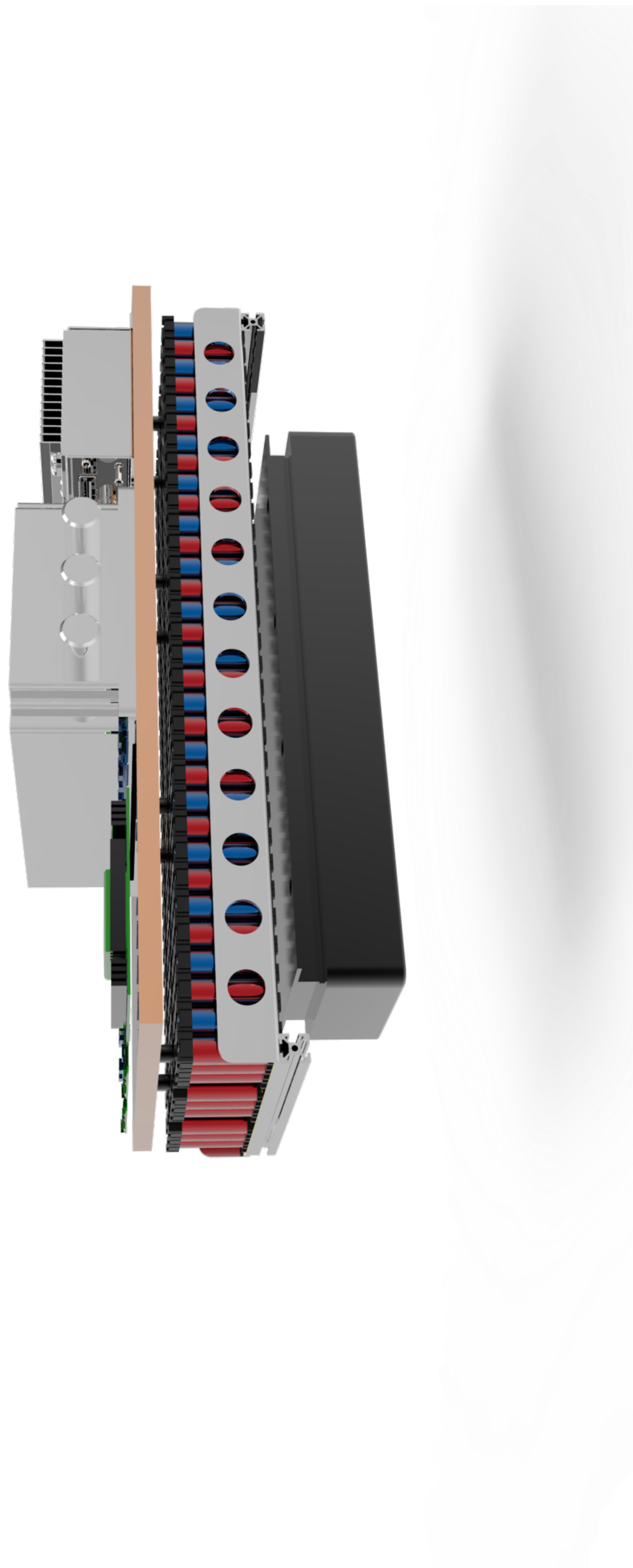

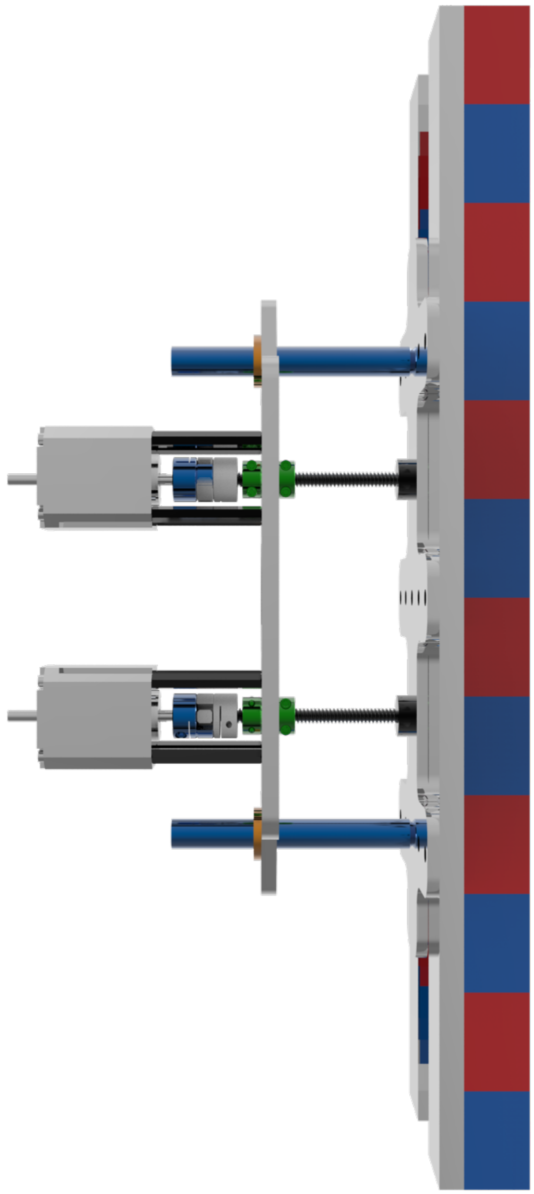

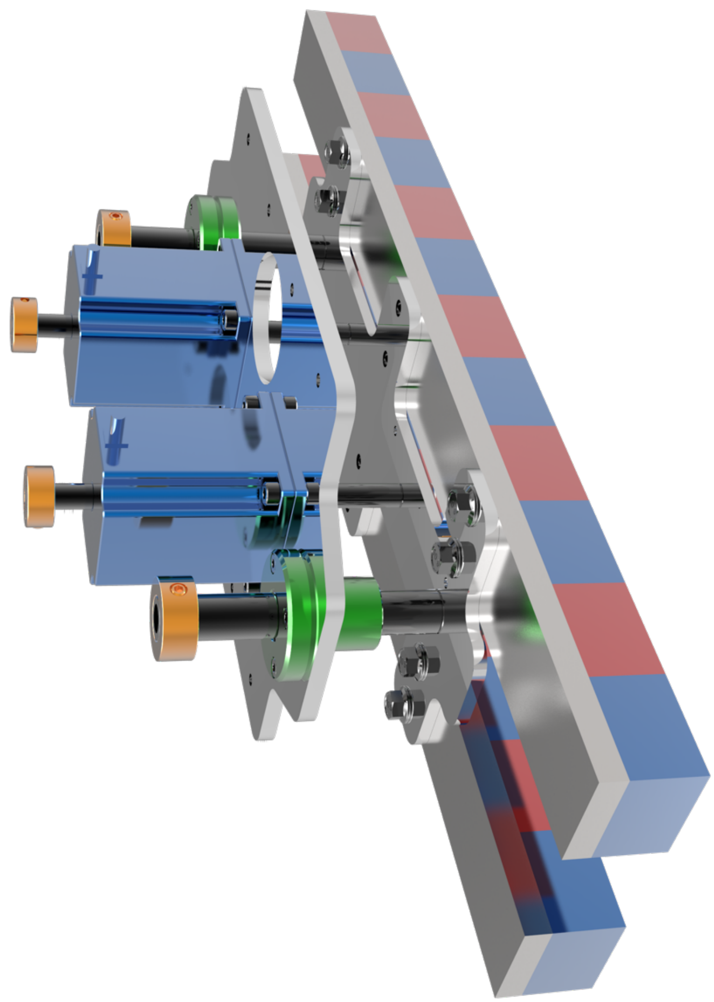

Appendix A.2 Modular Test Rig Prototype

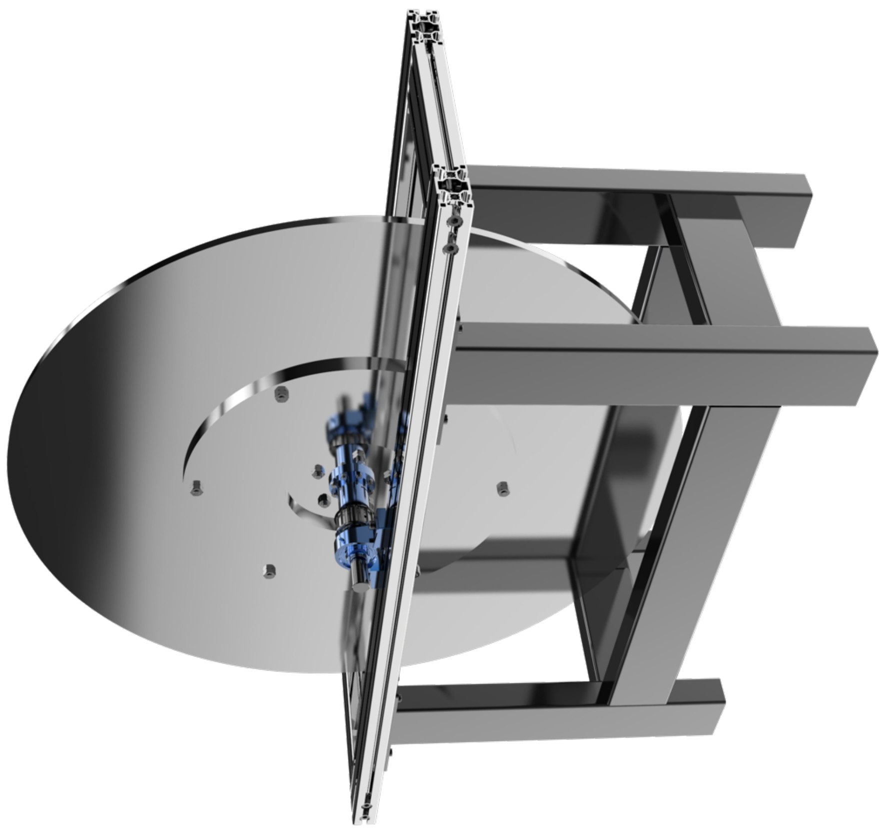

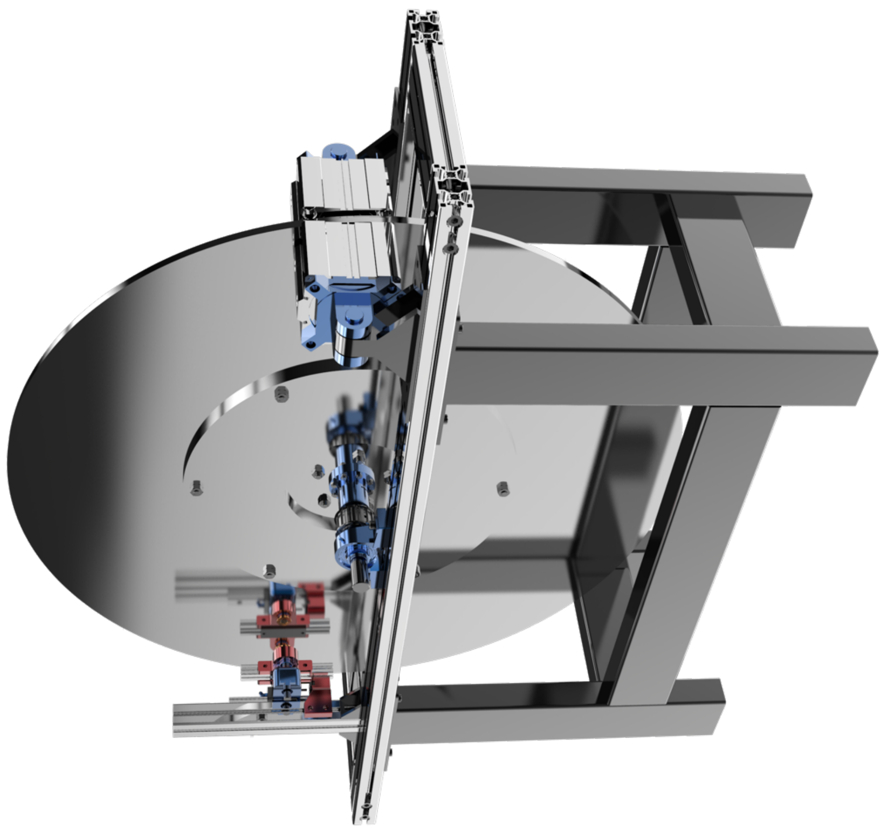

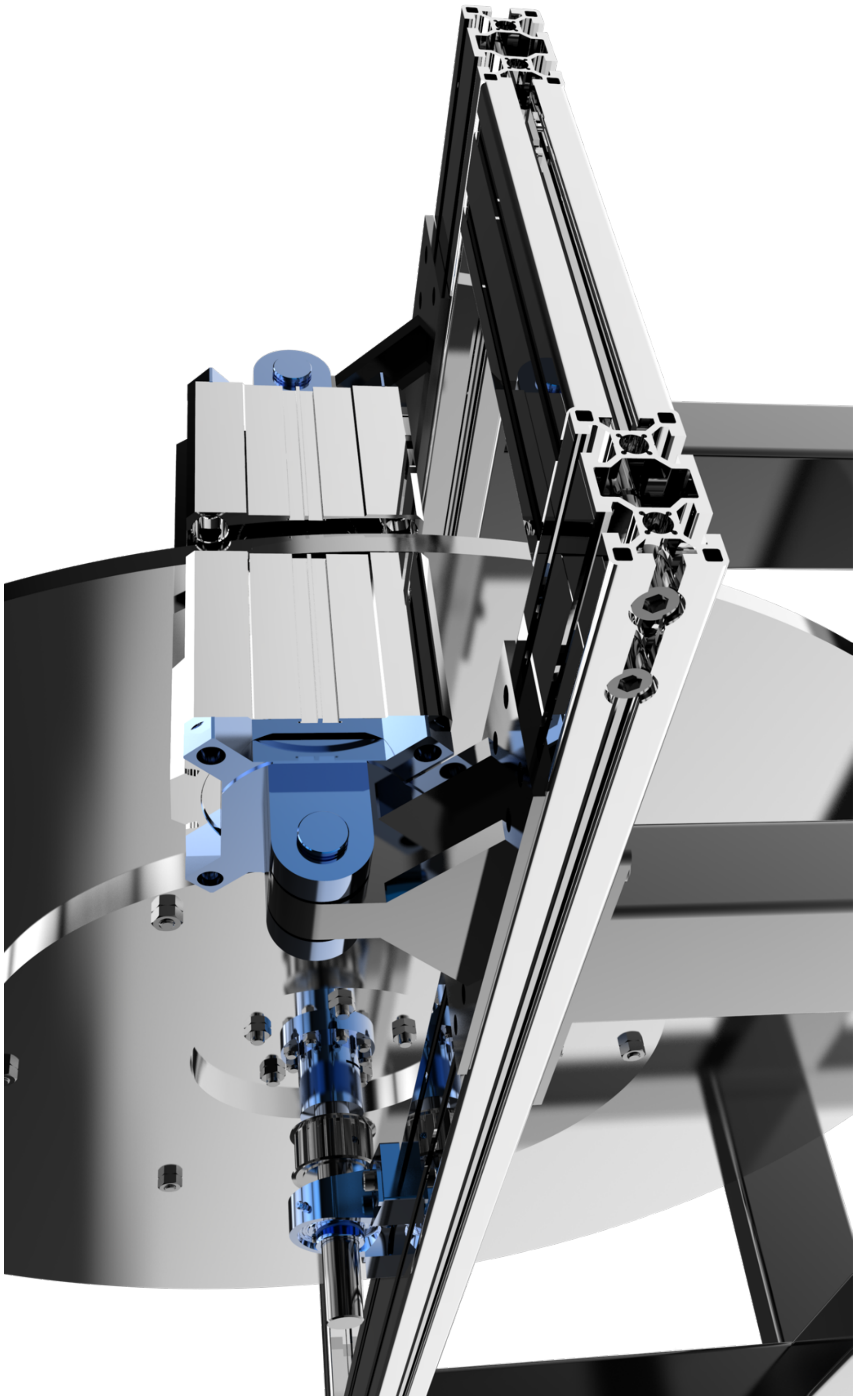

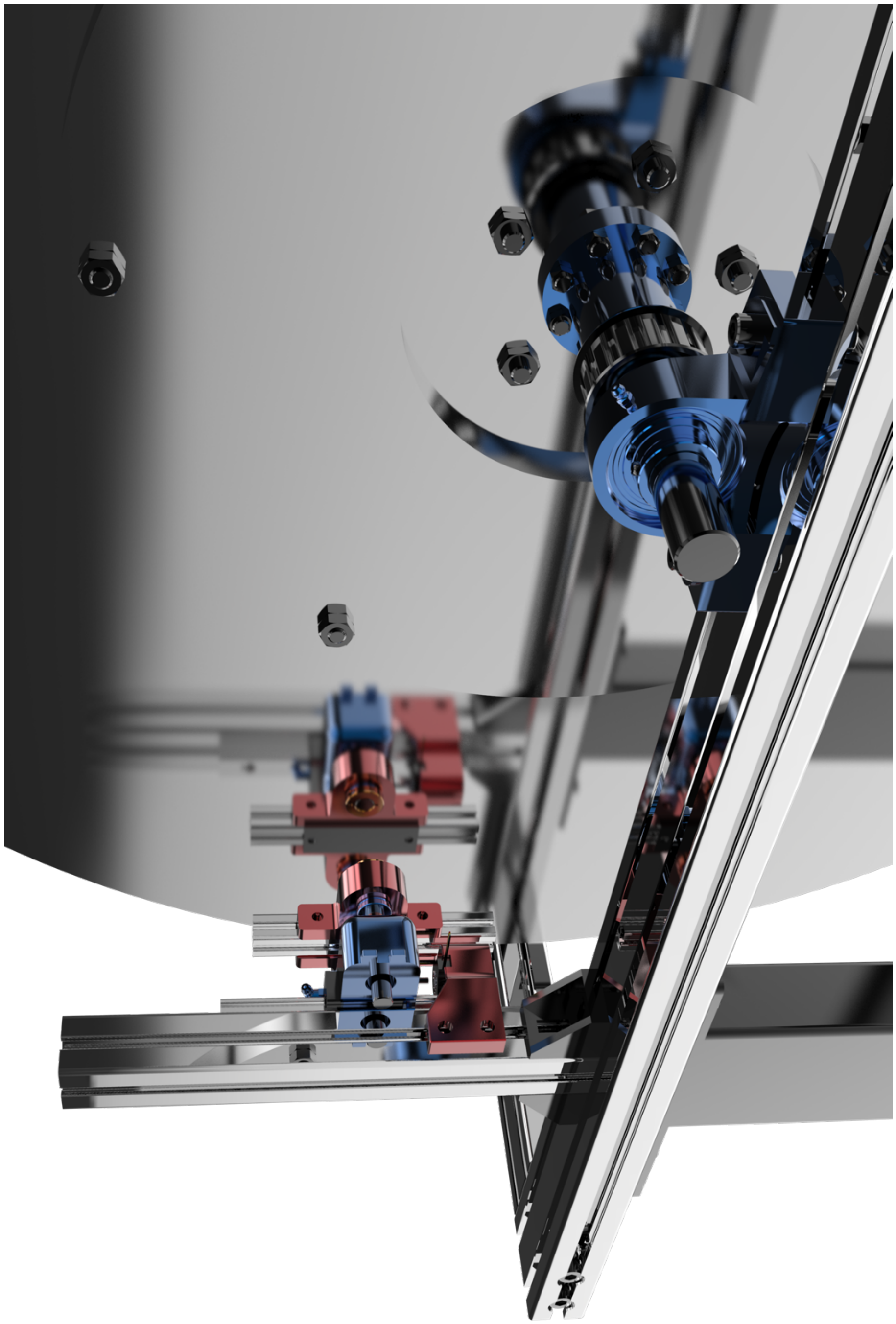

Appendix A.3 Pod Engineering Drawings

Front view
Scale: 1:1

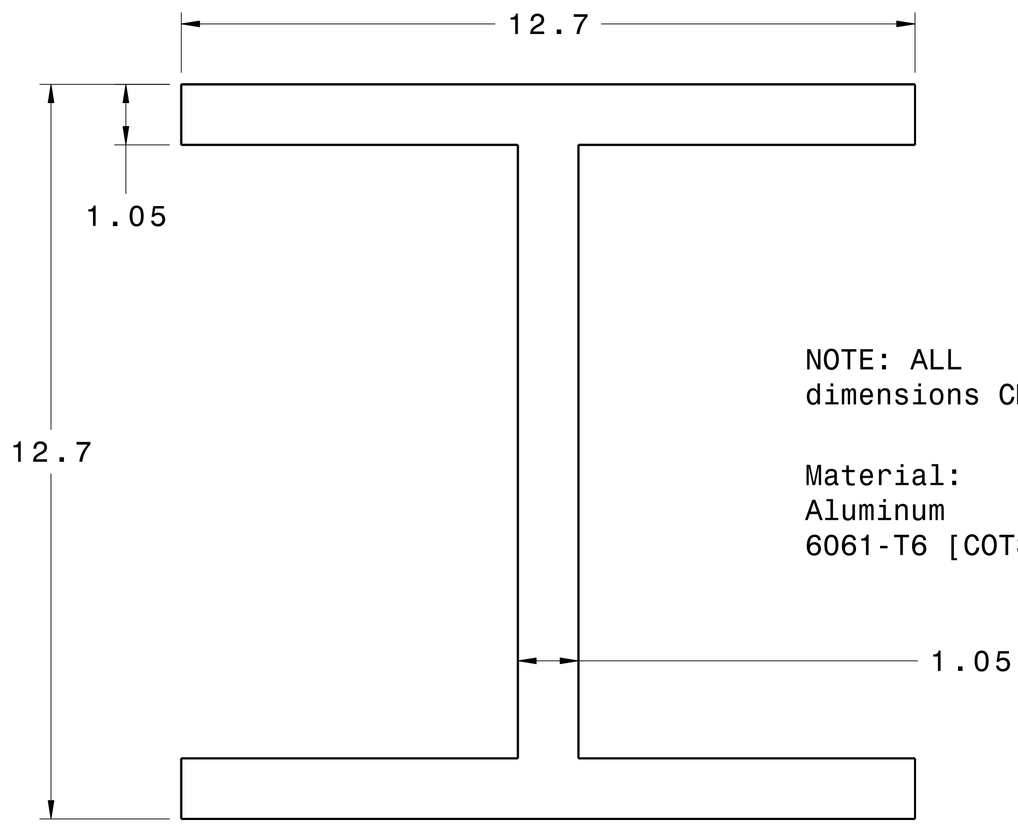

NOTE: ALL
dimensions CM

Material:
Aluminum
6061-T6 [COTS]

This drawing is our property. It can't be reproduced or communicated without our written agreement.		RYERSON INTERNATIONAL HYPERLOOP		
DRAWN BY: MOHI KHAN	DATE: 05/01/2019	DRAWING TITLE: RH - POD - I-BEAM		
CHECKED BY: MOHI KHAN	DATE: 05/01/2019	SIZE: Letter	DRAWING NUMBER: POD2019001	REV: A
DESIGNED BY: MOHI KHAN	DATE: 05/01/2019	SCALE 1:1	WEIGHT(kg) N/A	SHEET 1/1

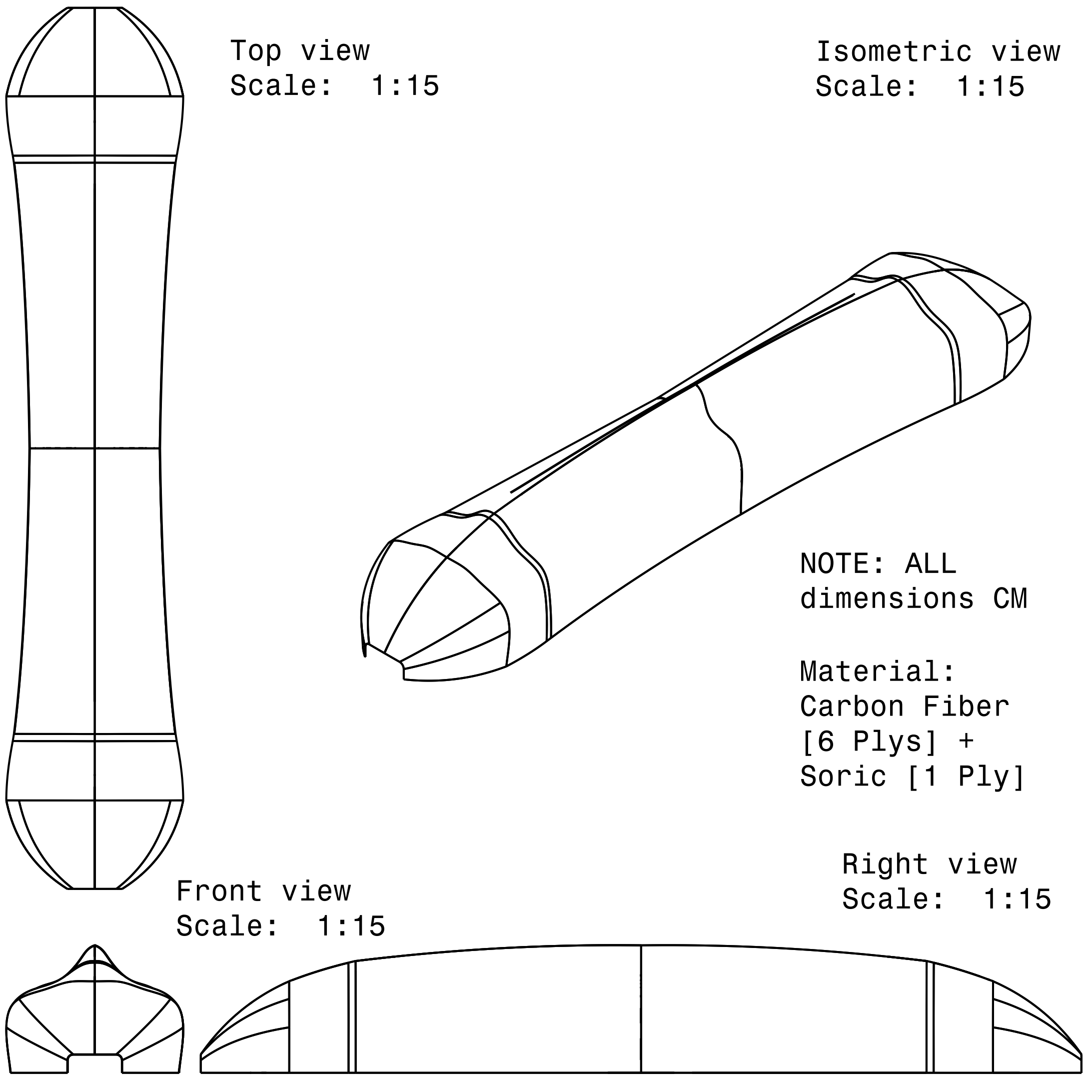

This drawing is our property. It can't be reproduced or communicated without our written agreement.

RYERSON INTERNATIONAL HYPERLOOP

DRAWN BY: MOHI KHAN	DATE: 05/01/2019	DRAWING TITLE: RH - POD - POD SHELL	
CHECKED BY: MOHI KHAN	DATE: 05/01/2019	SIZE: Letter	DRAWING NUMBER: STR PODSTR2019002 — REV: A
DESIGNED BY: MOHI KHAN	DATE: 05/01/2019	SCALE: 1:15	WEIGHT(kg): N/A — SHEET: 1/1

Front view
Scale: 1:3

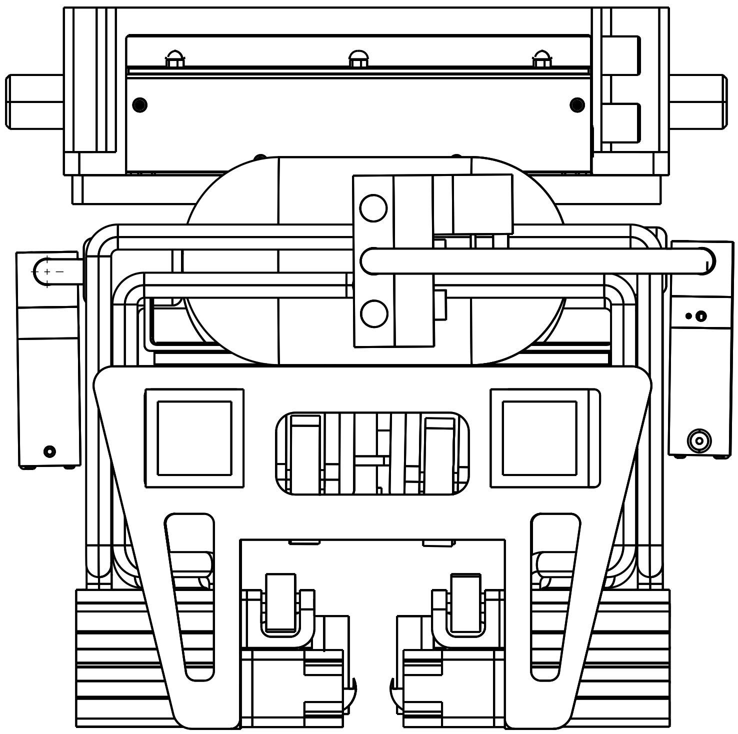

NOTE: ALL
dimensions CM

Material:
Various [SRAD]

This drawing is our property. It can't be reproduced or communicated without our written agreement.		RYERSON INTERNATIONAL HYPERLOOP				
DRAWN BY MOHI KHAN	DATE 05/01/2019	DRAWING TITLE RH - POD - POD FRONT				
CHECKED BY MOHI KHAN	DATE 05/01/2019	SIZE Letter	DRAWING NUMBER PODSTR2019003			REV A
DESIGNED BY MOHI KHAN	DATE 05/01/2019	SCALE 1:3	WEIGHT(kg) N/A		SHEET 1/1	

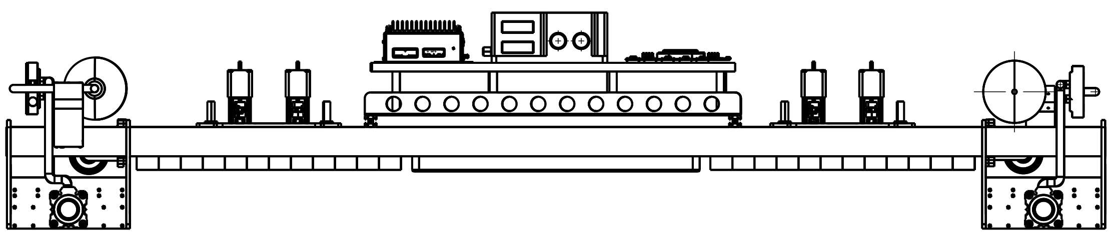

Right view
Scale: 1:10

NOTE: ALL
dimensions CM

Material:
Various [SRAD]

This drawing is our property. It can't be reproduced or communicated without our written agreement.		RYERSON INTERNATIONAL HYPERLOOP				
DRAWN BY MOHI KHAN	DATE 05/01/2019	DRAWING TITLE RH - POD - POD SIDE				
CHECKED BY MOHI KHAN	DATE 05/01/2019	SIZE Letter	DRAWING NUMBER PODSTR2019004			REV A
DESIGNED BY MOHI KHAN	DATE 05/01/2019	SCALE 1:10	WEIGHT(kg) N/A		SHEET 1/1	

Top view
Scale: 1:10

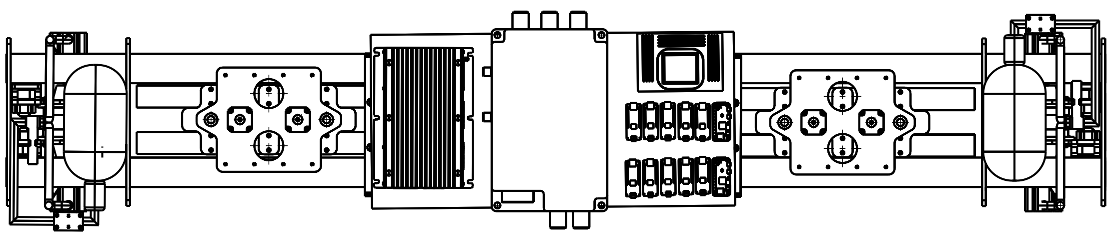

NOTE: ALL
dimensions CM

Material:
Various [SRAD]

RYERSON INTERNATIONAL HYPERLOOP

DRAWN BY: MOHI KHAN	DATE: 05/01/2019	DRAWING TITLE: RH - POD - POD TOP			
CHECKED BY: MOHI KHAN	DATE: 05/01/2019	SIZE: Letter	DRAWING NUMBER: PODSTR2019005		REV: A
DESIGNED BY: MOHI KHAN	DATE: 05/01/2019	SCALE 1:10	WEIGHT(kg) N/A		SHEET 1/1

Isometric view
Scale: 1:10

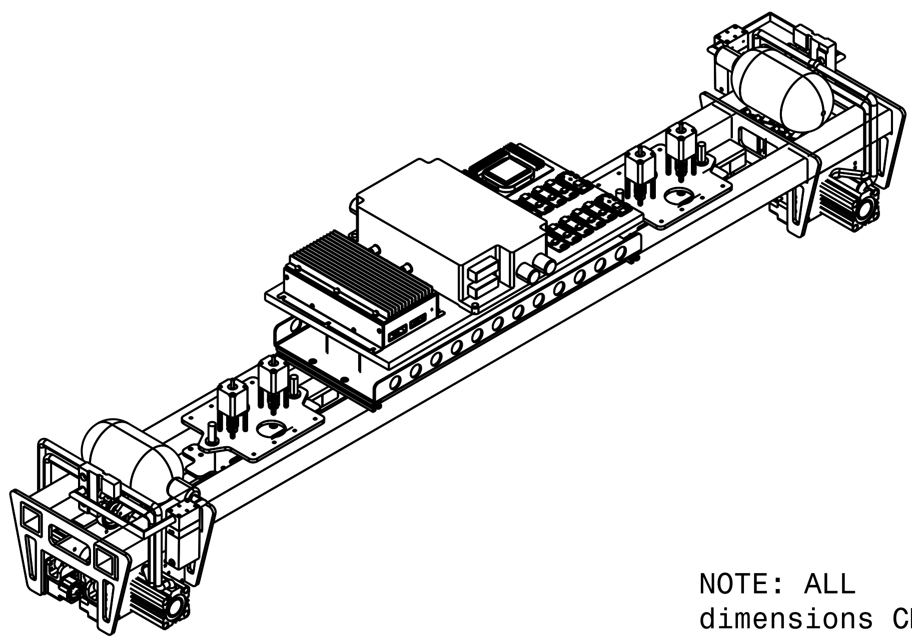

NOTE: ALL
dimensions CM

Material:
Various [SRAD]

RYERSON INTERNATIONAL HYPERLOOP

DRAWN BY: MOHI KHAN	DATE: 05/01/2019	DRAWING TITLE: RH - POD - POD ISOMETRIC		
CHECKED BY: MOHI KHAN	DATE: 05/01/2019	SIZE: Letter	DRAWING NUMBER: PODSTR2019006	REV: A
DESIGNED BY: MOHI KHAN	DATE: 05/01/2019	SCALE 1:10	WEIGHT(kg) N/A	SHEET 1/1

NOTE: ALL dimensions CM

Material: Aluminum 6061-T6 [SRAD]

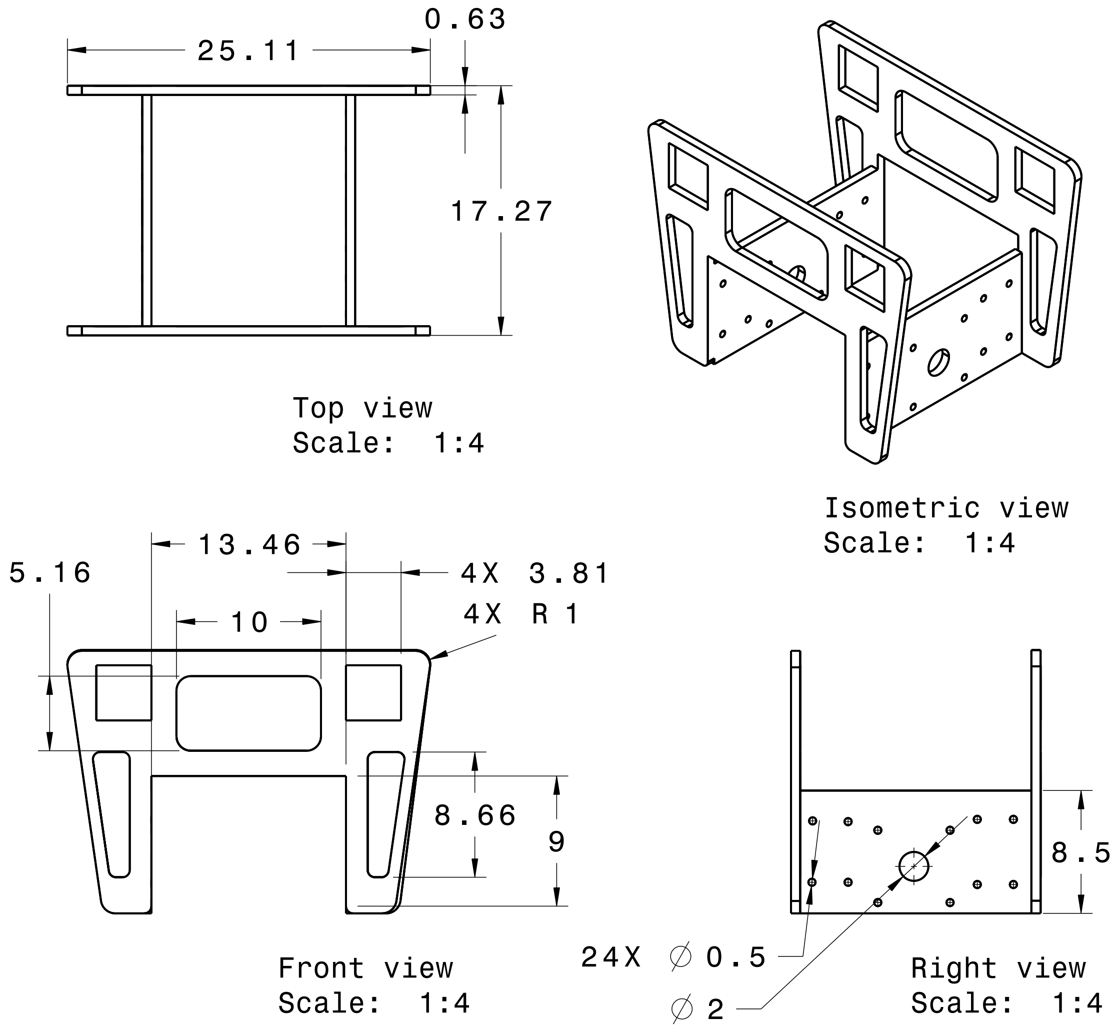

This drawing is our property. It can't be reproduced or communicated without our written agreement.		RYERSON INTERNATIONAL HYPERLOOP				
DRAWN BY MOHI KHAN	DATE 05/01/2019	DRAWING TITLE RH - POD - BULKHEAD				
CHECKED BY MOHI KHAN	DATE 05/01/2019	SIZE Letter	DRAWING NUMBER STR PODSTR2019007			REV A
DESIGNED BY MOHI KHAN	DATE 05/01/2019	SCALE 1:4	WEIGHT(kg) N/A		SHEET 1/1	

Top view
Scale: 1:3

Isometric view
Scale: 1:3

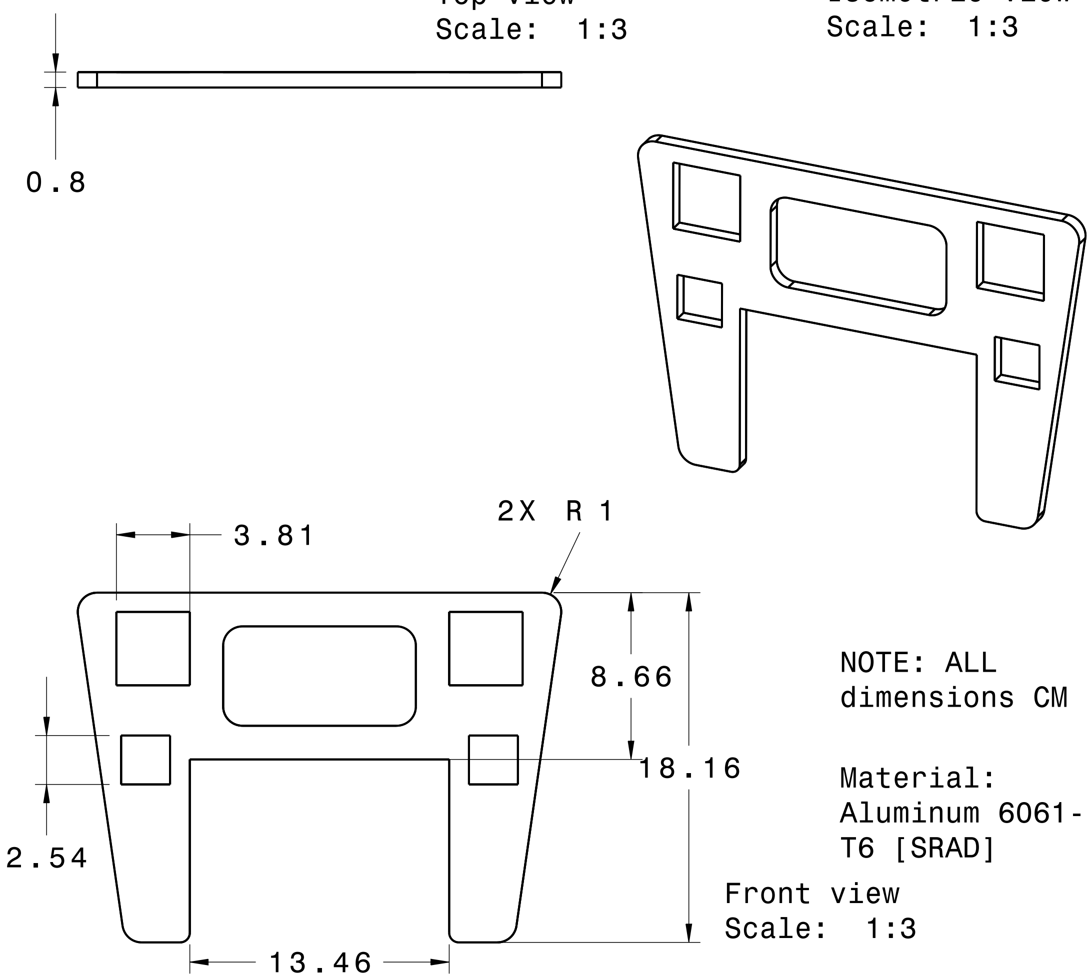

NOTE: ALL dimensions CM

Material: Aluminum 6061-T6 [SRAD]

Front view
Scale: 1:3

RYERSON INTERNATIONAL HYPERLOOP			
DRAWING TITLE: RH - POD - PRP BULKHEAD			
DRAWN BY: MOHI KHAN	DATE: 05/01/2019	SIZE: Letter	DRAWING NUMBER: STR PODSTR2019008
CHECKED BY: MOHI KHAN	DATE: 05/01/2019	REV: A	
DESIGNED BY: MOHI KHAN	DATE: 05/01/2019	SCALE: 1:3	WEIGHT(kg): N/A
SHEET: 1/1			

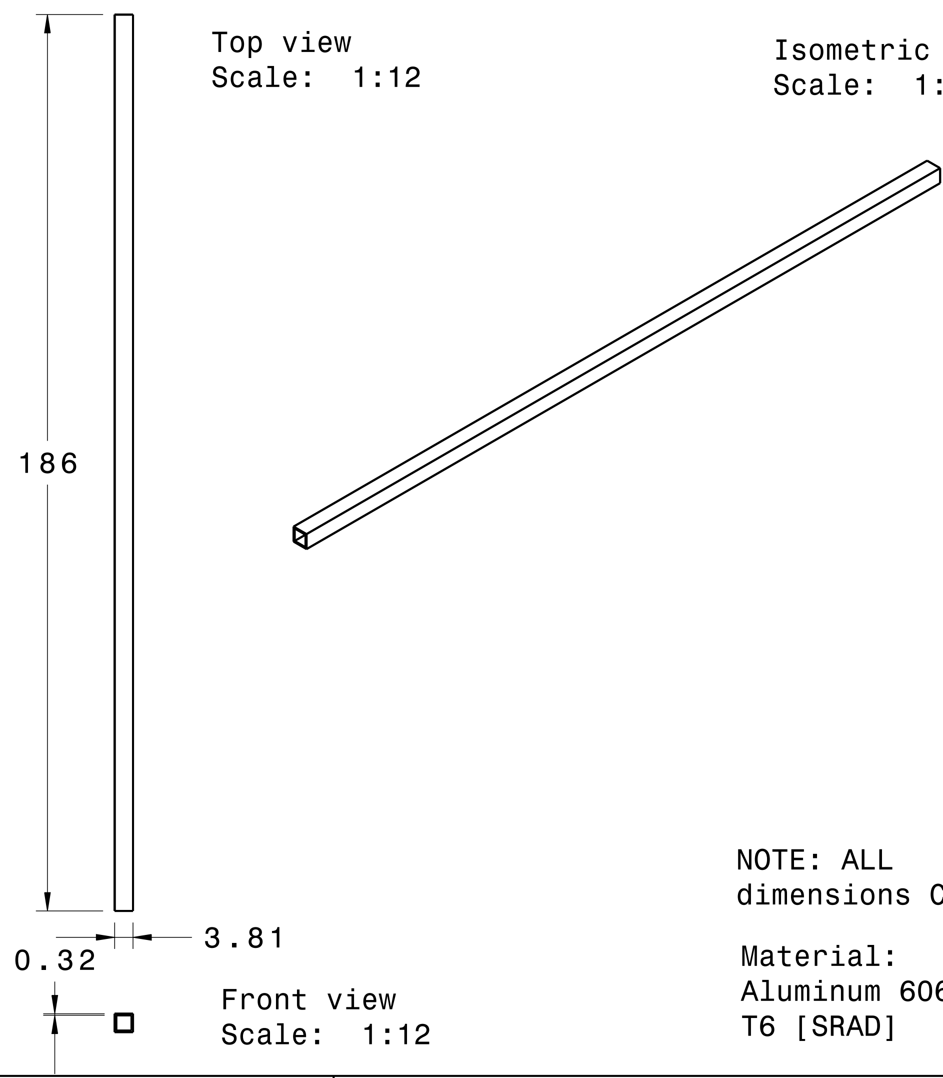

Top view
Scale: 1:12

Isometric view
Scale: 1:12

Front view
Scale: 1:12

NOTE: ALL dimensions CM

Material: Aluminum 6061-T6 [SRAD]

This drawing is our property. It can't be reproduced or communicated without our written agreement.		RYERSON INTERNATIONAL HYPERLOOP				
DRAWN BY MOHI KHAN	DATE 05/01/2019	DRAWING TITLE RH - POD - LCM				
CHECKED BY MOHI KHAN	DATE 05/01/2019	SIZE Letter	DRAWING NUMBER STR PODSTR2019009			REV A
DESIGNED BY MOHI KHAN	DATE 05/01/2019	SCALE 1:12	WEIGHT(kg) N/A		SHEET 1/1	

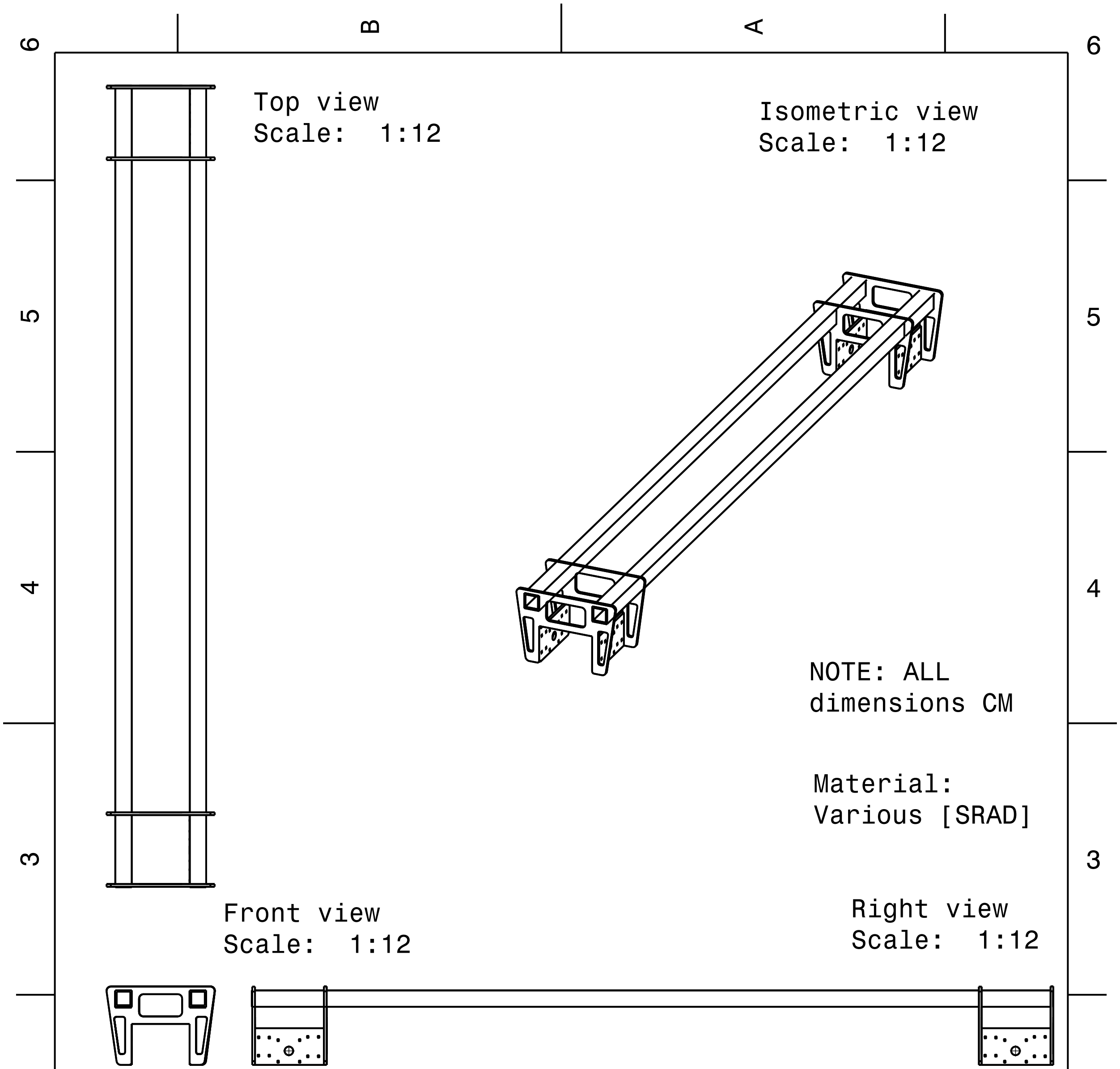

This drawing is our property. It can't be reproduced or communicated without our written agreement.		RYERSON INTERNATIONAL HYPERLOOP		
DRAWN BY MOHI KHAN	DATE 05/01/2019	DRAWING TITLE RH - POD - POD CHASSIS		
CHECKED BY MOHI KHAN	DATE 05/01/2019	SIZE Letter	DRAWING NUMBER STR PODSTR2019010	REV A
DESIGNED BY MOHI KHAN	DATE 05/01/2019	SCALE 1:12	WEIGHT(kg) N/A	SHEET 1/1

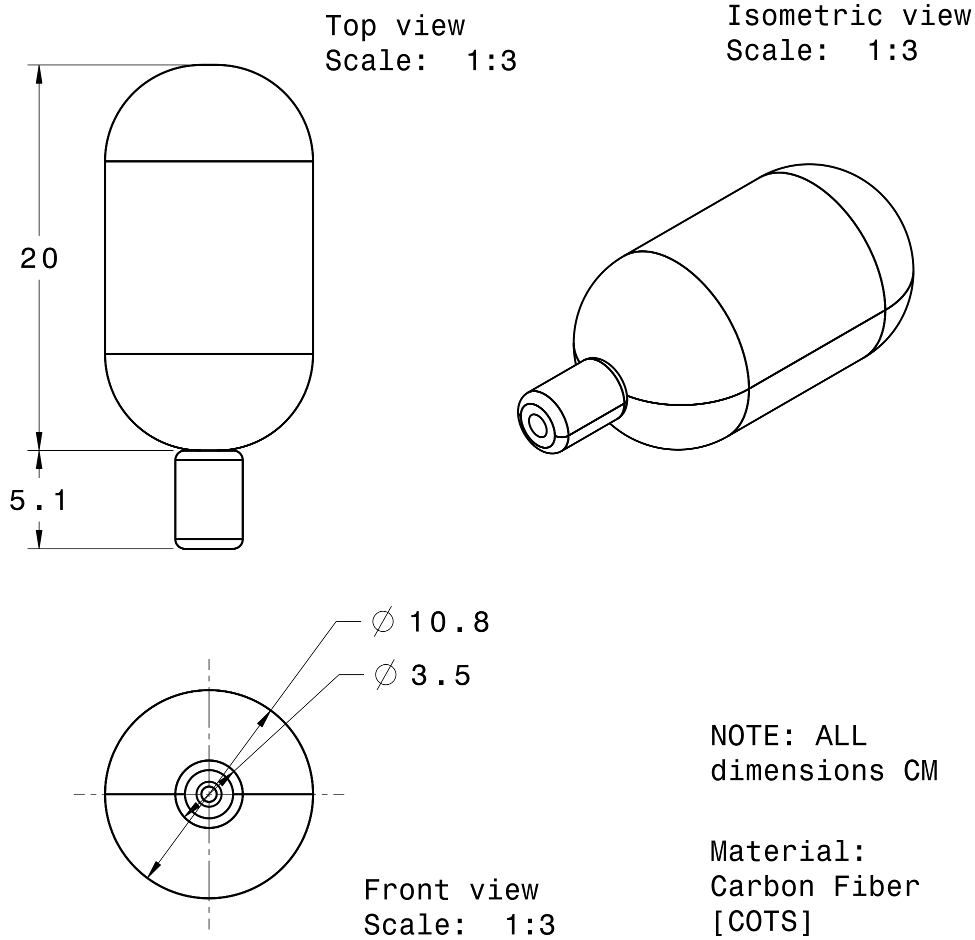

NOTE: ALL dimensions CM

Material:
Carbon Fiber
[COTS]

This drawing is our property. It can't be reproduced or communicated without our written agreement.		RYERSON INTERNATIONAL HYPERLOOP					
DRAWN BY MOHI KHAN	DATE 05/01/2019	DRAWING TITLE RH - POD - PRESSURE VESSEL					
CHECKED BY MOHI KHAN	DATE 05/01/2019	SIZE Letter	DRAWING NUMBER STR PODSTR2019011			REV A	
DESIGNED BY MOHI KHAN	DATE 05/01/2019	SCALE 1:3	WEIGHT(kg) N/A			SHEET 1/1	

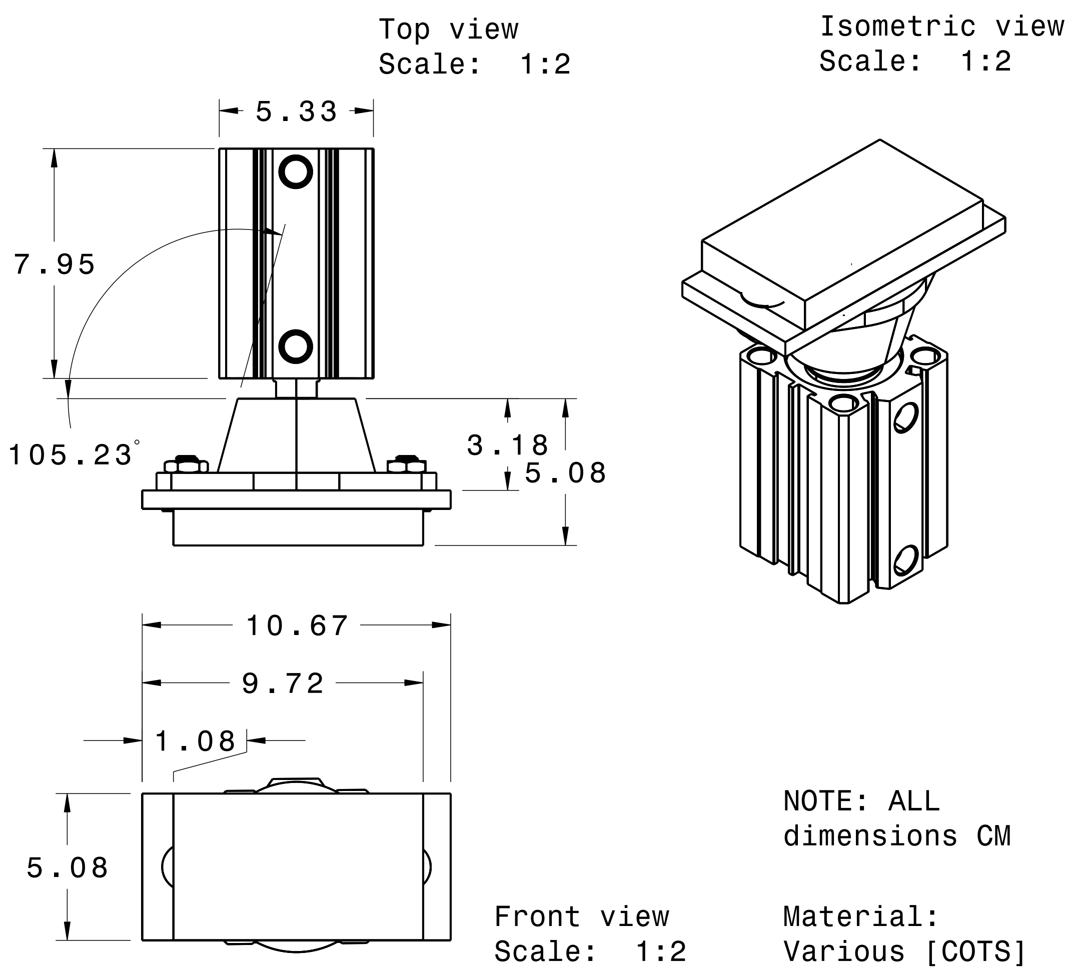

This drawing is our property. It can't be reproduced or communicated without our written agreement.		RYERSON INTERNATIONAL HYPERLOOP			
DRAWN BY MOHI KHAN	DATE 05/01/2019	DRAWING TITLE RH - POD - PNEUMATIC BRAKING PISTON			
CHECKED BY MOHI KHAN	DATE 05/01/2019	SIZE Letter	DRAWING NUMBER STR PODSTR2019012		REV A
DESIGNED BY MOHI KHAN	DATE 05/01/2019	SCALE 1:2	WEIGHT(kg) N/A		SHEET 1/1

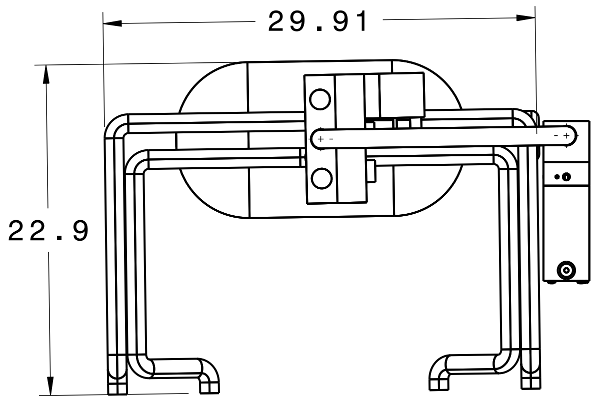

NOTE: ALL dimensions CM

Material: Various [SRAD]

Top view
Scale: 1:4

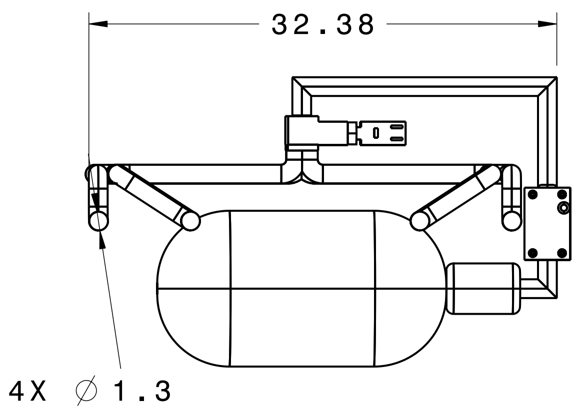

Front view
Scale: 1:4

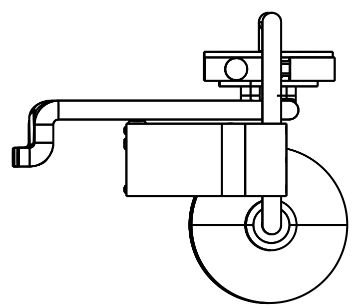

Right view
Scale: 1:4

This drawing is our property. It can't be reproduced or communicated without our written agreement.		RYERSON INTERNATIONAL HYPERLOOP	
DRAWN BY MOHI KHAN	DATE 05/01/2019	DRAWING TITLE RH - POD - POD BRAKING SYSTEM	
CHECKED BY MOHI KHAN	DATE 05/01/2019	SIZE Letter	DRAWING NUMBER STR PODSTR2019013 — REV A
DESIGNED BY MOHI KHAN	DATE 05/01/2019	SCALE 1:4	WEIGHT(kg) N/A — SHEET 1/1

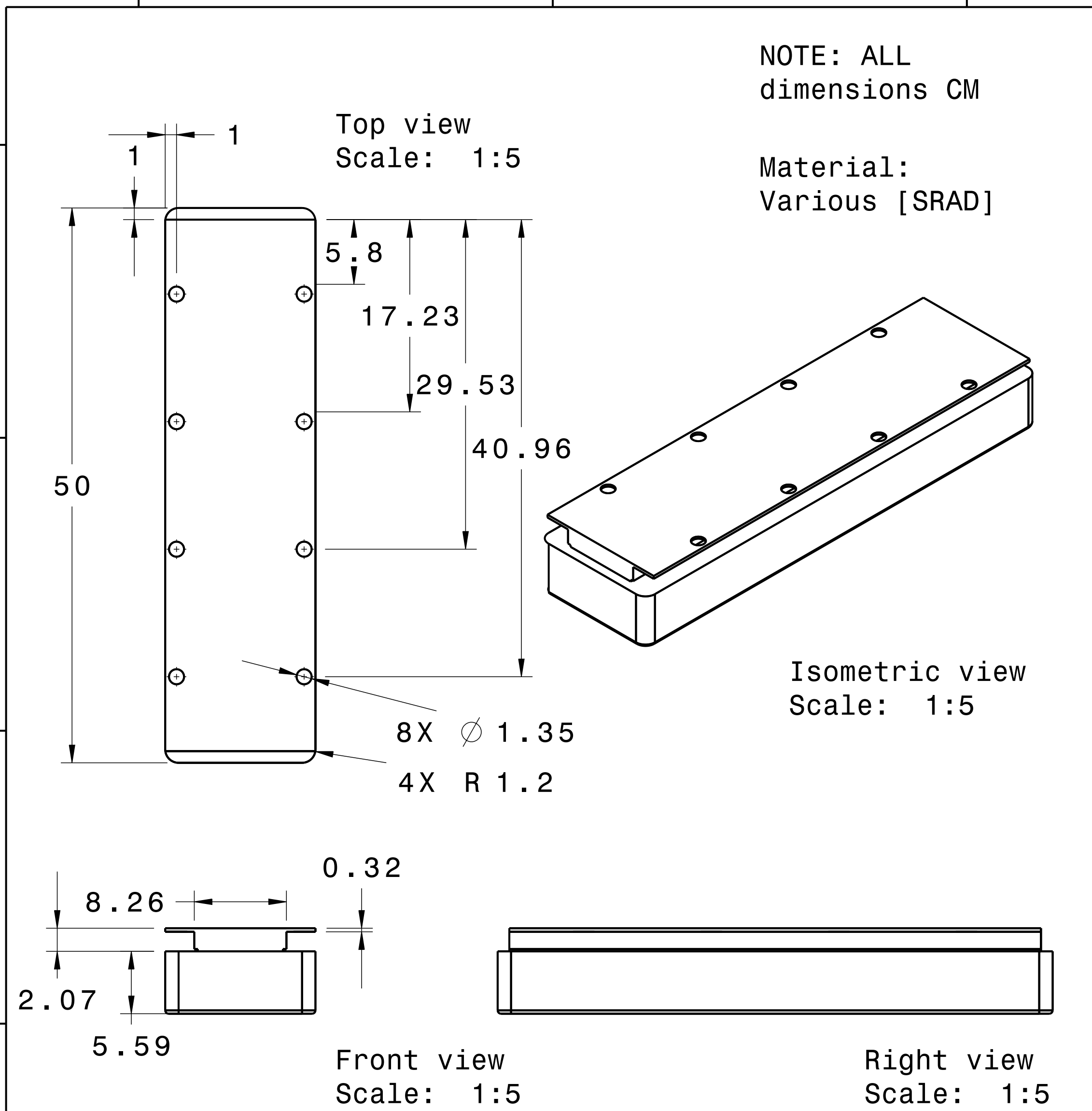

This drawing is our property. It can't be reproduced or communicated without our written agreement.		RYERSON INTERNATIONAL HYPERLOOP			
		DRAWING TITLE RH - POD - POD LIM			
DRAWN BY MOHI KHAN	DATE 05/01/2019				
CHECKED BY MOHI KHAN	DATE 05/01/2019	SIZE Letter	DRAWING NUMBER STR PODSTR2019014		REV A
DESIGNED BY MOHI KHAN	DATE 05/01/2019	SCALE 1:5	WEIGHT(kg) N/A		SHEET 1/1

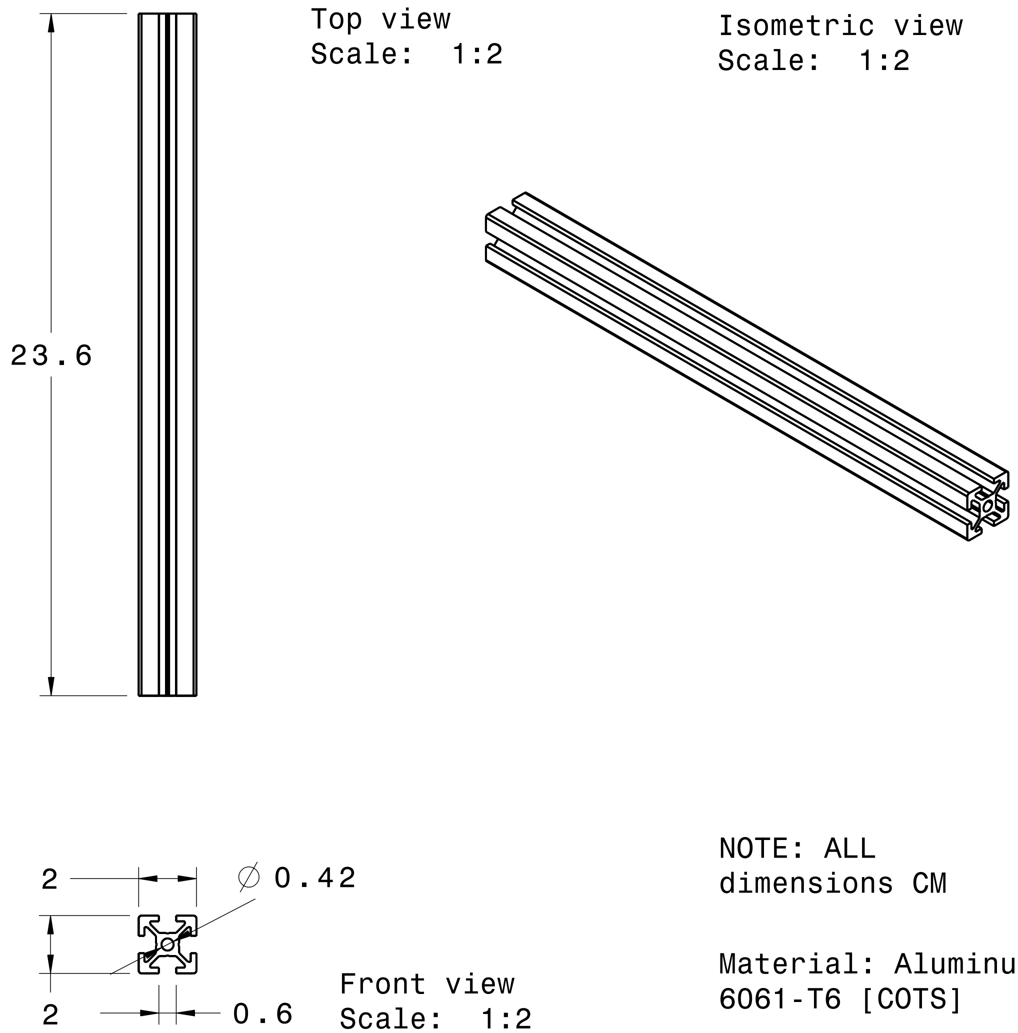

NOTE: ALL
dimensions CM

Material: Aluminum
6061-T6 [COTS]

RYERSON INTERNATIONAL HYPERLOOP

DRAWING TITLE
RH - POD - POD LIM EXTRUSION

DRAWN BY: MOHI KHAN	DATE: 05/01/2019		
CHECKED BY: MOHI KHAN	DATE: 05/01/2019	SIZE: Letter	DRAWING NUMBER: STR PODSTR2019015	REV: A
DESIGNED BY: MOHI KHAN	DATE: 05/01/2019	SCALE 1:2	WEIGHT(kg) N/A	SHEET 1/1

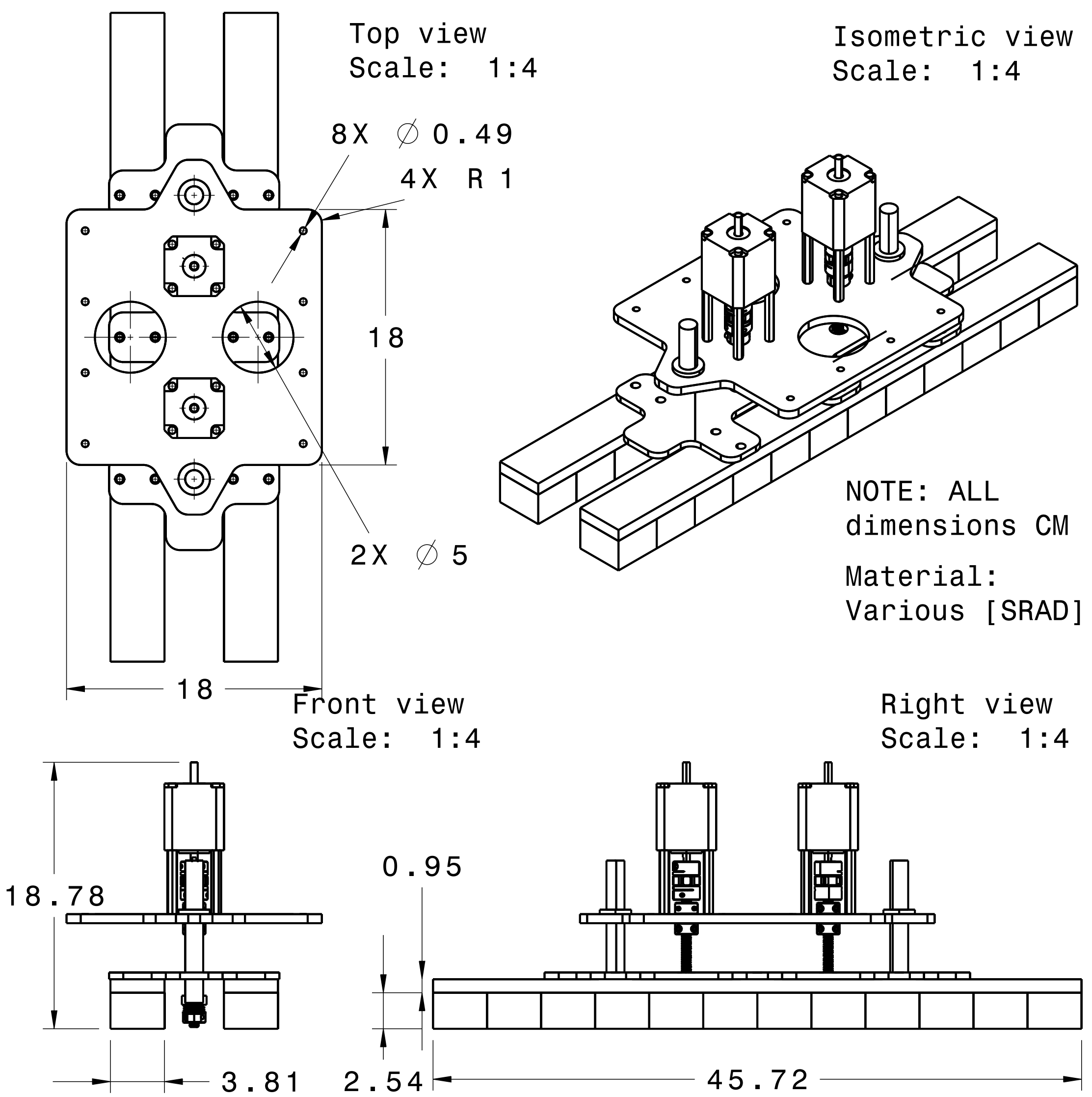

This drawing is our property. It can't be reproduced or communicated without our written agreement.		RYERSON INTERNATIONAL HYPERLOOP	
DRAWN BY MOHI KHAN	DATE 05/01/2019	DRAWING TITLE RH - POD - MAGLEV SYSTEM	
CHECKED BY MOHI KHAN	DATE 05/01/2019	SIZE Letter / DRAWING NUMBER STR PODSTR2019016	REV A
DESIGNED BY MOHI KHAN	DATE 05/01/2019	SCALE 1:4 / WEIGHT(kg) N/A	SHEET 1/1

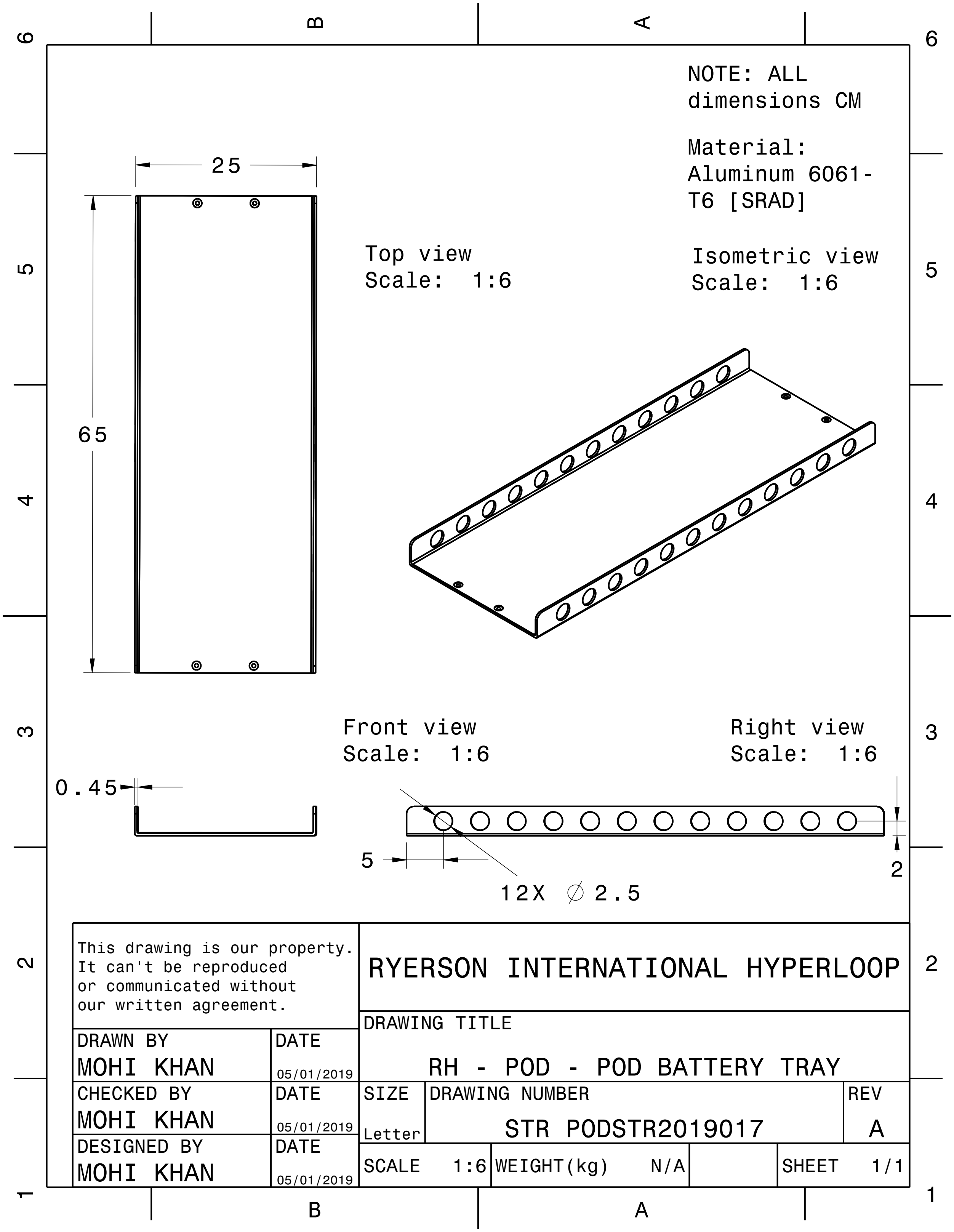
NOTE: ALL dimensions CM
Material: Aluminum 6061-T6 [SRAD]
Top view Scale: 1:6
Isometric view Scale: 1:6
Front view Scale: 1:6
Right view Scale: 1:6
25
65
0.45
5
2
12X ∅ 2.5
This drawing is our property. It can't be reproduced or communicated without our written agreement.
RYERSON INTERNATIONAL HYPERLOOP
DRAWING TITLE
RH - POD - POD BATTERY TRAY
DRAWN BY
MOHI KHAN
DATE
05/01/2019
CHECKED BY
MOHI KHAN
DATE
05/01/2019
DESIGNED BY
MOHI KHAN
DATE
05/01/2019
SIZE
Letter
DRAWING NUMBER
STR PODSTR2019017
REV
A
SCALE 1:6
WEIGHT(kg) N/A
SHEET 1/1

NOTE: ALL dimensions CM

Material: Various [SRAD]

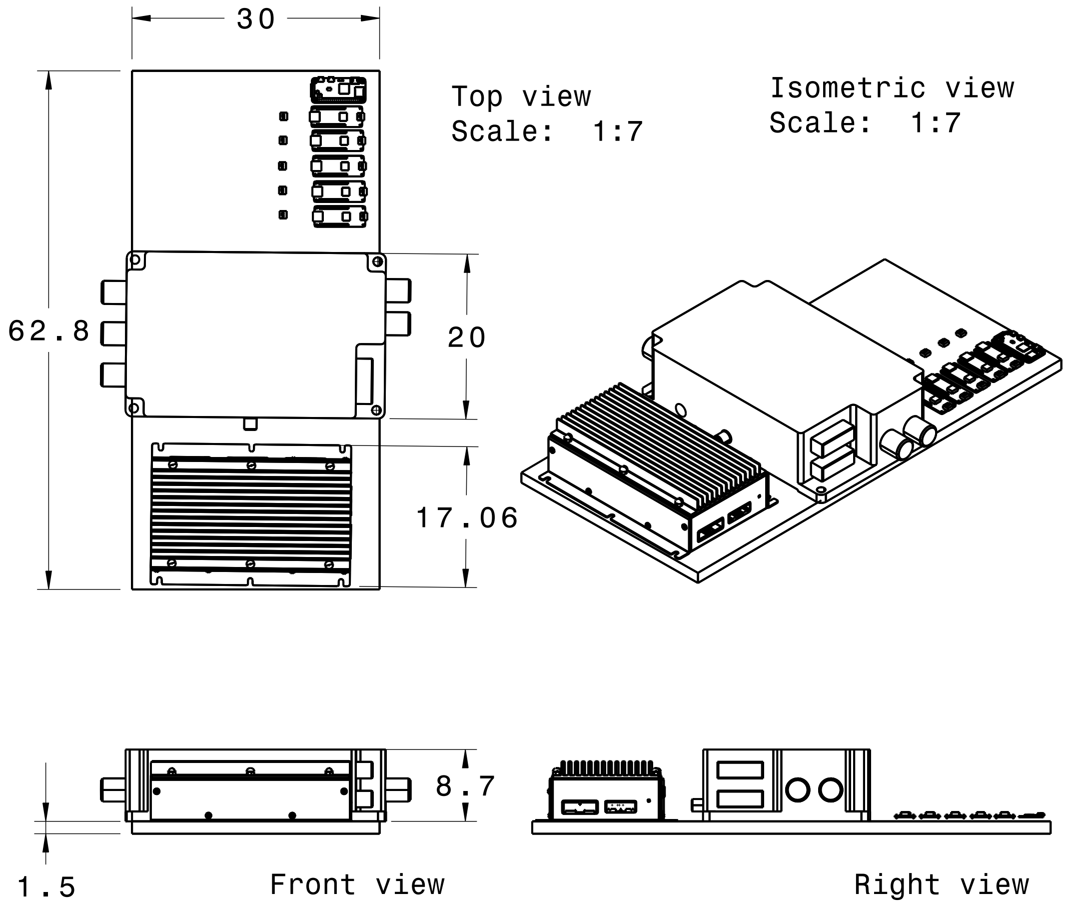

Top view
Scale: 1:7

Isometric view
Scale: 1:7

Front view
Scale: 1:7

Right view
Scale: 1:7

This drawing is our property. It can't be reproduced or communicated without our written agreement.		RYERSON INTERNATIONAL HYPERLOOP				
DRAWN BY MOHI KHAN	DATE 05/01/2019	DRAWING TITLE RH - POD - POD GNC SYSTEM				
CHECKED BY MOHI KHAN	DATE 05/01/2019	SIZE Letter	DRAWING NUMBER STR PODSTR2019018			REV A
DESIGNED BY MOHI KHAN	DATE 05/01/2019	SCALE 1:7	WEIGHT(kg) N/A		SHEET 1/1	

Appendix A.4 Modular Test Rig Engineering Drawings

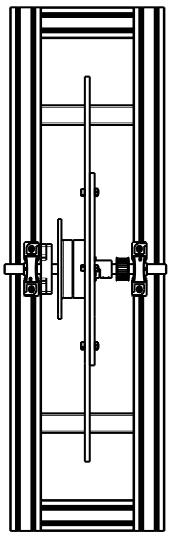

Top view
Scale: 1:15

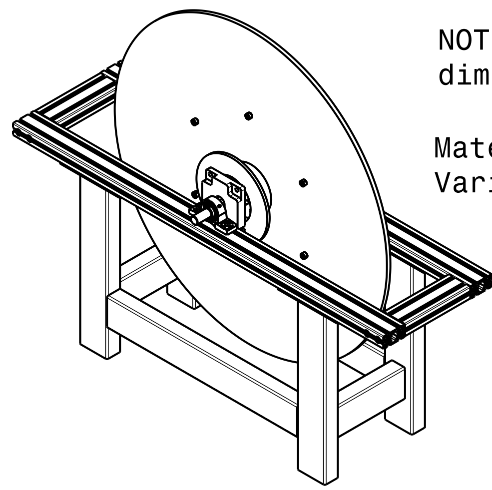

Isometric view
Scale: 1:15

NOTE: ALL dimensions CM

Material:
Various [SRAD]

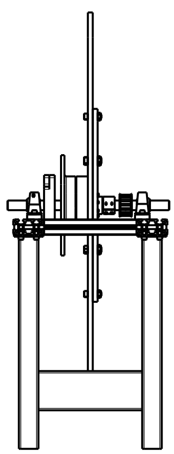

Front view
Scale: 1:15

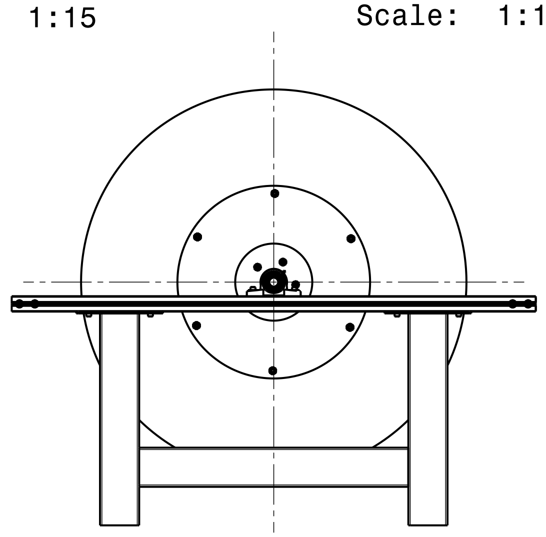

Right view
Scale: 1:15

RYERSON INTERNATIONAL HYPERLOOP

DRAWN BY MOHI KHAN	DATE 05/01/2019	DRAWING TITLE RH - MTR - MTR ASSEMBLY	
CHECKED BY MOHI KHAN	DATE 05/01/2019	SIZE Letter	DRAWING NUMBER MTR STR2019001 — REV A
DESIGNED BY MOHI KHAN	DATE 05/01/2019	SCALE 1:15	WEIGHT(kg) N/A — SHEET 1/1

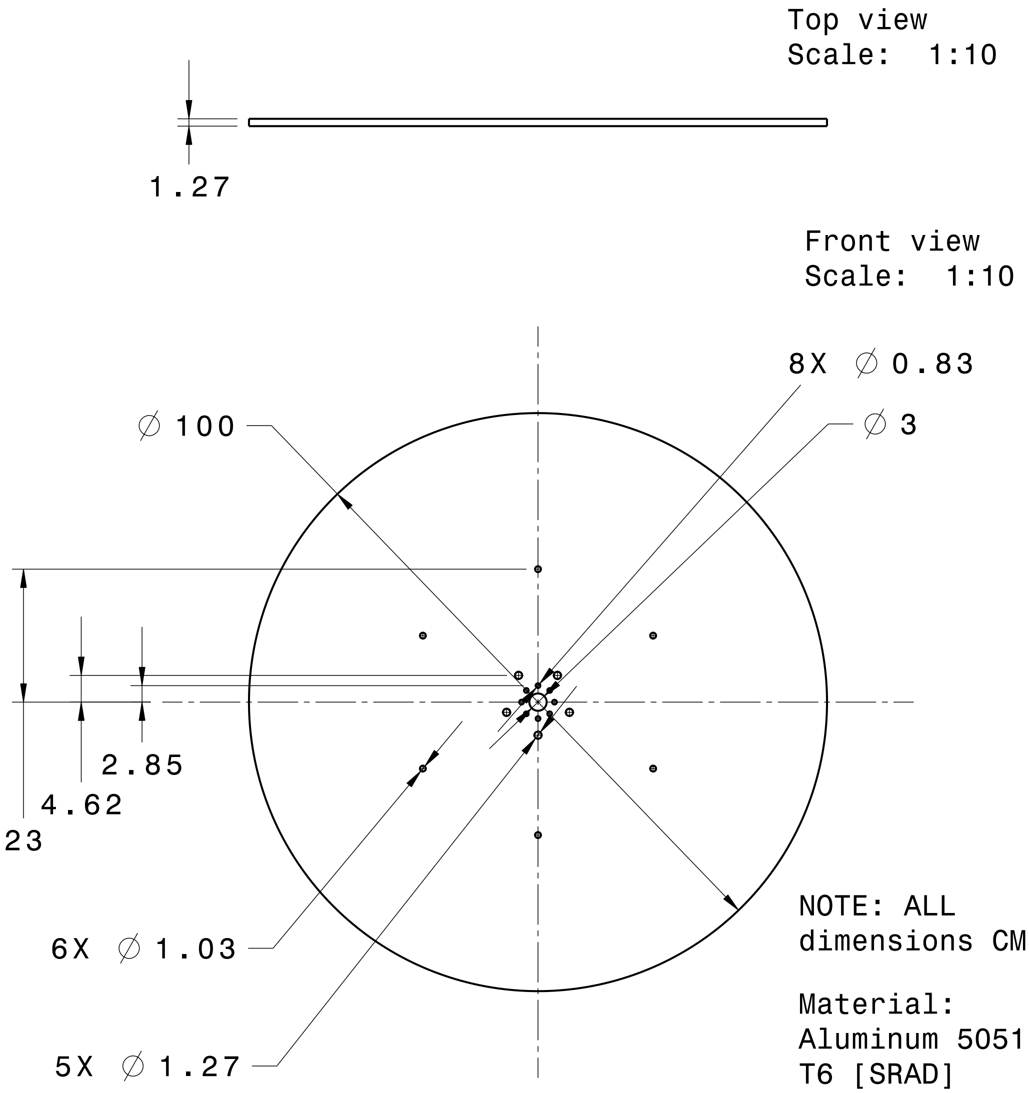

NOTE: ALL dimensions CM

Material:
Aluminum 5051-T6 [SRAD]

This drawing is our property. It can't be reproduced or communicated without our written agreement.

RYERSON INTERNATIONAL HYPERLOOP

DRAWN BY: MOHI KHAN	DATE: 05/01/2019	DRAWING TITLE: RH - MTR - TRACK	
CHECKED BY: MOHI KHAN	DATE: 05/01/2019	SIZE: Letter	DRAWING NUMBER: MTR STR2019002 — REV: A
DESIGNED BY: MOHI KHAN	DATE: 05/01/2019	SCALE 1:10	WEIGHT(kg) N/A — SHEET 1/1

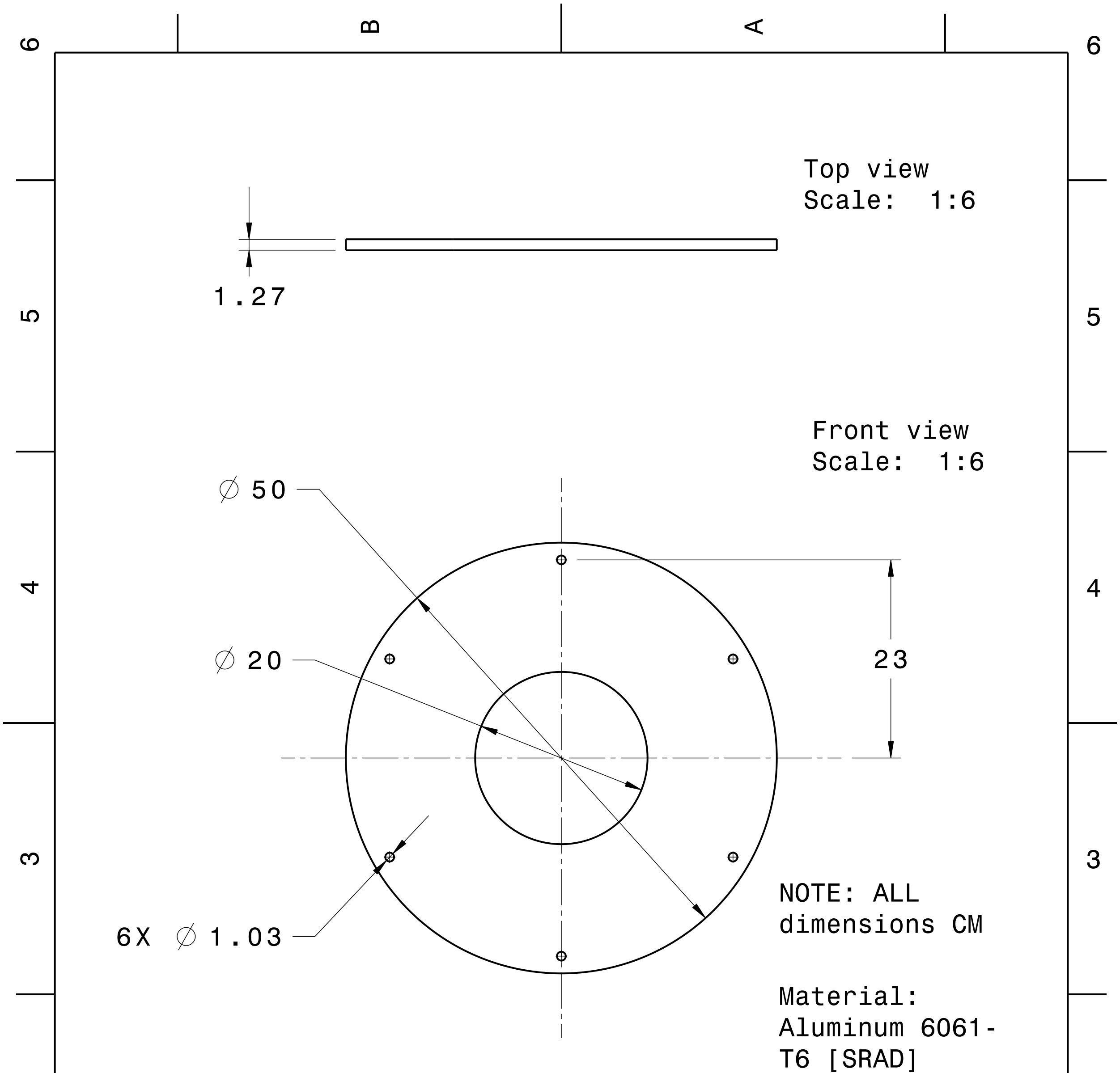

This drawing is our property. It can't be reproduced or communicated without our written agreement.

RYERSON INTERNATIONAL HYPERLOOP

DRAWN BY: MOHI KHAN	DATE: 05/01/2019	DRAWING TITLE: RH - MTR - STIFFNER PLATE	
CHECKED BY: MOHI KHAN	DATE: 05/01/2019	SIZE: Letter	DRAWING NUMBER: MTR STR2019003	REV: A
DESIGNED BY: MOHI KHAN	DATE: 05/01/2019	SCALE 1:6	WEIGHT(kg) N/A	SHEET 1/1

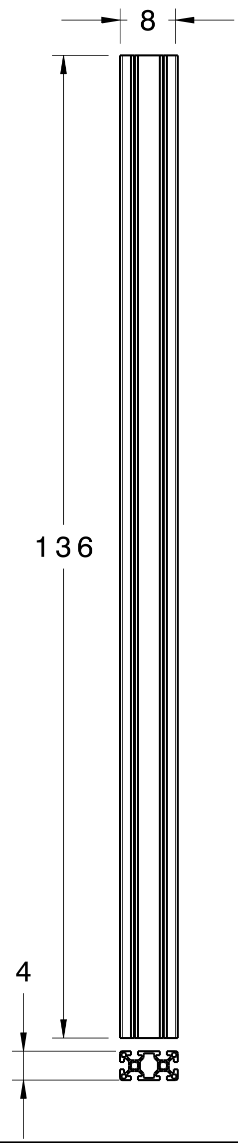

Top view
Scale: 1:8

Front view
Scale: 1:8

NOTE: ALL
dimensions CM

Material:
Aluminum 6061-
T6 [COTS]

This drawing is our property. It can't be reproduced or communicated without our written agreement.		RYERSON INTERNATIONAL HYPERLOOP			
DRAWN BY MOHI KHAN	DATE 05/01/2019	DRAWING TITLE RH - MTR - MAIN EXTRUSION			
CHECKED BY MOHI KHAN	DATE 05/01/2019	SIZE Letter	DRAWING NUMBER MTR STR2019004		REV A
DESIGNED BY MOHI KHAN	DATE 05/01/2019	SCALE 1:8	WEIGHT(kg) N/A		SHEET 1/1

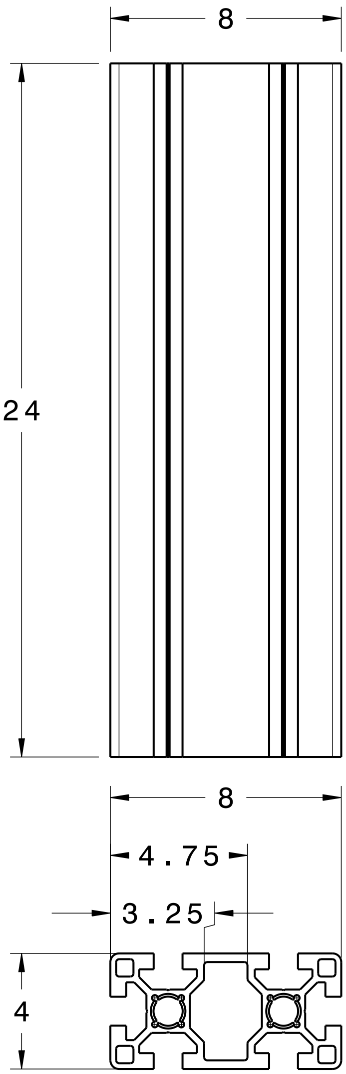

Top view
Scale: 1:2

NOTE: ALL dimensions CM

Material: Aluminum 6061-T6 [COTS]

Front view
Scale: 1:2

This drawing is our property. It can't be reproduced or communicated without our written agreement.		RYERSON INTERNATIONAL HYPERLOOP			
DRAWN BY MOHI KHAN	DATE 05/01/2019	DRAWING TITLE RH - MTR - SIDE EXTRUSION			
CHECKED BY MOHI KHAN	DATE 05/01/2019	SIZE Letter	DRAWING NUMBER MTR STR2019005		REV A
DESIGNED BY MOHI KHAN	DATE 05/01/2019	SCALE 1:2	WEIGHT(kg) N/A		SHEET 1/1

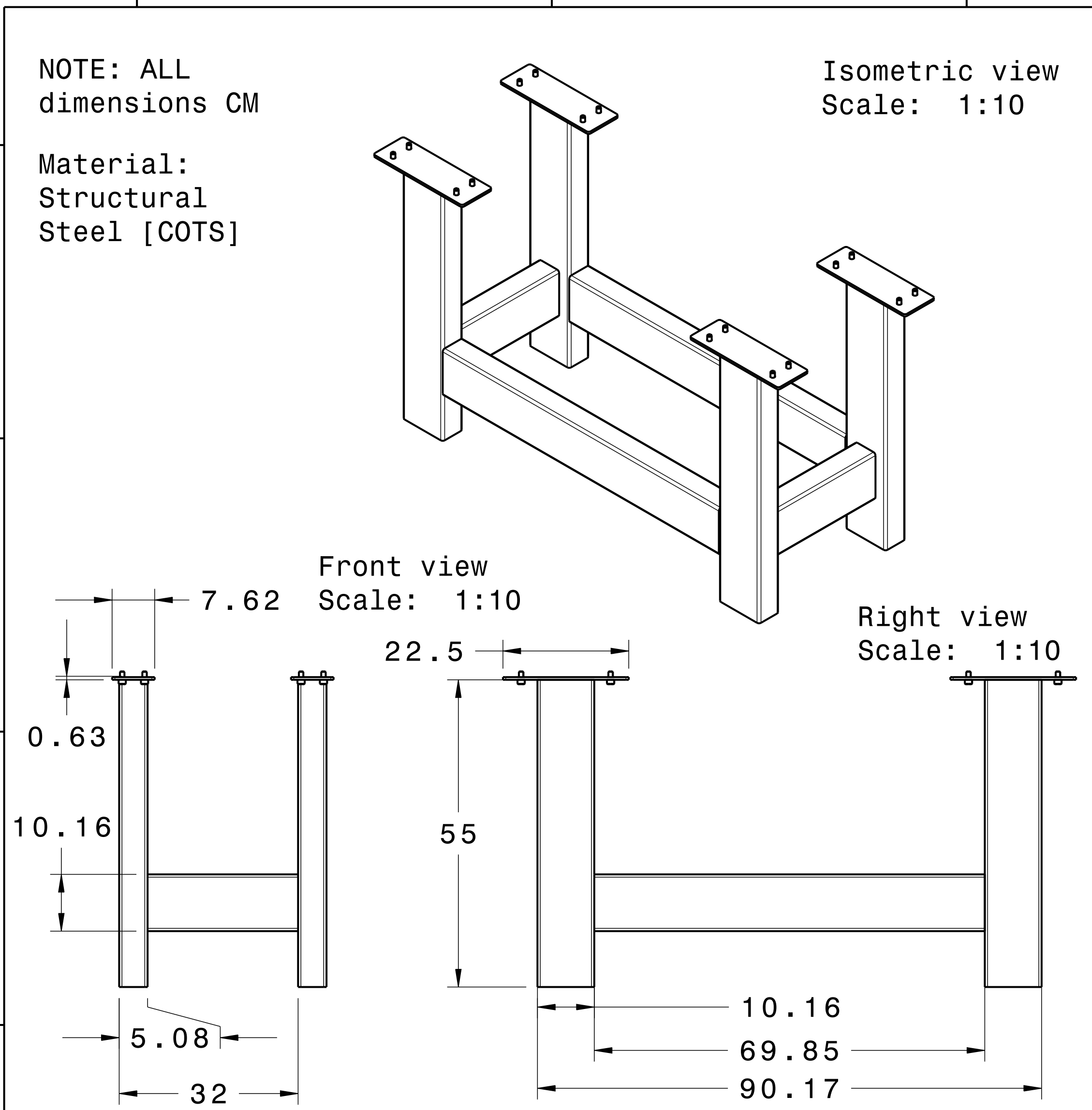

This drawing is our property. It can't be reproduced or communicated without our written agreement.		RYERSON INTERNATIONAL HYPERLOOP
DRAWN BY MOHI KHAN	DATE 05/01/2019	DRAWING TITLE RH - MTR - SUPPORT FRAME
CHECKED BY MOHI KHAN	DATE 05/01/2019	SIZE: Letter; DRAWING NUMBER: MTR STR2019006; REV: A
DESIGNED BY MOHI KHAN	DATE 05/01/2019	SCALE 1:10; WEIGHT(kg) N/A; SHEET 1/1

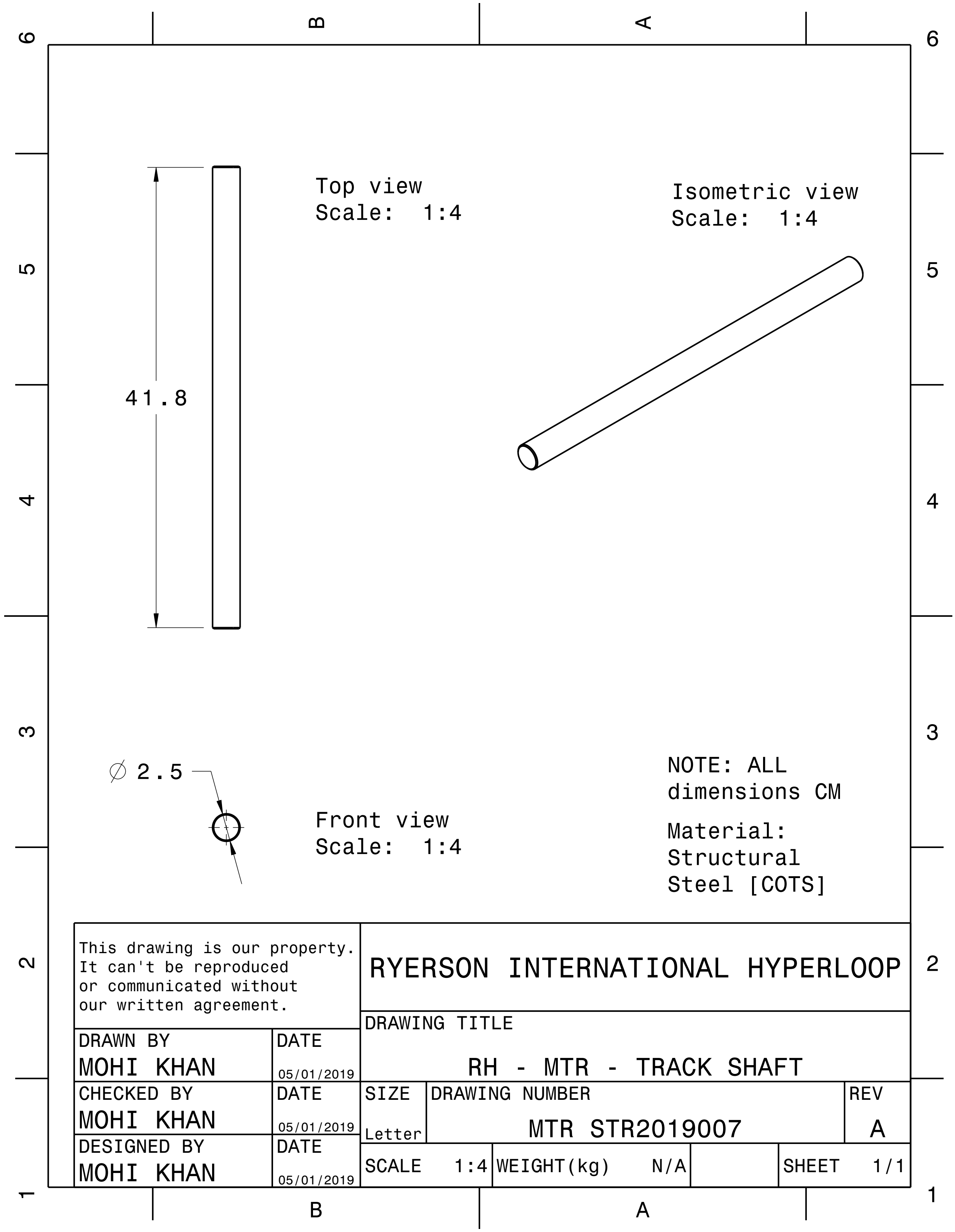
Top view
Scale: 1:4
41.8
Isometric view
Scale: 1:4
∅ 2.5
Front view
Scale: 1:4
NOTE: ALL dimensions CM
Material: Structural Steel [COTS]
This drawing is our property. It can't be reproduced or communicated without our written agreement.
RYERSON INTERNATIONAL HYPERLOOP
DRAWN BY
MOHI KHAN
DATE
05/01/2019
CHECKED BY
MOHI KHAN
DATE
05/01/2019
DESIGNED BY
MOHI KHAN
DATE
05/01/2019
DRAWING TITLE
RH - MTR - TRACK SHAFT
SIZE
Letter
DRAWING NUMBER
MTR STR2019007
REV
A
SCALE 1:4
WEIGHT(kg) N/A
SHEET 1/1

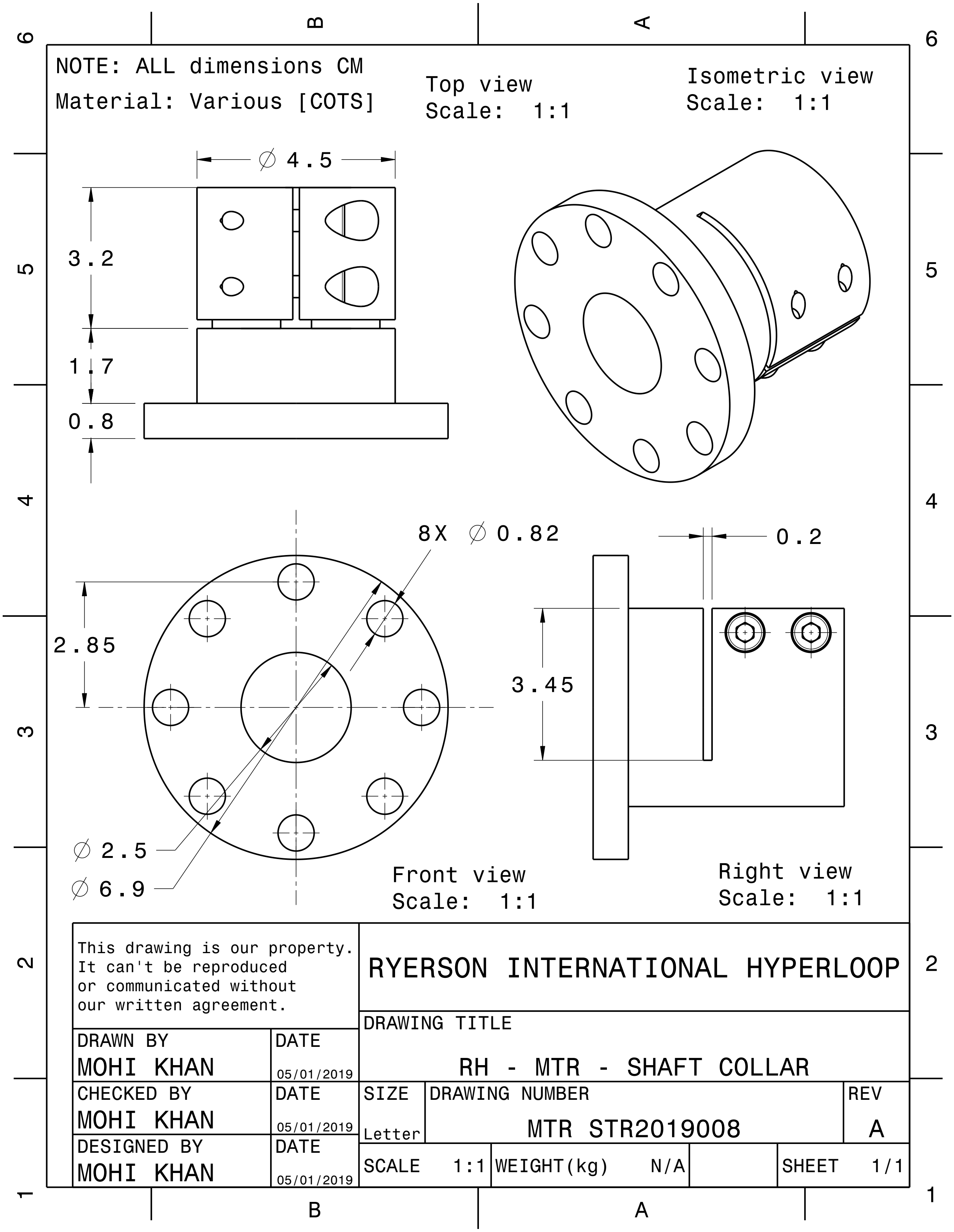
NOTE: ALL dimensions CM
Material: Various [COTS]
Top view
Scale: 1:1
Isometric view
Scale: 1:1
∅ 4.5
3.2
1.7
0.8
8X ∅ 0.82
0.2
2.85
3.45
∅ 2.5
∅ 6.9
Front view
Scale: 1:1
Right view
Scale: 1:1
This drawing is our property. It can't be reproduced or communicated without our written agreement.
RYERSON INTERNATIONAL HYPERLOOP
DRAWING TITLE
RH - MTR - SHAFT COLLAR
DRAWN BY
MOHI KHAN
DATE
05/01/2019
CHECKED BY
MOHI KHAN
DATE
05/01/2019
DESIGNED BY
MOHI KHAN
DATE
05/01/2019
SIZE
Letter
DRAWING NUMBER
MTR STR2019008
REV
A
SCALE 1:1
WEIGHT(kg) N/A
SHEET 1/1

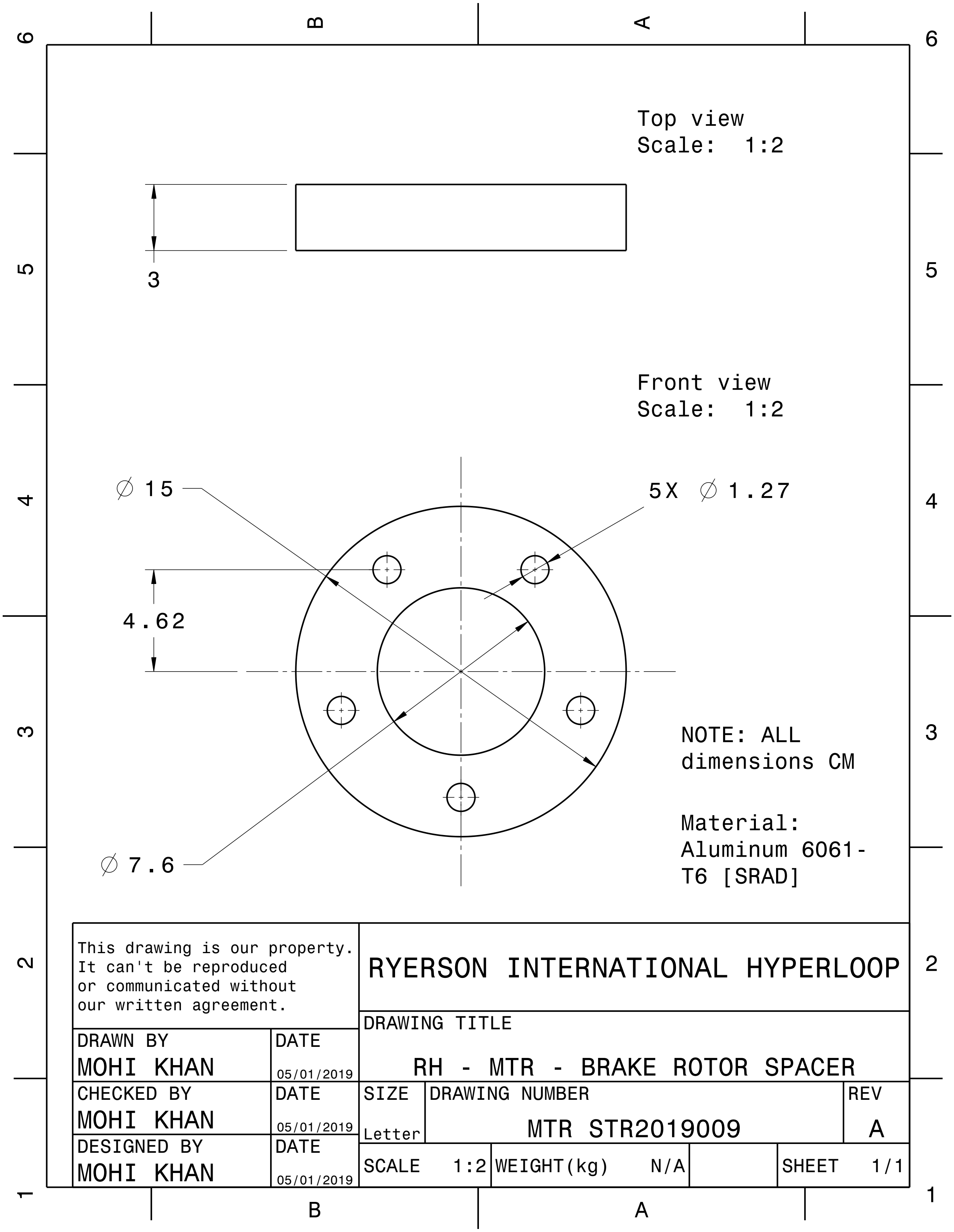
Top view
Scale: 1:2
3
Front view
Scale: 1:2
∅ 15
5X ∅ 1.27
4.62
∅ 7.6
NOTE: ALL dimensions CM
Material: Aluminum 6061-T6 [SRAD]
This drawing is our property. It can't be reproduced or communicated without our written agreement.
RYERSON INTERNATIONAL HYPERLOOP
DRAWING TITLE
RH - MTR - BRAKE ROTOR SPACER
DRAWN BY
MOHI KHAN
DATE
05/01/2019
CHECKED BY
MOHI KHAN
DATE
05/01/2019
DESIGNED BY
MOHI KHAN
DATE
05/01/2019
SIZE
Letter
DRAWING NUMBER
MTR STR2019009
REV
A
SCALE 1:2
WEIGHT(kg) N/A
SHEET 1/1

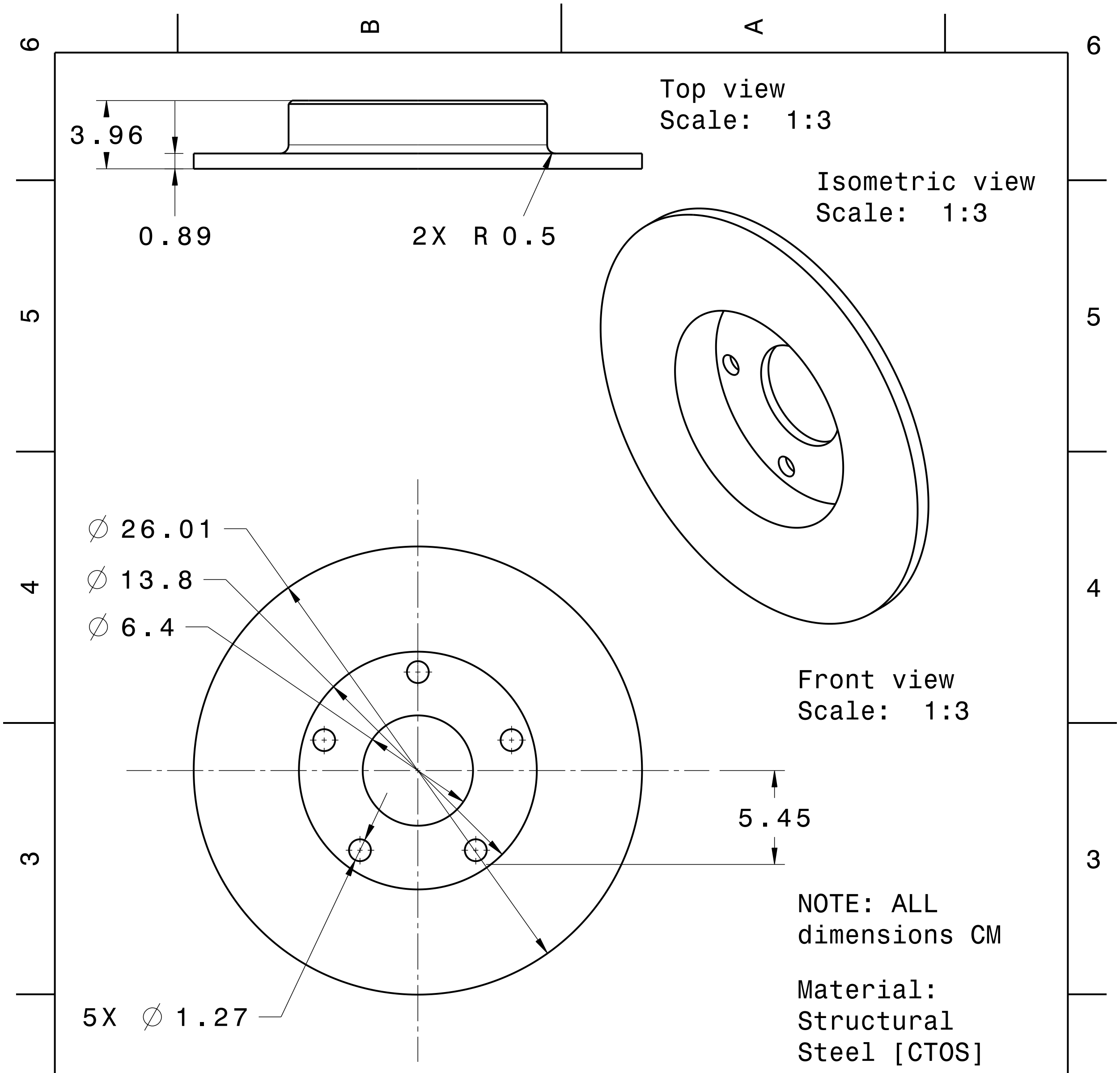

This drawing is our property. It can't be reproduced or communicated without our written agreement.		RYERSON INTERNATIONAL HYPERLOOP			
DRAWN BY MOHI KHAN	DATE 05/01/2019	DRAWING TITLE RH - MTR - BRAKE ROTOR			
CHECKED BY MOHI KHAN	DATE 05/01/2019	SIZE Letter	DRAWING NUMBER MTR STR2019010		REV A
DESIGNED BY MOHI KHAN	DATE 05/01/2019	SCALE 1:3	WEIGHT(kg) N/A		SHEET 1/1

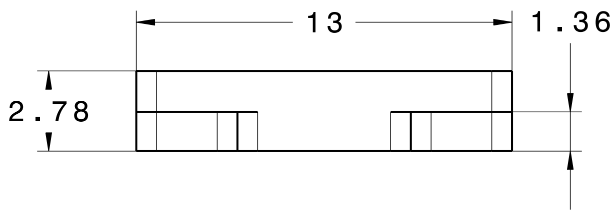

Top view
Scale: 1:2

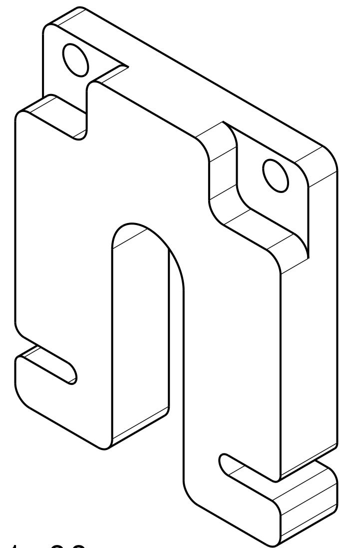

Isometric view
Scale: 1:2

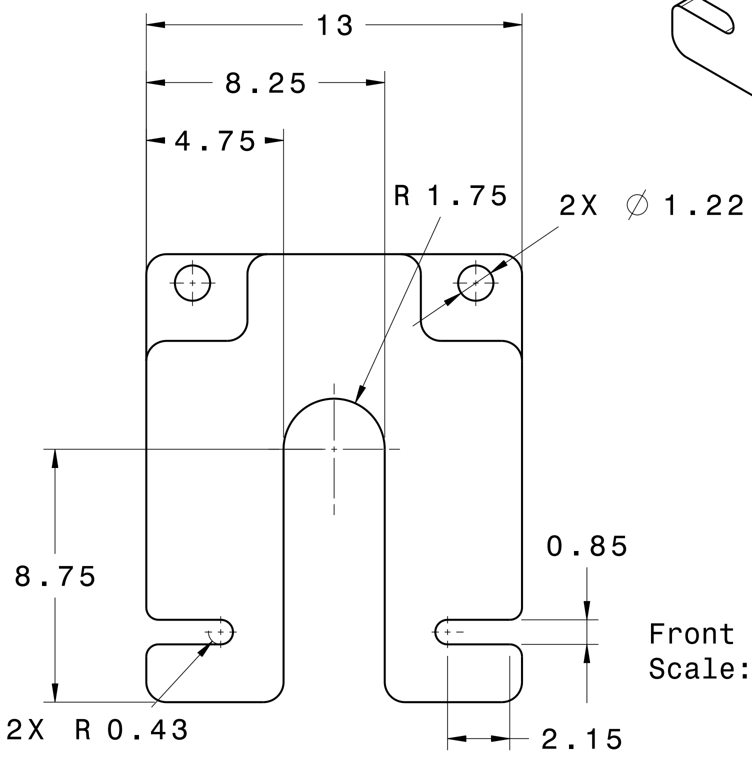

Front view
Scale: 1:2

NOTE: ALL dimensions CM

Material: Aluminum 6061-T6 [SRAD]

RYERSON INTERNATIONAL HYPERLOOP

DRAWN BY: MOHI KHAN	DATE: 05/01/2019	DRAWING TITLE: RH - MTR - BRAKE CALIPER BRACKET	
CHECKED BY: MOHI KHAN	DATE: 05/01/2019	SIZE: Letter	DRAWING NUMBER: MTR STR2019011 / REV: A
DESIGNED BY: MOHI KHAN	DATE: 05/01/2019	SCALE 1:2	WEIGHT(kg) N/A / SHEET 1/1

Appendix A.5 LCM Load Case I (Pod Staging) Analysis Report

Project*

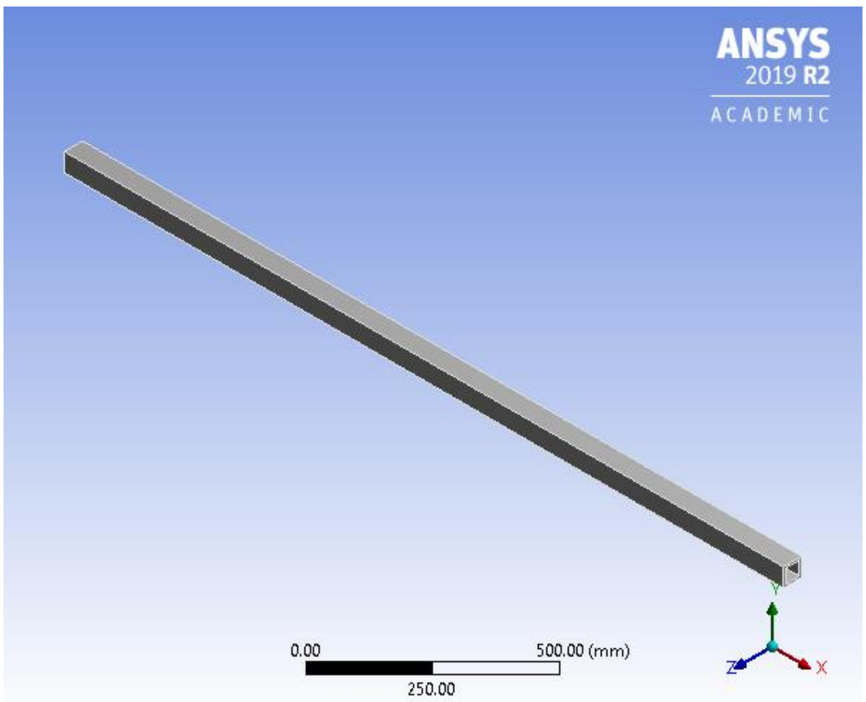

Contents

Units

TABLE 1

Unit System	Metric (mm, kg, N, s, mV, mA) Degrees rad/s Celsius
Angle	Degrees
Rotational Velocity	rad/s
Temperature	Celsius

Model (C4)

Geometry

TABLE 2
Model (C4) > Geometry

Object Name	*Geometry*
State	Fully Defined
Definition	
Source	C:\Users\DIAPM599\OneDrive - Dentsply Sirona\Desktop\ANSYS Analysis\LCM_files\dp0\Geom\DM\Geom.scdoc
Type	SpaceClaim
Length Unit	Meters
Element Control	Program Controlled
Display Style	Body Color
Bounding Box	
Length X	2000. mm
Length Y	50.8 mm
Length Z	50.8 mm

Properties	
Volume	2.2581e+006 mm³
Mass	6.2548 kg
Scale Factor Value	1.
Statistics	
Bodies	1
Active Bodies	1
Nodes	2261
Elements	1143
Mesh Metric	None
Update Options	
Assign Default Material	No
Basic Geometry Options	
Solid Bodies	Yes
Surface Bodies	Yes
Line Bodies	Yes
Parameters	Independent
Parameter Key	
Attributes	Yes
Attribute Key	
Named Selections	Yes
Named Selection Key	
Material Properties	Yes
Advanced Geometry Options	
Use Associativity	Yes
Coordinate Systems	Yes
Coordinate System Key	
Reader Mode Saves Updated File	No
Use Instances	Yes
Smart CAD Update	Yes
Compare Parts On Update	No
Analysis Type	3-D
Mixed Import Resolution	None
Clean Bodies On Import	No
Stitch Surfaces On Import	None
Decompose Disjoint Geometry	Yes
Enclosure and Symmetry Processing	Yes

TABLE 3
Model (C4) > Geometry > Parts

Object Name	*Geom\PartBody*
State	Meshed
Graphics Properties	

Visible	Yes
Transparency	1
Definition	
Suppressed	No
Stiffness Behavior	Flexible
Coordinate System	Default Coordinate System
Reference Temperature	By Environment
Treatment	None
Material	
Assignment	Aluminum Alloy
Nonlinear Effects	Yes
Thermal Strain Effects	Yes
Bounding Box	
Length X	2000. mm
Length Y	50.8 mm
Length Z	50.8 mm
Properties	
Volume	2.2581e+006 mm³
Mass	6.2548 kg
Centroid X	-1000. mm
Centroid Y	25.4 mm
Centroid Z	25.4 mm
Moment of Inertia Ip1	4203.5 kg·mm²
Moment of Inertia Ip2	2.087e+006 kg·mm²
Moment of Inertia Ip3	2.087e+006 kg·mm²
Statistics	
Nodes	2261
Elements	1143
Mesh Metric	None
CAD Attributes	
PartTolerance:	0.00000001
Color:175.143.175	

FIGURE 1
Model (C4) > Geometry > Figure

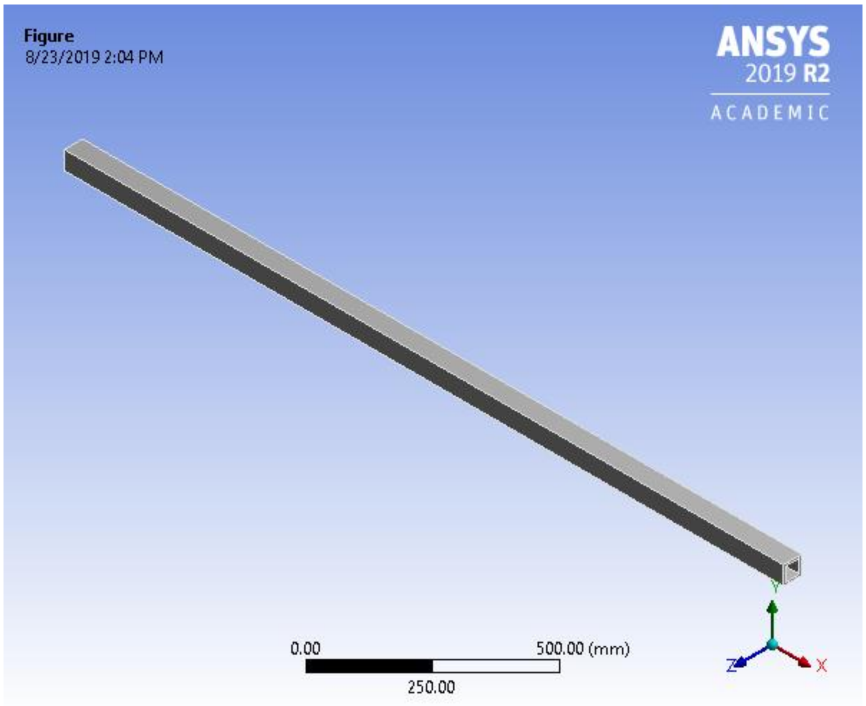

TABLE 4
Model (C4) > Materials

Object Name	*Materials*
State	Fully Defined
Statistics	
Materials	2
Material Assignments	0

Coordinate Systems

TABLE 5
Model (C4) > Coordinate Systems > Coordinate System

Object Name	*Global Coordinate System*
State	Fully Defined
Definition	
Type	Cartesian
Coordinate System ID	0.
Origin	
Origin X	0. mm

Origin Y	0. mm
Origin Z	0. mm
Directional Vectors	
X Axis Data	[1. 0. 0.]
Y Axis Data	[0. 1. 0.]
Z Axis Data	[0. 0. 1.]

Mesh

TABLE 6
Model (C4) > Mesh

Object Name	*Mesh*
State	Solved
Display	
Display Style	Use Geometry Setting
Defaults	
Physics Preference	Mechanical
Element Order	Program Controlled
Element Size	Default
Sizing	
Use Adaptive Sizing	Yes
Resolution	Default (2)
Mesh Defeaturing	Yes
Defeature Size	Default
Transition	Fast
Span Angle Center	Fine
Initial Size Seed	Assembly
Bounding Box Diagonal	2001.3 mm
Average Surface Area	71346 mm²
Minimum Edge Length	38.1 mm
Quality	
Check Mesh Quality	Yes, Errors
Error Limits	Standard Mechanical
Target Quality	Default (0.050000)
Smoothing	Medium
Mesh Metric	None
Inflation	
Use Automatic Inflation	None
Inflation Option	Smooth Transition
Transition Ratio	0.272
Maximum Layers	5
Growth Rate	1.2
Inflation Algorithm	Pre
View Advanced Options	No
Advanced	
Number of CPUs for Parallel Part Meshing	Program Controlled
Straight Sided Elements	No
Rigid Body Behavior	Dimensionally Reduced

Triangle Surface Mesher	Program Controlled
Topology Checking	Yes
Pinch Tolerance	Please Define
Generate Pinch on Refresh	No
Statistics	
Nodes	2261
Elements	1143

TABLE 7
Model (C4) > Mesh > Mesh Controls

Object Name	*Patch Conforming Method*
State	Fully Defined
Scope	
Scoping Method	Geometry Selection
Geometry	1 Body
Definition	
Suppressed	No
Method	Tetrahedrons
Algorithm	Patch Conforming
Element Order	Use Global Setting

FIGURE 2
Model (C4) > Mesh > Figure

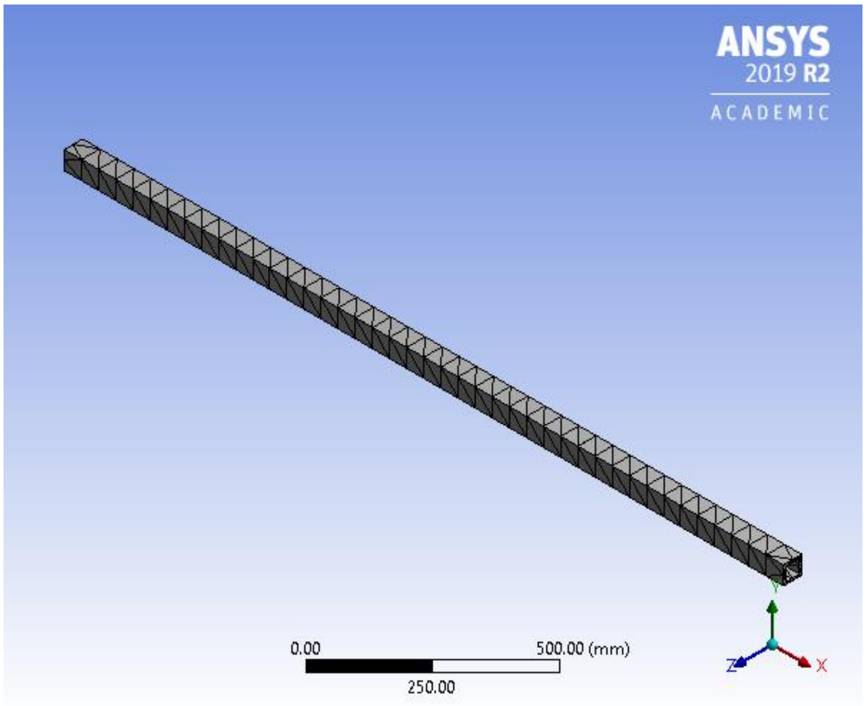

Static Structural (C5)

TABLE 8
Model (C4) > Analysis

Object Name	*Static Structural (C5)*
State	Solved
Definition	
Physics Type	Structural
Analysis Type	Static Structural
Solver Target	Mechanical APDL
Options	
Environment Temperature	22. °C
Generate Input Only	No

TABLE 9
Model (C4) > Static Structural (C5) > Analysis Settings

Object Name	*Analysis Settings*
State	Fully Defined
Step Controls	

Number Of Steps	1.
Current Step Number	1.
Step End Time	1. s
Auto Time Stepping	Program Controlled
Solver Controls	
Solver Type	Program Controlled
Weak Springs	Off
Solver Pivot Checking	Program Controlled
Large Deflection	Off
Inertia Relief	Off
Rotordynamics Controls	
Coriolis Effect	Off
Restart Controls	
Generate Restart Points	Program Controlled
Retain Files After Full Solve	No
Combine Restart Files	Program Controlled
Nonlinear Controls	
Newton-Raphson Option	Program Controlled
Force Convergence	Program Controlled
Moment Convergence	Program Controlled
Displacement Convergence	Program Controlled
Rotation Convergence	Program Controlled
Line Search	Program Controlled
Stabilization	Program Controlled
Output Controls	
Stress	Yes
Surface Stress	No
Back Stress	No
Strain	Yes
Contact Data	Yes
Nonlinear Data	No
Nodal Forces	No
Contact Miscellaneous	No
General Miscellaneous	No
Store Results At	All Time Points
Result File Compression	Program Controlled
Analysis Data Management	
Solver Files Directory	C:\Users\DIAPM599\OneDrive - Dentsply Sirona\Desktop\ANSYS Analysis\LCM_files\dp0\SYS\MECH\
Future Analysis	None
Scratch Solver Files Directory	
Save MAPDL db	No
Contact Summary	Program Controlled

Delete Unneeded Files	Yes
Nonlinear Solution	No
Solver Units	Active System
Solver Unit System	nmm

FIGURE 3
Model (C4) > Static Structural (C5) > Figure

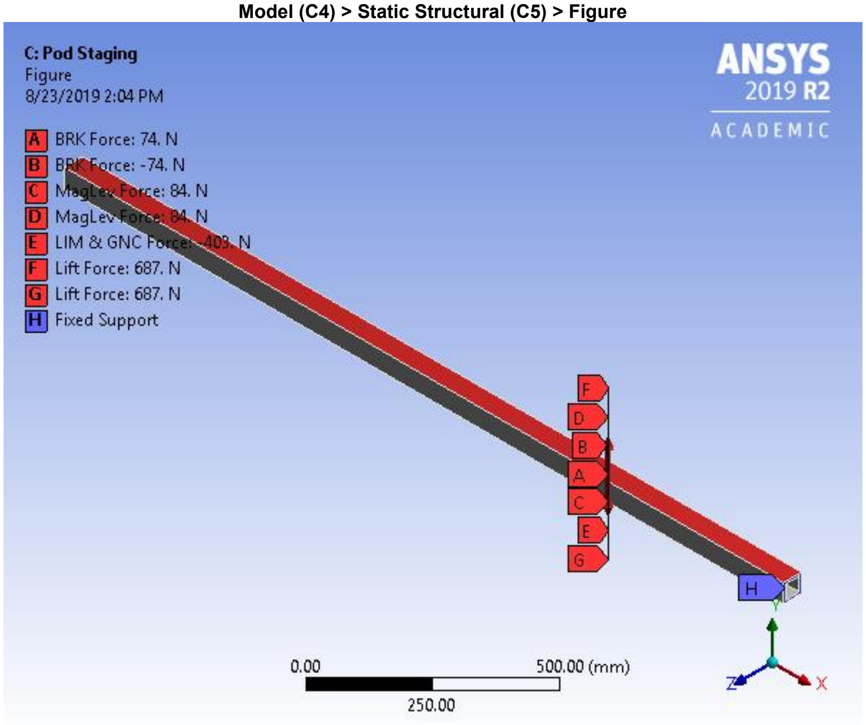

TABLE 10
Model (C4) > Static Structural (C5) > Loads

Object Name	*BRK Force*	*BRK Force*	*MagLev Force*	*MagLev Force*	*LIM & GNC Force*	*Lift Force*	*Lift Force*	*Thermal Condition*	*Fixed Support*
State	Fully Defined								
Scope									
Scoping Method	Geometry Selection								
Geometry	1 Face							1 Body	2 Faces
Definition									

Type	Force						Thermal Condition	Fixed Support
Define By	Components	Vector	Components	Vector	Components	Vector		
Coordinate System	Global Coordinate System		Global Coordinate System		Global Coordinate System			
X Component	0. N (ramped)		0. N (ramped)		0. N (ramped)			
Y Component	-74. N (ramped)		-84. N (ramped)		687. N (ramped)			
Z Component	0. N (ramped)		0. N (ramped)		0. N (ramped)			
Suppressed	No							
Magnitude		-74. N (ramped)		-403. N (ramped)		687. N (ramped)	80. °C (ramped)	
Direction		Defined		Defined		Defined		

FIGURE 4
Model (C4) > Static Structural (C5) > BRK Force

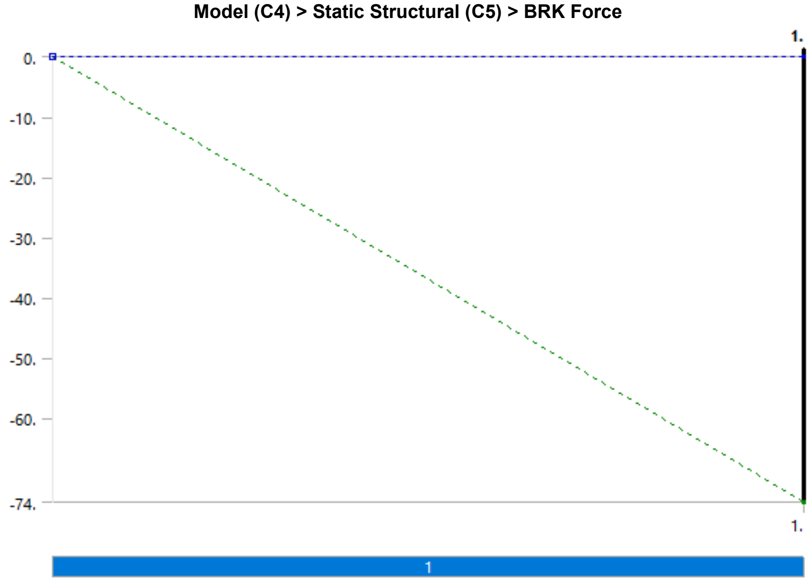

FIGURE 5
Model (C4) > Static Structural (C5) > BRK Force

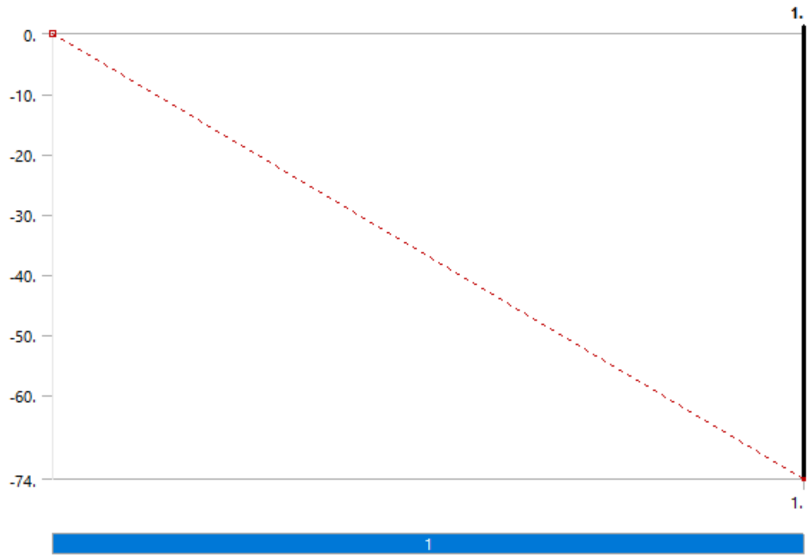

FIGURE 6
Model (C4) > Static Structural (C5) > MagLev Force

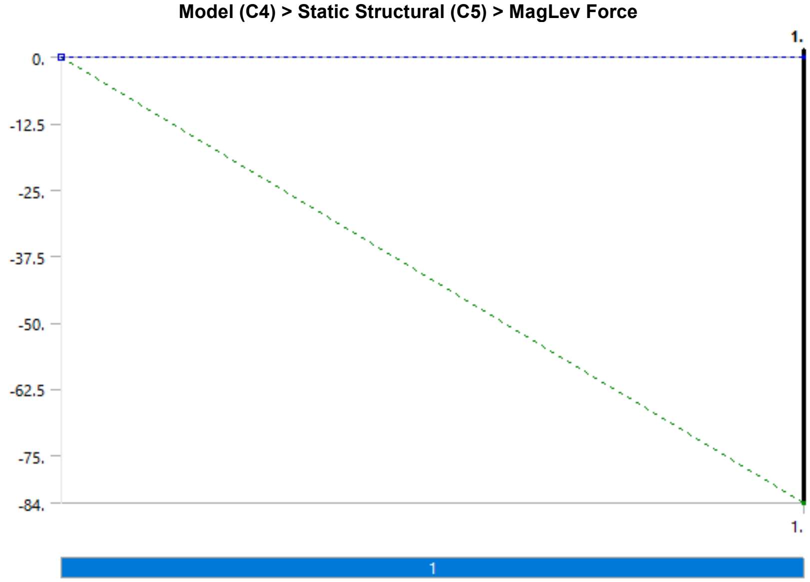

FIGURE 7
Model (C4) > Static Structural (C5) > MagLev Force

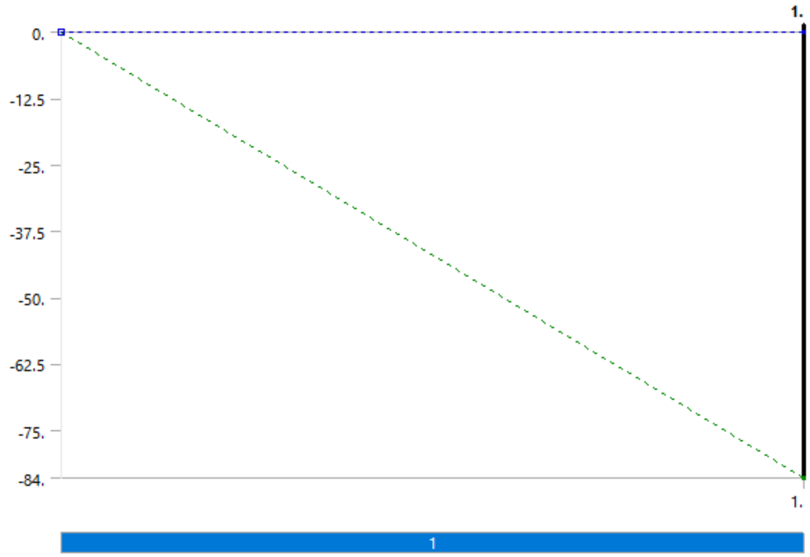

FIGURE 8
Model (C4) > Static Structural (C5) > LIM & GNC Force

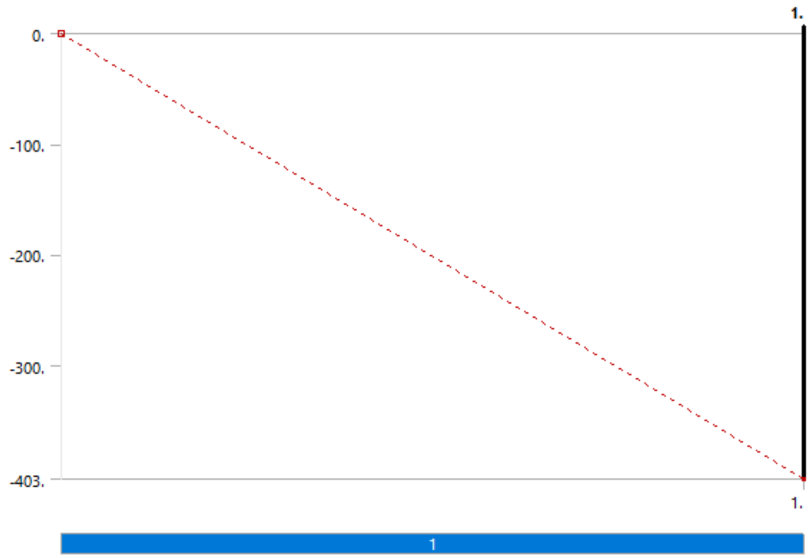

FIGURE 9
Model (C4) > Static Structural (C5) > Lift Force

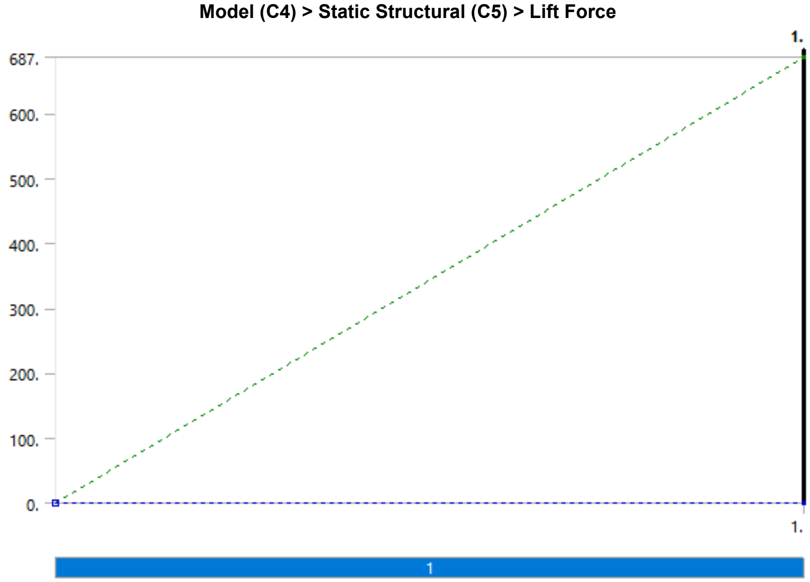

FIGURE 10
Model (C4) > Static Structural (C5) > Lift Force

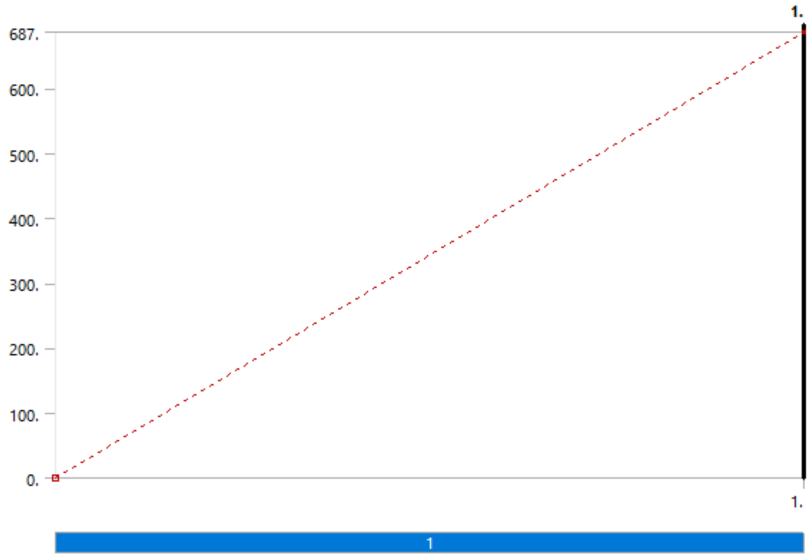

FIGURE 11
Model (C4) > Static Structural (C5) > Thermal Condition

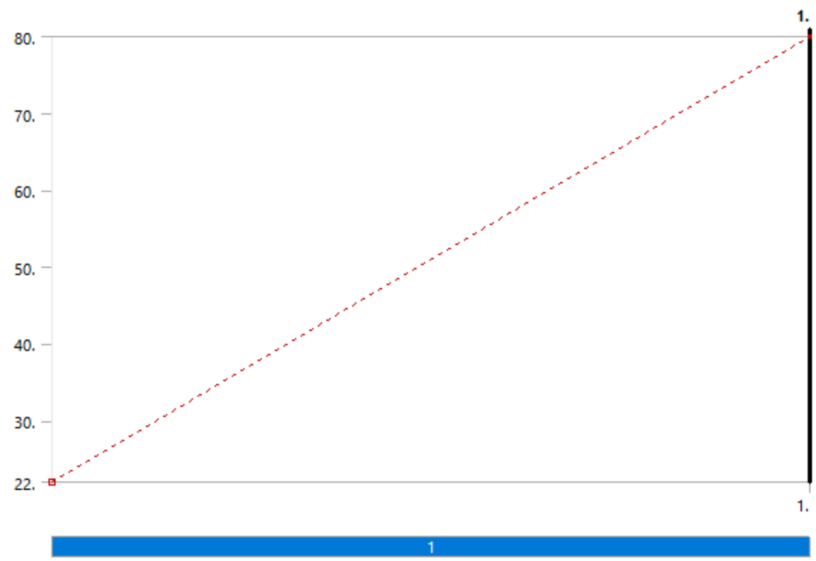

Solution (C6)

TABLE 11
Model (C4) > Static Structural (C5) > Solution

Object Name	*Solution (C6)*
State	Solved
Adaptive Mesh Refinement	
Max Refinement Loops	1.
Refinement Depth	2.
Information	
Status	Done
MAPDL Elapsed Time	3. s
MAPDL Memory Used	266. MB
MAPDL Result File Size	1.25 MB
Post Processing	
Beam Section Results	No
On Demand Stress/Strain	No

TABLE 12
Model (C4) > Static Structural (C5) > Solution (C6) > Solution Information

Object Name	*Solution Information*
State	Solved
Solution Information	
Solution Output	Solver Output
Newton-Raphson Residuals	0

Identify Element Violations	0
Update Interval	2.5 s
Display Points	All
FE Connection Visibility	
Activate Visibility	Yes
Display	All FE Connectors
Draw Connections Attached To	All Nodes
Line Color	Connection Type
Visible on Results	No
Line Thickness	Single
Display Type	Lines

TABLE 13
Model (C4) > Static Structural (C5) > Solution (C6) > Results

Object Name	*Total Deformation*	*Equivalent Stress*
State	Solved	
Scope		
Scoping Method	Geometry Selection	
Geometry	All Bodies	
Definition		
Type	Total Deformation	Equivalent (von-Mises) Stress
By	Time	
Display Time	Last	
Calculate Time History	Yes	
Identifier		
Suppressed	No	
Results		
Minimum	0. mm	34.987 MPa
Maximum	0.55549 mm	165.71 MPa
Average	0.26761 mm	95.926 MPa
Minimum Occurs On	Geom\PartBody	
Maximum Occurs On	Geom\PartBody	
Information		
Time	1. s	
Load Step	1	
Substep	1	
Iteration Number	1	
Integration Point Results		
Display Option		Averaged
Average Across Bodies		No

FIGURE 12
Model (C4) > Static Structural (C5) > Solution (C6) > Total Deformation

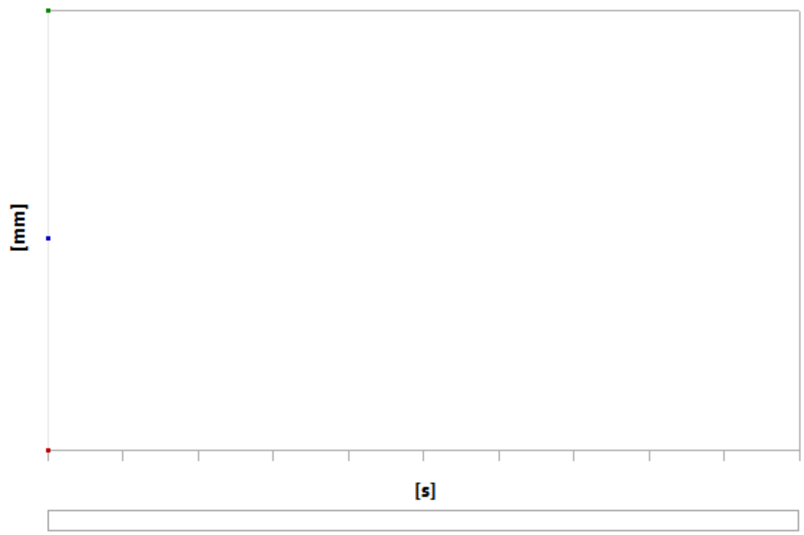

TABLE 14
Model (C4) > Static Structural (C5) > Solution (C6) > Total Deformation

Time [s]	Minimum [mm]	Maximum [mm]	Average [mm]
1.	0.	0.55549	0.26761

FIGURE 13
Model (C4) > Static Structural (C5) > Solution (C6) > Total Deformation > Figure

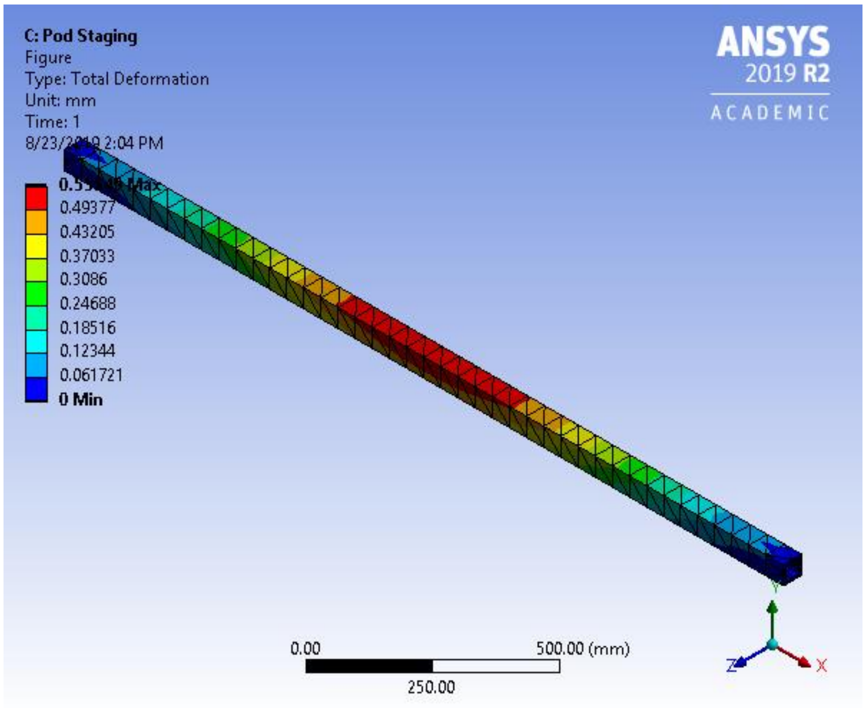

FIGURE 14
Model (C4) > Static Structural (C5) > Solution (C6) > Equivalent Stress

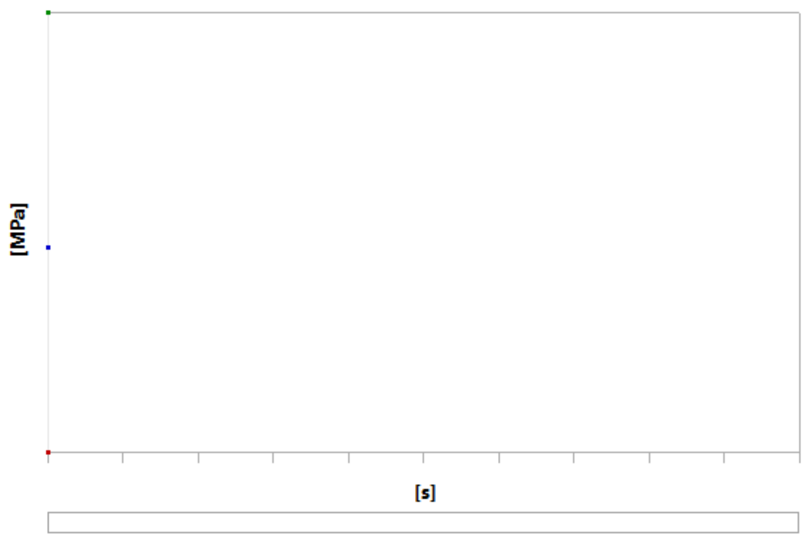

TABLE 15
Model (C4) > Static Structural (C5) > Solution (C6) > Equivalent Stress

Time [s]	Minimum [MPa]	Maximum [MPa]	Average [MPa]
1.	34.987	165.71	95.926

FIGURE 15
Model (C4) > Static Structural (C5) > Solution (C6) > Equivalent Stress > Figure

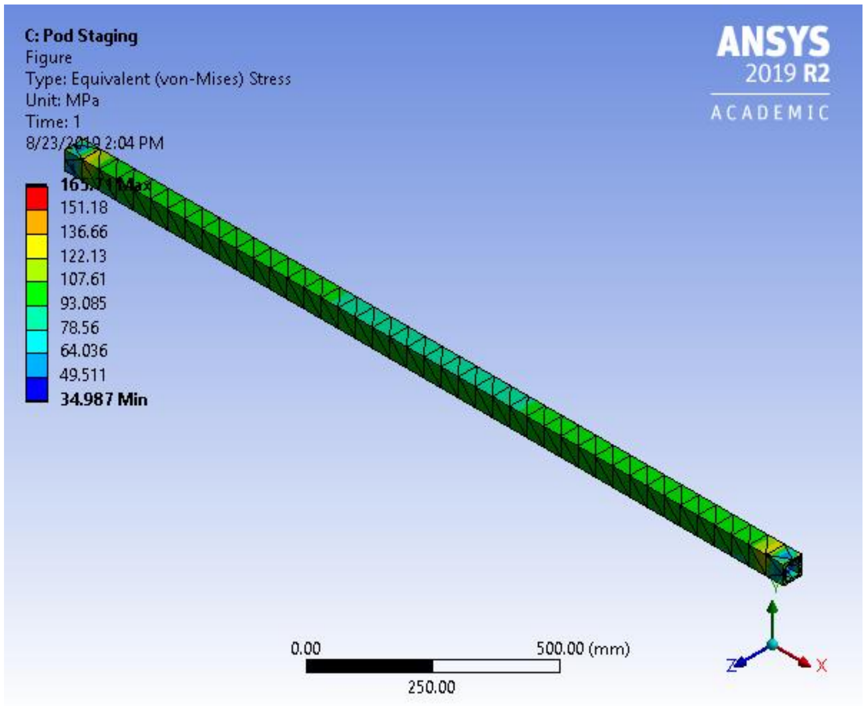

Material Data

Aluminum Alloy

TABLE 16
Aluminum Alloy > Constants

Density	2.77e-006 kg mm^-3
Coefficient of Thermal Expansion	2.3e-005 C^-1
Specific Heat	8.75e+005 mJ kg^-1 C^-1

TABLE 17
Aluminum Alloy > Color

Red	Green	Blue
138	104	46

TABLE 18
Aluminum Alloy > Compressive Ultimate Strength

Compressive Ultimate Strength MPa
0

TABLE 19
Aluminum Alloy > Compressive Yield Strength

Compressive Yield Strength MPa
280

TABLE 20
Aluminum Alloy > Tensile Yield Strength

Tensile Yield Strength MPa
280

TABLE 21
Aluminum Alloy > Tensile Ultimate Strength

Tensile Ultimate Strength MPa
310

TABLE 22
Aluminum Alloy > Isotropic Secant Coefficient of Thermal Expansion

Zero-Thermal-Strain Reference Temperature C
22

TABLE 23
Aluminum Alloy > Isotropic Thermal Conductivity

Thermal Conductivity W mm^-1 C^-1	Temperature C
0.114	-100
0.144	0
0.165	100
0.175	200

TABLE 24
Aluminum Alloy > S-N Curve

Alternating Stress MPa	Cycles	R-Ratio
275.8	1700	-1
241.3	5000	-1
206.8	34000	-1
172.4	1.4e+005	-1
137.9	8.e+005	-1
117.2	2.4e+006	-1
89.63	5.5e+007	-1
82.74	1.e+008	-1
170.6	50000	-0.5
139.6	3.5e+005	-0.5
108.6	3.7e+006	-0.5
87.91	1.4e+007	-0.5
77.57	5.e+007	-0.5
72.39	1.e+008	-0.5
144.8	50000	0
120.7	1.9e+005	0
103.4	1.3e+006	0
93.08	4.4e+006	0

86.18	1.2e+007	0
72.39	1.e+008	0
74.12	3.e+005	0.5
70.67	1.5e+006	0.5
66.36	1.2e+007	0.5
62.05	1.e+008	0.5

TABLE 25
Aluminum Alloy > Isotropic Resistivity

Resistivity ohm mm	Temperature C
2.43e-005	0
2.67e-005	20
3.63e-005	100

TABLE 26
Aluminum Alloy > Isotropic Elasticity

Young's Modulus MPa	Poisson's Ratio	Bulk Modulus MPa	Shear Modulus MPa	Temperature C
71000	0.33	69608	26692	

TABLE 27
Aluminum Alloy > Isotropic Relative Permeability

Relative Permeability
1

Appendix A.6 LCM Load Case II (Launch Phase) Analysis Report

ANSYS

Project

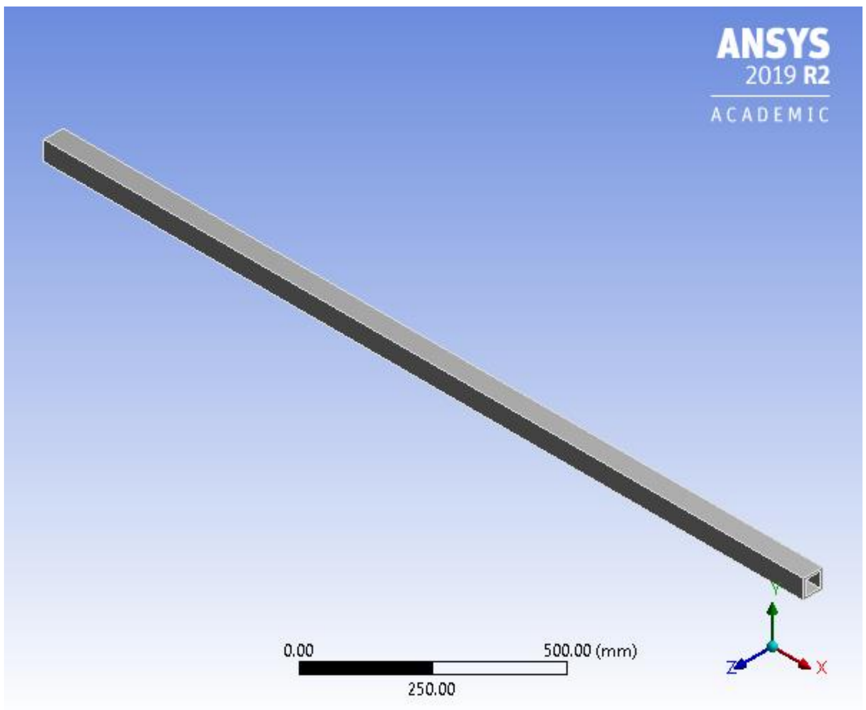

Contents

Units

TABLE 1

Unit System	Metric (mm, kg, N, s, mV, mA) Degrees rad/s Celsius
Angle	Degrees
Rotational Velocity	rad/s
Temperature	Celsius

Model (D4)

Geometry

TABLE 2
Model (D4) > Geometry

Object Name	*Geometry*
State	Fully Defined
Definition	
Source	C:\Users\DIAPM599\OneDrive - Dentsply Sirona\Desktop\ANSYS Analysis\LCM_files\dp0\Geom\DM\Geom.scdoc
Type	SpaceClaim
Length Unit	Meters
Element Control	Program Controlled
Display Style	Body Color
Bounding Box	
Length X	2000. mm
Length Y	50.8 mm
Length Z	50.8 mm

Properties	
Volume	2.2581e+006 mm³
Mass	6.2548 kg
Scale Factor Value	1.
Statistics	
Bodies	1
Active Bodies	1
Nodes	2261
Elements	1143
Mesh Metric	None
Update Options	
Assign Default Material	No
Basic Geometry Options	
Solid Bodies	Yes
Surface Bodies	Yes
Line Bodies	Yes
Parameters	Independent
Parameter Key	
Attributes	Yes
Attribute Key	
Named Selections	Yes
Named Selection Key	
Material Properties	Yes
Advanced Geometry Options	
Use Associativity	Yes
Coordinate Systems	Yes
Coordinate System Key	
Reader Mode Saves Updated File	No
Use Instances	Yes
Smart CAD Update	Yes
Compare Parts On Update	No
Analysis Type	3-D
Mixed Import Resolution	None
Clean Bodies On Import	No
Stitch Surfaces On Import	None
Decompose Disjoint Geometry	Yes
Enclosure and Symmetry Processing	Yes

TABLE 3
Model (D4) > Geometry > Parts

Object Name	*Geom\PartBody*
State	Meshed
Graphics Properties	

Visible	Yes
Transparency	1
Definition	
Suppressed	No
Stiffness Behavior	Flexible
Coordinate System	Default Coordinate System
Reference Temperature	By Environment
Treatment	None
Material	
Assignment	Aluminum Alloy
Nonlinear Effects	Yes
Thermal Strain Effects	Yes
Bounding Box	
Length X	2000. mm
Length Y	50.8 mm
Length Z	50.8 mm
Properties	
Volume	2.2581e+006 mm³
Mass	6.2548 kg
Centroid X	-1000. mm
Centroid Y	25.4 mm
Centroid Z	25.4 mm
Moment of Inertia Ip1	4203.5 kg·mm²
Moment of Inertia Ip2	2.087e+006 kg·mm²
Moment of Inertia Ip3	2.087e+006 kg·mm²
Statistics	
Nodes	2261
Elements	1143
Mesh Metric	None
CAD Attributes	
PartTolerance:	0.00000001
Color:175.143.175	

FIGURE 1
Model (D4) > Geometry > Figure

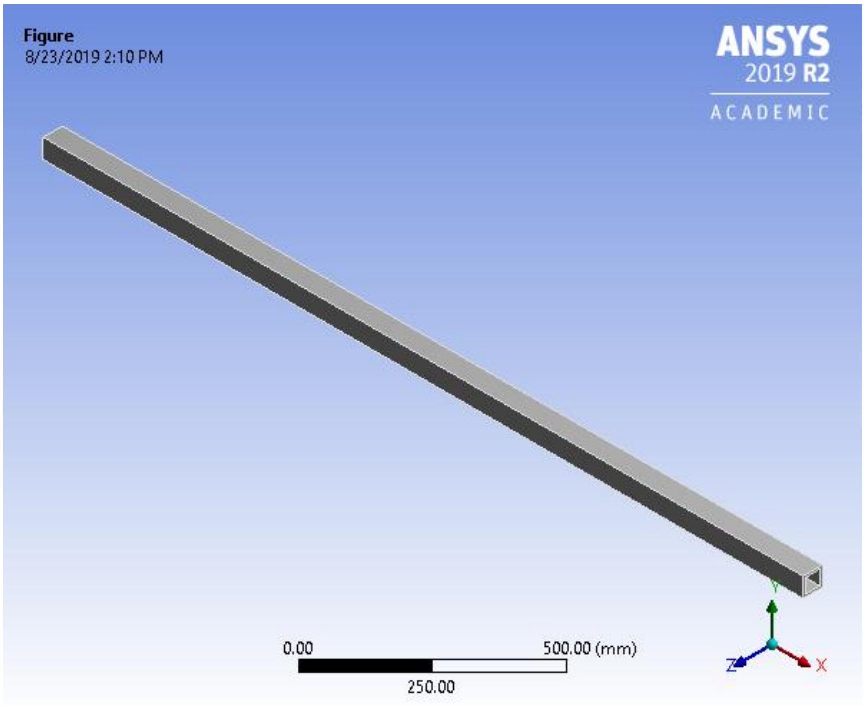

TABLE 4
Model (D4) > Materials

Object Name	*Materials*
State	Fully Defined
Statistics	
Materials	2
Material Assignments	0

Coordinate Systems

TABLE 5
Model (D4) > Coordinate Systems > Coordinate System

Object Name	*Global Coordinate System*
State	Fully Defined
Definition	
Type	Cartesian
Coordinate System ID	0.
Origin	
Origin X	0. mm

Origin Y	0. mm
Origin Z	0. mm
Directional Vectors	
X Axis Data	[1. 0. 0.]
Y Axis Data	[0. 1. 0.]
Z Axis Data	[0. 0. 1.]

Mesh

TABLE 6
Model (D4) > Mesh

Object Name	*Mesh*
State	Solved
Display	
Display Style	Use Geometry Setting
Defaults	
Physics Preference	Mechanical
Element Order	Program Controlled
Element Size	Default
Sizing	
Use Adaptive Sizing	Yes
Resolution	Default (2)
Mesh Defeaturing	Yes
Defeature Size	Default
Transition	Fast
Span Angle Center	Fine
Initial Size Seed	Assembly
Bounding Box Diagonal	2001.3 mm
Average Surface Area	71346 mm²
Minimum Edge Length	38.1 mm
Quality	
Check Mesh Quality	Yes, Errors
Error Limits	Standard Mechanical
Target Quality	Default (0.050000)
Smoothing	Medium
Mesh Metric	None
Inflation	
Use Automatic Inflation	None
Inflation Option	Smooth Transition
Transition Ratio	0.272
Maximum Layers	5
Growth Rate	1.2
Inflation Algorithm	Pre
View Advanced Options	No
Advanced	
Number of CPUs for Parallel Part Meshing	Program Controlled
Straight Sided Elements	No
Rigid Body Behavior	Dimensionally Reduced

Triangle Surface Mesher	Program Controlled
Topology Checking	Yes
Pinch Tolerance	Please Define
Generate Pinch on Refresh	No
Statistics	
Nodes	2261
Elements	1143

TABLE 7
Model (D4) > Mesh > Mesh Controls

Object Name	*Patch Conforming Method*
State	Fully Defined
Scope	
Scoping Method	Geometry Selection
Geometry	1 Body
Definition	
Suppressed	No
Method	Tetrahedrons
Algorithm	Patch Conforming
Element Order	Use Global Setting

FIGURE 2
Model (D4) > Mesh > Figure

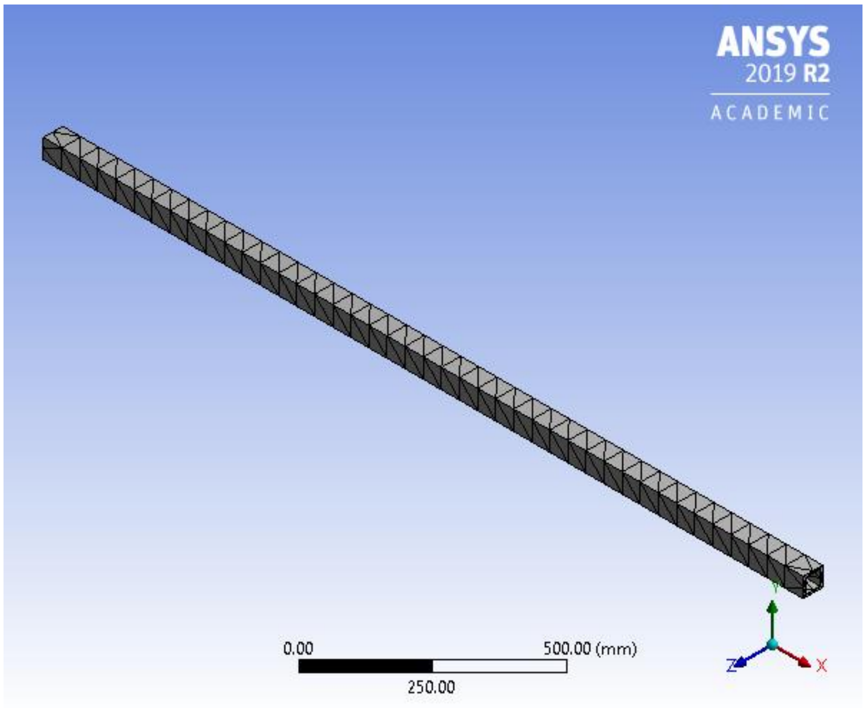

Static Structural (D5)

TABLE 8
Model (D4) > Analysis

Object Name	*Static Structural (D5)*
State	Solved
Definition	
Physics Type	Structural
Analysis Type	Static Structural
Solver Target	Mechanical APDL
Options	
Environment Temperature	22. °C
Generate Input Only	No

TABLE 9
Model (D4) > Static Structural (D5) > Analysis Settings

Object Name	*Analysis Settings*
State	Fully Defined
Step Controls	

Number Of Steps	1.
Current Step Number	1.
Step End Time	1. s
Auto Time Stepping	Program Controlled
Solver Controls	
Solver Type	Program Controlled
Weak Springs	Off
Solver Pivot Checking	Program Controlled
Large Deflection	Off
Inertia Relief	Off
Rotordynamics Controls	
Coriolis Effect	Off
Restart Controls	
Generate Restart Points	Program Controlled
Retain Files After Full Solve	No
Combine Restart Files	Program Controlled
Nonlinear Controls	
Newton-Raphson Option	Program Controlled
Force Convergence	Program Controlled
Moment Convergence	Program Controlled
Displacement Convergence	Program Controlled
Rotation Convergence	Program Controlled
Line Search	Program Controlled
Stabilization	Program Controlled
Output Controls	
Stress	Yes
Surface Stress	No
Back Stress	No
Strain	Yes
Contact Data	Yes
Nonlinear Data	No
Nodal Forces	No
Contact Miscellaneous	No
General Miscellaneous	No
Store Results At	All Time Points
Result File Compression	Program Controlled
Analysis Data Management	
Solver Files Directory	C:\Users\DIAPM599\OneDrive - Dentsply Sirona\Desktop\ANSYS Analysis\LCM_files\dp0\SYS-1\MECH\
Future Analysis	None
Scratch Solver Files Directory	
Save MAPDL db	No
Contact Summary	Program Controlled
Delete Unneeded Files	Yes

Nonlinear Solution	No
Solver Units	Active System
Solver Unit System	nmm

FIGURE 3
Model (D4) > Static Structural (D5) > Figure

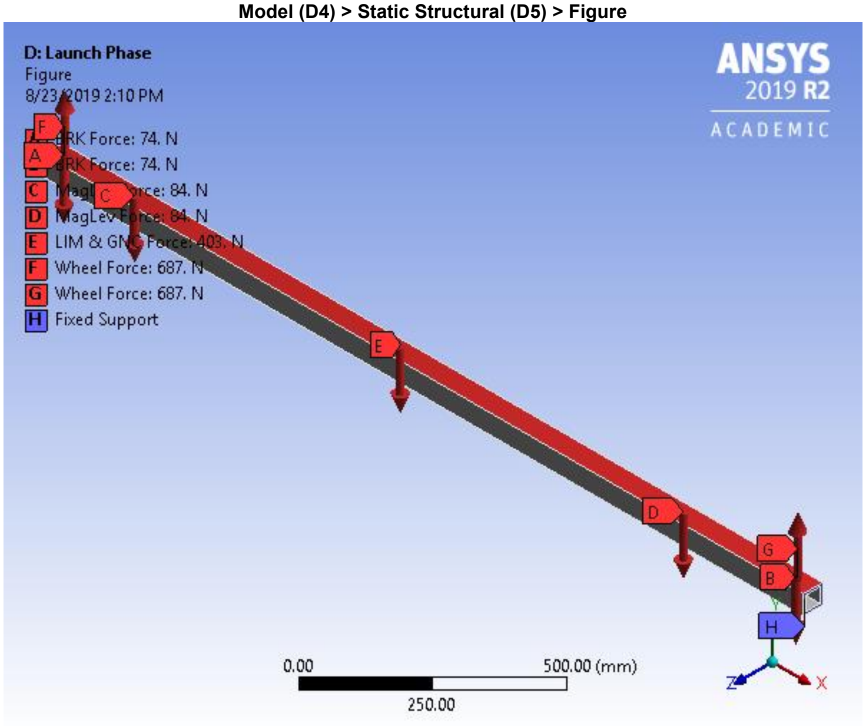

TABLE 10
Model (D4) > Static Structural (D5) > Loads

Object Name	*Thermal Condition*	*BRK Force*	*BRK Force*	*MagLev Force*	*MagLev Force*	*LIM & GNC Force*	*Wheel Force*	*Wheel Force*	*Fixed Support*
State	Fully Defined								
Scope									
Scoping Method	Geometry Selection								
Geometry	1 Body	1 Face							2 Faces
Definition									
Type	Thermal Condition	Force							Fixed Support

Magnitude	80. °C (ramped)					
Suppressed	No					
Define By		Components				
Coordinate System		Global Coordinate System				
X Component		0. N (ramped)				
Y Component		-74. N (ramped)	-84. N (ramped)	-403. N (ramped)	687. N (ramped)	
Z Component		0. N (ramped)				

FIGURE 4
Model (D4) > Static Structural (D5) > Thermal Condition

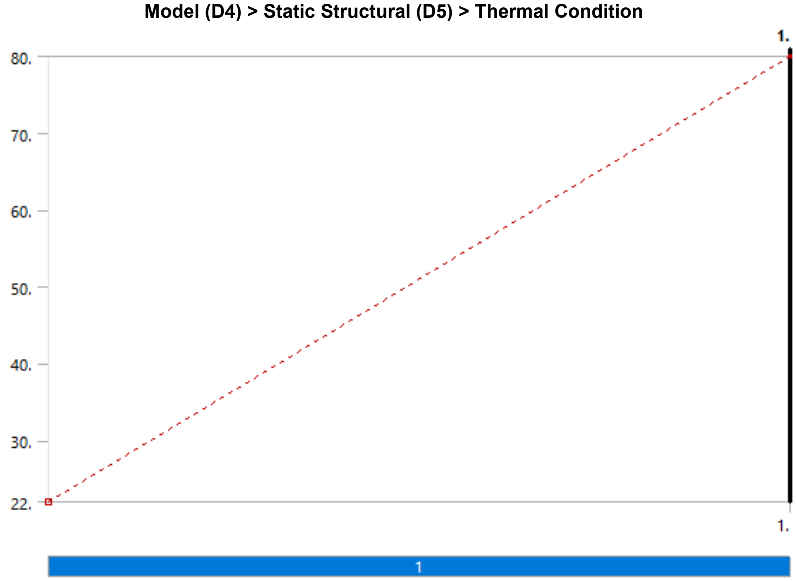

FIGURE 5
Model (D4) > Static Structural (D5) > BRK Force

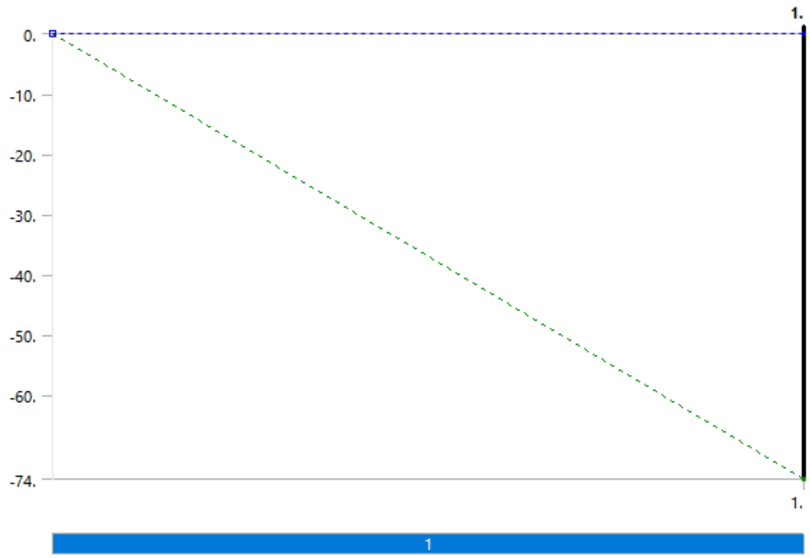

FIGURE 6
Model (D4) > Static Structural (D5) > BRK Force

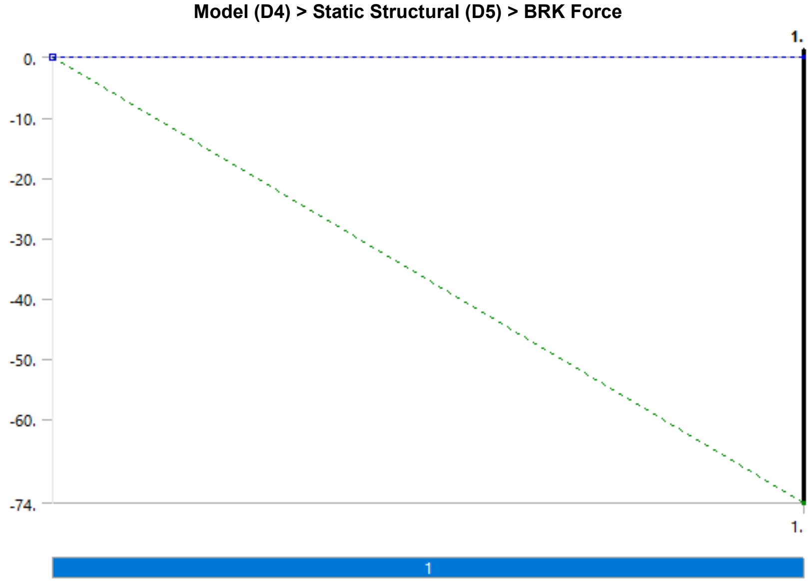

FIGURE 7
Model (D4) > Static Structural (D5) > MagLev Force

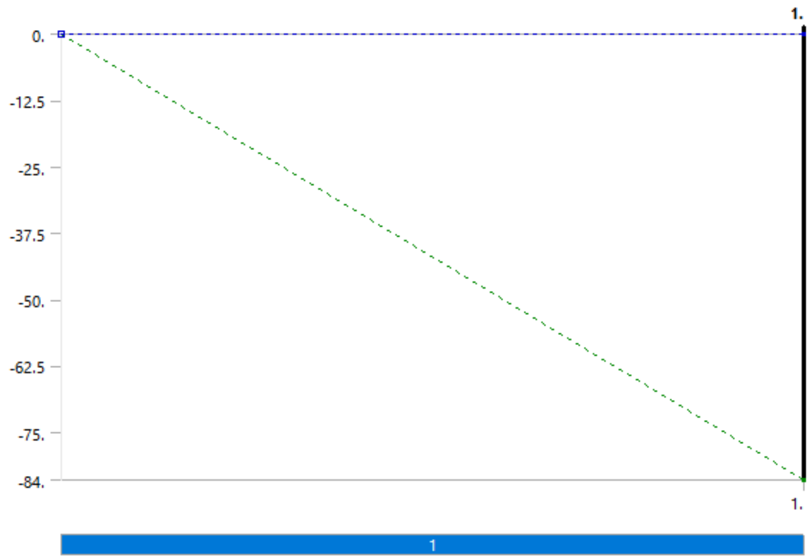

FIGURE 8
Model (D4) > Static Structural (D5) > MagLev Force

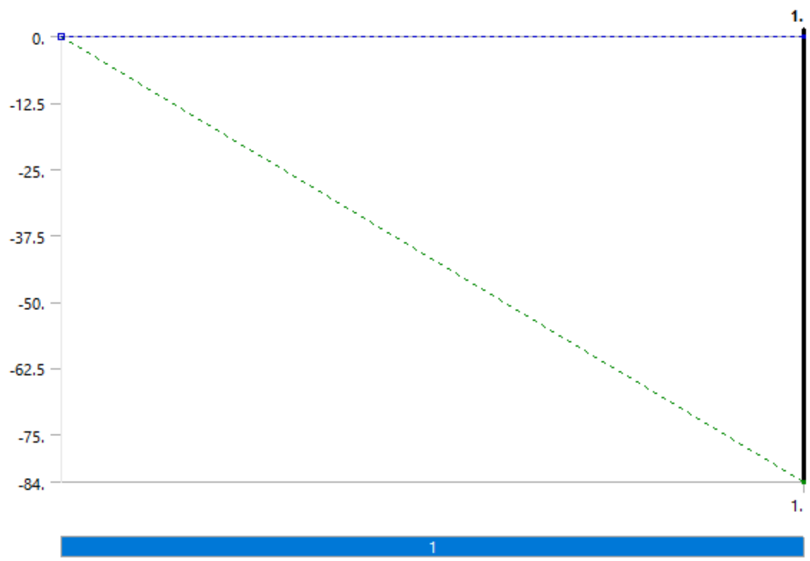

FIGURE 9
Model (D4) > Static Structural (D5) > LIM & GNC Force

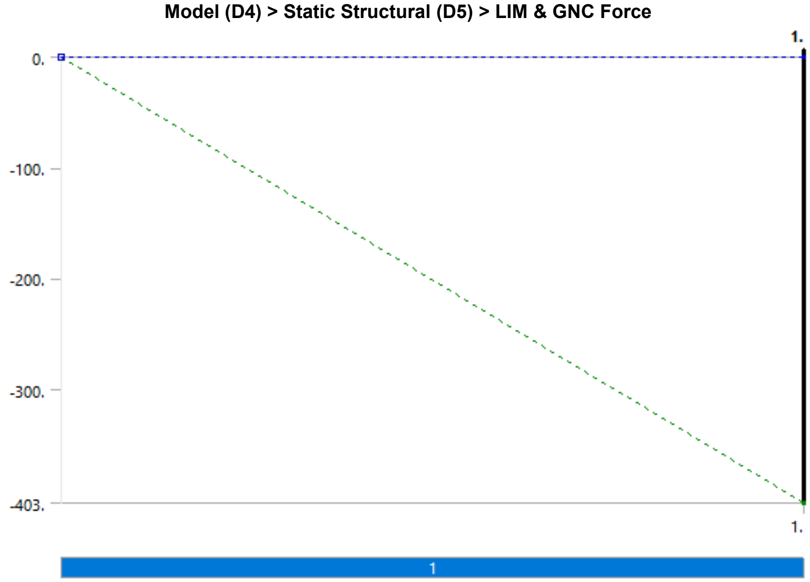

FIGURE 10
Model (D4) > Static Structural (D5) > Wheel Force

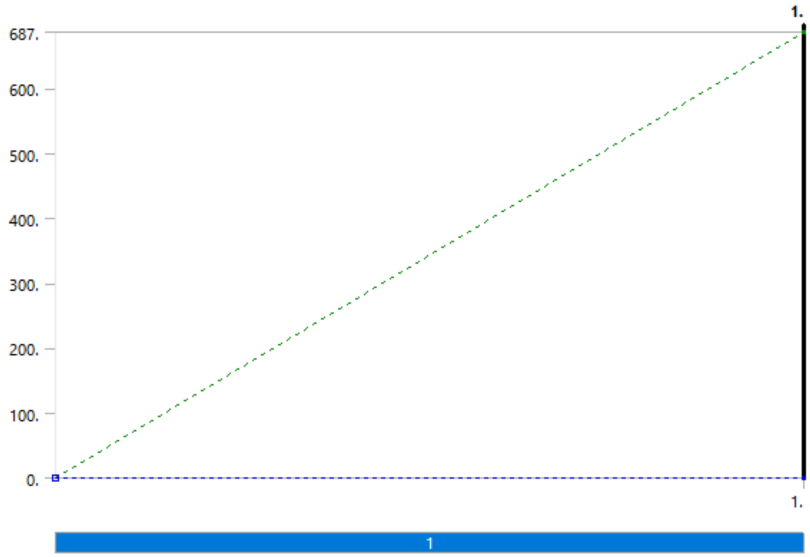

FIGURE 11
Model (D4) > Static Structural (D5) > Wheel Force

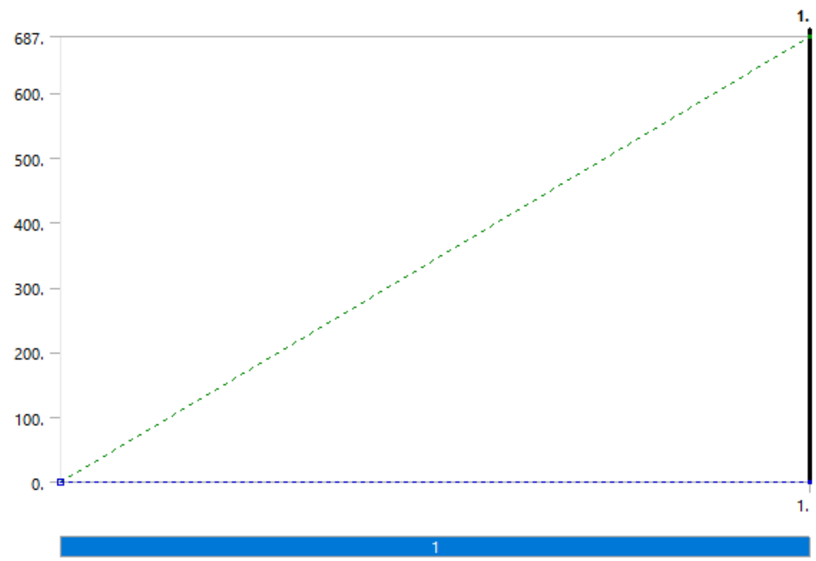

Solution (D6)

TABLE 11
Model (D4) > Static Structural (D5) > Solution

Object Name	*Solution (D6)*
State	Solved
Adaptive Mesh Refinement	
Max Refinement Loops	1.
Refinement Depth	2.
Information	
Status	Done
MAPDL Elapsed Time	3. s
MAPDL Memory Used	266. MB
MAPDL Result File Size	1.25 MB
Post Processing	
Beam Section Results	No
On Demand Stress/Strain	No

TABLE 12
Model (D4) > Static Structural (D5) > Solution (D6) > Solution Information

Object Name	*Solution Information*
State	Solved
Solution Information	
Solution Output	Solver Output
Newton-Raphson Residuals	0

Identify Element Violations	0
Update Interval	2.5 s
Display Points	All
FE Connection Visibility	
Activate Visibility	Yes
Display	All FE Connectors
Draw Connections Attached To	All Nodes
Line Color	Connection Type
Visible on Results	No
Line Thickness	Single
Display Type	Lines

TABLE 13
Model (D4) > Static Structural (D5) > Solution (D6) > Results

Object Name	*Total Deformation*	*Equivalent Stress*
State	Solved	
Scope		
Scoping Method	Geometry Selection	
Geometry	All Bodies	
Definition		
Type	Total Deformation	Equivalent (von-Mises) Stress
By	Time	
Display Time	Last	
Calculate Time History	Yes	
Identifier		
Suppressed	No	
Results		
Minimum	0. mm	34.987 MPa
Maximum	0.55549 mm	165.71 MPa
Average	0.26761 mm	95.926 MPa
Minimum Occurs On	Geom\PartBody	
Maximum Occurs On	Geom\PartBody	
Information		
Time	1. s	
Load Step	1	
Substep	1	
Iteration Number	1	
Integration Point Results		
Display Option		Averaged
Average Across Bodies		No

FIGURE 12
Model (D4) > Static Structural (D5) > Solution (D6) > Total Deformation

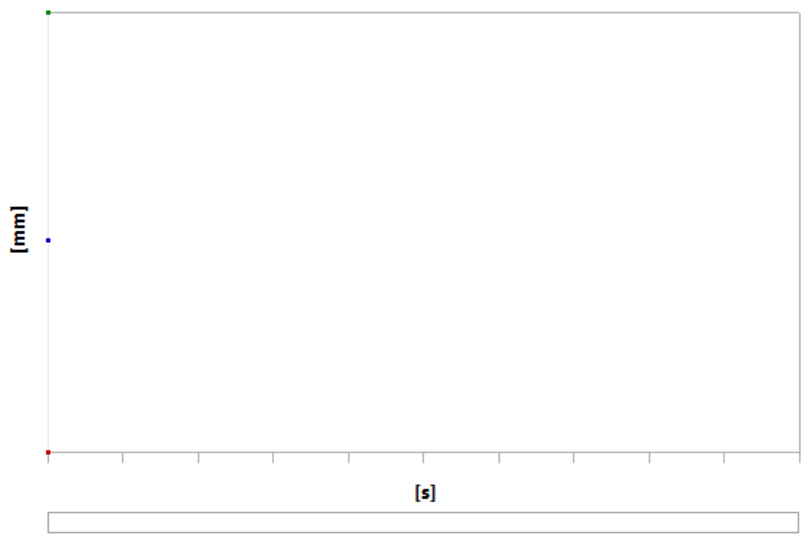

TABLE 14
Model (D4) > Static Structural (D5) > Solution (D6) > Total Deformation

Time [s]	Minimum [mm]	Maximum [mm]	Average [mm]
1.	0.	0.55549	0.26761

FIGURE 13
Model (D4) > Static Structural (D5) > Solution (D6) > Total Deformation > Figure

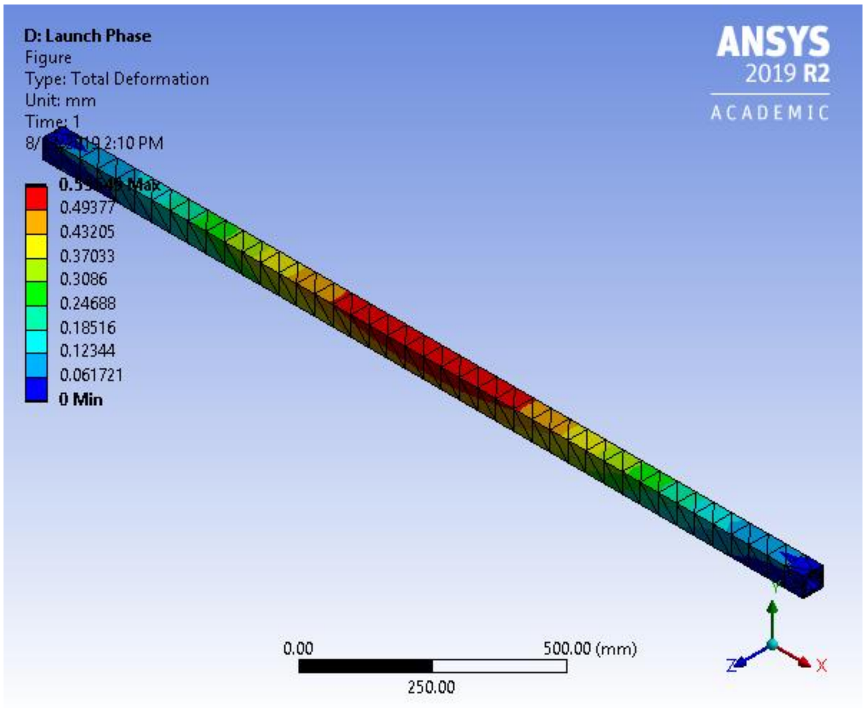

FIGURE 14
Model (D4) > Static Structural (D5) > Solution (D6) > Equivalent Stress

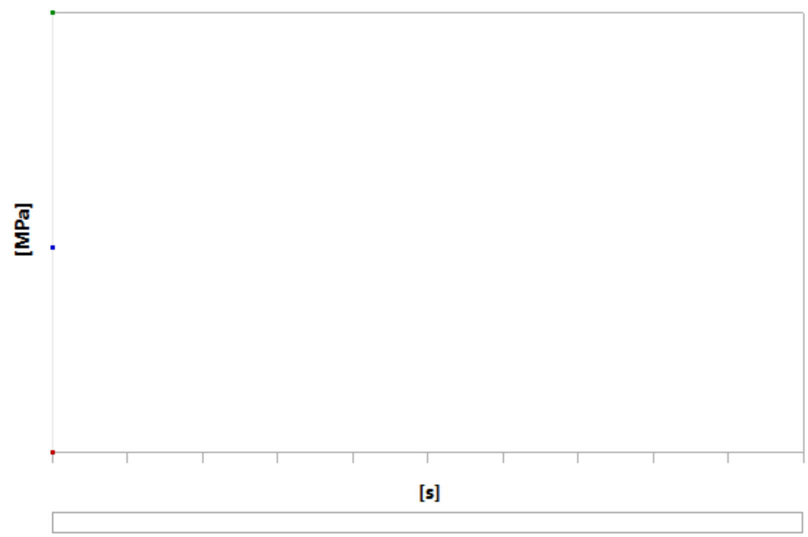

TABLE 15
Model (D4) > Static Structural (D5) > Solution (D6) > Equivalent Stress

Time [s]	Minimum [MPa]	Maximum [MPa]	Average [MPa]
1.	34.987	165.71	95.926

FIGURE 15
Model (D4) > Static Structural (D5) > Solution (D6) > Equivalent Stress > Figure

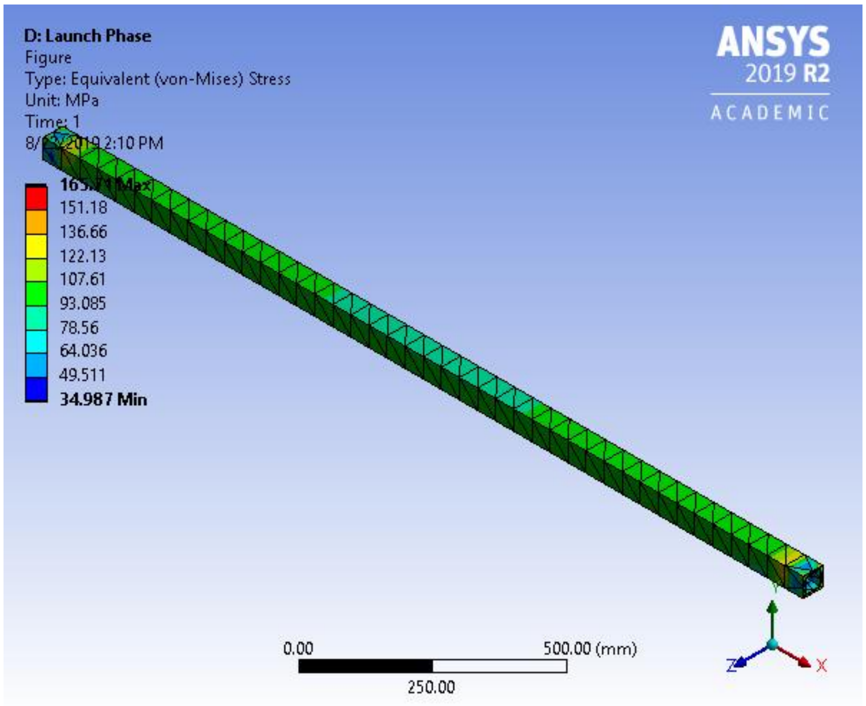

Material Data

Aluminum Alloy

TABLE 16
Aluminum Alloy > Constants

Density	2.77e-006 kg mm^-3
Coefficient of Thermal Expansion	2.3e-005 C^-1
Specific Heat	8.75e+005 mJ kg^-1 C^-1

TABLE 17
Aluminum Alloy > Color

Red	Green	Blue
138	104	46

TABLE 18
Aluminum Alloy > Compressive Ultimate Strength

Compressive Ultimate Strength MPa
0

TABLE 19
Aluminum Alloy > Compressive Yield Strength

Compressive Yield Strength MPa
280

TABLE 20
Aluminum Alloy > Tensile Yield Strength

Tensile Yield Strength MPa
280

TABLE 21
Aluminum Alloy > Tensile Ultimate Strength

Tensile Ultimate Strength MPa
310

TABLE 22
Aluminum Alloy > Isotropic Secant Coefficient of Thermal Expansion

Zero-Thermal-Strain Reference Temperature C
22

TABLE 23
Aluminum Alloy > Isotropic Thermal Conductivity

Thermal Conductivity W mm^-1 C^-1	Temperature C
0.114	-100
0.144	0
0.165	100
0.175	200

TABLE 24
Aluminum Alloy > S-N Curve

Alternating Stress MPa	Cycles	R-Ratio
275.8	1700	-1
241.3	5000	-1
206.8	34000	-1
172.4	1.4e+005	-1
137.9	8.e+005	-1
117.2	2.4e+006	-1
89.63	5.5e+007	-1
82.74	1.e+008	-1
170.6	50000	-0.5
139.6	3.5e+005	-0.5
108.6	3.7e+006	-0.5
87.91	1.4e+007	-0.5
77.57	5.e+007	-0.5
72.39	1.e+008	-0.5
144.8	50000	0
120.7	1.9e+005	0
103.4	1.3e+006	0
93.08	4.4e+006	0

86.18	1.2e+007	0
72.39	1.e+008	0
74.12	3.e+005	0.5
70.67	1.5e+006	0.5
66.36	1.2e+007	0.5
62.05	1.e+008	0.5

TABLE 25
Aluminum Alloy > Isotropic Resistivity

Resistivity ohm mm	Temperature C
2.43e-005	0
2.67e-005	20
3.63e-005	100

TABLE 26
Aluminum Alloy > Isotropic Elasticity

Young's Modulus MPa	Poisson's Ratio	Bulk Modulus MPa	Shear Modulus MPa	Temperature C
71000	0.33	69608	26692	

TABLE 27
Aluminum Alloy > Isotropic Relative Permeability

Relative Permeability
1

Appendix A.7 LCM Load Case III (Levitation Phase) Analysis Report

ANSYS

Project

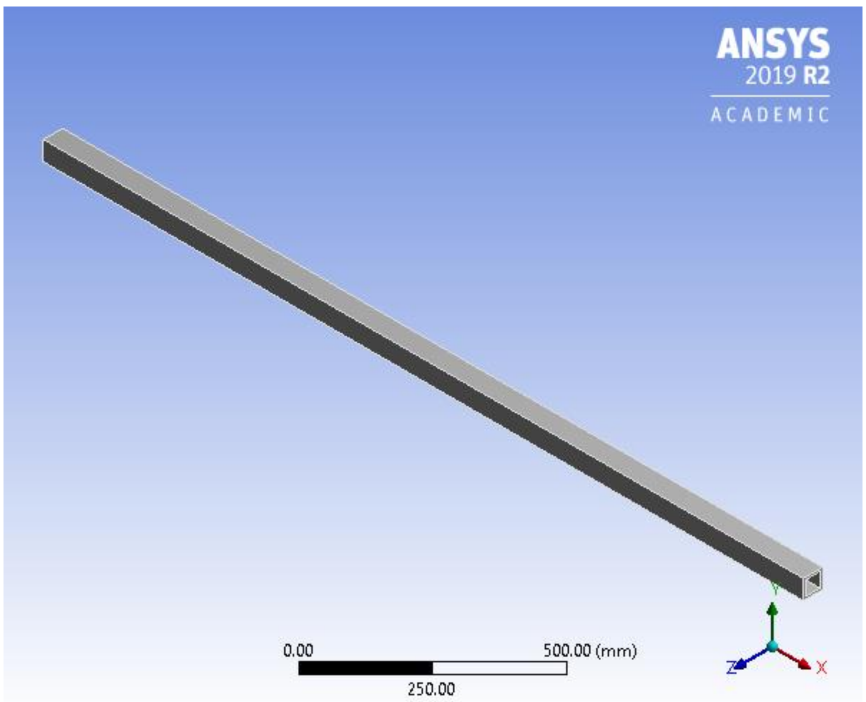

Contents

Units

TABLE 1

Unit System	Metric (mm, kg, N, s, mV, mA) Degrees rad/s Celsius
Angle	Degrees
Rotational Velocity	rad/s
Temperature	Celsius

Model (E4)

Geometry

TABLE 2
Model (E4) > Geometry

Object Name	*Geometry*
State	Fully Defined
Definition	
Source	C:\Users\DIAPM599\OneDrive - Dentsply Sirona\Desktop\ANSYS Analysis\LCM_files\dp0\Geom\DM\Geom.scdoc
Type	SpaceClaim
Length Unit	Meters
Element Control	Program Controlled
Display Style	Body Color
Bounding Box	
Length X	2000. mm
Length Y	50.8 mm
Length Z	50.8 mm

Properties	
Volume	2.2581e+006 mm³
Mass	6.2548 kg
Scale Factor Value	1.
Statistics	
Bodies	1
Active Bodies	1
Nodes	2261
Elements	1143
Mesh Metric	None
Update Options	
Assign Default Material	No
Basic Geometry Options	
Solid Bodies	Yes
Surface Bodies	Yes
Line Bodies	Yes
Parameters	Independent
Parameter Key	
Attributes	Yes
Attribute Key	
Named Selections	Yes
Named Selection Key	
Material Properties	Yes
Advanced Geometry Options	
Use Associativity	Yes
Coordinate Systems	Yes
Coordinate System Key	
Reader Mode Saves Updated File	No
Use Instances	Yes
Smart CAD Update	Yes
Compare Parts On Update	No
Analysis Type	3-D
Mixed Import Resolution	None
Clean Bodies On Import	No
Stitch Surfaces On Import	None
Decompose Disjoint Geometry	Yes
Enclosure and Symmetry Processing	Yes

TABLE 3
Model (E4) > Geometry > Parts

Object Name	*Geom\PartBody*
State	Meshed
Graphics Properties	

Visible	Yes
Transparency	1
Definition	
Suppressed	No
Stiffness Behavior	Flexible
Coordinate System	Default Coordinate System
Reference Temperature	By Environment
Treatment	None
Material	
Assignment	Aluminum Alloy
Nonlinear Effects	Yes
Thermal Strain Effects	Yes
Bounding Box	
Length X	2000. mm
Length Y	50.8 mm
Length Z	50.8 mm
Properties	
Volume	2.2581e+006 mm³
Mass	6.2548 kg
Centroid X	-1000. mm
Centroid Y	25.4 mm
Centroid Z	25.4 mm
Moment of Inertia Ip1	4203.5 kg·mm²
Moment of Inertia Ip2	2.087e+006 kg·mm²
Moment of Inertia Ip3	2.087e+006 kg·mm²
Statistics	
Nodes	2261
Elements	1143
Mesh Metric	None
CAD Attributes	
PartTolerance:	0.00000001
Color:175.143.175	

FIGURE 1
Model (E4) > Geometry > Geom > PartBody > Figure

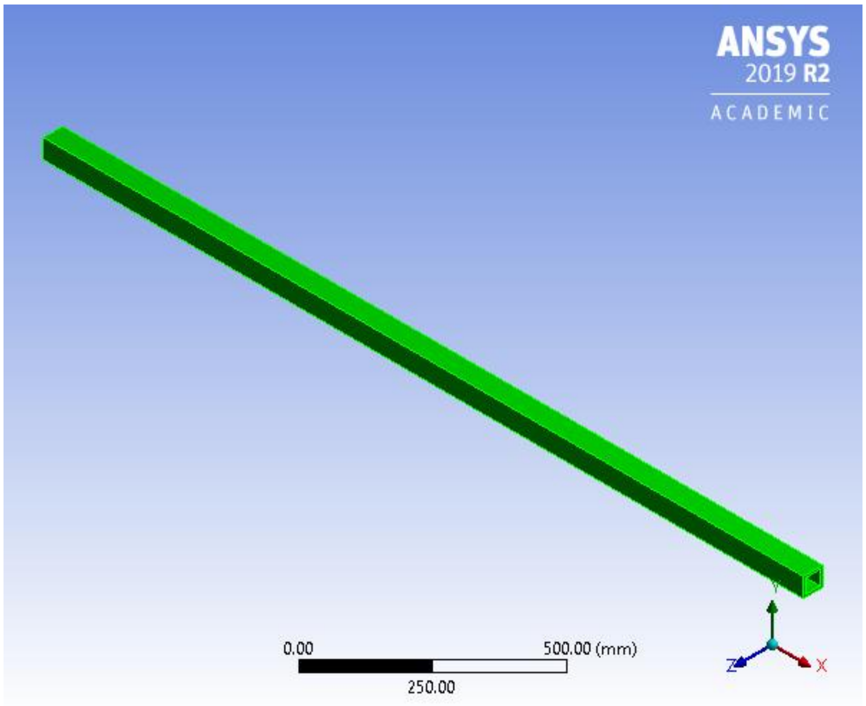

TABLE 4
Model (E4) > Materials

Object Name	*Materials*
State	Fully Defined
Statistics	
Materials	2
Material Assignments	0

Coordinate Systems

TABLE 5
Model (E4) > Coordinate Systems > Coordinate System

Object Name	*Global Coordinate System*
State	Fully Defined
Definition	
Type	Cartesian
Coordinate System ID	0.
Origin	
Origin X	0. mm

Origin Y	0. mm
Origin Z	0. mm
Directional Vectors	
X Axis Data	[1. 0. 0.]
Y Axis Data	[0. 1. 0.]
Z Axis Data	[0. 0. 1.]

Mesh

TABLE 6
Model (E4) > Mesh

Object Name	*Mesh*
State	Solved
Display	
Display Style	Use Geometry Setting
Defaults	
Physics Preference	Mechanical
Element Order	Program Controlled
Element Size	Default
Sizing	
Use Adaptive Sizing	Yes
Resolution	Default (2)
Mesh Defeaturing	Yes
Defeature Size	Default
Transition	Fast
Span Angle Center	Fine
Initial Size Seed	Assembly
Bounding Box Diagonal	2001.3 mm
Average Surface Area	71346 mm²
Minimum Edge Length	38.1 mm
Quality	
Check Mesh Quality	Yes, Errors
Error Limits	Standard Mechanical
Target Quality	Default (0.050000)
Smoothing	Medium
Mesh Metric	None
Inflation	
Use Automatic Inflation	None
Inflation Option	Smooth Transition
Transition Ratio	0.272
Maximum Layers	5
Growth Rate	1.2
Inflation Algorithm	Pre
View Advanced Options	No
Advanced	
Number of CPUs for Parallel Part Meshing	Program Controlled
Straight Sided Elements	No
Rigid Body Behavior	Dimensionally Reduced

Triangle Surface Mesher	Program Controlled
Topology Checking	Yes
Pinch Tolerance	Please Define
Generate Pinch on Refresh	No
Statistics	
Nodes	2261
Elements	1143

TABLE 7
Model (E4) > Mesh > Mesh Controls

Object Name	*Patch Conforming Method*
State	Fully Defined
Scope	
Scoping Method	Geometry Selection
Geometry	1 Body
Definition	
Suppressed	No
Method	Tetrahedrons
Algorithm	Patch Conforming
Element Order	Use Global Setting

FIGURE 2
Model (E4) > Mesh > Figure

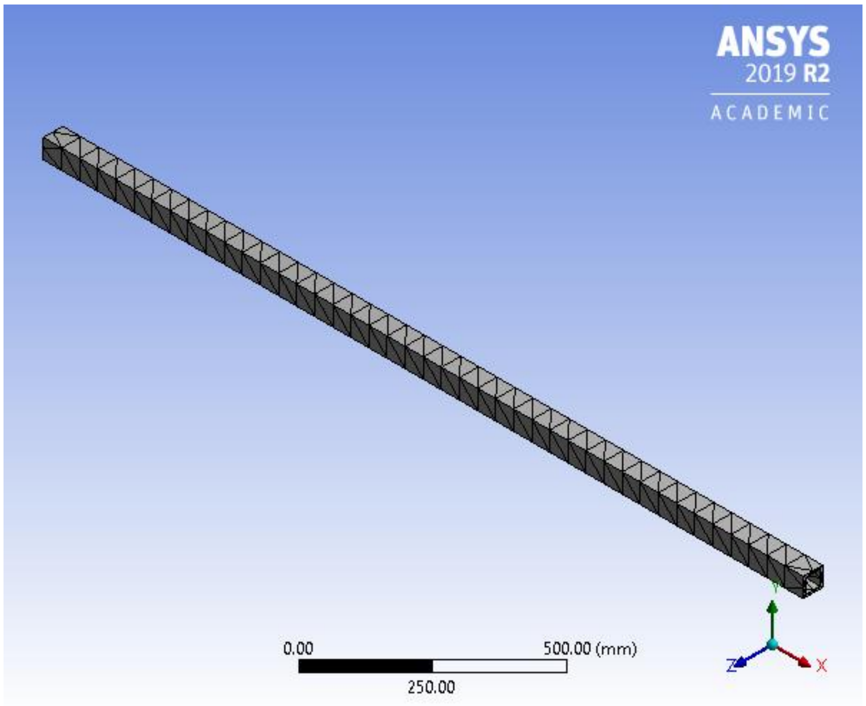

Static Structural (E5)

TABLE 8
Model (E4) > Analysis

Object Name	*Static Structural (E5)*
State	Solved
Definition	
Physics Type	Structural
Analysis Type	Static Structural
Solver Target	Mechanical APDL
Options	
Environment Temperature	22. °C
Generate Input Only	No

TABLE 9
Model (E4) > Static Structural (E5) > Analysis Settings

Object Name	*Analysis Settings*
State	Fully Defined
Step Controls	

Number Of Steps	1.
Current Step Number	1.
Step End Time	1. s
Auto Time Stepping	Program Controlled
Solver Controls	
Solver Type	Program Controlled
Weak Springs	Off
Solver Pivot Checking	Program Controlled
Large Deflection	Off
Inertia Relief	Off
Rotordynamics Controls	
Coriolis Effect	Off
Restart Controls	
Generate Restart Points	Program Controlled
Retain Files After Full Solve	No
Combine Restart Files	Program Controlled
Nonlinear Controls	
Newton-Raphson Option	Program Controlled
Force Convergence	Program Controlled
Moment Convergence	Program Controlled
Displacement Convergence	Program Controlled
Rotation Convergence	Program Controlled
Line Search	Program Controlled
Stabilization	Program Controlled
Output Controls	
Stress	Yes
Surface Stress	No
Back Stress	No
Strain	Yes
Contact Data	Yes
Nonlinear Data	No
Nodal Forces	No
Contact Miscellaneous	No
General Miscellaneous	No
Store Results At	All Time Points
Result File Compression	Program Controlled
Analysis Data Management	
Solver Files Directory	C:\Users\DIAPM599\OneDrive - Dentsply Sirona\Desktop\ANSYS Analysis\LCM_files\dp0\SYS-2\MECH\
Future Analysis	None
Scratch Solver Files Directory	
Save MAPDL db	No
Contact Summary	Program Controlled
Delete Unneeded Files	Yes

Nonlinear Solution	No
Solver Units	Active System
Solver Unit System	nmm

FIGURE 3
Model (E4) > Static Structural (E5) > Figure

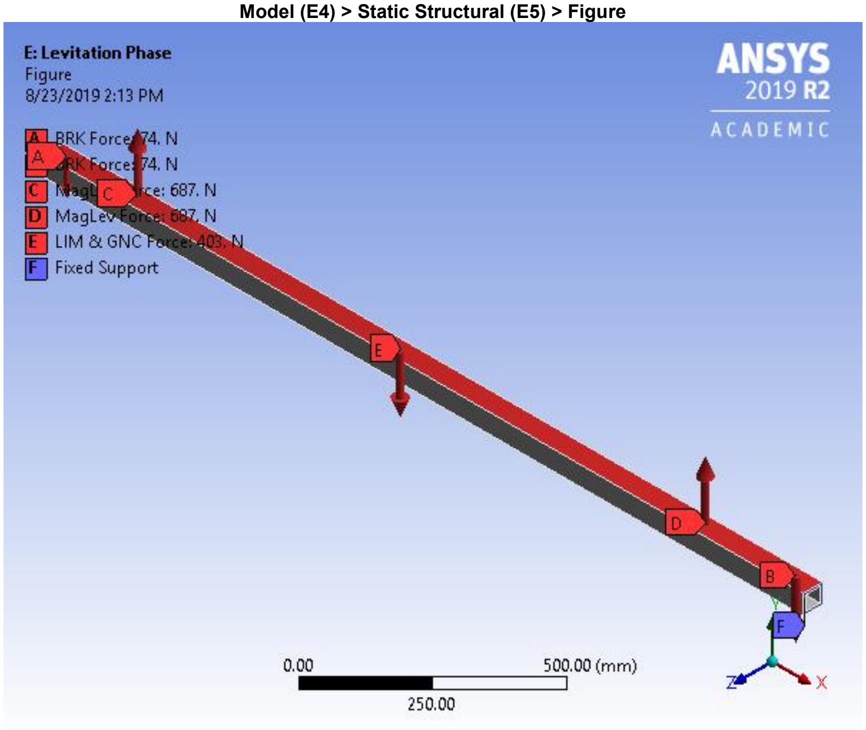

TABLE 10
Model (E4) > Static Structural (E5) > Loads

Object Name	*Thermal Condition*	*BRK Force*	*BRK Force*	*MagLev Force*	*MagLev Force*	*LIM & GNC Force*	*Fixed Support*
State	Fully Defined						
Scope							
Scoping Method	Geometry Selection						
Geometry	1 Body	1 Face					2 Faces
Definition							
Type	Thermal Condition	Force					Fixed Support
Magnitude	80. °C (ramped)						

Suppressed	No				
Define By		Components			
Coordinate System		Global Coordinate System			
X Component		0. N (ramped)			
Y Component		-74. N (ramped)	687. N (ramped)	-403. N (ramped)	
Z Component		0. N (ramped)			

FIGURE 4
Model (E4) > Static Structural (E5) > Thermal Condition

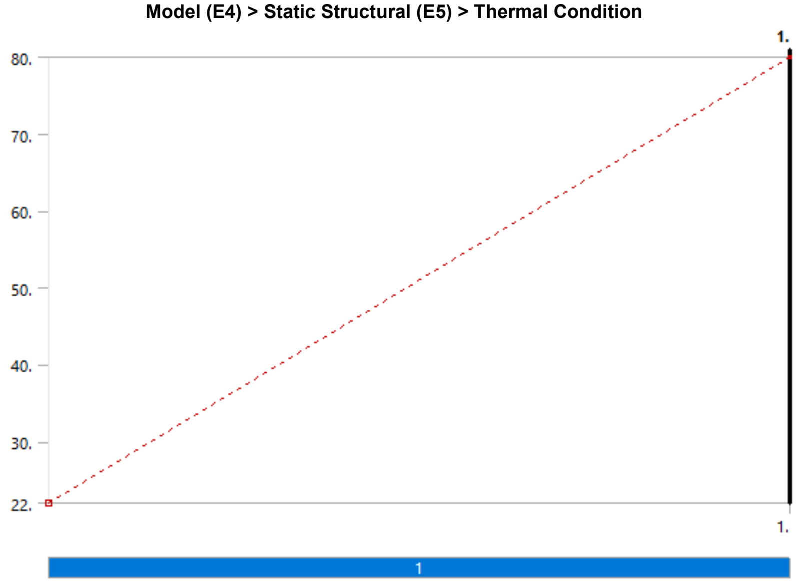

FIGURE 5
Model (E4) > Static Structural (E5) > BRK Force

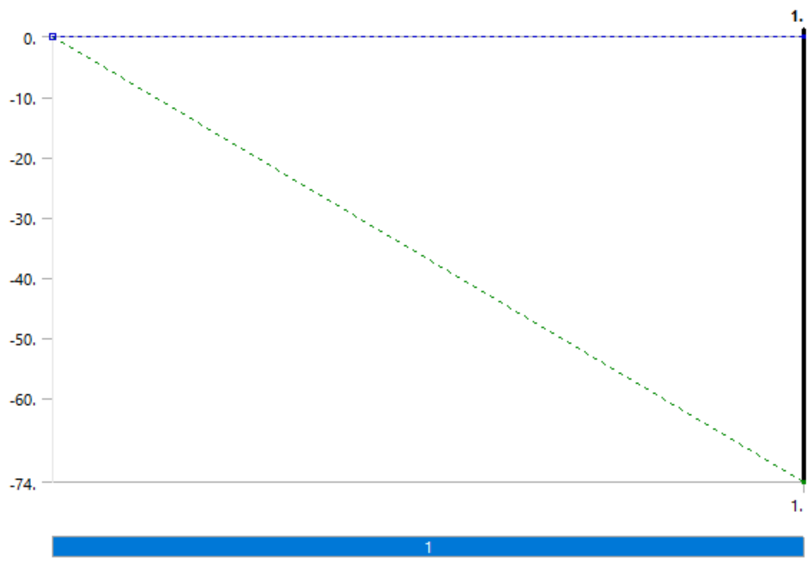

FIGURE 6
Model (E4) > Static Structural (E5) > BRK Force

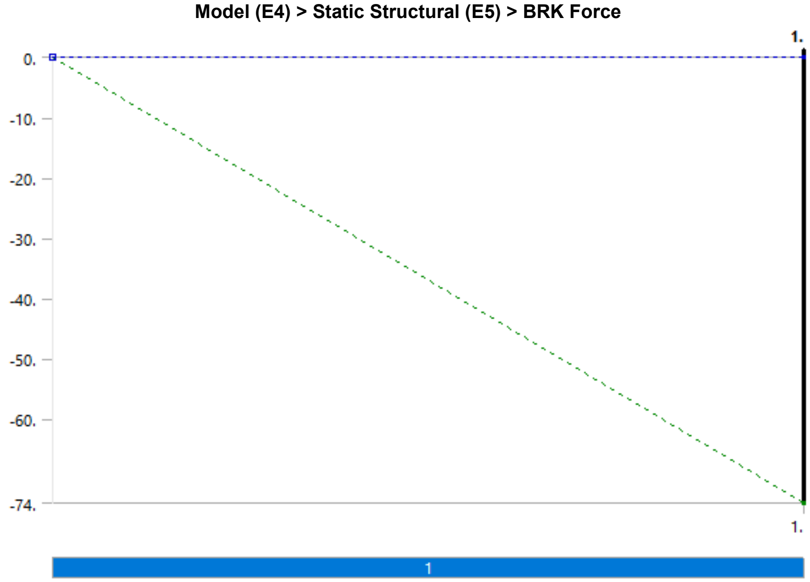

FIGURE 7
Model (E4) > Static Structural (E5) > MagLev Force

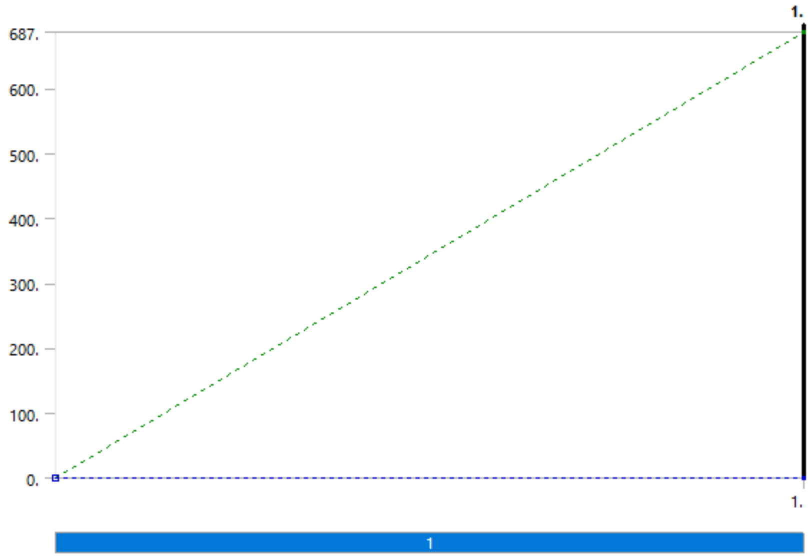

FIGURE 8
Model (E4) > Static Structural (E5) > MagLev Force

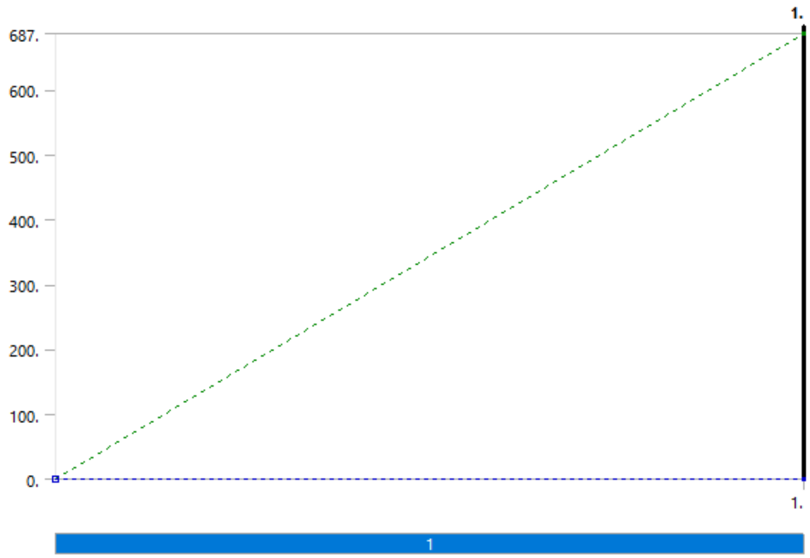

FIGURE 9
Model (E4) > Static Structural (E5) > LIM & GNC Force

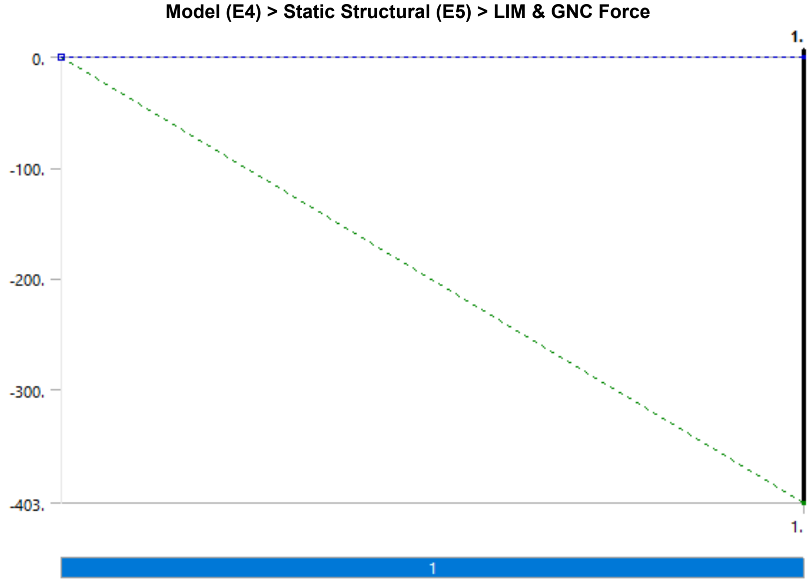

Solution (E6)

TABLE 11
Model (E4) > Static Structural (E5) > Solution

Object Name	*Solution (E6)*
State	Solved
Adaptive Mesh Refinement	
Max Refinement Loops	1.
Refinement Depth	2.
Information	
Status	Done
MAPDL Elapsed Time	2. s
MAPDL Memory Used	266. MB
MAPDL Result File Size	1.1875 MB
Post Processing	
Beam Section Results	No
On Demand Stress/Strain	No

TABLE 12
Model (E4) > Static Structural (E5) > Solution (E6) > Solution Information

Object Name	*Solution Information*
State	Solved
Solution Information	
Solution Output	Solver Output
Newton-Raphson Residuals	0
Identify Element Violations	0
Update Interval	2.5 s
Display Points	All
FE Connection Visibility	
Activate Visibility	Yes
Display	All FE Connectors
Draw Connections Attached To	All Nodes
Line Color	Connection Type
Visible on Results	No
Line Thickness	Single
Display Type	Lines

TABLE 13
Model (E4) > Static Structural (E5) > Solution (E6) > Results

Object Name	*Total Deformation*	*Equivalent Stress*
State	Solved	
Scope		
Scoping Method	Geometry Selection	
Geometry	All Bodies	
Definition		
Type	Total Deformation	Equivalent (von-Mises) Stress
By	Time	
Display Time	Last	
Calculate Time History	Yes	

Identifier		
Suppressed	No	
Results		
Minimum	0. mm	34.165 MPa
Maximum	0.68558 mm	165.09 MPa
Average	0.33298 mm	95.935 MPa
Minimum Occurs On	Geom\PartBody	
Maximum Occurs On	Geom\PartBody	
Information		
Time	1. s	
Load Step	1	
Substep	1	
Iteration Number	1	
Integration Point Results		
Display Option		Averaged
Average Across Bodies		No

FIGURE 10
Model (E4) > Static Structural (E5) > Solution (E6) > Total Deformation

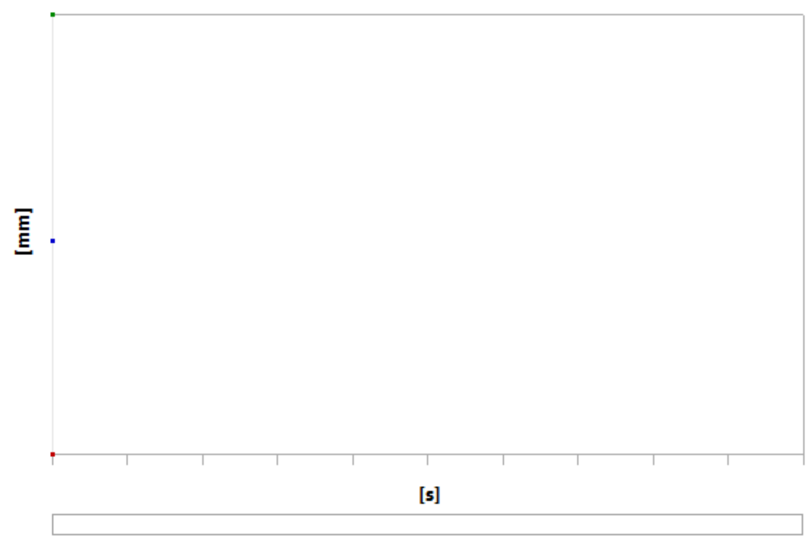

TABLE 14
Model (E4) > Static Structural (E5) > Solution (E6) > Total Deformation

Time [s]	Minimum [mm]	Maximum [mm]	Average [mm]
1.	0.	0.68558	0.33298

FIGURE 11
Model (E4) > Static Structural (E5) > Solution (E6) > Total Deformation > Figure

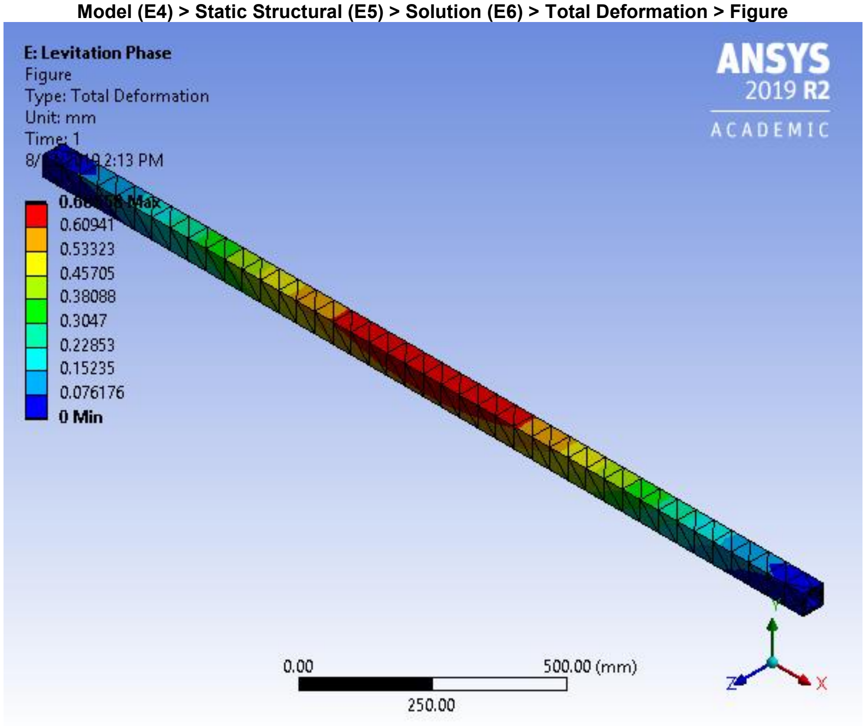

FIGURE 12
Model (E4) > Static Structural (E5) > Solution (E6) > Equivalent Stress

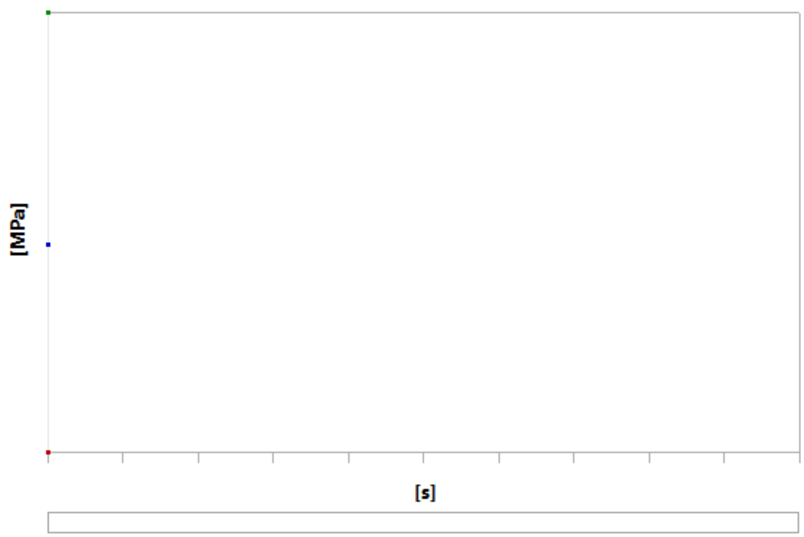

TABLE 15
Model (E4) > Static Structural (E5) > Solution (E6) > Equivalent Stress

Time [s]	Minimum [MPa]	Maximum [MPa]	Average [MPa]
1.	34.165	165.09	95.935

FIGURE 13
Model (E4) > Static Structural (E5) > Solution (E6) > Equivalent Stress > Figure

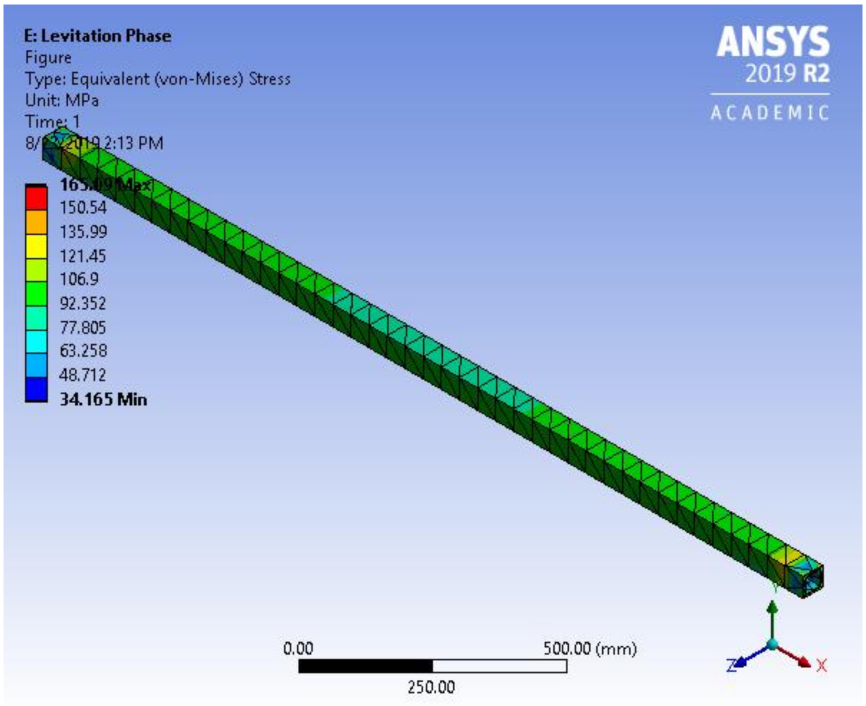

Material Data

Aluminum Alloy

TABLE 16
Aluminum Alloy > Constants

Density	2.77e-006 kg mm^-3
Coefficient of Thermal Expansion	2.3e-005 C^-1
Specific Heat	8.75e+005 mJ kg^-1 C^-1

TABLE 17
Aluminum Alloy > Color

Red	Green	Blue
138	104	46

TABLE 18
Aluminum Alloy > Compressive Ultimate Strength

Compressive Ultimate Strength MPa
0

TABLE 19
Aluminum Alloy > Compressive Yield Strength

Compressive Yield Strength MPa
280

TABLE 20
Aluminum Alloy > Tensile Yield Strength

Tensile Yield Strength MPa
280

TABLE 21
Aluminum Alloy > Tensile Ultimate Strength

Tensile Ultimate Strength MPa
310

TABLE 22
Aluminum Alloy > Isotropic Secant Coefficient of Thermal Expansion

Zero-Thermal-Strain Reference Temperature C
22

TABLE 23
Aluminum Alloy > Isotropic Thermal Conductivity

Thermal Conductivity W mm^-1 C^-1	Temperature C
0.114	-100
0.144	0
0.165	100
0.175	200

TABLE 24
Aluminum Alloy > S-N Curve

Alternating Stress MPa	Cycles	R-Ratio
275.8	1700	-1
241.3	5000	-1
206.8	34000	-1
172.4	1.4e+005	-1
137.9	8.e+005	-1
117.2	2.4e+006	-1
89.63	5.5e+007	-1
82.74	1.e+008	-1
170.6	50000	-0.5
139.6	3.5e+005	-0.5
108.6	3.7e+006	-0.5
87.91	1.4e+007	-0.5
77.57	5.e+007	-0.5
72.39	1.e+008	-0.5
144.8	50000	0
120.7	1.9e+005	0
103.4	1.3e+006	0
93.08	4.4e+006	0

86.18	1.2e+007	0
72.39	1.e+008	0
74.12	3.e+005	0.5
70.67	1.5e+006	0.5
66.36	1.2e+007	0.5
62.05	1.e+008	0.5

TABLE 25
Aluminum Alloy > Isotropic Resistivity

Resistivity ohm mm	Temperature C
2.43e-005	0
2.67e-005	20
3.63e-005	100

TABLE 26
Aluminum Alloy > Isotropic Elasticity

Young's Modulus MPa	Poisson's Ratio	Bulk Modulus MPa	Shear Modulus MPa	Temperature C
71000	0.33	69608	26692	

TABLE 27
Aluminum Alloy > Isotropic Relative Permeability

Relative Permeability
1

Appendix A.8 LCM Load Case IV (Braking Phase) Analysis Report

Project

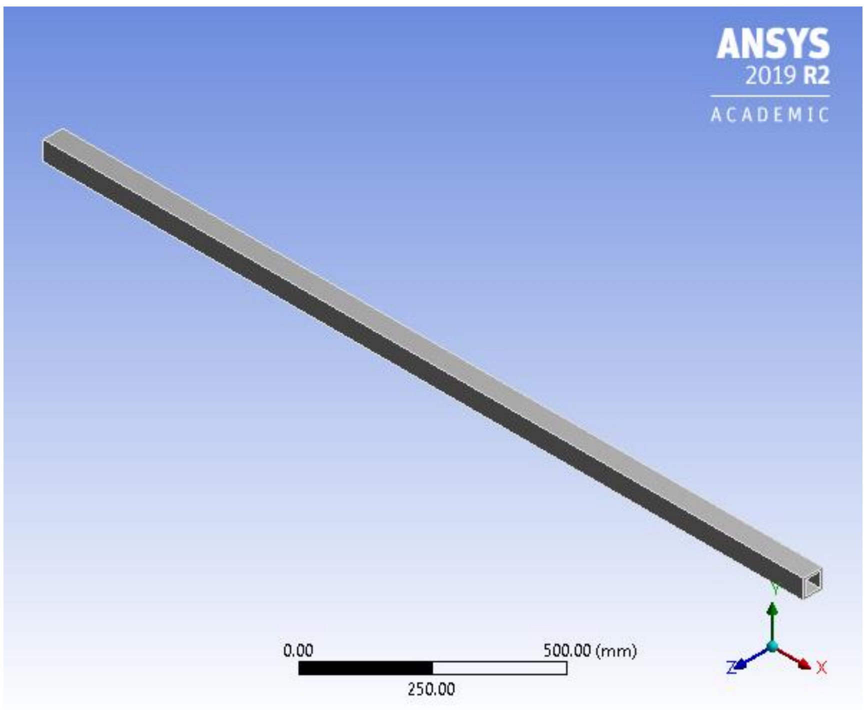

Contents

Units

TABLE 1

Unit System	Metric (mm, kg, N, s, mV, mA) Degrees rad/s Celsius
Angle	Degrees
Rotational Velocity	rad/s
Temperature	Celsius

Model (F4)

Geometry

TABLE 2
Model (F4) > Geometry

Object Name	*Geometry*
State	Fully Defined
Definition	
Source	C:\Users\DIAPM599\OneDrive - Dentsply Sirona\Desktop\ANSYS Analysis\LCM_files\dp0\Geom\DM\Geom.scdoc
Type	SpaceClaim
Length Unit	Meters
Element Control	Program Controlled
Display Style	Body Color
Bounding Box	
Length X	2000. mm
Length Y	50.8 mm
Length Z	50.8 mm

Properties	
Volume	2.2581e+006 mm³
Mass	6.2548 kg
Scale Factor Value	1.
Statistics	
Bodies	1
Active Bodies	1
Nodes	2261
Elements	1143
Mesh Metric	None
Update Options	
Assign Default Material	No
Basic Geometry Options	
Solid Bodies	Yes
Surface Bodies	Yes
Line Bodies	Yes
Parameters	Independent
Parameter Key	
Attributes	Yes
Attribute Key	
Named Selections	Yes
Named Selection Key	
Material Properties	Yes
Advanced Geometry Options	
Use Associativity	Yes
Coordinate Systems	Yes
Coordinate System Key	
Reader Mode Saves Updated File	No
Use Instances	Yes
Smart CAD Update	Yes
Compare Parts On Update	No
Analysis Type	3-D
Mixed Import Resolution	None
Clean Bodies On Import	No
Stitch Surfaces On Import	None
Decompose Disjoint Geometry	Yes
Enclosure and Symmetry Processing	Yes

TABLE 3
Model (F4) > Geometry > Parts

Object Name	*Geom\PartBody*
State	Meshed
Graphics Properties	

Visible	Yes
Transparency	1
Definition	
Suppressed	No
Stiffness Behavior	Flexible
Coordinate System	Default Coordinate System
Reference Temperature	By Environment
Treatment	None
Material	
Assignment	Aluminum Alloy
Nonlinear Effects	Yes
Thermal Strain Effects	Yes
Bounding Box	
Length X	2000. mm
Length Y	50.8 mm
Length Z	50.8 mm
Properties	
Volume	2.2581e+006 mm³
Mass	6.2548 kg
Centroid X	-1000. mm
Centroid Y	25.4 mm
Centroid Z	25.4 mm
Moment of Inertia Ip1	4203.5 kg·mm²
Moment of Inertia Ip2	2.087e+006 kg·mm²
Moment of Inertia Ip3	2.087e+006 kg·mm²
Statistics	
Nodes	2261
Elements	1143
Mesh Metric	None
CAD Attributes	
PartTolerance:	0.00000001
Color:175.143.175	

FIGURE 1
Model (F4) > Geometry > Geom > PartBody > Figure

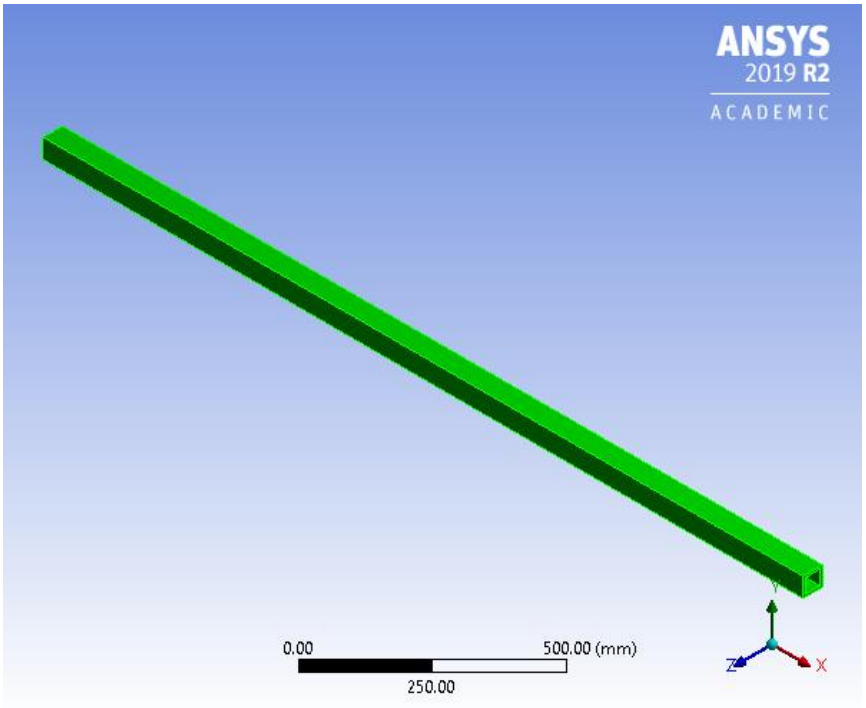

TABLE 4
Model (F4) > Materials

Object Name	*Materials*
State	Fully Defined
Statistics	
Materials	2
Material Assignments	0

Coordinate Systems

TABLE 5
Model (F4) > Coordinate Systems > Coordinate System

Object Name	*Global Coordinate System*
State	Fully Defined
Definition	
Type	Cartesian
Coordinate System ID	0.
Origin	
Origin X	0. mm

Origin Y	0. mm
Origin Z	0. mm
Directional Vectors	
X Axis Data	[1. 0. 0.]
Y Axis Data	[0. 1. 0.]
Z Axis Data	[0. 0. 1.]

Mesh

TABLE 6
Model (F4) > Mesh

Object Name	*Mesh*
State	Solved
Display	
Display Style	Use Geometry Setting
Defaults	
Physics Preference	Mechanical
Element Order	Program Controlled
Element Size	Default
Sizing	
Use Adaptive Sizing	Yes
Resolution	Default (2)
Mesh Defeaturing	Yes
Defeature Size	Default
Transition	Fast
Span Angle Center	Fine
Initial Size Seed	Assembly
Bounding Box Diagonal	2001.3 mm
Average Surface Area	71346 mm²
Minimum Edge Length	38.1 mm
Quality	
Check Mesh Quality	Yes, Errors
Error Limits	Standard Mechanical
Target Quality	Default (0.050000)
Smoothing	Medium
Mesh Metric	None
Inflation	
Use Automatic Inflation	None
Inflation Option	Smooth Transition
Transition Ratio	0.272
Maximum Layers	5
Growth Rate	1.2
Inflation Algorithm	Pre
View Advanced Options	No
Advanced	
Number of CPUs for Parallel Part Meshing	Program Controlled
Straight Sided Elements	No
Rigid Body Behavior	Dimensionally Reduced

Triangle Surface Mesher	Program Controlled
Topology Checking	Yes
Pinch Tolerance	Please Define
Generate Pinch on Refresh	No
Statistics	
Nodes	2261
Elements	1143

TABLE 7
Model (F4) > Mesh > Mesh Controls

Object Name	*Patch Conforming Method*
State	Fully Defined
Scope	
Scoping Method	Geometry Selection
Geometry	1 Body
Definition	
Suppressed	No
Method	Tetrahedrons
Algorithm	Patch Conforming
Element Order	Use Global Setting

FIGURE 2
Model (F4) > Mesh > Figure

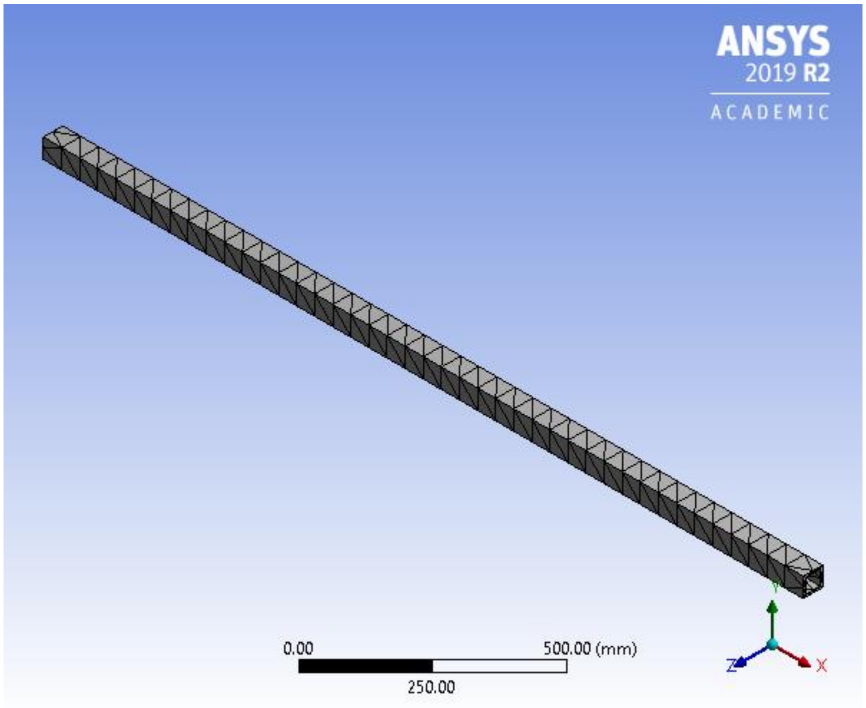

Static Structural (F5)

TABLE 8
Model (F4) > Analysis

Object Name	*Static Structural (F5)*
State	Solved
Definition	
Physics Type	Structural
Analysis Type	Static Structural
Solver Target	Mechanical APDL
Options	
Environment Temperature	22. °C
Generate Input Only	No

TABLE 9
Model (F4) > Static Structural (F5) > Analysis Settings

Object Name	*Analysis Settings*
State	Fully Defined
Step Controls	

Number Of Steps	1.
Current Step Number	1.
Step End Time	1. s
Auto Time Stepping	Program Controlled
Solver Controls	
Solver Type	Program Controlled
Weak Springs	Off
Solver Pivot Checking	Program Controlled
Large Deflection	Off
Inertia Relief	Off
Rotordynamics Controls	
Coriolis Effect	Off
Restart Controls	
Generate Restart Points	Program Controlled
Retain Files After Full Solve	No
Combine Restart Files	Program Controlled
Nonlinear Controls	
Newton-Raphson Option	Program Controlled
Force Convergence	Program Controlled
Moment Convergence	Program Controlled
Displacement Convergence	Program Controlled
Rotation Convergence	Program Controlled
Line Search	Program Controlled
Stabilization	Program Controlled
Output Controls	
Stress	Yes
Surface Stress	No
Back Stress	No
Strain	Yes
Contact Data	Yes
Nonlinear Data	No
Nodal Forces	No
Contact Miscellaneous	No
General Miscellaneous	No
Store Results At	All Time Points
Result File Compression	Program Controlled
Analysis Data Management	
Solver Files Directory	C:\Users\DIAPM599\OneDrive - Dentsply Sirona\Desktop\ANSYS Analysis\LCM_files\dp0\SYS-3\MECH\
Future Analysis	None
Scratch Solver Files Directory	
Save MAPDL db	No
Contact Summary	Program Controlled
Delete Unneeded Files	Yes

Nonlinear Solution	No
Solver Units	Active System
Solver Unit System	nmm

FIGURE 3
Model (F4) > Static Structural (F5) > Figure

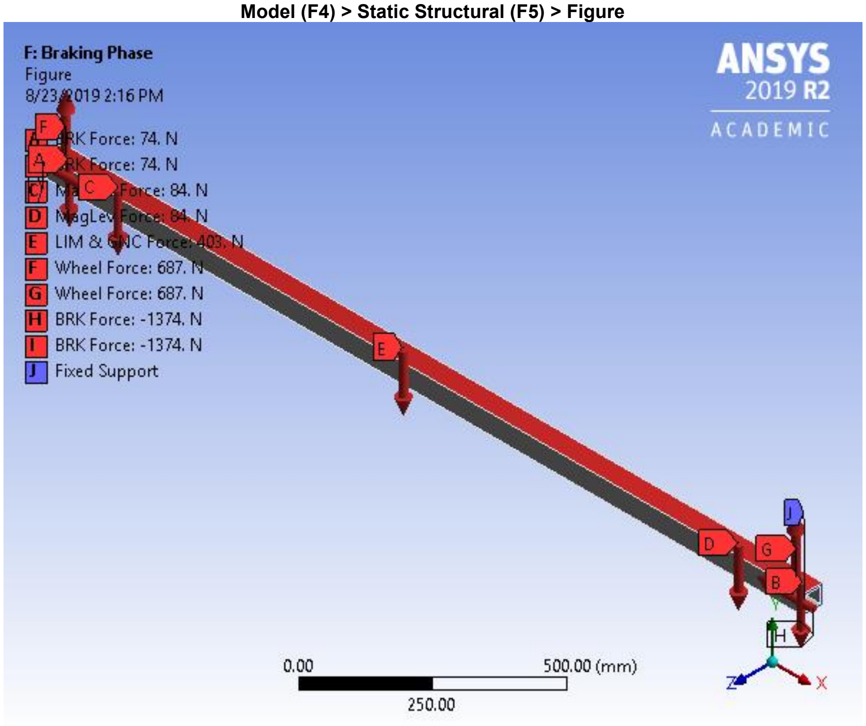

TABLE 10
Model (F4) > Static Structural (F5) > Loads

Object Name	*Thermal Condition*	*BRK Force*	*BRK Force*	*MagLev Force*	*MagLev Force*	*LIM & GNC Force*	*Wheel Force*	*Wheel Force*	*BRK Force*	*BRK Force*	*Fixed Support*
State	Fully Defined										
Scope											
Scoping Method	Geometry Selection										
Geometry	1 Body	1 Face									2 Faces
Definition											
Type	Thermal Condition	Force									Fixed Support

Magnitude	80. °C (ramped)					-1374. N (ramped)	
Suppressed	No						
Define By		Components				Vector	
Coordinate System		Global Coordinate System					
X Component		0. N (ramped)					
Y Component		-74. N (ramped)	-84. N (ramped)	-403. N (ramped)	687. N (ramped)		
Z Component		0. N (ramped)					
Direction						Defined	

FIGURE 4
Model (F4) > Static Structural (F5) > Thermal Condition

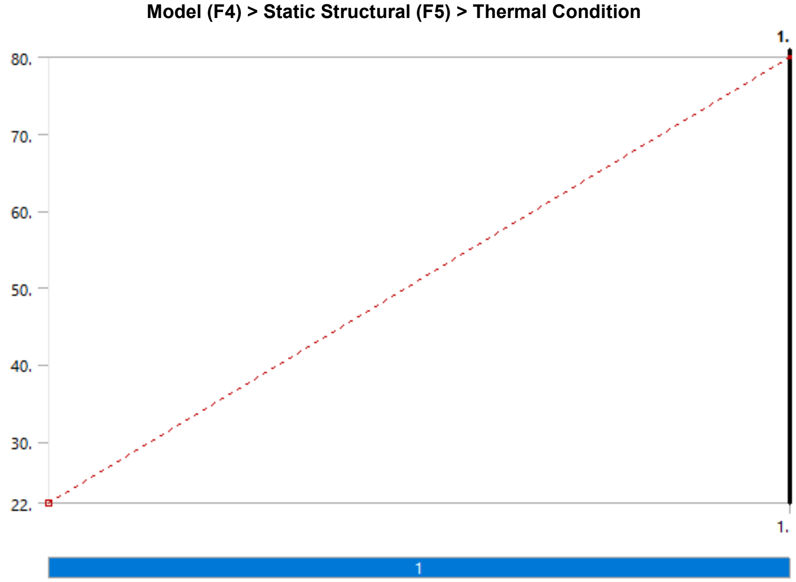

FIGURE 5
Model (F4) > Static Structural (F5) > BRK Force

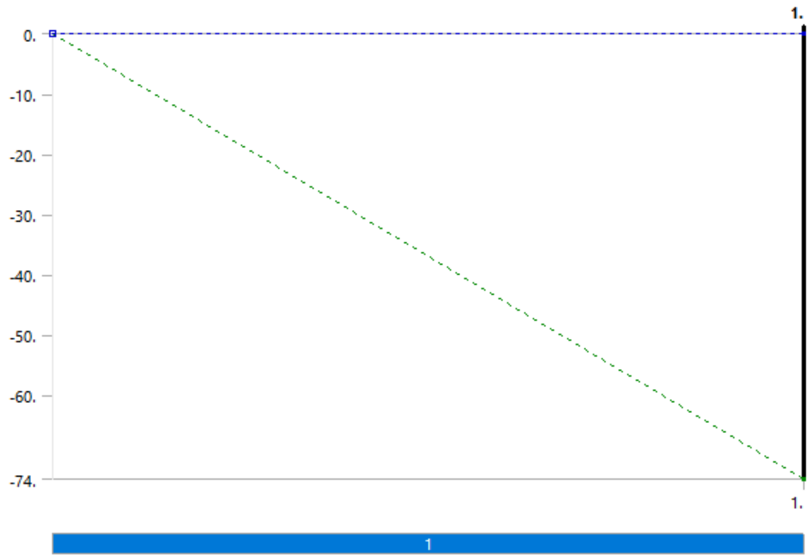

FIGURE 6
Model (F4) > Static Structural (F5) > BRK Force

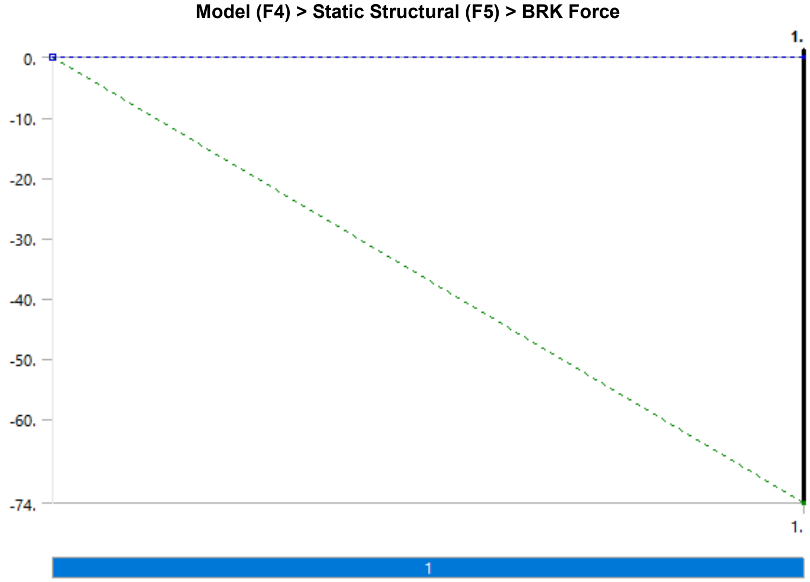

FIGURE 7
Model (F4) > Static Structural (F5) > MagLev Force

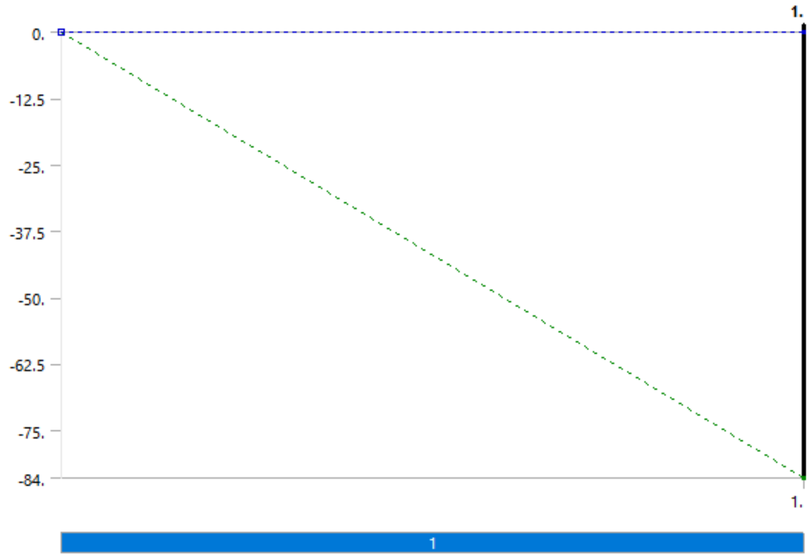

FIGURE 8
Model (F4) > Static Structural (F5) > MagLev Force

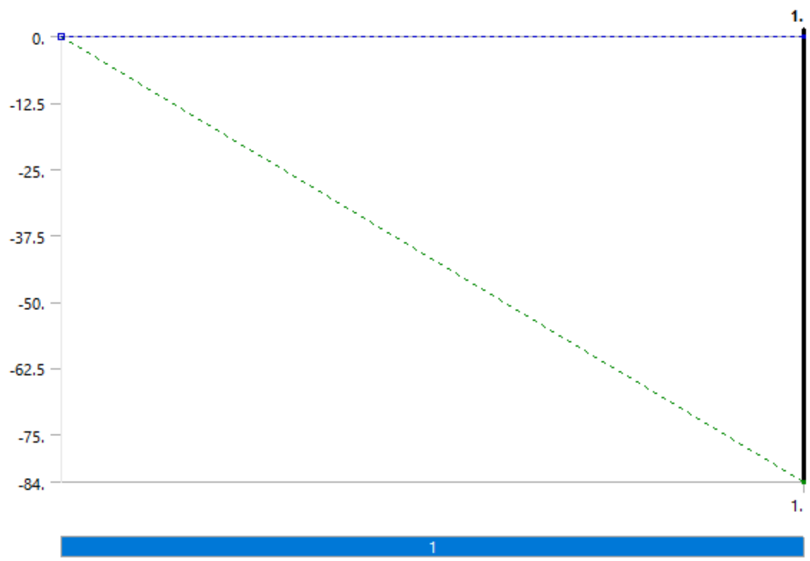

FIGURE 9
Model (F4) > Static Structural (F5) > LIM & GNC Force

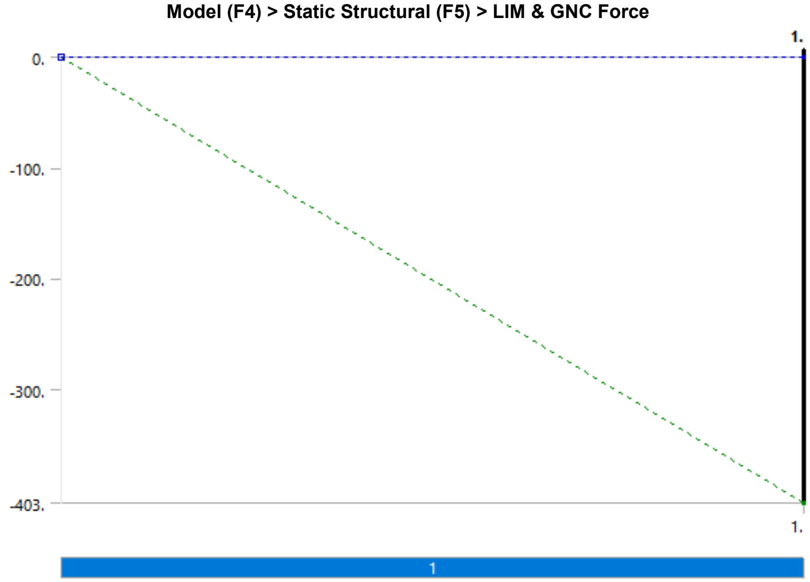

FIGURE 10
Model (F4) > Static Structural (F5) > Wheel Force

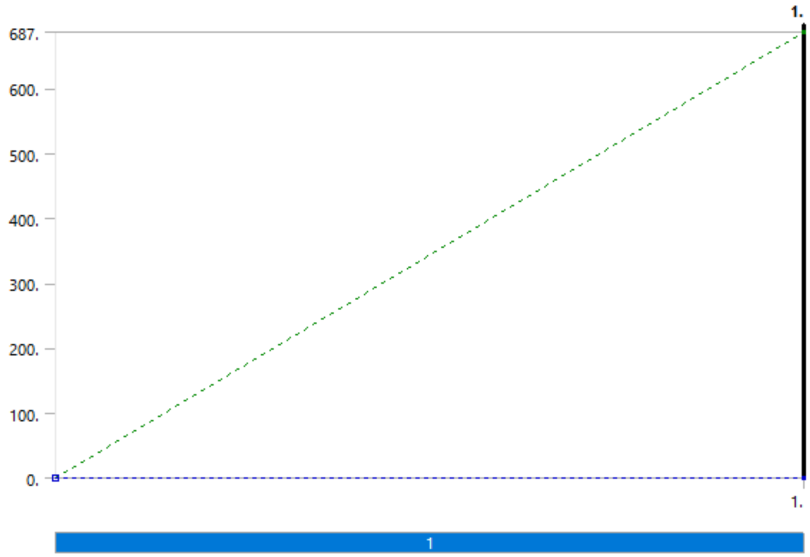

FIGURE 11
Model (F4) > Static Structural (F5) > Wheel Force

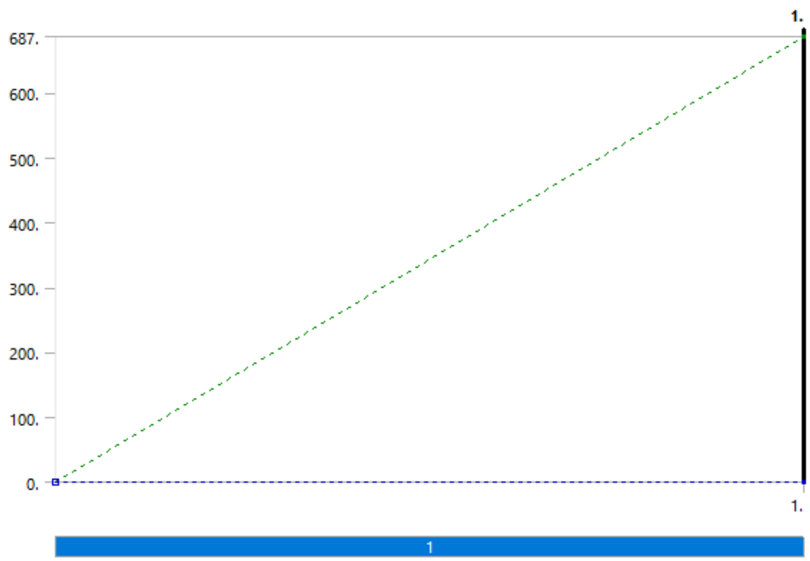

FIGURE 12
Model (F4) > Static Structural (F5) > BRK Force

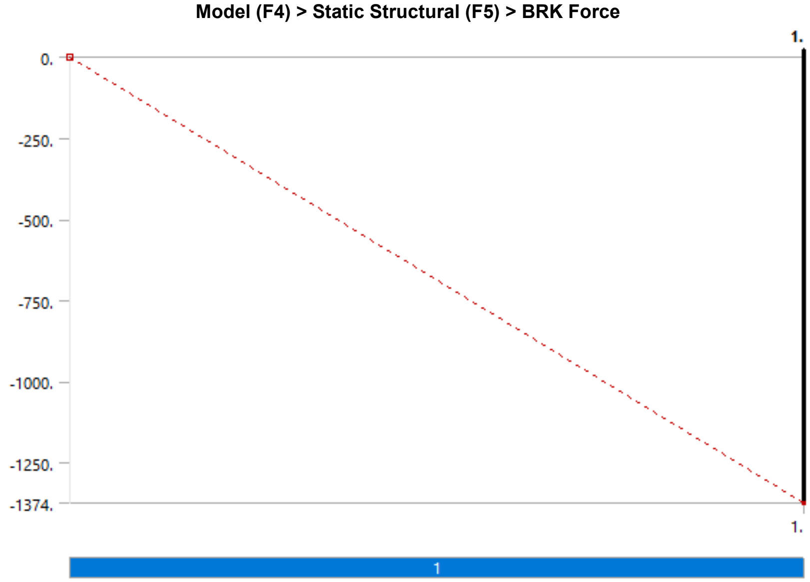

FIGURE 13
Model (F4) > Static Structural (F5) > BRK Force

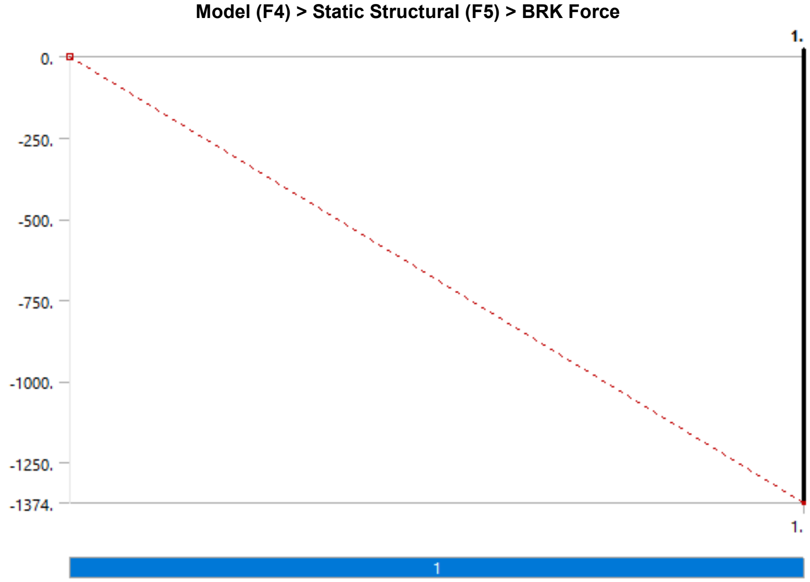

Solution (F6)

TABLE 11
Model (F4) > Static Structural (F5) > Solution

Object Name	*Solution (F6)*
State	Solved
Adaptive Mesh Refinement	
Max Refinement Loops	1.
Refinement Depth	2.
Information	
Status	Done
MAPDL Elapsed Time	2. s
MAPDL Memory Used	266. MB
MAPDL Result File Size	1.25 MB
Post Processing	
Beam Section Results	No
On Demand Stress/Strain	No

TABLE 12
Model (F4) > Static Structural (F5) > Solution (F6) > Solution Information

Object Name	*Solution Information*
State	Solved
Solution Information	

Solution Output	Solver Output
Newton-Raphson Residuals	0
Identify Element Violations	0
Update Interval	2.5 s
Display Points	All
FE Connection Visibility	
Activate Visibility	Yes
Display	All FE Connectors
Draw Connections Attached To	All Nodes
Line Color	Connection Type
Visible on Results	No
Line Thickness	Single
Display Type	Lines

TABLE 13
Model (F4) > Static Structural (F5) > Solution (F6) > Results

Object Name	*Total Deformation*	*Equivalent Stress*
State	Solved	
Scope		
Scoping Method	Geometry Selection	
Geometry	All Bodies	
Definition		
Type	Total Deformation	Equivalent (von-Mises) Stress
By	Time	
Display Time	Last	
Calculate Time History	Yes	
Identifier		
Suppressed	No	
Results		
Minimum	0. mm	34.987 MPa
Maximum	0.55549 mm	165.71 MPa
Average	0.26761 mm	95.926 MPa
Minimum Occurs On	Geom\PartBody	
Maximum Occurs On	Geom\PartBody	
Information		
Time	1. s	
Load Step	1	
Substep	1	
Iteration Number	1	
Integration Point Results		
Display Option		Averaged
Average Across Bodies		No

FIGURE 14
Model (F4) > Static Structural (F5) > Solution (F6) > Total Deformation

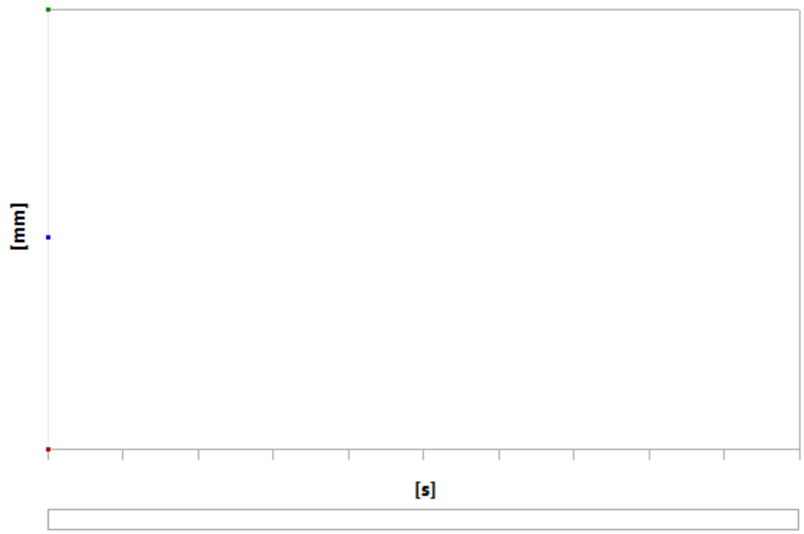

TABLE 14
Model (F4) > Static Structural (F5) > Solution (F6) > Total Deformation

Time [s]	Minimum [mm]	Maximum [mm]	Average [mm]
1.	0.	0.55549	0.26761

FIGURE 15
Model (F4) > Static Structural (F5) > Solution (F6) > Total Deformation > Figure

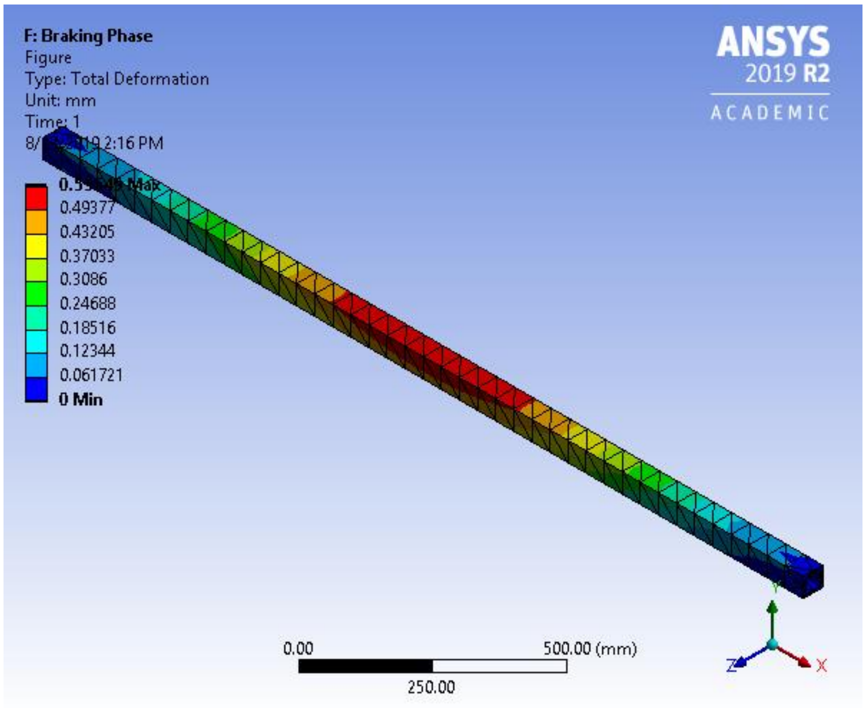

FIGURE 16
Model (F4) > Static Structural (F5) > Solution (F6) > Equivalent Stress

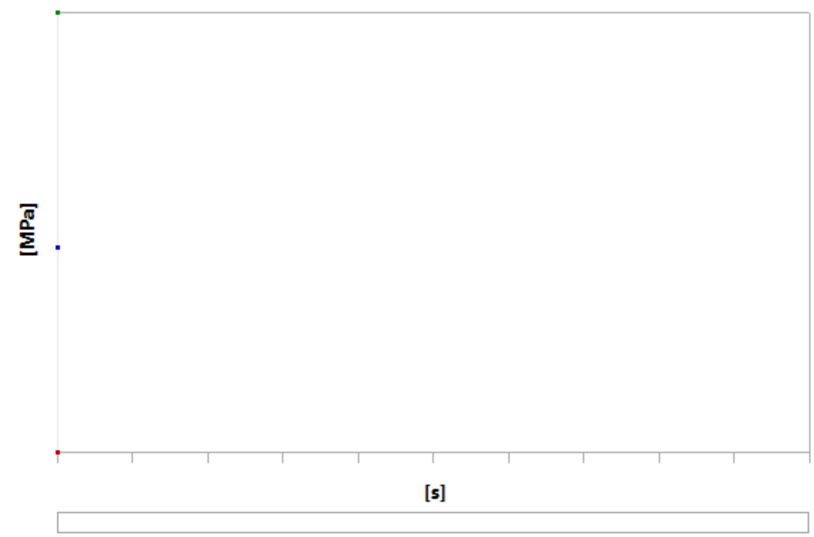

TABLE 15
Model (F4) > Static Structural (F5) > Solution (F6) > Equivalent Stress

Time [s]	Minimum [MPa]	Maximum [MPa]	Average [MPa]
1.	34.987	165.71	95.926

FIGURE 17
Model (F4) > Static Structural (F5) > Solution (F6) > Equivalent Stress > Figure

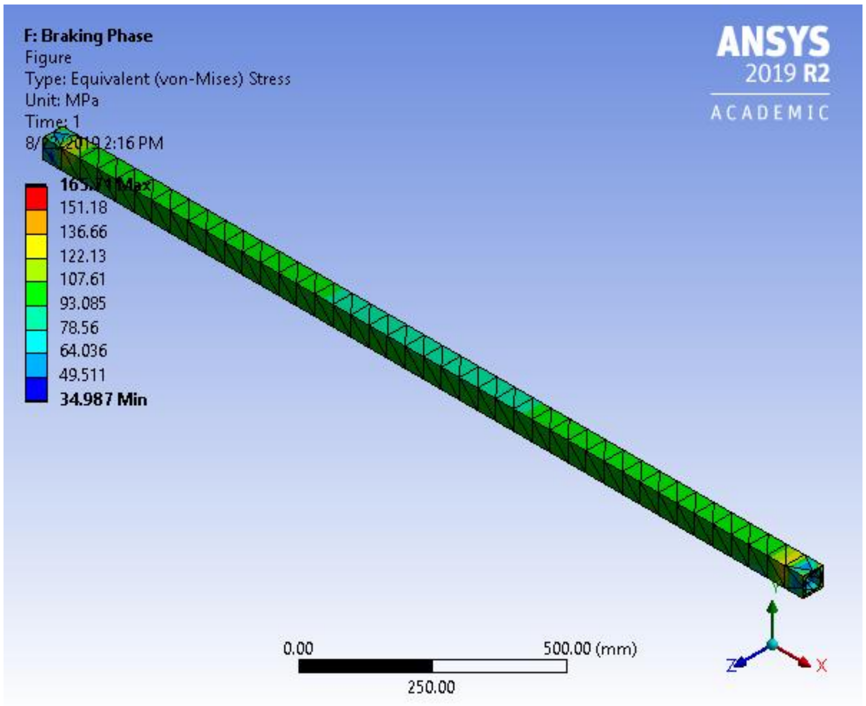

Material Data

Aluminum Alloy

TABLE 16
Aluminum Alloy > Constants

Density	2.77e-006 kg mm^-3
Coefficient of Thermal Expansion	2.3e-005 C^-1
Specific Heat	8.75e+005 mJ kg^-1 C^-1

TABLE 17
Aluminum Alloy > Color

Red	Green	Blue
138	104	46

TABLE 18
Aluminum Alloy > Compressive Ultimate Strength

Compressive Ultimate Strength MPa
0

TABLE 19
Aluminum Alloy > Compressive Yield Strength

Compressive Yield Strength MPa
280

TABLE 20
Aluminum Alloy > Tensile Yield Strength

Tensile Yield Strength MPa
280

TABLE 21
Aluminum Alloy > Tensile Ultimate Strength

Tensile Ultimate Strength MPa
310

TABLE 22
Aluminum Alloy > Isotropic Secant Coefficient of Thermal Expansion

Zero-Thermal-Strain Reference Temperature C
22

TABLE 23
Aluminum Alloy > Isotropic Thermal Conductivity

Thermal Conductivity W mm^-1 C^-1	Temperature C
0.114	-100
0.144	0
0.165	100
0.175	200

TABLE 24
Aluminum Alloy > S-N Curve

Alternating Stress MPa	Cycles	R-Ratio
275.8	1700	-1
241.3	5000	-1
206.8	34000	-1
172.4	1.4e+005	-1
137.9	8.e+005	-1
117.2	2.4e+006	-1
89.63	5.5e+007	-1
82.74	1.e+008	-1
170.6	50000	-0.5
139.6	3.5e+005	-0.5
108.6	3.7e+006	-0.5
87.91	1.4e+007	-0.5
77.57	5.e+007	-0.5
72.39	1.e+008	-0.5
144.8	50000	0
120.7	1.9e+005	0
103.4	1.3e+006	0
93.08	4.4e+006	0

86.18	1.2e+007	0
72.39	1.e+008	0
74.12	3.e+005	0.5
70.67	1.5e+006	0.5
66.36	1.2e+007	0.5
62.05	1.e+008	0.5

TABLE 25
Aluminum Alloy > Isotropic Resistivity

Resistivity ohm mm	Temperature C
2.43e-005	0
2.67e-005	20
3.63e-005	100

TABLE 26
Aluminum Alloy > Isotropic Elasticity

Young's Modulus MPa	Poisson's Ratio	Bulk Modulus MPa	Shear Modulus MPa	Temperature C
71000	0.33	69608	26692	

TABLE 27
Aluminum Alloy > Isotropic Relative Permeability

Relative Permeability
1

Appendix A.9 Bulkhead Load Case (Braking Phase) Analysis Report

Project

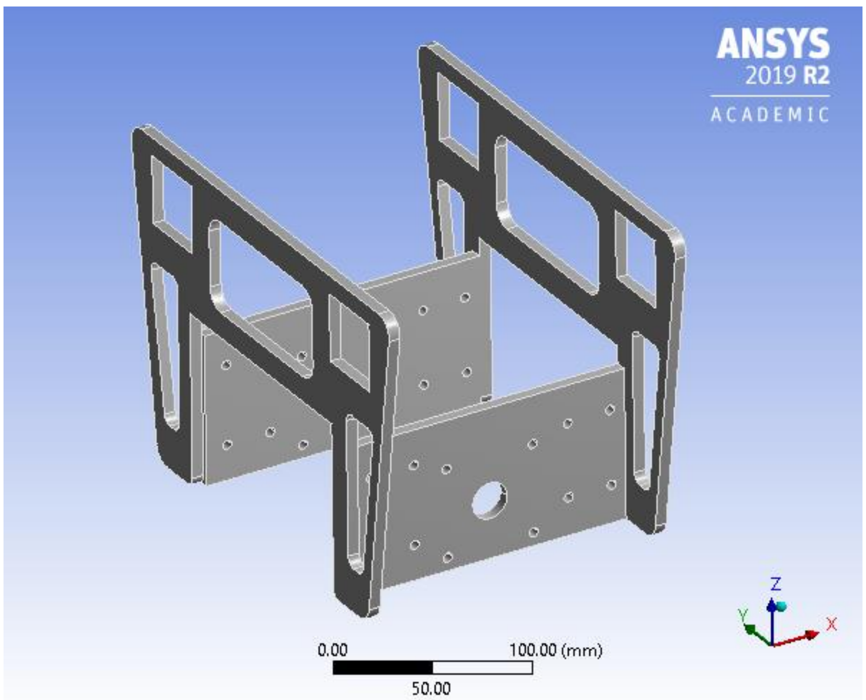

Contents

Units

TABLE 1

Unit System	Metric (mm, kg, N, s, mV, mA) Degrees rad/s Celsius
Angle	Degrees
Rotational Velocity	rad/s
Temperature	Celsius

Model (C4)

Geometry

TABLE 2
Model (C4) > Geometry

Object Name	*Geometry*
State	Fully Defined
Definition	
Source	D:\RH_PRP_Chassis_BulkHead.igs
Type	Iges
Length Unit	Millimeters
Element Control	Program Controlled
Display Style	Body Color
Bounding Box	
Length X	172.7 mm
Length Y	251.12 mm
Length Z	182.12 mm
Properties	

Volume	3.8104e+005 mm³
Mass	1.0555 kg
Scale Factor Value	1.
Statistics	
Bodies	1
Active Bodies	1
Nodes	11908
Elements	5576
Mesh Metric	None
Update Options	
Assign Default Material	No
Basic Geometry Options	
Solid Bodies	Yes
Surface Bodies	Yes
Line Bodies	No
Parameters	Independent
Parameter Key	ANS;DS
Attributes	No
Named Selections	No
Material Properties	No
Advanced Geometry Options	
Use Associativity	Yes
Coordinate Systems	No
Reader Mode Saves Updated File	No
Use Instances	Yes
Smart CAD Update	Yes
Compare Parts On Update	No
Analysis Type	3-D
Mixed Import Resolution	None
Clean Bodies On Import	No
Stitch Surfaces On Import	Program Tolerance
Decompose Disjoint Geometry	Yes
Enclosure and Symmetry Processing	Yes

TABLE 3
Model (C4) > Geometry > Parts

Object Name	*RH_PRP_Chassis_BulkHead-FreeParts|PartBody*
State	Meshed
Graphics Properties	
Visible	Yes
Transparency	1
Definition	
Suppressed	No
Stiffness Behavior	Flexible
Coordinate System	Default Coordinate System
Reference Temperature	By Environment
Treatment	None
Material	
Assignment	Aluminum Alloy

Nonlinear Effects	Yes
Thermal Strain Effects	Yes
Bounding Box	
Length X	172.7 mm
Length Y	251.12 mm
Length Z	182.12 mm
Properties	
Volume	3.8104e+005 mm³
Mass	1.0555 kg
Centroid X	86.745 mm
Centroid Y	0.17852 mm
Centroid Z	16.361 mm
Moment of Inertia Ip1	9126.2 kg·mm²
Moment of Inertia Ip2	8230.3 kg·mm²
Moment of Inertia Ip3	11149 kg·mm²
Statistics	
Nodes	11908
Elements	5576
Mesh Metric	None

FIGURE 1
Model (C4) > Geometry > RH_PRP_Chassis_BulkHead-FreeParts|PartBody > Figure

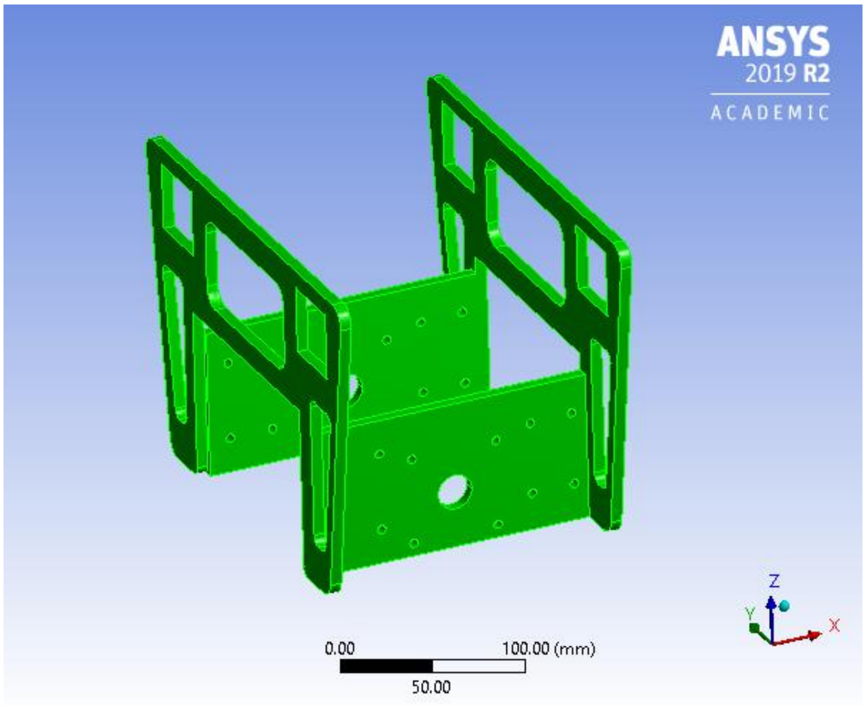

TABLE 4
Model (C4) > Materials

Object Name	*Materials*
State	Fully Defined
Statistics	
Materials	2
Material Assignments	0

Coordinate Systems

TABLE 5
Model (C4) > Coordinate Systems > Coordinate System

Object Name	*Global Coordinate System*
State	Fully Defined
Definition	
Type	Cartesian
Coordinate System ID	0.
Origin	
Origin X	0. mm

Origin Y	0. mm
Origin Z	0. mm
Directional Vectors	
X Axis Data	[1. 0. 0.]
Y Axis Data	[0. 1. 0.]
Z Axis Data	[0. 0. 1.]

Mesh

TABLE 6
Model (C4) > Mesh

Object Name	*Mesh*
State	Solved
Display	
Display Style	Use Geometry Setting
Defaults	
Physics Preference	Mechanical
Element Order	Program Controlled
Element Size	Default
Sizing	
Use Adaptive Sizing	Yes
Resolution	Default (2)
Mesh Defeaturing	Yes
Defeature Size	Default
Transition	Fast
Span Angle Center	Coarse
Initial Size Seed	Assembly
Bounding Box Diagonal	355.04 mm
Average Surface Area	980.37 mm²
Minimum Edge Length	0.21228 mm
Quality	
Check Mesh Quality	Yes, Errors
Error Limits	Standard Mechanical
Target Quality	Default (0.050000)
Smoothing	Medium
Mesh Metric	None
Inflation	
Use Automatic Inflation	None
Inflation Option	Smooth Transition
Transition Ratio	0.272
Maximum Layers	5
Growth Rate	1.2
Inflation Algorithm	Pre
View Advanced Options	No
Advanced	
Number of CPUs for Parallel Part Meshing	Program Controlled
Straight Sided Elements	No
Rigid Body Behavior	Dimensionally Reduced

Triangle Surface Mesher	Program Controlled
Topology Checking	Yes
Pinch Tolerance	Please Define
Generate Pinch on Refresh	No
Statistics	
Nodes	11908
Elements	5576

TABLE 7
Model (C4) > Mesh > Mesh Controls

Object Name	*Patch Conforming Method*
State	Fully Defined
Scope	
Scoping Method	Geometry Selection
Geometry	1 Body
Definition	
Suppressed	No
Method	Tetrahedrons
Algorithm	Patch Conforming
Element Order	Use Global Setting

FIGURE 2
Model (C4) > Mesh > Figure

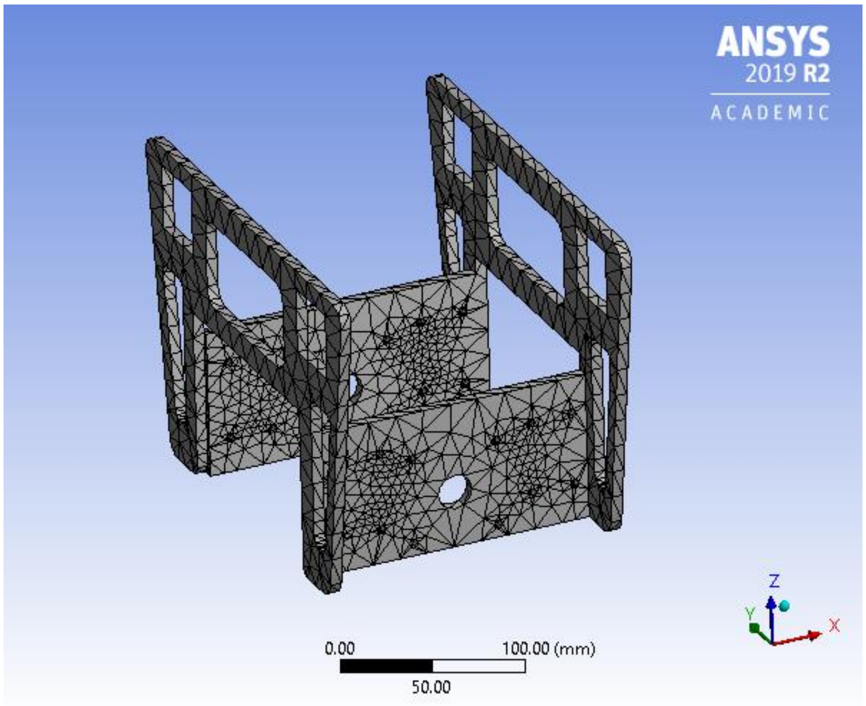

Static Structural (C5)

TABLE 8
Model (C4) > Analysis

Object Name	*Static Structural (C5)*
State	Solved
Definition	
Physics Type	Structural
Analysis Type	Static Structural
Solver Target	Mechanical APDL
Options	
Environment Temperature	22. °C
Generate Input Only	No

TABLE 9
Model (C4) > Static Structural (C5) > Analysis Settings

Object Name	*Analysis Settings*
State	Fully Defined
Step Controls	

Number Of Steps	1.
Current Step Number	1.
Step End Time	1. s
Auto Time Stepping	Program Controlled
Solver Controls	
Solver Type	Program Controlled
Weak Springs	Off
Solver Pivot Checking	Program Controlled
Large Deflection	Off
Inertia Relief	Off
Rotordynamics Controls	
Coriolis Effect	Off
Restart Controls	
Generate Restart Points	Program Controlled
Retain Files After Full Solve	No
Combine Restart Files	Program Controlled
Nonlinear Controls	
Newton-Raphson Option	Program Controlled
Force Convergence	Program Controlled
Moment Convergence	Program Controlled
Displacement Convergence	Program Controlled
Rotation Convergence	Program Controlled
Line Search	Program Controlled
Stabilization	Program Controlled
Output Controls	
Stress	Yes
Surface Stress	No
Back Stress	No
Strain	Yes
Contact Data	Yes
Nonlinear Data	No
Nodal Forces	No
Contact Miscellaneous	No
General Miscellaneous	No
Store Results At	All Time Points
Result File Compression	Program Controlled
Analysis Data Management	
Solver Files Directory	C:\Users\DIAPM599\OneDrive - Dentsply Sirona\Desktop\ANSYS Analysis\Bulkhead_files\dp0\SYS\MECH\
Future Analysis	None
Scratch Solver Files Directory	
Save MAPDL db	No
Contact Summary	Program Controlled

Delete Unneeded Files	Yes
Nonlinear Solution	No
Solver Units	Active System
Solver Unit System	nmm

TABLE 10
Model (C4) > Static Structural (C5) > Loads

Object Name	*Thermal Condition*	*BRK Force*	*BRK Force*	*BRK Force*	*BRK Force*	*Fixed Support*
State	Fully Defined					
Scope						
Scoping Method	Geometry Selection					
Geometry	1 Body	1 Face				16 Faces
Definition						
Type	Thermal Condition	Force				Fixed Support
Magnitude	80. °C (ramped)	1957. N (ramped)		-1374. N (ramped)		
Suppressed	No					
Define By		Vector				
Direction		Defined				

FIGURE 3
Model (C4) > Static Structural (C5) > Thermal Condition

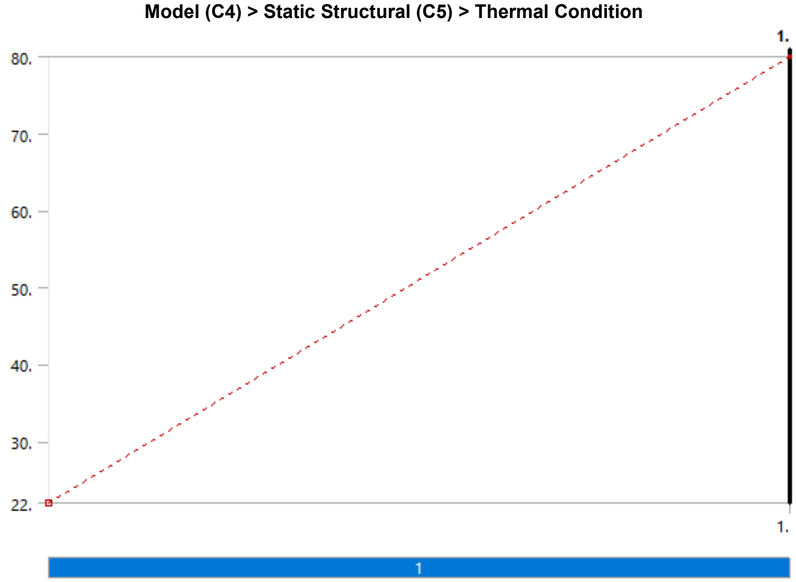

FIGURE 4
Model (C4) > Static Structural (C5) > BRK Force

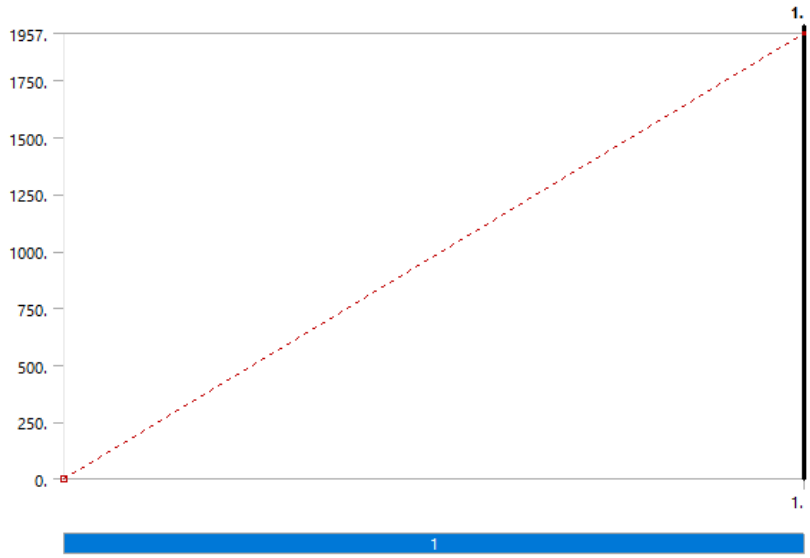

FIGURE 5
Model (C4) > Static Structural (C5) > BRK Force

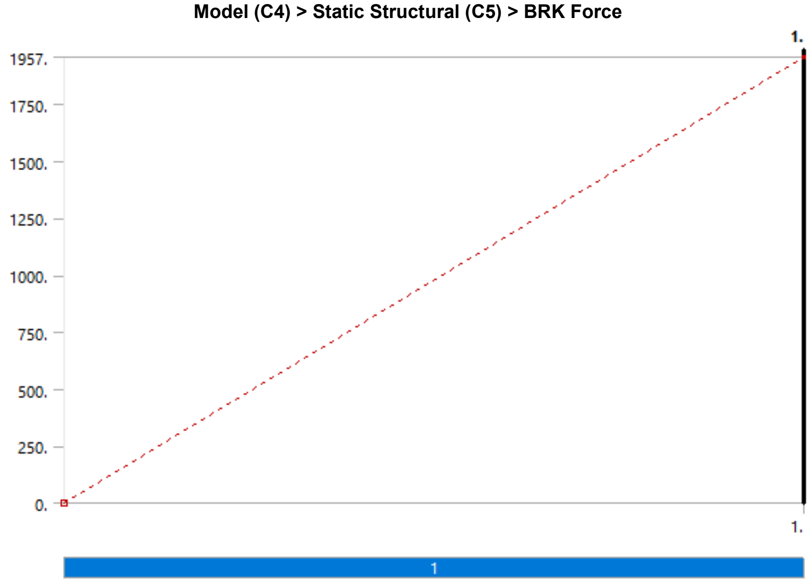

FIGURE 6
Model (C4) > Static Structural (C5) > BRK Force

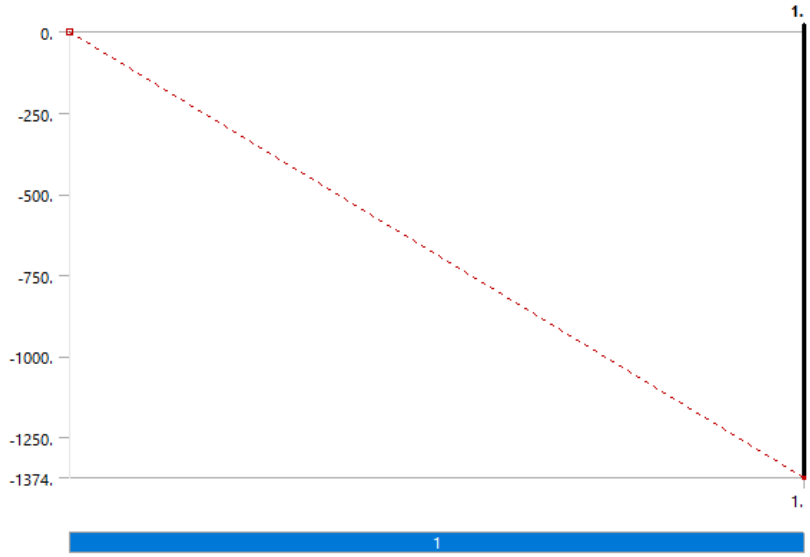

FIGURE 7
Model (C4) > Static Structural (C5) > BRK Force

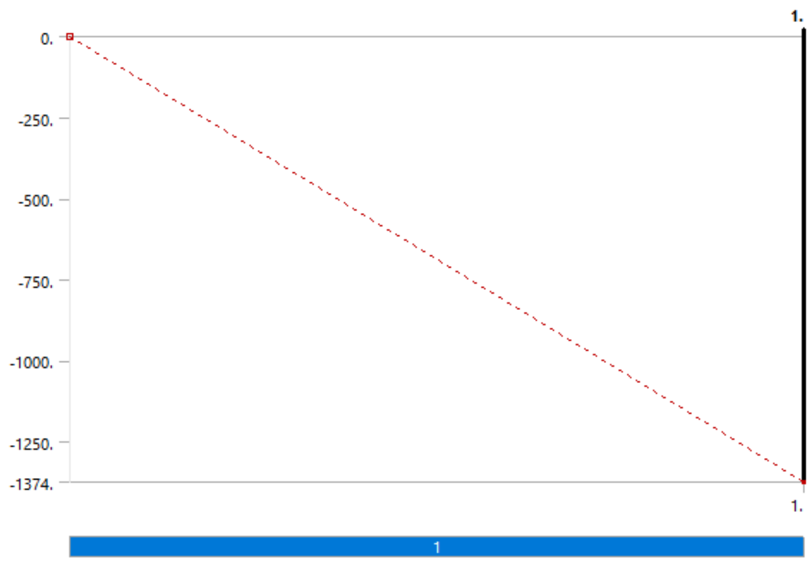

Solution (C6)

TABLE 11
Model (C4) > Static Structural (C5) > Solution

Object Name	*Solution (C6)*
State	Solved
Adaptive Mesh Refinement	
Max Refinement Loops	1.
Refinement Depth	2.
Information	
Status	Done
MAPDL Elapsed Time	4. s
MAPDL Memory Used	325. MB
MAPDL Result File Size	4.5625 MB
Post Processing	
Beam Section Results	No
On Demand Stress/Strain	No

TABLE 12
Model (C4) > Static Structural (C5) > Solution (C6) > Solution Information

Object Name	*Solution Information*
State	Solved
Solution Information	
Solution Output	Solver Output
Newton-Raphson Residuals	0

Identify Element Violations	0
Update Interval	2.5 s
Display Points	All
FE Connection Visibility	
Activate Visibility	Yes
Display	All FE Connectors
Draw Connections Attached To	All Nodes
Line Color	Connection Type
Visible on Results	No
Line Thickness	Single
Display Type	Lines

TABLE 13
Model (C4) > Static Structural (C5) > Solution (C6) > Results

Object Name	*Total Deformation*	*Equivalent Stress*
State	Solved	
Scope		
Scoping Method	Geometry Selection	
Geometry	All Bodies	
Definition		
Type	Total Deformation	Equivalent (von-Mises) Stress
By	Time	
Display Time	Last	
Calculate Time History	Yes	
Identifier		
Suppressed	No	
Results		
Minimum	0. mm	0.52937 MPa
Maximum	1.0151 mm	193.69 MPa
Average	0.47214 mm	31.029 MPa
Minimum Occurs On	RH_PRP_Chassis_BulkHead-FreeParts|PartBody	
Maximum Occurs On	RH_PRP_Chassis_BulkHead-FreeParts|PartBody	
Information		
Time	1. s	
Load Step	1	
Substep	1	
Iteration Number	1	
Integration Point Results		
Display Option		Averaged
Average Across Bodies		No

FIGURE 8
Model (C4) > Static Structural (C5) > Solution (C6) > Total Deformation

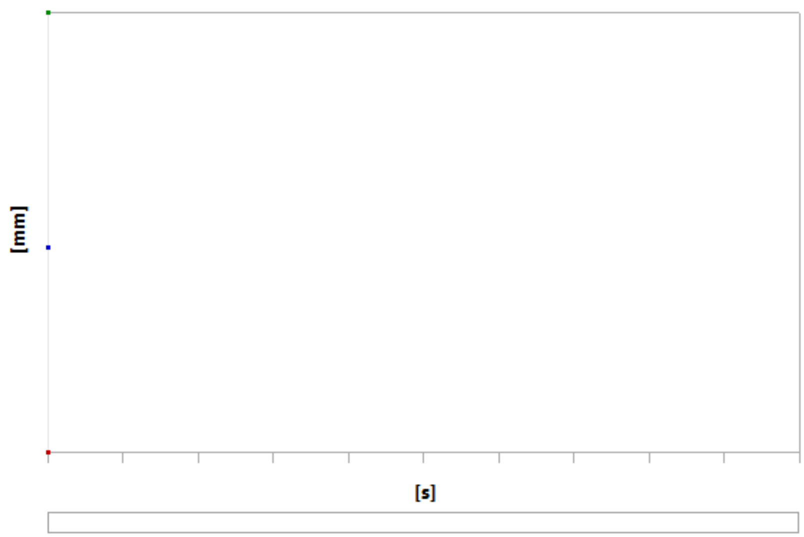

TABLE 14
Model (C4) > Static Structural (C5) > Solution (C6) > Total Deformation

Time [s]	Minimum [mm]	Maximum [mm]	Average [mm]
1.	0.	1.0151	0.47214

FIGURE 9
Model (C4) > Static Structural (C5) > Solution (C6) > Total Deformation > Figure

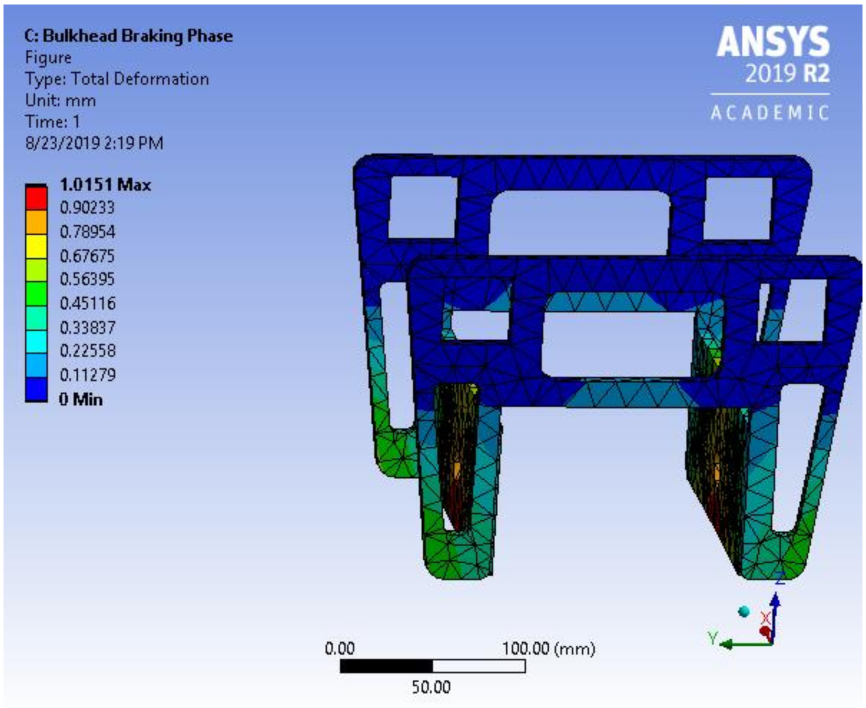

FIGURE 10
Model (C4) > Static Structural (C5) > Solution (C6) > Equivalent Stress

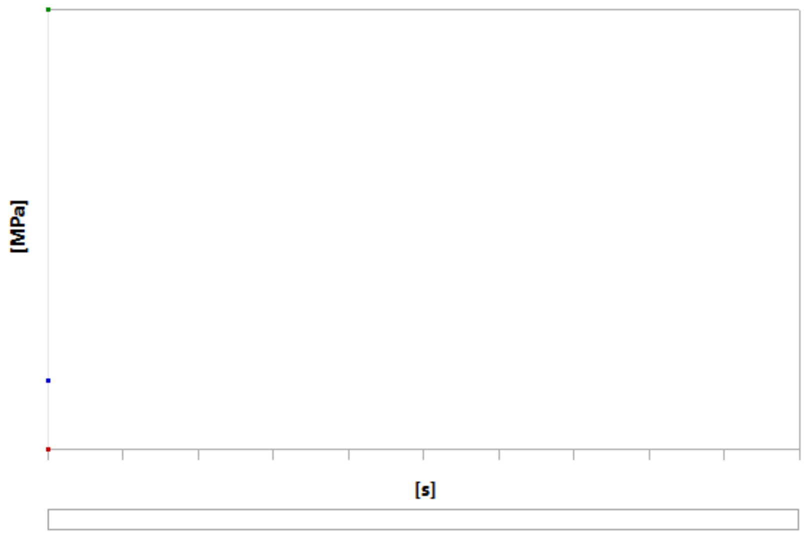

TABLE 15
Model (C4) > Static Structural (C5) > Solution (C6) > Equivalent Stress

Time [s]	Minimum [MPa]	Maximum [MPa]	Average [MPa]
1.	0.52937	193.69	31.029

FIGURE 11
Model (C4) > Static Structural (C5) > Solution (C6) > Equivalent Stress > Figure

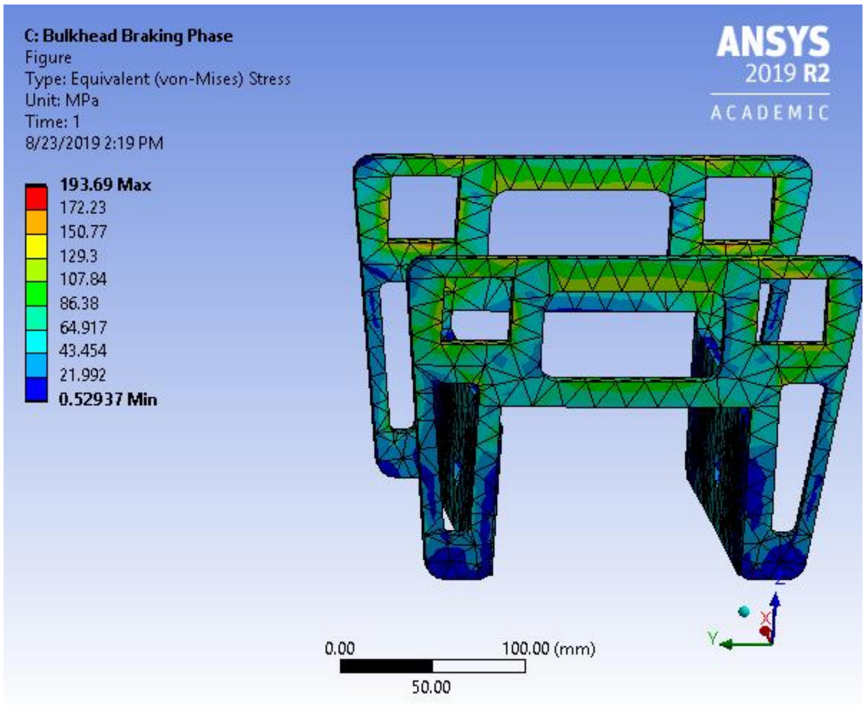

Material Data

Aluminum Alloy

TABLE 16
Aluminum Alloy > Constants

Density	2.77e-006 kg mm^-3
Coefficient of Thermal Expansion	2.3e-005 C^-1
Specific Heat	8.75e+005 mJ kg^-1 C^-1

TABLE 17
Aluminum Alloy > Color

Red	Green	Blue
138	104	46

TABLE 18
Aluminum Alloy > Compressive Ultimate Strength

Compressive Ultimate Strength MPa
0

TABLE 19
Aluminum Alloy > Compressive Yield Strength

Compressive Yield Strength MPa
280

TABLE 20
Aluminum Alloy > Tensile Yield Strength

Tensile Yield Strength MPa
280

TABLE 21
Aluminum Alloy > Tensile Ultimate Strength

Tensile Ultimate Strength MPa
310

TABLE 22
Aluminum Alloy > Isotropic Secant Coefficient of Thermal Expansion

Zero-Thermal-Strain Reference Temperature C
22

TABLE 23
Aluminum Alloy > Isotropic Thermal Conductivity

Thermal Conductivity W mm^-1 C^-1	Temperature C
0.114	-100
0.144	0
0.165	100
0.175	200

TABLE 24
Aluminum Alloy > S-N Curve

Alternating Stress MPa	Cycles	R-Ratio
275.8	1700	-1
241.3	5000	-1
206.8	34000	-1
172.4	1.4e+005	-1
137.9	8.e+005	-1
117.2	2.4e+006	-1
89.63	5.5e+007	-1
82.74	1.e+008	-1
170.6	50000	-0.5
139.6	3.5e+005	-0.5
108.6	3.7e+006	-0.5
87.91	1.4e+007	-0.5
77.57	5.e+007	-0.5
72.39	1.e+008	-0.5
144.8	50000	0
120.7	1.9e+005	0
103.4	1.3e+006	0
93.08	4.4e+006	0

86.18	1.2e+007	0
72.39	1.e+008	0
74.12	3.e+005	0.5
70.67	1.5e+006	0.5
66.36	1.2e+007	0.5
62.05	1.e+008	0.5

TABLE 25
Aluminum Alloy > Isotropic Resistivity

Resistivity ohm mm	Temperature C
2.43e-005	0
2.67e-005	20
3.63e-005	100

TABLE 26
Aluminum Alloy > Isotropic Elasticity

Young's Modulus MPa	Poisson's Ratio	Bulk Modulus MPa	Shear Modulus MPa	Temperature C
71000	0.33	69608	26692	

TABLE 27
Aluminum Alloy > Isotropic Relative Permeability

Relative Permeability
1

Appendix A.10 Chassis Load Case (Braking Phase) Analysis Report

ANSYS

Project

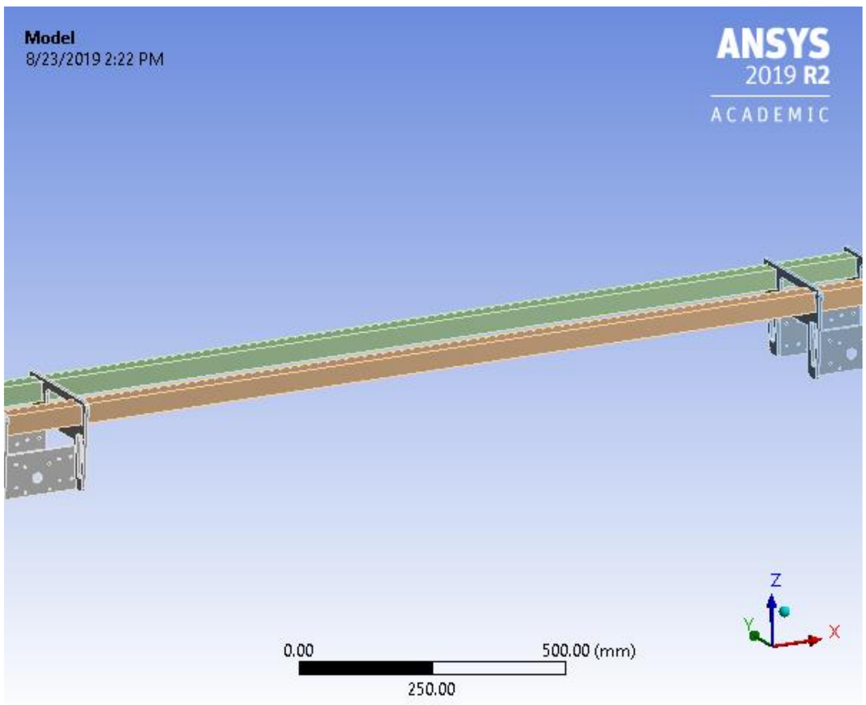

Contents

Units

TABLE 1

Unit System	Metric (mm, kg, N, s, mV, mA) Degrees rad/s Celsius
Angle	Degrees
Rotational Velocity	rad/s
Temperature	Celsius

Model (C4)

Geometry

TABLE 2
Model (C4) > Geometry

Object Name	*Geometry*
State	Fully Defined
Definition	
Source	D:\RH_PRP_Chassis_PODAssembly_V1.2_YO_04012019.igs
Type	Iges
Length Unit	Millimeters
Element Control	Program Controlled
Display Style	Body Color
Bounding Box	
Length X	1860. mm
Length Y	251.5 mm

Length Z	182.12 mm
Properties	
Volume	2.4121e+006 mm³
Mass	6.6814 kg
Scale Factor Value	1.
Statistics	
Bodies	4
Active Bodies	4
Nodes	25790
Elements	12206
Mesh Metric	None
Update Options	
Assign Default Material	No
Basic Geometry Options	
Solid Bodies	Yes
Surface Bodies	Yes
Line Bodies	No
Parameters	Independent
Parameter Key	ANS;DS
Attributes	No
Named Selections	No
Material Properties	No
Advanced Geometry Options	
Use Associativity	Yes
Coordinate Systems	No
Reader Mode Saves Updated File	No
Use Instances	Yes
Smart CAD Update	Yes
Compare Parts On Update	No
Analysis Type	3-D
Mixed Import Resolution	None
Clean Bodies On Import	No
Stitch Surfaces On Import	Program Tolerance
Decompose Disjoint Geometry	Yes
Enclosure and Symmetry Processing	Yes

TABLE 3
Model (C4) > Geometry > Parts

Object Name	*Part2|PartBody*	*Part2|PartBody[2]*	*Part3|PartBody*	*Part3|PartBody[2]*
State	Meshed			
Graphics Properties				
Visible	Yes			
Transparency	1			
Definition				
Suppressed	No			
Stiffness Behavior	Flexible			
Coordinate System	Default Coordinate System			
Reference Temperature	By Environment			
Treatment	None			

Material				
Assignment	Aluminum Alloy			
Nonlinear Effects	Yes			
Thermal Strain Effects	Yes			
Bounding Box				
Length X	172.7 mm		1860. mm	
Length Y	251.12 mm		38.1 mm	
Length Z	182.12 mm		38.1 mm	
Properties				
Volume	3.8104e+005 mm³		8.25e+005 mm³	
Mass	1.0555 kg		2.2852 kg	
Centroid X	117.42 mm	1803.7 mm	960.67 mm	
Centroid Y	-4.2843 mm	-4.6664 mm	81.897 mm	-90.823 mm
Centroid Z	30.577 mm		103.1 mm	103.31 mm
Moment of Inertia Ip1	9126.2 kg·mm²		936.83 kg·mm²	
Moment of Inertia Ip2	8230.3 kg·mm²		6.593e+005 kg·mm²	
Moment of Inertia Ip3	11149 kg·mm²		6.593e+005 kg·mm²	
Statistics				
Nodes	10838		2057	
Elements	5090		1013	
Mesh Metric	None			

FIGURE 1
Model (C4) > Geometry > Figure

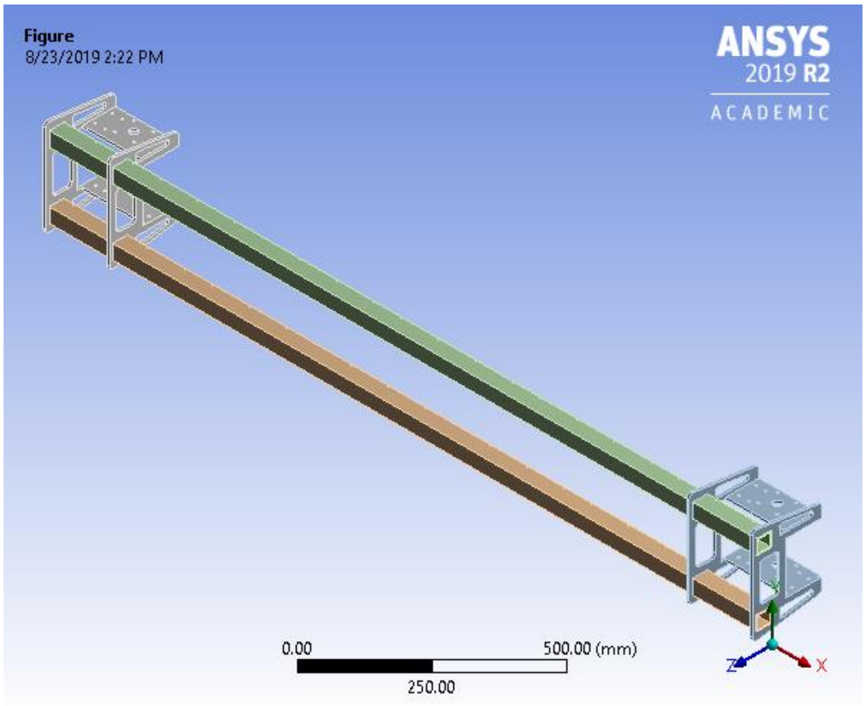

TABLE 4
Model (C4) > Materials

Object Name	*Materials*
State	Fully Defined
Statistics	
Materials	2
Material Assignments	0

Coordinate Systems

TABLE 5
Model (C4) > Coordinate Systems > Coordinate System

Object Name	*Global Coordinate System*
State	Fully Defined
Definition	
Type	Cartesian
Coordinate System ID	0.
Origin	
Origin X	0. mm

Origin Y	0. mm
Origin Z	0. mm
Directional Vectors	
X Axis Data	[1. 0. 0.]
Y Axis Data	[0. 1. 0.]
Z Axis Data	[0. 0. 1.]

Connections

TABLE 6
Model (C4) > Connections

Object Name	*Connections*
State	Fully Defined
Auto Detection	
Generate Automatic Connection On Refresh	Yes
Transparency	
Enabled	Yes

TABLE 7
Model (C4) > Connections > Contacts

Object Name	*Contacts*
State	Fully Defined
Definition	
Connection Type	Contact
Scope	
Scoping Method	Geometry Selection
Geometry	All Bodies
Auto Detection	
Tolerance Type	Slider
Tolerance Slider	0.
Tolerance Value	4.7144 mm
Use Range	No
Face/Face	Yes
Face-Face Angle Tolerance	75. °
Face Overlap Tolerance	Off
Cylindrical Faces	Include
Face/Edge	No
Edge/Edge	No
Priority	Include All
Group By	Bodies
Search Across	Bodies
Statistics	
Connections	4
Active Connections	4

TABLE 8
Model (C4) > Connections > Contacts > Contact Regions

Object Name	*Contact Region*	*Contact Region 2*	*Contact Region 3*	*Contact Region 4*
State	Fully Defined			

<table>
<tr><th colspan="5">Scope</th></tr>
<tr><td>Scoping Method</td><td colspan="4">Geometry Selection</td></tr>
<tr><td>Contact</td><td colspan="4">8 Faces</td></tr>
<tr><td>Target</td><td colspan="4">4 Faces</td></tr>
<tr><td>Contact Bodies</td><td colspan="2">Part2|PartBody</td><td colspan="2">Part2|PartBody[2]</td></tr>
<tr><td>Target Bodies</td><td>Part3|PartBody</td><td>Part3|PartBody[2]</td><td>Part3|PartBody</td><td>Part3|PartBody[2]</td></tr>
<tr><td>Protected</td><td colspan="4">No</td></tr>
<tr><th colspan="5">Definition</th></tr>
<tr><td>Type</td><td colspan="4">Bonded</td></tr>
<tr><td>Scope Mode</td><td colspan="4">Automatic</td></tr>
<tr><td>Behavior</td><td colspan="4">Program Controlled</td></tr>
<tr><td>Trim Contact</td><td colspan="4">Program Controlled</td></tr>
<tr><td>Trim Tolerance</td><td colspan="4">4.7144 mm</td></tr>
<tr><td>Suppressed</td><td colspan="4">No</td></tr>
<tr><th colspan="5">Advanced</th></tr>
<tr><td>Formulation</td><td colspan="4">Program Controlled</td></tr>
<tr><td>Small Sliding</td><td colspan="4">Program Controlled</td></tr>
<tr><td>Detection Method</td><td colspan="4">Program Controlled</td></tr>
<tr><td>Penetration Tolerance</td><td colspan="4">Program Controlled</td></tr>
<tr><td>Elastic Slip Tolerance</td><td colspan="4">Program Controlled</td></tr>
<tr><td>Normal Stiffness</td><td colspan="4">Program Controlled</td></tr>
<tr><td>Update Stiffness</td><td colspan="4">Program Controlled</td></tr>
<tr><td>Pinball Region</td><td colspan="4">Program Controlled</td></tr>
<tr><th colspan="5">Geometric Modification</th></tr>
<tr><td>Contact Geometry Correction</td><td colspan="4">None</td></tr>
<tr><td>Target Geometry Correction</td><td colspan="4">None</td></tr>
</table>

Mesh

TABLE 9
Model (C4) > Mesh

Object Name	*Mesh*
State	Solved
Display	
Display Style	Use Geometry Setting
Defaults	
Physics Preference	Mechanical
Element Order	Program Controlled
Element Size	Default
Sizing	
Use Adaptive Sizing	Yes
Resolution	Default (2)
Mesh Defeaturing	Yes
Defeature Size	Default
Transition	Fast
Span Angle Center	Coarse
Initial Size Seed	Assembly
Bounding Box Diagonal	1885.7 mm

Average Surface Area	4094.8 mm²
Minimum Edge Length	0.21228 mm
Quality	
Check Mesh Quality	Yes, Errors
Error Limits	Standard Mechanical
Target Quality	Default (0.050000)
Smoothing	Medium
Mesh Metric	None
Inflation	
Use Automatic Inflation	None
Inflation Option	Smooth Transition
Transition Ratio	0.272
Maximum Layers	5
Growth Rate	1.2
Inflation Algorithm	Pre
View Advanced Options	No
Advanced	
Number of CPUs for Parallel Part Meshing	Program Controlled
Straight Sided Elements	No
Rigid Body Behavior	Dimensionally Reduced
Triangle Surface Mesher	Program Controlled
Topology Checking	Yes
Pinch Tolerance	Please Define
Generate Pinch on Refresh	No
Statistics	
Nodes	25790
Elements	12206

TABLE 10
Model (C4) > Mesh > Mesh Controls

Object Name	*Patch Conforming Method*
State	Fully Defined
Scope	
Scoping Method	Geometry Selection
Geometry	4 Bodies
Definition	
Suppressed	No
Method	Tetrahedrons
Algorithm	Patch Conforming
Element Order	Use Global Setting

FIGURE 2
Model (C4) > Mesh > Figure

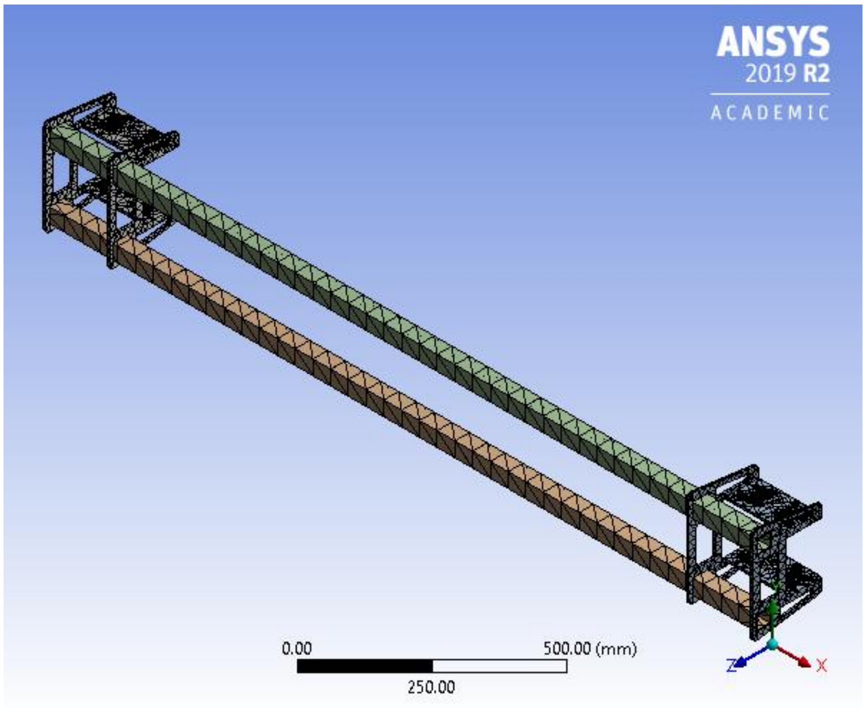

Static Structural (C5)

TABLE 11
Model (C4) > Analysis

Object Name	*Static Structural (C5)*
State	Solved
Definition	
Physics Type	Structural
Analysis Type	Static Structural
Solver Target	Mechanical APDL
Options	
Environment Temperature	22. °C
Generate Input Only	No

TABLE 12
Model (C4) > Static Structural (C5) > Analysis Settings

Object Name	*Analysis Settings*
State	Fully Defined
Step Controls	

Number Of Steps	1.
Current Step Number	1.
Step End Time	1. s
Auto Time Stepping	Program Controlled
Solver Controls	
Solver Type	Program Controlled
Weak Springs	Off
Solver Pivot Checking	Program Controlled
Large Deflection	Off
Inertia Relief	Off
Rotordynamics Controls	
Coriolis Effect	Off
Restart Controls	
Generate Restart Points	Program Controlled
Retain Files After Full Solve	No
Combine Restart Files	Program Controlled
Nonlinear Controls	
Newton-Raphson Option	Program Controlled
Force Convergence	Program Controlled
Moment Convergence	Program Controlled
Displacement Convergence	Program Controlled
Rotation Convergence	Program Controlled
Line Search	Program Controlled
Stabilization	Program Controlled
Output Controls	
Stress	Yes
Surface Stress	No
Back Stress	No
Strain	Yes
Contact Data	Yes
Nonlinear Data	No
Nodal Forces	No
Contact Miscellaneous	No
General Miscellaneous	No
Store Results At	All Time Points
Result File Compression	Program Controlled
Analysis Data Management	
Solver Files Directory	C:\Users\DIAPM599\OneDrive - Dentsply Sirona\Desktop\ANSYS Analysis\Chassis_files\dp0\SYS\MECH\
Future Analysis	None
Scratch Solver Files Directory	
Save MAPDL db	No
Contact Summary	Program Controlled

Delete Unneeded Files	Yes
Nonlinear Solution	No
Solver Units	Active System
Solver Unit System	nmm

TABLE 13
Model (C4) > Static Structural (C5) > Loads

Object Name	*Thermal Condition*	*BRK Force*	*BRK Force*	*BRK Force*	*BRK Force*	*MagLev Force*	*MagLev Force*	*MagLev Force*	*MagLev Force*	*LIM & GNC Force*	*LIM & GNC Force*
State	Fully Defined										
Scope											
Scoping Method	Geometry Selection										
Geometry	4 Bodies	1 Face									
Definition											
Type	Thermal Condition	Force									
Magnitude	80. °C (ramped)										
Suppressed	No										
Define By		Components									
Coordinate System		Global Coordinate System									
X Component		0. N (ramped)									
Y Component		0. N (ramped)									
Z Component		-37. N (ramped)				-42. N (ramped)				-202. N (ramped)	

FIGURE 3
Model (C4) > Static Structural (C5) > Thermal Condition

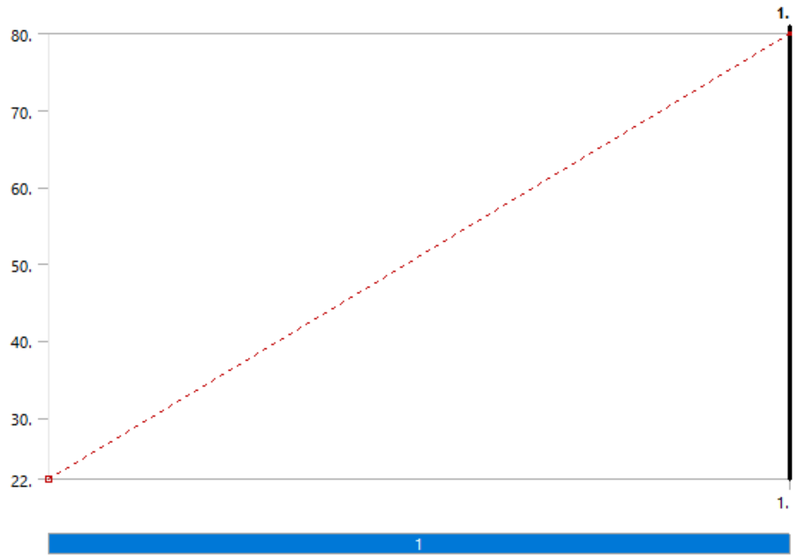

FIGURE 4
Model (C4) > Static Structural (C5) > BRK Force

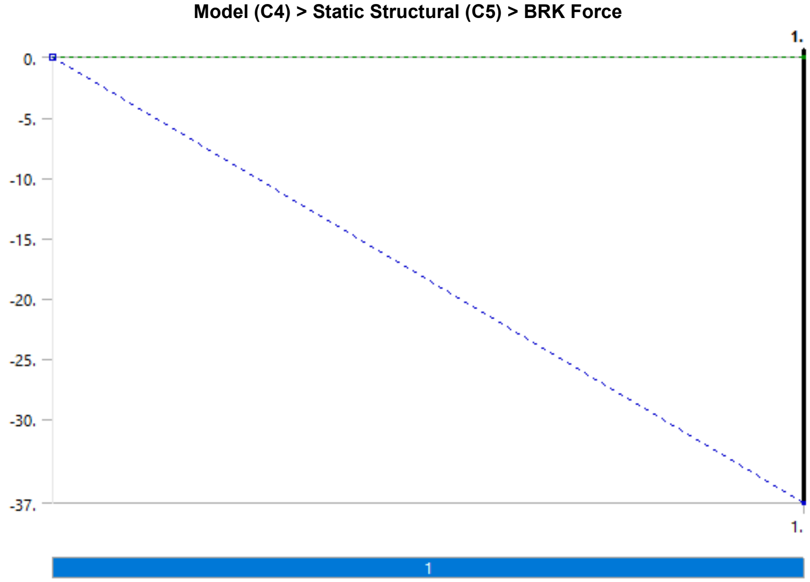

FIGURE 5
Model (C4) > Static Structural (C5) > BRK Force

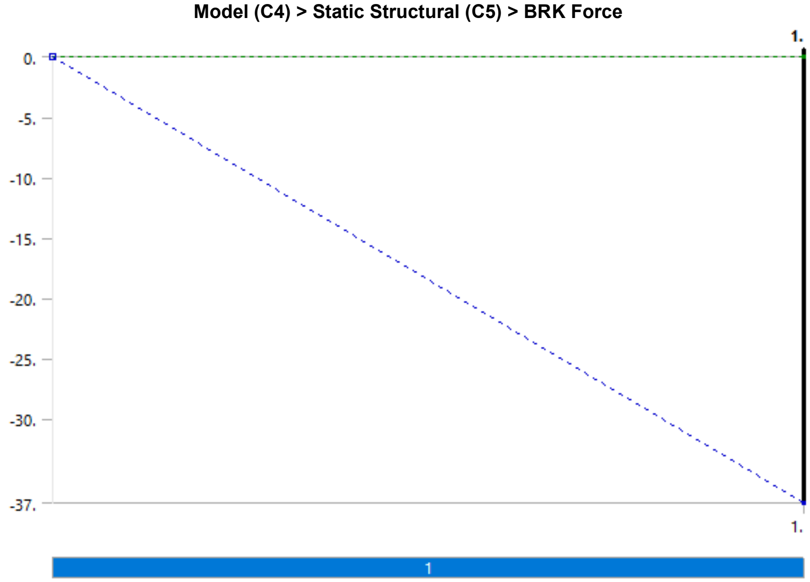

FIGURE 6
Model (C4) > Static Structural (C5) > BRK Force

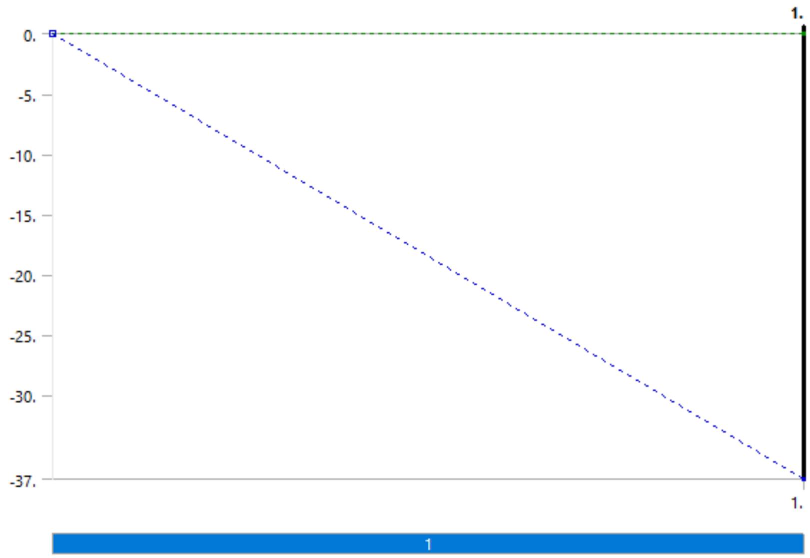

FIGURE 7
Model (C4) > Static Structural (C5) > BRK Force

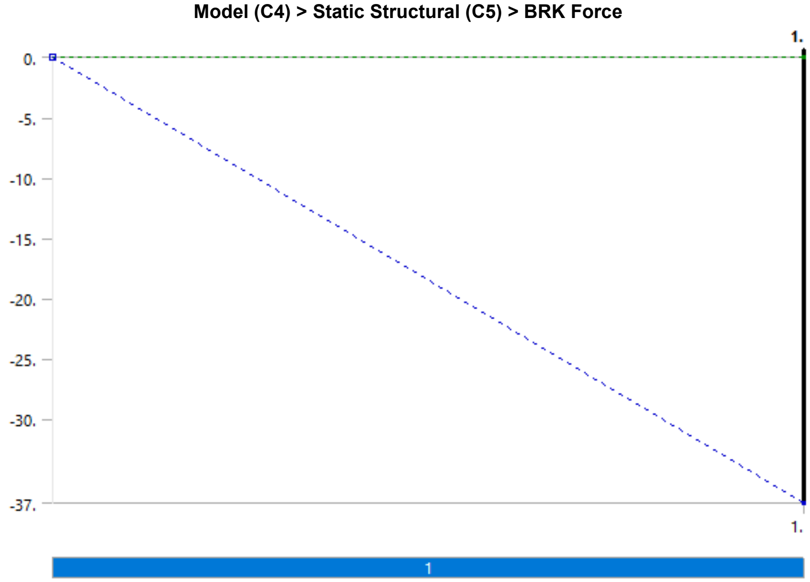

FIGURE 8
Model (C4) > Static Structural (C5) > MagLev Force

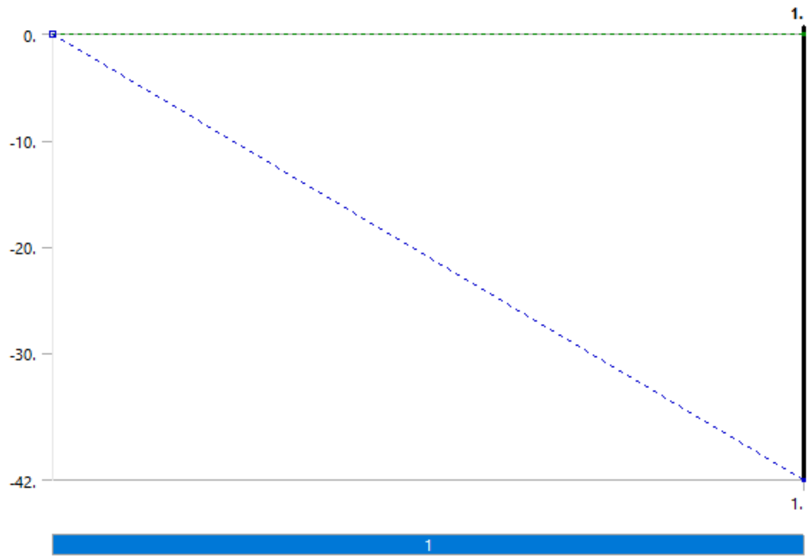

FIGURE 9
Model (C4) > Static Structural (C5) > MagLev Force

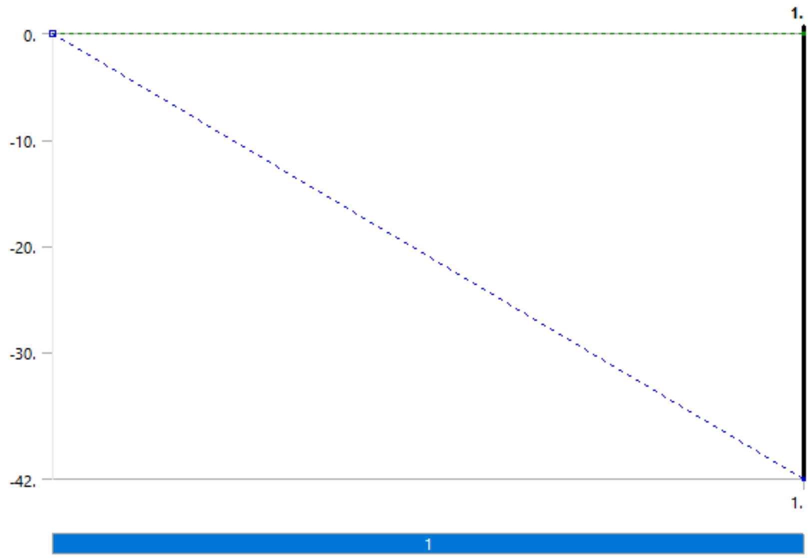

FIGURE 10
Model (C4) > Static Structural (C5) > MagLev Force

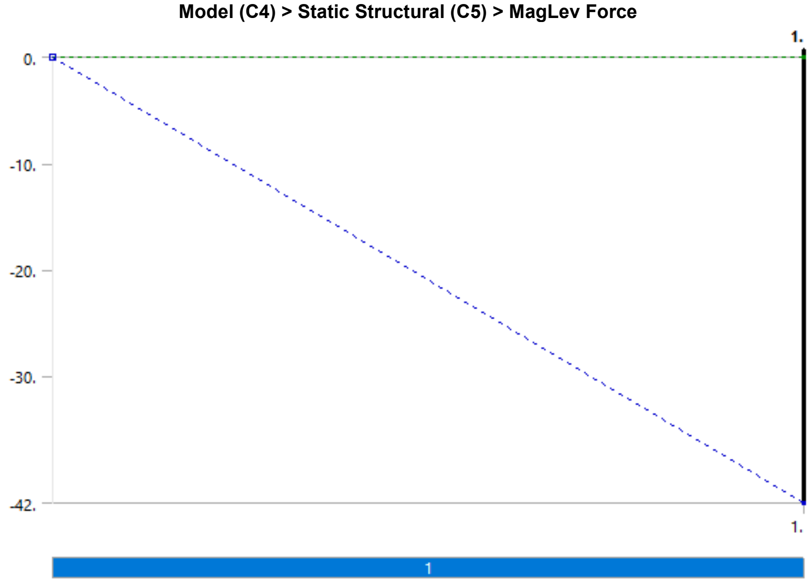

FIGURE 11
Model (C4) > Static Structural (C5) > MagLev Force

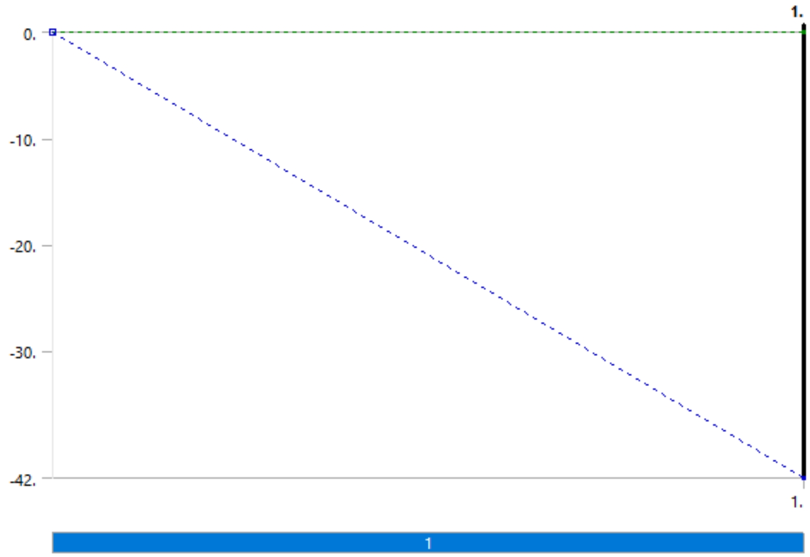

FIGURE 12
Model (C4) > Static Structural (C5) > LIM & GNC Force

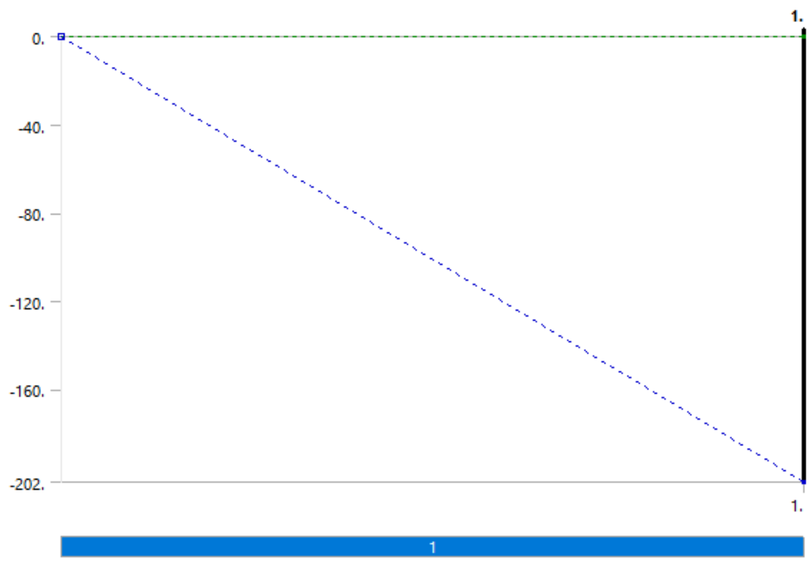

FIGURE 13
Model (C4) > Static Structural (C5) > LIM & GNC Force

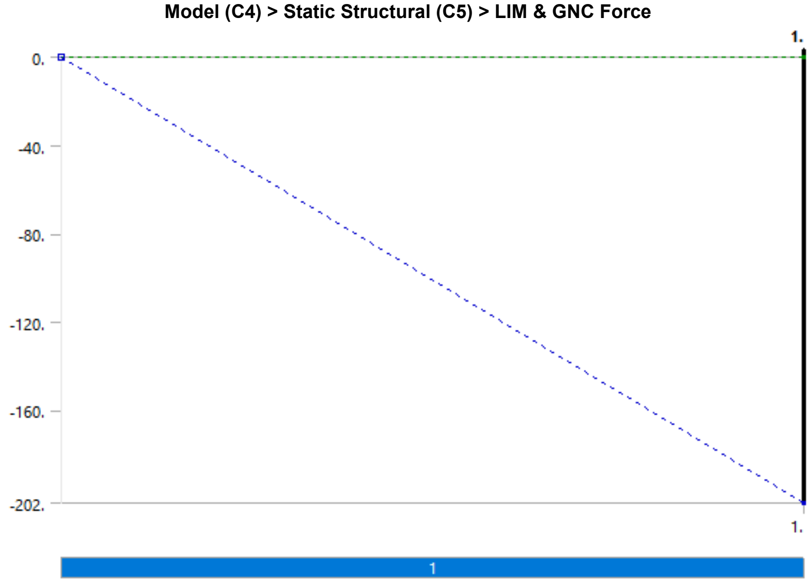

TABLE 14
Model (C4) > Static Structural (C5) > Loads

Object Name	*BRK Force*	*BRK Force*	*BRK Force*	*BRK Force*	*Lockup Force*	*Fixed Support*
State	Fully Defined					
Scope						
Scoping Method	Geometry Selection					
Geometry	1 Face					
Definition						
Type	Force					Fixed Support
Define By	Vector					
Magnitude	1957. N (ramped)				-1374. N (ramped)	
Direction	Defined					
Suppressed	No					

FIGURE 14
Model (C4) > Static Structural (C5) > BRK Force

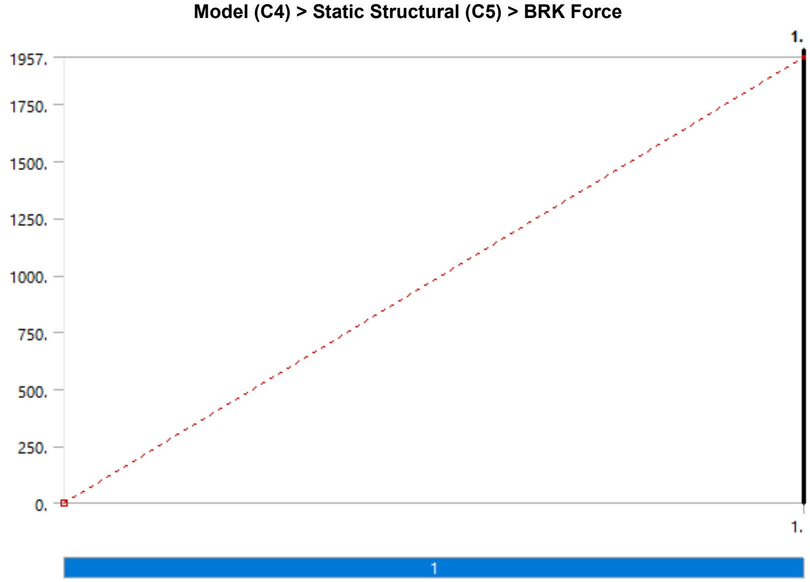

FIGURE 15
Model (C4) > Static Structural (C5) > BRK Force

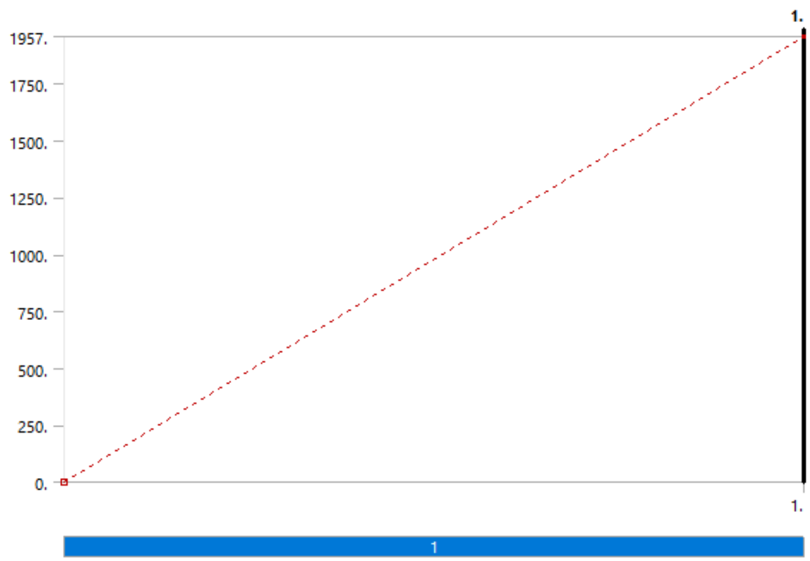

FIGURE 16
Model (C4) > Static Structural (C5) > BRK Force

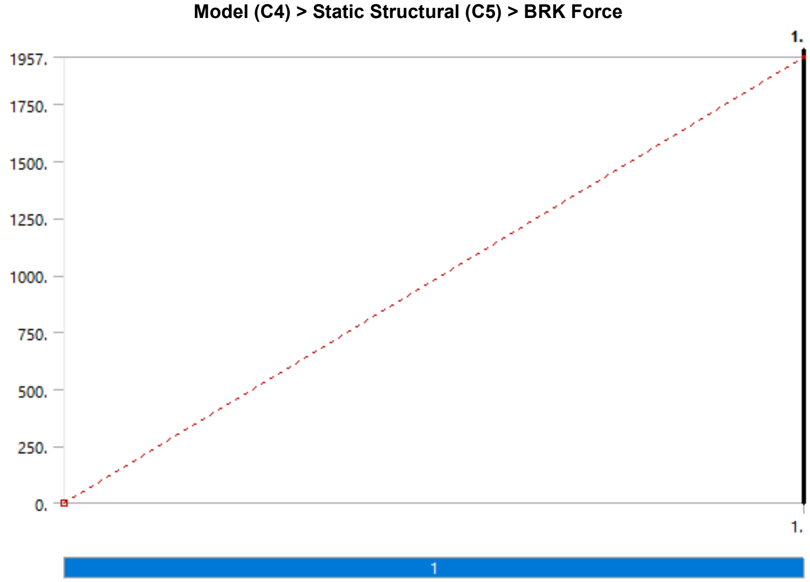

FIGURE 17
Model (C4) > Static Structural (C5) > BRK Force

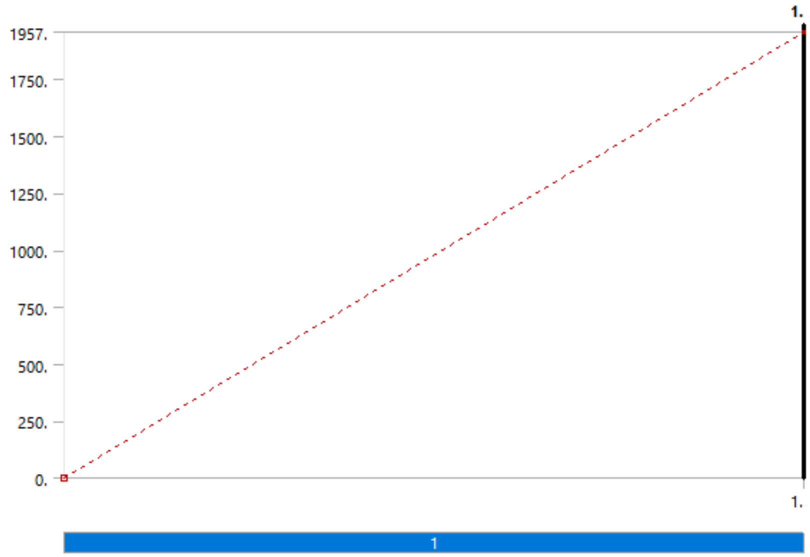

FIGURE 18
Model (C4) > Static Structural (C5) > Lockup Force

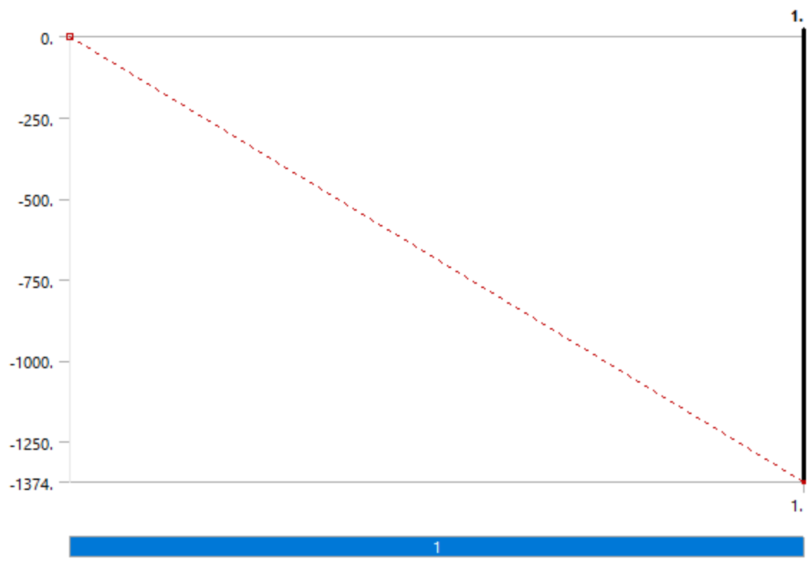

FIGURE 19
Model (C4) > Static Structural (C5) > Fixed Support > Figure

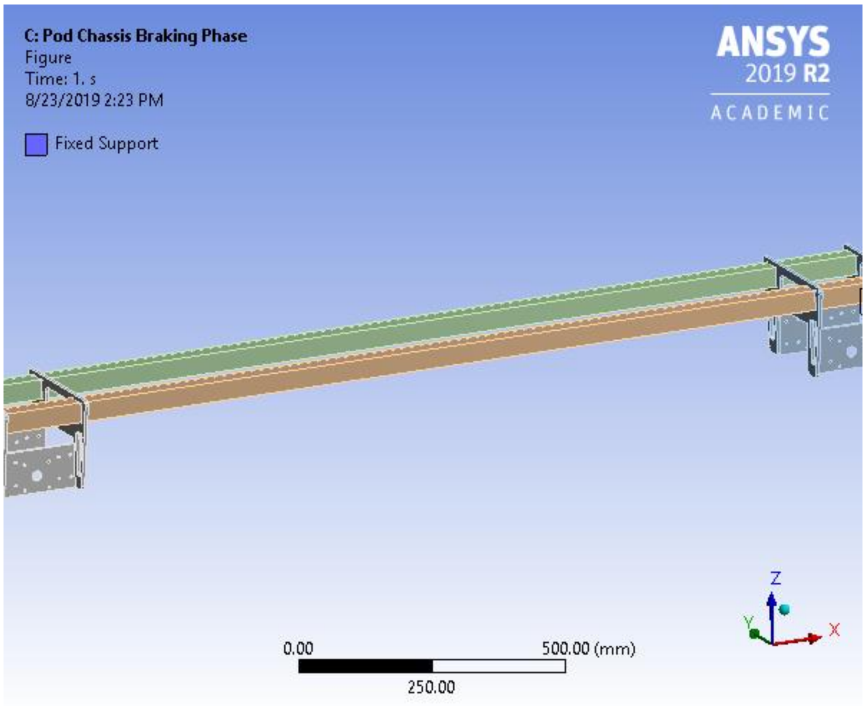

Solution (C6)

TABLE 15
Model (C4) > Static Structural (C5) > Solution

Object Name	*Solution (C6)*
State	Solved
Adaptive Mesh Refinement	
Max Refinement Loops	1.
Refinement Depth	2.
Information	
Status	Done
MAPDL Elapsed Time	4. s
MAPDL Memory Used	405. MB
MAPDL Result File Size	9.625 MB
Post Processing	
Beam Section Results	No
On Demand Stress/Strain	No

TABLE 16
Model (C4) > Static Structural (C5) > Solution (C6) > Solution Information

Object Name	*Solution Information*
State	Solved
Solution Information	
Solution Output	Solver Output
Newton-Raphson Residuals	0
Identify Element Violations	0
Update Interval	2.5 s
Display Points	All
FE Connection Visibility	
Activate Visibility	Yes
Display	All FE Connectors
Draw Connections Attached To	All Nodes
Line Color	Connection Type
Visible on Results	No
Line Thickness	Single
Display Type	Lines

TABLE 17
Model (C4) > Static Structural (C5) > Solution (C6) > Results

Object Name	*Total Deformation*	*Equivalent Stress*
State	Solved	
Scope		
Scoping Method	Geometry Selection	
Geometry	All Bodies	
Definition		
Type	Total Deformation	Equivalent (von-Mises) Stress
By	Time	
Display Time	Last	
Calculate Time History	Yes	
Identifier		
Suppressed	No	
Results		
Minimum	0. mm	0.36597 MPa
Maximum	14.162 mm	354.03 MPa
Average	6.8722 mm	26.305 MPa
Minimum Occurs On	Part2|PartBody[2]	Part3|PartBody
Maximum Occurs On	Part2|PartBody	Part2|PartBody[2]
Information		
Time	1. s	
Load Step	1	
Substep	1	
Iteration Number	1	
Integration Point Results		
Display Option		Averaged
Average Across Bodies		No

FIGURE 20
Model (C4) > Static Structural (C5) > Solution (C6) > Total Deformation

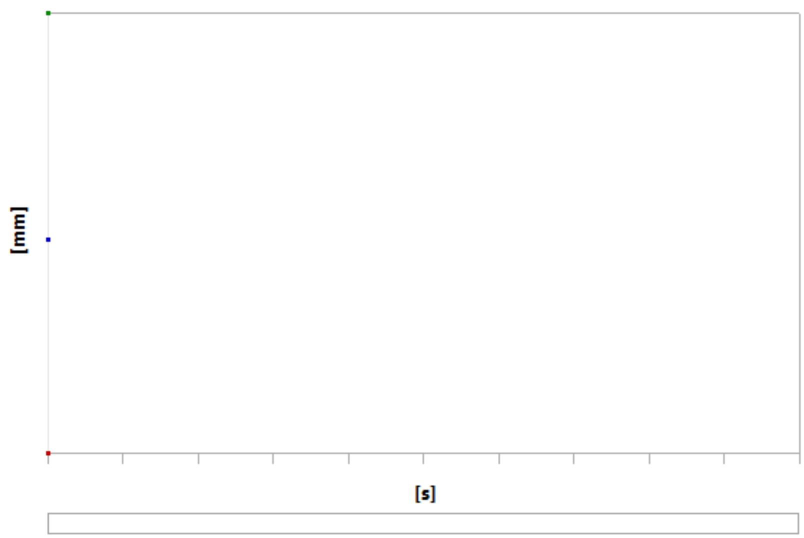

TABLE 18
Model (C4) > Static Structural (C5) > Solution (C6) > Total Deformation

Time [s]	Minimum [mm]	Maximum [mm]	Average [mm]
1.	0.	14.162	6.8722

FIGURE 21
Model (C4) > Static Structural (C5) > Solution (C6) > Total Deformation > Figure

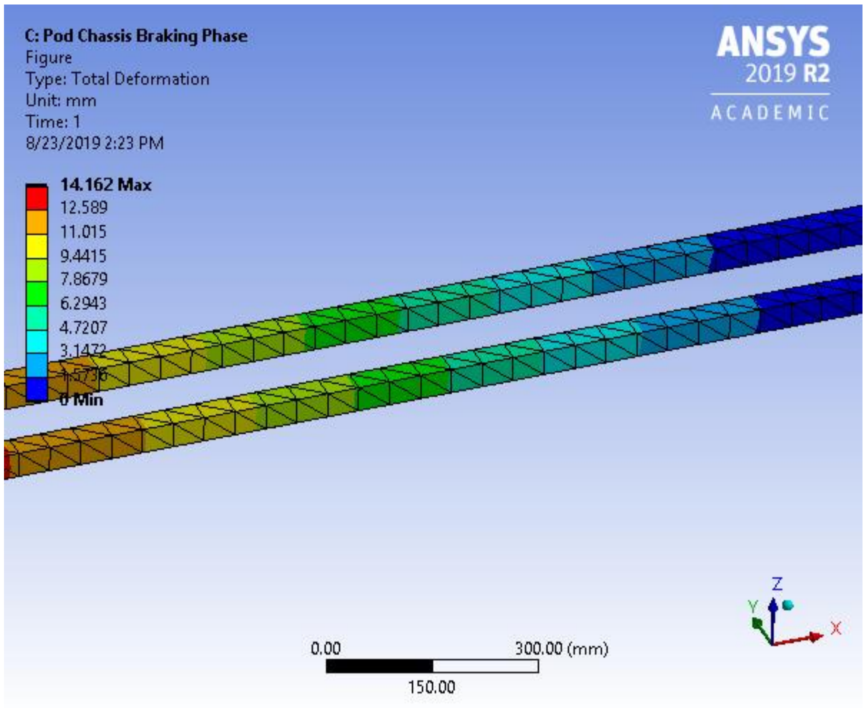

FIGURE 22
Model (C4) > Static Structural (C5) > Solution (C6) > Equivalent Stress

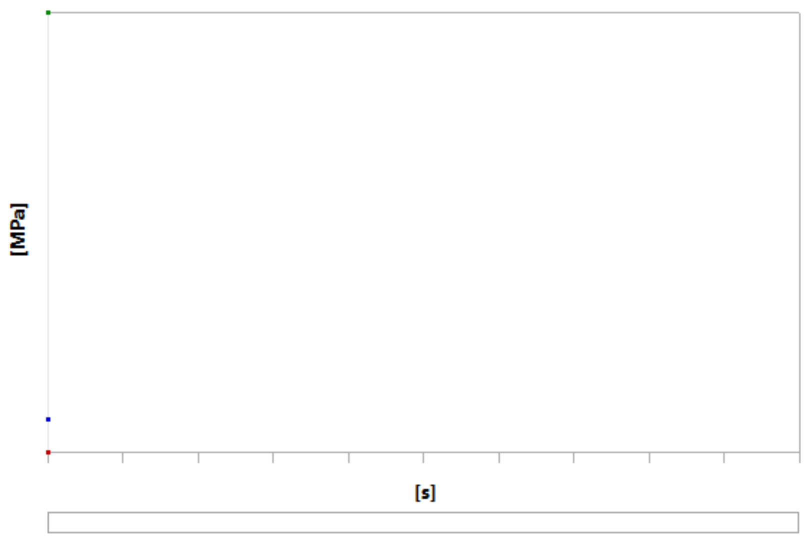

TABLE 19
Model (C4) > Static Structural (C5) > Solution (C6) > Equivalent Stress

Time [s]	Minimum [MPa]	Maximum [MPa]	Average [MPa]
1.	0.36597	354.03	26.305

FIGURE 23
Model (C4) > Static Structural (C5) > Solution (C6) > Equivalent Stress > Figure

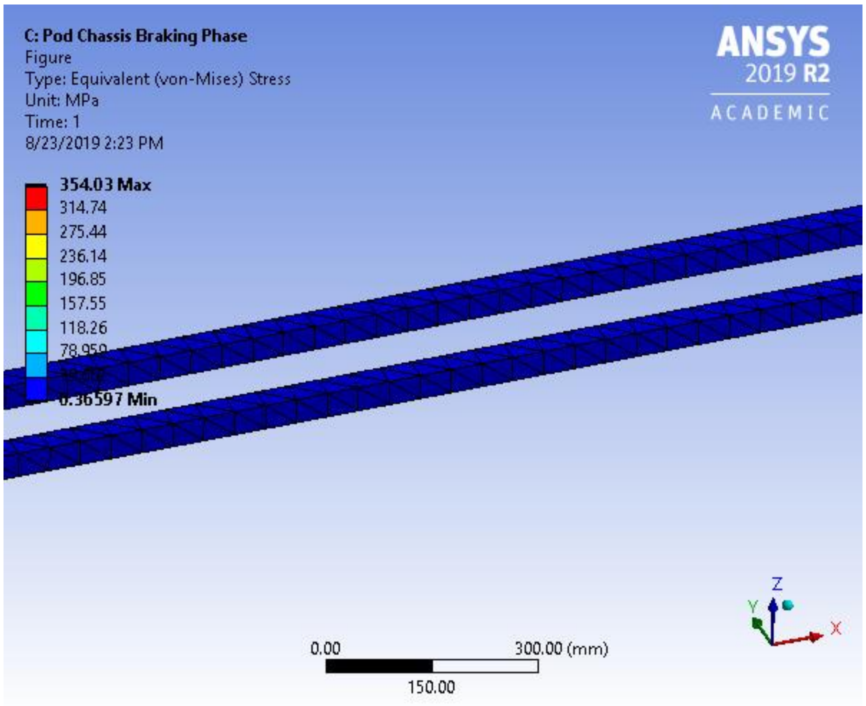

Material Data

Aluminum Alloy

TABLE 20
Aluminum Alloy > Constants

Density	2.77e-006 kg mm^-3
Coefficient of Thermal Expansion	2.3e-005 C^-1
Specific Heat	8.75e+005 mJ kg^-1 C^-1

TABLE 21
Aluminum Alloy > Color

Red	Green	Blue
138	104	46

TABLE 22
Aluminum Alloy > Compressive Ultimate Strength

Compressive Ultimate Strength MPa
0

TABLE 23
Aluminum Alloy > Compressive Yield Strength

Compressive Yield Strength MPa
280

TABLE 24
Aluminum Alloy > Tensile Yield Strength

Tensile Yield Strength MPa
280

TABLE 25
Aluminum Alloy > Tensile Ultimate Strength

Tensile Ultimate Strength MPa
310

TABLE 26
Aluminum Alloy > Isotropic Secant Coefficient of Thermal Expansion

Zero-Thermal-Strain Reference Temperature C
22

TABLE 27
Aluminum Alloy > Isotropic Thermal Conductivity

Thermal Conductivity W mm^-1 C^-1	Temperature C
0.114	-100
0.144	0
0.165	100
0.175	200

TABLE 28
Aluminum Alloy > S-N Curve

Alternating Stress MPa	Cycles	R-Ratio
275.8	1700	-1
241.3	5000	-1
206.8	34000	-1
172.4	1.4e+005	-1
137.9	8.e+005	-1
117.2	2.4e+006	-1
89.63	5.5e+007	-1
82.74	1.e+008	-1
170.6	50000	-0.5
139.6	3.5e+005	-0.5
108.6	3.7e+006	-0.5
87.91	1.4e+007	-0.5
77.57	5.e+007	-0.5
72.39	1.e+008	-0.5
144.8	50000	0
120.7	1.9e+005	0
103.4	1.3e+006	0
93.08	4.4e+006	0

86.18	1.2e+007	0
72.39	1.e+008	0
74.12	3.e+005	0.5
70.67	1.5e+006	0.5
66.36	1.2e+007	0.5
62.05	1.e+008	0.5

TABLE 29
Aluminum Alloy > Isotropic Resistivity

Resistivity ohm mm	Temperature C
2.43e-005	0
2.67e-005	20
3.63e-005	100

TABLE 30
Aluminum Alloy > Isotropic Elasticity

Young's Modulus MPa	Poisson's Ratio	Bulk Modulus MPa	Shear Modulus MPa	Temperature C
71000	0.33	69608	26692	

TABLE 31
Aluminum Alloy > Isotropic Relative Permeability

Relative Permeability
1

Appendix A.11 MTR Track Load Case (Overspeed) Analysis Report

Project*

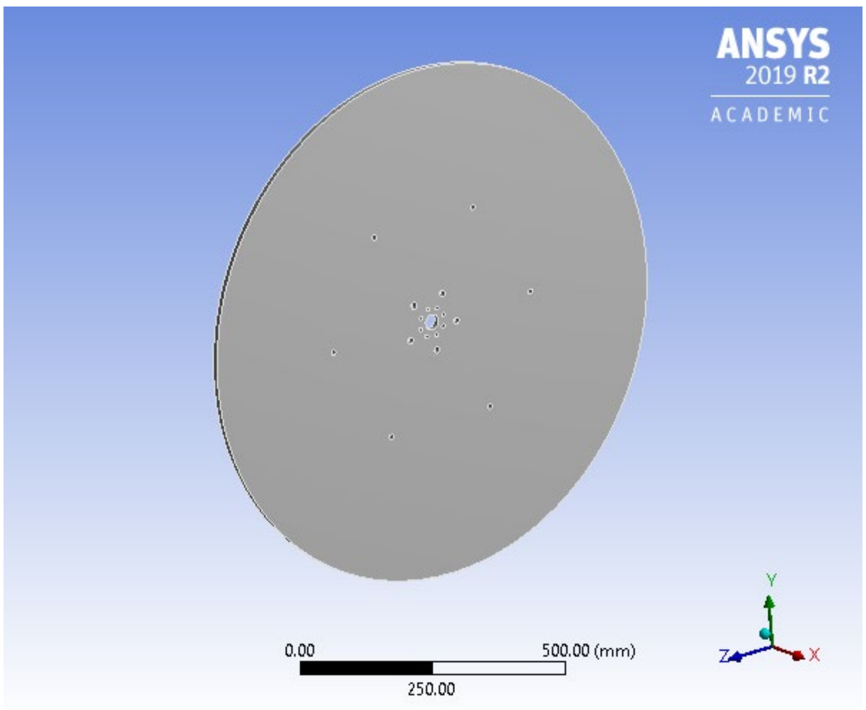

Contents

Units

TABLE 1

Unit System	Metric (mm, kg, N, s, mV, mA) Degrees rad/s Celsius
Angle	Degrees
Rotational Velocity	rad/s
Temperature	Celsius

Model (C4)

Geometry

TABLE 2
Model (C4) > Geometry

Object Name	*Geometry*
State	Fully Defined
Definition	
Source	C:\Users\DIAPM599\AppData\Local\Temp\WB_C0010-DIAPM599A_diapm599_18756_2\unsaved_project_files\dp0\Geom\DM\Geom.scdoc
Type	SpaceClaim
Length Unit	Meters
Element Control	Program Controlled
Display Style	Body Color
Bounding Box	
Length X	12.7 mm
Length Y	1361.8 mm

Length Z	1361.8 mm
Properties	
Volume	9.9457e+006 mm³
Mass	27.55 kg
Scale Factor Value	1.
Statistics	
Bodies	1
Active Bodies	1
Nodes	9539
Elements	1288
Mesh Metric	None
Update Options	
Assign Default Material	No
Basic Geometry Options	
Solid Bodies	Yes
Surface Bodies	Yes
Line Bodies	Yes
Parameters	Independent
Parameter Key	
Attributes	Yes
Attribute Key	
Named Selections	Yes
Named Selection Key	
Material Properties	Yes
Advanced Geometry Options	
Use Associativity	Yes
Coordinate Systems	Yes
Coordinate System Key	
Reader Mode Saves Updated File	No
Use Instances	Yes
Smart CAD Update	Yes
Compare Parts On Update	No
Analysis Type	3-D

Mixed Import Resolution	None
Clean Bodies On Import	No
Stitch Surfaces On Import	None
Decompose Disjoint Geometry	Yes
Enclosure and Symmetry Processing	Yes

TABLE 3
Model (C4) > Geometry > Parts

Object Name	*Track Wheel_rev0\Solid1*
State	Meshed
Graphics Properties	
Visible	Yes
Transparency	1
Definition	
Suppressed	No
Stiffness Behavior	Flexible
Coordinate System	Default Coordinate System
Reference Temperature	By Environment
Treatment	None
Material	
Assignment	Aluminum Alloy
Nonlinear Effects	Yes
Thermal Strain Effects	Yes
Bounding Box	
Length X	12.7 mm
Length Y	1361.8 mm
Length Z	1361.8 mm
Properties	
Volume	9.9457e+006 mm³
Mass	27.55 kg
Centroid X	-180. mm
Centroid Y	401.34 mm
Centroid Z	-203.5 mm
Moment of Inertia Ip1	1.7235e+006 kg·mm²
Moment of Inertia Ip2	1.7235e+006 kg·mm²
Moment of Inertia Ip3	3.4462e+006 kg·mm²
Statistics	
Nodes	9539
Elements	1288
Mesh Metric	None
CAD Attributes	

PartTolerance:	0.00000001
Color:143.143.175	

FIGURE 1
Model (C4) > Geometry > Track Wheel_rev0 > Solid1 > Figure

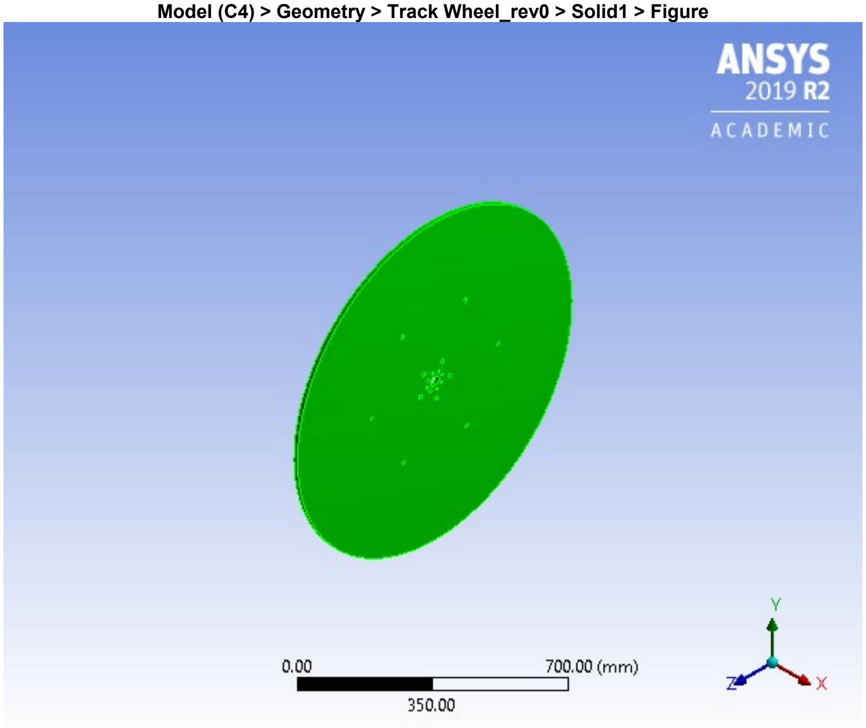

TABLE 4
Model (C4) > Materials

Object Name	*Materials*
State	Fully Defined
Statistics	
Materials	2
Material Assignments	0

Coordinate Systems

TABLE 5
Model (C4) > Coordinate Systems > Coordinate System

Object Name	*Global Coordinate System*
State	Fully Defined

Definition	
Type	Cartesian
Coordinate System ID	0.
Origin	
Origin X	0. mm
Origin Y	0. mm
Origin Z	0. mm
Directional Vectors	
X Axis Data	[1. 0. 0.]
Y Axis Data	[0. 1. 0.]
Z Axis Data	[0. 0. 1.]

Mesh

TABLE 6
Model (C4) > Mesh

Object Name	*Mesh*
State	Solved
Display	
Display Style	Use Geometry Setting
Defaults	
Physics Preference	Mechanical
Element Order	Program Controlled
Element Size	Default
Sizing	
Use Adaptive Sizing	Yes
Resolution	Default (2)
Mesh Defeaturing	Yes
Defeature Size	Default
Transition	Fast
Span Angle Center	Coarse
Initial Size Seed	Assembly
Bounding Box Diagonal	1925.9 mm
Average Surface Area	70154 mm²
Minimum Edge Length	26.075 mm
Quality	
Check Mesh Quality	Yes, Errors
Error Limits	Standard Mechanical
Target Quality	Default (0.050000)
Smoothing	Medium
Mesh Metric	None
Inflation	
Use Automatic Inflation	None
Inflation Option	Smooth Transition
Transition Ratio	0.272
Maximum Layers	5
Growth Rate	1.2
Inflation Algorithm	Pre

View Advanced Options	No
Advanced	
Number of CPUs for Parallel Part Meshing	Program Controlled
Straight Sided Elements	No
Rigid Body Behavior	Dimensionally Reduced
Triangle Surface Mesher	Program Controlled
Topology Checking	Yes
Pinch Tolerance	Please Define
Generate Pinch on Refresh	No
Statistics	
Nodes	9539
Elements	1288

TABLE 7
Model (C4) > Mesh > Mesh Controls

Object Name	*Automatic Method*
State	Fully Defined
Scope	
Scoping Method	Geometry Selection
Geometry	1 Body
Definition	
Suppressed	No
Method	Automatic
Element Order	Use Global Setting

FIGURE 2
Model (C4) > Mesh > Figure

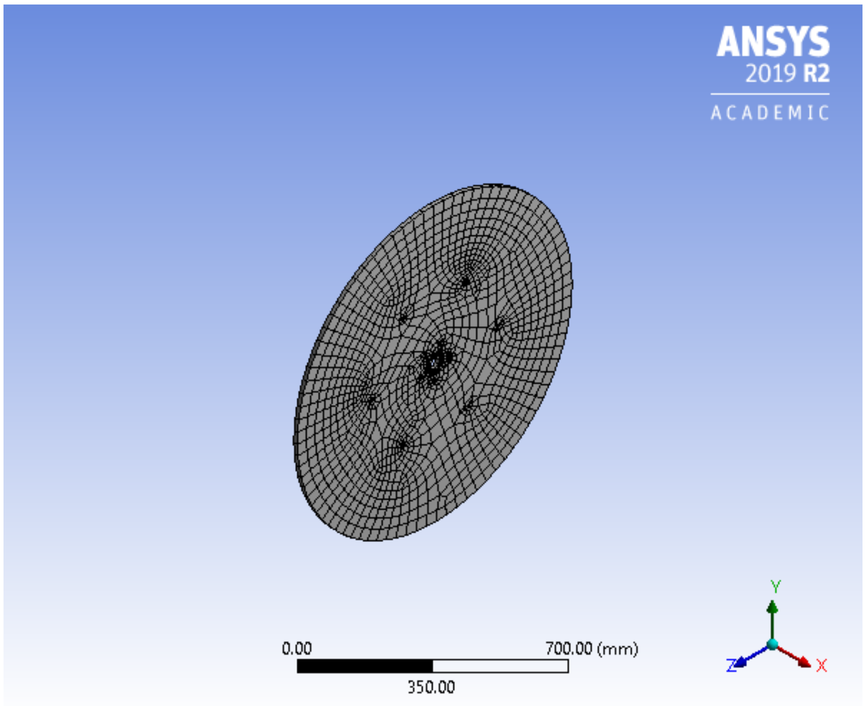

Static Structural (C5)

TABLE 8
Model (C4) > Analysis

Object Name	*Static Structural (C5)*
State	Solved
Definition	
Physics Type	Structural
Analysis Type	Static Structural
Solver Target	Mechanical APDL
Options	
Environment Temperature	22. °C
Generate Input Only	No

TABLE 9
Model (C4) > Static Structural (C5) > Analysis Settings

Object Name	*Analysis Settings*
State	Fully Defined
Step Controls	

Number Of Steps	1.
Current Step Number	1.
Step End Time	1. s
Auto Time Stepping	Program Controlled
Solver Controls	
Solver Type	Program Controlled
Weak Springs	Off
Solver Pivot Checking	Program Controlled
Large Deflection	Off
Inertia Relief	Off
Rotordynamics Controls	
Coriolis Effect	Off
Restart Controls	
Generate Restart Points	Program Controlled
Retain Files After Full Solve	No
Combine Restart Files	Program Controlled
Nonlinear Controls	
Newton-Raphson Option	Program Controlled
Force Convergence	Program Controlled
Moment Convergence	Program Controlled
Displacement Convergence	Program Controlled
Rotation Convergence	Program Controlled
Line Search	Program Controlled
Stabilization	Program Controlled
Output Controls	
Stress	Yes
Surface Stress	No
Back Stress	No
Strain	Yes
Contact Data	Yes
Nonlinear Data	No
Nodal Forces	No
Contact Miscellaneous	No
General Miscellaneous	No
Store Results At	All Time Points
Result File Compression	Program Controlled

Analysis Data Management	
Solver Files Directory	C:\Users\DIAPM599\AppData\Local\Temp\WB_C0010-DIAPM599A_diapm599_18756_2\unsaved_project_files\dp0\SYS\MECH\
Future Analysis	None
Scratch Solver Files Directory	
Save MAPDL db	No
Contact Summary	Program Controlled
Delete Unneeded Files	Yes
Nonlinear Solution	No
Solver Units	Active System
Solver Unit System	nmm

TABLE 10
Model (C4) > Static Structural (C5) > Rotations

Object Name	*Rotational Velocity*
State	Fully Defined
Scope	
Scoping Method	Geometry Selection
Geometry	All Bodies
Definition	
Define By	Vector
Magnitude	50. rad/s (ramped)
Axis	Defined
Suppressed	No

FIGURE 3
Model (C4) > Static Structural (C5) > Rotational Velocity

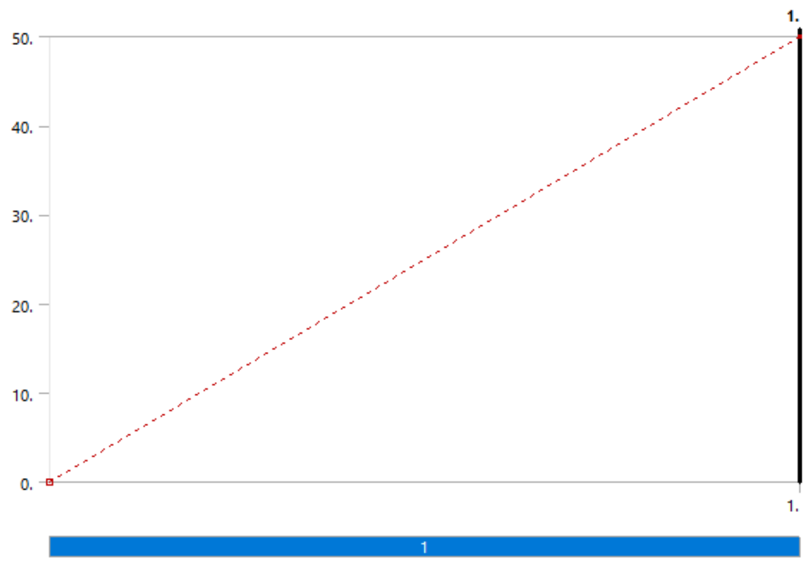

TABLE 11
Model (C4) > Static Structural (C5) > Loads

Object Name	*Thermal Condition*	*Fixed Support*	*Cylindrical Support*
State	Fully Defined		Suppressed
Scope			
Scoping Method	Geometry Selection		
Geometry	1 Body	1 Face	
Definition			
Type	Thermal Condition	Fixed Support	Cylindrical Support
Magnitude	22. °C (ramped)		
Suppressed	No		Yes
Radial			Fixed
Axial			Fixed
Tangential			Fixed

FIGURE 4
Model (C4) > Static Structural (C5) > Thermal Condition

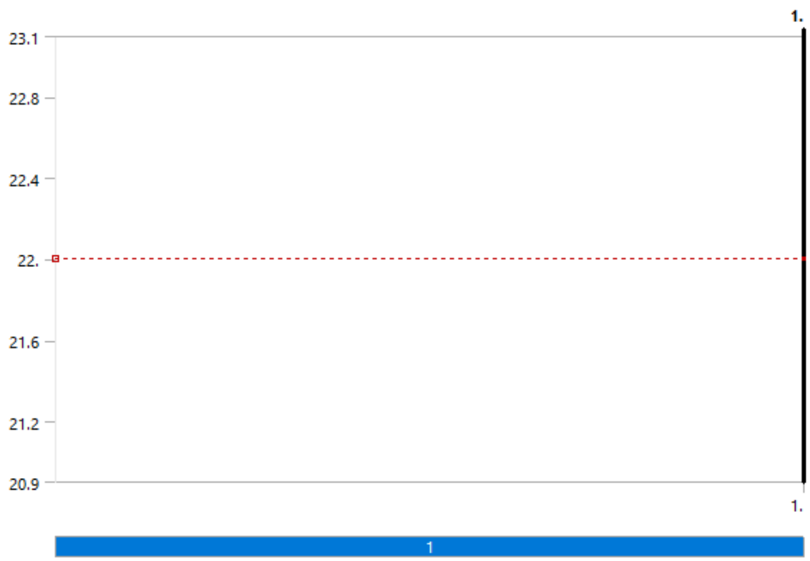

FIGURE 5
Model (C4) > Static Structural (C5) > Figure

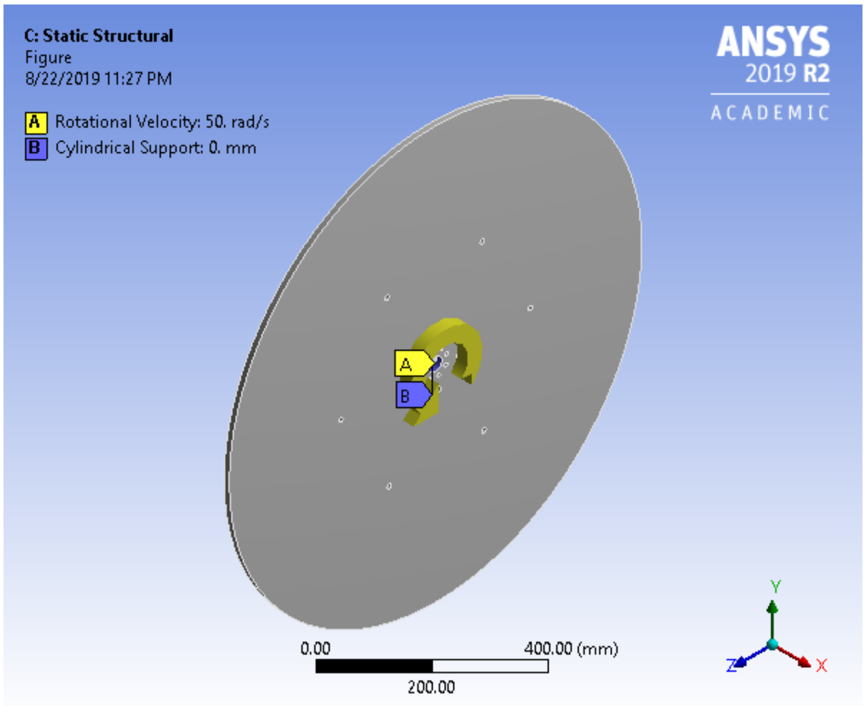

Solution (C6)

TABLE 12
Model (C4) > Static Structural (C5) > Solution

Object Name	*Solution (C6)*
State	Solved
Adaptive Mesh Refinement	
Max Refinement Loops	1.
Refinement Depth	2.
Information	
Status	Done
MAPDL Elapsed Time	3. s
MAPDL Memory Used	317. MB
MAPDL Result File Size	2. MB
Post Processing	
Beam Section Results	No
On Demand Stress/Strain	No

TABLE 13
Model (C4) > Static Structural (C5) > Solution (C6) > Solution Information

Object Name	*Solution Information*
State	Solved
Solution Information	
Solution Output	Solver Output
Newton-Raphson Residuals	0
Identify Element Violations	0
Update Interval	2.5 s
Display Points	All
FE Connection Visibility	
Activate Visibility	Yes
Display	All FE Connectors
Draw Connections Attached To	All Nodes
Line Color	Connection Type
Visible on Results	No
Line Thickness	Single
Display Type	Lines

TABLE 14
Model (C4) > Static Structural (C5) > Solution (C6) > Results

Object Name	*Total Deformation*	*Equivalent Stress*
State	Solved	
Scope		
Scoping Method	Geometry Selection	
Geometry	All Bodies	
Definition		
Type	Total Deformation	Equivalent (von-Mises) Stress
By	Time	
Display Time	Last	
Calculate Time History	Yes	
Identifier		
Suppressed	No	
Results		
Minimum	0. mm	0.29176 MPa
Maximum	2.0848e-003 mm	1.978 MPa
Average	1.4607e-003 mm	0.59689 MPa
Minimum Occurs On	Track Wheel_rev0\Solid1	
Maximum Occurs On	Track Wheel_rev0\Solid1	
Information		
Time	1. s	
Load Step	1	
Substep	1	
Iteration Number	1	
Integration Point Results		
Display Option		Averaged
Average Across Bodies		No

FIGURE 6
Model (C4) > Static Structural (C5) > Solution (C6) > Total Deformation

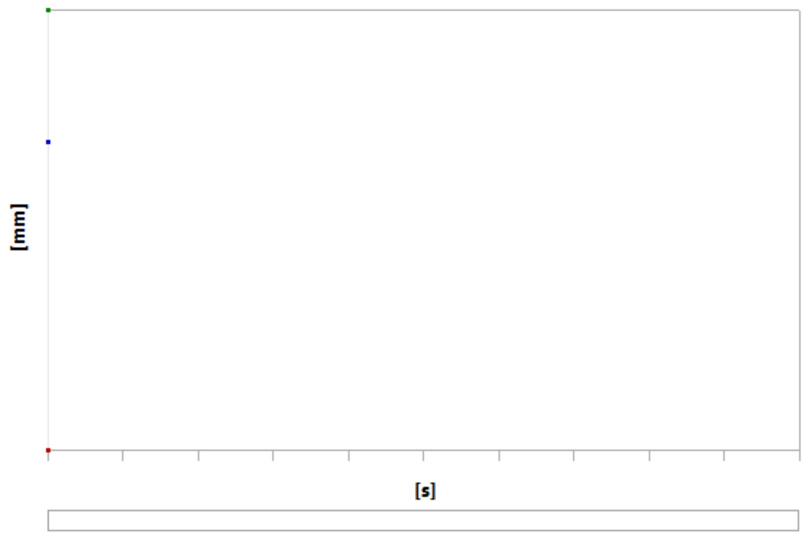

TABLE 15
Model (C4) > Static Structural (C5) > Solution (C6) > Total Deformation

Time [s]	Minimum [mm]	Maximum [mm]	Average [mm]
1.	0.	2.0848e-003	1.4607e-003

FIGURE 7
Model (C4) > Static Structural (C5) > Solution (C6) > Total Deformation > Figure

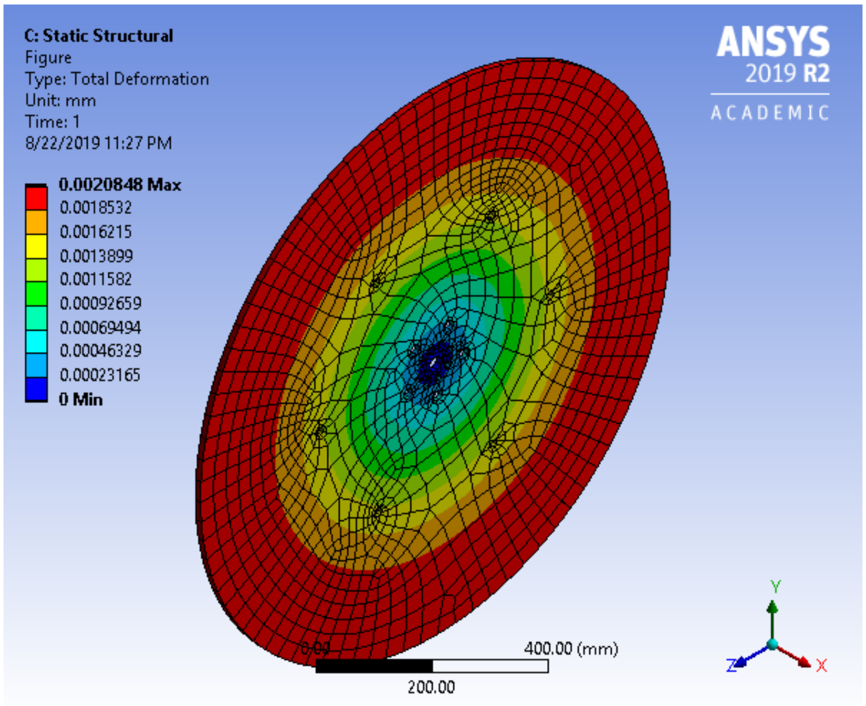

FIGURE 8
Model (C4) > Static Structural (C5) > Solution (C6) > Equivalent Stress

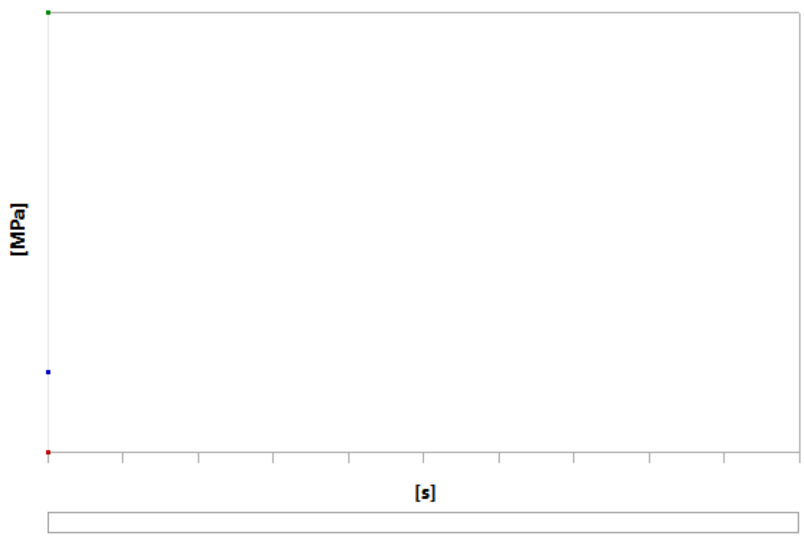

TABLE 16
Model (C4) > Static Structural (C5) > Solution (C6) > Equivalent Stress

Time [s]	Minimum [MPa]	Maximum [MPa]	Average [MPa]
1.	0.29176	1.978	0.59689

FIGURE 9
Model (C4) > Static Structural (C5) > Solution (C6) > Equivalent Stress > Figure

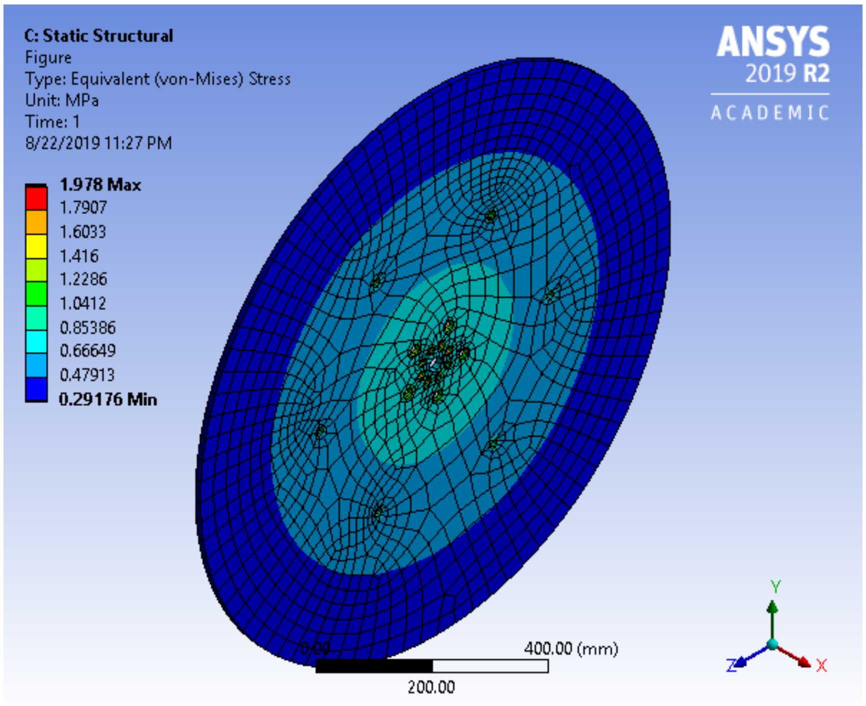

Material Data

Aluminum Alloy

TABLE 17
Aluminum Alloy > Constants

Density	2.77e-006 kg mm^-3
Coefficient of Thermal Expansion	2.3e-005 C^-1
Specific Heat	8.75e+005 mJ kg^-1 C^-1

TABLE 18
Aluminum Alloy > Color

Red	Green	Blue
138	104	46

TABLE 19
Aluminum Alloy > Compressive Ultimate Strength

Compressive Ultimate Strength MPa
0

TABLE 20
Aluminum Alloy > Compressive Yield Strength

Compressive Yield Strength MPa
280

TABLE 21
Aluminum Alloy > Tensile Yield Strength

Tensile Yield Strength MPa
280

TABLE 22
Aluminum Alloy > Tensile Ultimate Strength

Tensile Ultimate Strength MPa
310

TABLE 23
Aluminum Alloy > Isotropic Secant Coefficient of Thermal Expansion

Zero-Thermal-Strain Reference Temperature C
22

TABLE 24
Aluminum Alloy > Isotropic Thermal Conductivity

Thermal Conductivity W mm^-1 C^-1	Temperature C
0.114	-100
0.144	0
0.165	100
0.175	200

TABLE 25
Aluminum Alloy > S-N Curve

Alternating Stress MPa	Cycles	R-Ratio
275.8	1700	-1
241.3	5000	-1
206.8	34000	-1
172.4	1.4e+005	-1
137.9	8.e+005	-1
117.2	2.4e+006	-1
89.63	5.5e+007	-1
82.74	1.e+008	-1
170.6	50000	-0.5
139.6	3.5e+005	-0.5
108.6	3.7e+006	-0.5
87.91	1.4e+007	-0.5
77.57	5.e+007	-0.5
72.39	1.e+008	-0.5
144.8	50000	0
120.7	1.9e+005	0
103.4	1.3e+006	0
93.08	4.4e+006	0

86.18	1.2e+007	0
72.39	1.e+008	0
74.12	3.e+005	0.5
70.67	1.5e+006	0.5
66.36	1.2e+007	0.5
62.05	1.e+008	0.5

TABLE 26
Aluminum Alloy > Isotropic Resistivity

Resistivity ohm mm	Temperature C
2.43e-005	0
2.67e-005	20
3.63e-005	100

TABLE 27
Aluminum Alloy > Isotropic Elasticity

Young's Modulus MPa	Poisson's Ratio	Bulk Modulus MPa	Shear Modulus MPa	Temperature C
71000	0.33	69608	26692	

TABLE 28
Aluminum Alloy > Isotropic Relative Permeability

Relative Permeability
1

Appendix A.12 MTR Shaft Load Case (Lock Up) Analysis Report

Project*

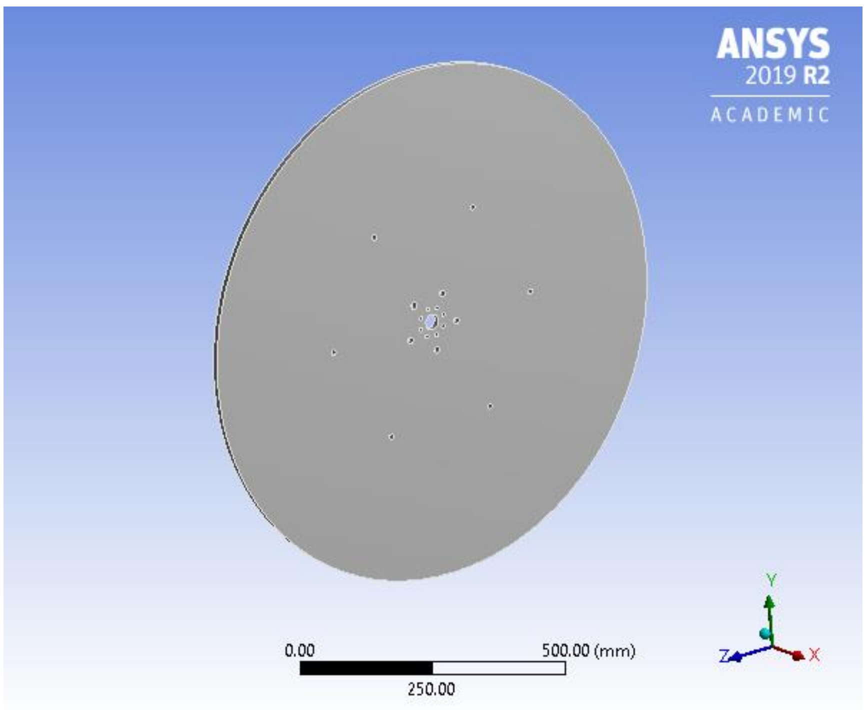

Contents

Units

TABLE 1

Unit System	Metric (mm, kg, N, s, mV, mA) Degrees rad/s Celsius
Angle	Degrees
Rotational Velocity	rad/s
Temperature	Celsius

Model (C4)

Geometry

TABLE 2
Model (C4) > Geometry

Object Name	*Geometry*
State	Fully Defined
Definition	
Source	C:\Users\DIAPM599\AppData\Local\Temp\WB_C0010-DIAPM599A_diapm599_18756_2\unsaved_project_files\dp0\Geom\DM\Geom.scdoc
Type	SpaceClaim
Length Unit	Meters
Element Control	Program Controlled
Display Style	Body Color
Bounding Box	
Length X	420. mm
Length Y	34.044 mm

Length Z	34.044 mm
Properties	
Volume	2.0609e+005 mm³
Mass	0.57088 kg
Scale Factor Value	1.
Statistics	
Bodies	1
Active Bodies	1
Nodes	2162
Elements	1064
Mesh Metric	None
Update Options	
Assign Default Material	No
Basic Geometry Options	
Solid Bodies	Yes
Surface Bodies	Yes
Line Bodies	Yes
Parameters	Independent
Parameter Key	
Attributes	Yes
Attribute Key	
Named Selections	Yes
Named Selection Key	
Material Properties	Yes
Advanced Geometry Options	
Use Associativity	Yes
Coordinate Systems	Yes
Coordinate System Key	
Reader Mode Saves Updated File	No
Use Instances	Yes
Smart CAD Update	Yes
Compare Parts On Update	No
Analysis Type	3-D

Mixed Import Resolution	None
Clean Bodies On Import	No
Stitch Surfaces On Import	None
Decompose Disjoint Geometry	Yes
Enclosure and Symmetry Processing	Yes

TABLE 3
Model (C4) > Geometry > Parts

Object Name	*Shaft\Solid1*
State	Meshed
Graphics Properties	
Visible	Yes
Transparency	1
Definition	
Suppressed	No
Stiffness Behavior	Flexible
Coordinate System	Default Coordinate System
Reference Temperature	By Environment
Treatment	None
Material	
Assignment	Aluminum Alloy
Nonlinear Effects	Yes
Thermal Strain Effects	Yes
Bounding Box	
Length X	420. mm
Length Y	34.044 mm
Length Z	34.044 mm
Properties	
Volume	2.0609e+005 mm³
Mass	0.57088 kg
Centroid X	-175.03 mm
Centroid Y	401.34 mm
Centroid Z	-203.5 mm
Moment of Inertia Ip1	8365.2 kg·mm²
Moment of Inertia Ip2	8365.2 kg·mm²
Moment of Inertia Ip3	44.134 kg·mm²
Statistics	
Nodes	2162
Elements	1064
Mesh Metric	None
CAD Attributes	

PartTolerance:	0.00000001
Color:143.143.175	

FIGURE 1
Model (C4) > Geometry > Shaft > Solid1 > Figure

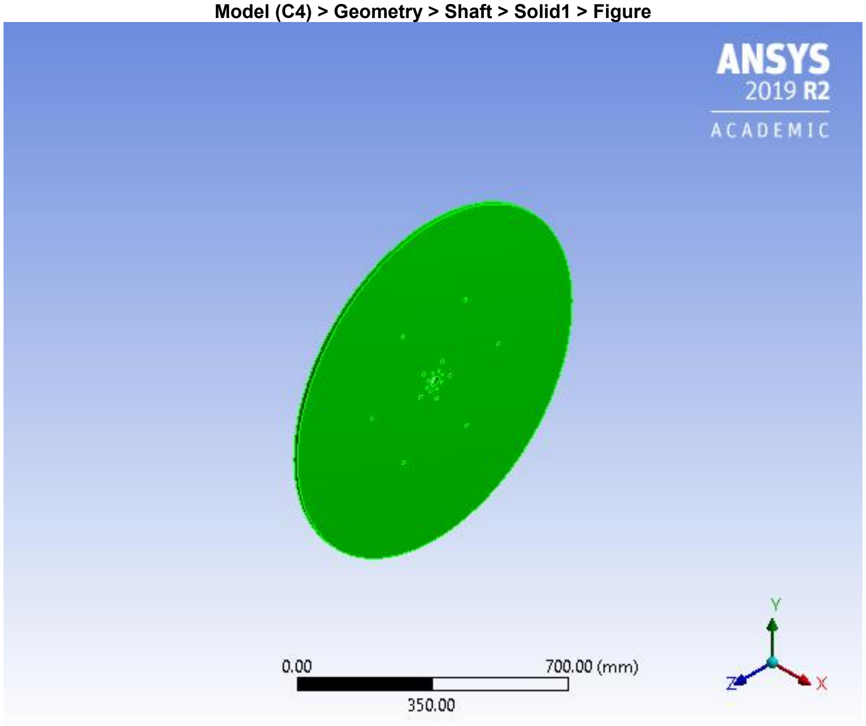

TABLE 4
Model (C4) > Materials

Object Name	*Materials*
State	Fully Defined
Statistics	
Materials	2
Material Assignments	0

Coordinate Systems

TABLE 5
Model (C4) > Coordinate Systems > Coordinate System

Object Name	*Global Coordinate System*
State	Fully Defined

Definition	
Type	Cartesian
Coordinate System ID	0.
Origin	
Origin X	0. mm
Origin Y	0. mm
Origin Z	0. mm
Directional Vectors	
X Axis Data	[1. 0. 0.]
Y Axis Data	[0. 1. 0.]
Z Axis Data	[0. 0. 1.]

Mesh

TABLE 6
Model (C4) > Mesh

Object Name	*Mesh*
State	Solved
Display	
Display Style	Use Geometry Setting
Defaults	
Physics Preference	Mechanical
Element Order	Program Controlled
Element Size	Default
Sizing	
Use Adaptive Sizing	Yes
Resolution	Default (2)
Mesh Defeaturing	Yes
Defeature Size	Default
Transition	Fast
Span Angle Center	Fine
Initial Size Seed	Assembly
Bounding Box Diagonal	422.75 mm
Average Surface Area	6765.5 mm²
Minimum Edge Length	72.257 mm
Quality	
Check Mesh Quality	Yes, Errors
Error Limits	Standard Mechanical
Target Quality	Default (0.050000)
Smoothing	Medium
Mesh Metric	None
Inflation	
Use Automatic Inflation	None
Inflation Option	Smooth Transition
Transition Ratio	0.272
Maximum Layers	5
Growth Rate	1.2
Inflation Algorithm	Pre

View Advanced Options	No
Advanced	
Number of CPUs for Parallel Part Meshing	Program Controlled
Straight Sided Elements	No
Rigid Body Behavior	Dimensionally Reduced
Triangle Surface Mesher	Program Controlled
Topology Checking	Yes
Pinch Tolerance	Please Define
Generate Pinch on Refresh	No
Statistics	
Nodes	2162
Elements	1064

TABLE 7
Model (C4) > Mesh > Mesh Controls

Object Name	*Patch Conforming Method*
State	Fully Defined
Scope	
Scoping Method	Geometry Selection
Geometry	1 Body
Definition	
Suppressed	No
Method	Tetrahedrons
Algorithm	Patch Conforming
Element Order	Use Global Setting

FIGURE 2
Model (C4) > Mesh > Figure

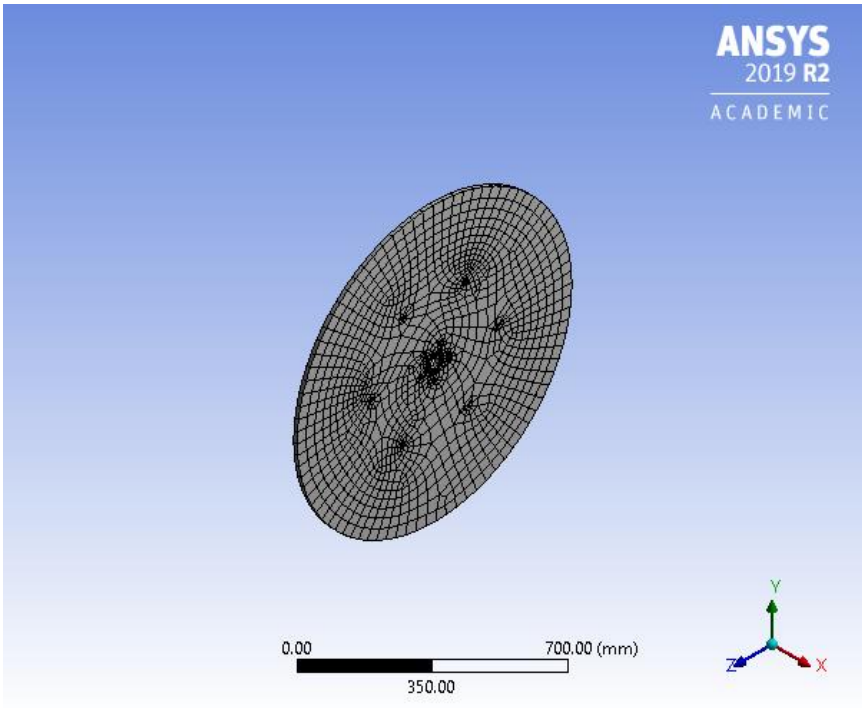

Static Structural (C5)

TABLE 8
Model (C4) > Analysis

Object Name	*Static Structural (C5)*
State	Solved
Definition	
Physics Type	Structural
Analysis Type	Static Structural
Solver Target	Mechanical APDL
Options	
Environment Temperature	22. °C
Generate Input Only	No

TABLE 9
Model (C4) > Static Structural (C5) > Analysis Settings

Object Name	*Analysis Settings*
State	Fully Defined
Step Controls	

Number Of Steps	1.
Current Step Number	1.
Step End Time	1. s
Auto Time Stepping	Program Controlled
Solver Controls	
Solver Type	Program Controlled
Weak Springs	Off
Solver Pivot Checking	Program Controlled
Large Deflection	Off
Inertia Relief	Off
Rotordynamics Controls	
Coriolis Effect	Off
Restart Controls	
Generate Restart Points	Program Controlled
Retain Files After Full Solve	No
Combine Restart Files	Program Controlled
Nonlinear Controls	
Newton-Raphson Option	Program Controlled
Force Convergence	Program Controlled
Moment Convergence	Program Controlled
Displacement Convergence	Program Controlled
Rotation Convergence	Program Controlled
Line Search	Program Controlled
Stabilization	Program Controlled
Output Controls	
Stress	Yes
Surface Stress	No
Back Stress	No
Strain	Yes
Contact Data	Yes
Nonlinear Data	No
Nodal Forces	No
Contact Miscellaneous	No
General Miscellaneous	No
Store Results At	All Time Points
Result File Compression	Program Controlled

Analysis Data Management	
Solver Files Directory	C:\Users\DIAPM599\AppData\Local\Temp\WB_C0010-DIAPM599A_diapm599_18756_2\unsaved_project_files\dp0\SYS\MECH\
Future Analysis	None
Scratch Solver Files Directory	
Save MAPDL db	No
Contact Summary	Program Controlled
Delete Unneeded Files	Yes
Nonlinear Solution	No
Solver Units	Active System
Solver Unit System	nmm

TABLE 10
Model (C4) > Static Structural (C5) > Loads

Object Name	*Fixed Support*
State	Fully Defined
Scope	
Scoping Method	Geometry Selection
Geometry	2 Faces
Definition	
Type	Fixed Support
Suppressed	No

TABLE 11
Model (C4) > Static Structural (C5) > Rotations

Object Name	*Rotational Velocity*
State	Fully Defined
Scope	
Scoping Method	Geometry Selection
Geometry	All Bodies
Definition	
Define By	Components
Coordinate System	Global Coordinate System
X Component	50. rad/s (ramped)
Y Component	0. rad/s (ramped)
Z Component	0. rad/s (ramped)
X Coordinate	0. mm
Y Coordinate	0. mm
Z Coordinate	0. mm
Suppressed	No

FIGURE 3
Model (C4) > Static Structural (C5) > Rotational Velocity

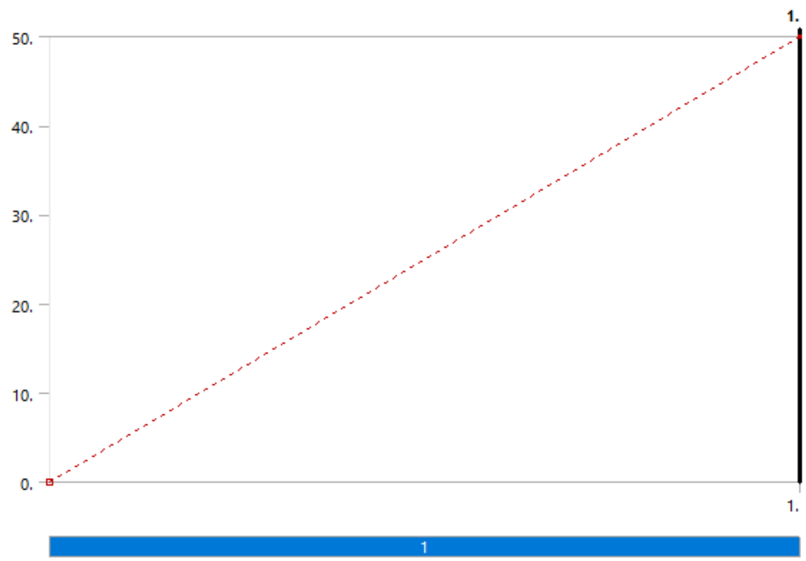

FIGURE 4
Model (C4) > Static Structural (C5) > Figure

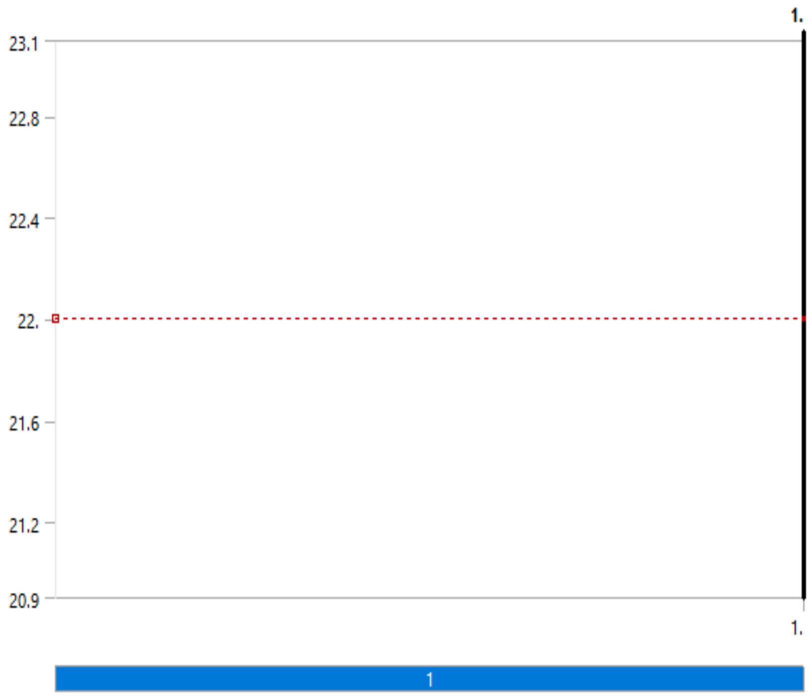

Solution (C6)

TABLE 12
Model (C4) > Static Structural (C5) > Solution

Object Name	*Solution (C6)*
State	Solved
Adaptive Mesh Refinement	
Max Refinement Loops	1.
Refinement Depth	2.
Information	
Status	Done
MAPDL Elapsed Time	3. s
MAPDL Memory Used	265. MB
MAPDL Result File Size	1. MB
Post Processing	
Beam Section Results	No
On Demand Stress/Strain	No

TABLE 13
Model (C4) > Static Structural (C5) > Solution (C6) > Solution Information

Object Name	*Solution Information*
State	Solved
Solution Information	
Solution Output	Solver Output
Newton-Raphson Residuals	0
Identify Element Violations	0
Update Interval	2.5 s
Display Points	All
FE Connection Visibility	
Activate Visibility	Yes
Display	All FE Connectors
Draw Connections Attached To	All Nodes
Line Color	Connection Type
Visible on Results	No
Line Thickness	Single
Display Type	Lines

TABLE 14
Model (C4) > Static Structural (C5) > Solution (C6) > Results

Object Name	*Total Deformation*	*Equivalent Stress*
State	Solved	
Scope		
Scoping Method	Geometry Selection	
Geometry	All Bodies	
Definition		
Type	Total Deformation	Equivalent (von-Mises) Stress
By	Time	
Display Time	Last	
Calculate Time History	Yes	
Identifier		
Suppressed	No	
Results		
Minimum	0. mm	0.11575 MPa
Maximum	9.2547e-002 mm	25.615 MPa
Average	1.2127e-002 mm	6.0968 MPa
Minimum Occurs On	Shaft\Solid1	
Maximum Occurs On	Shaft\Solid1	
Information		
Time	1. s	
Load Step	1	
Substep	1	
Iteration Number	1	
Integration Point Results		
Display Option		Averaged
Average Across Bodies		No

FIGURE 5
Model (C4) > Static Structural (C5) > Solution (C6) > Total Deformation

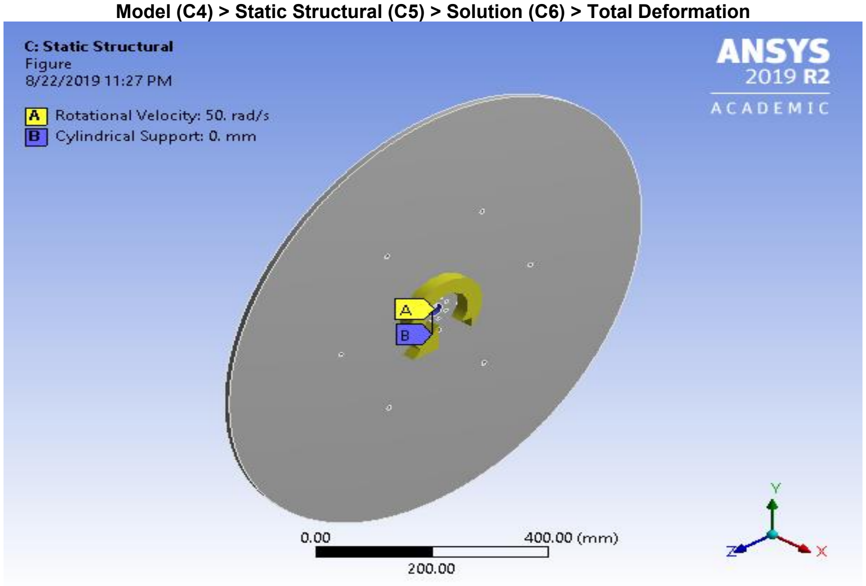

TABLE 15
Model (C4) > Static Structural (C5) > Solution (C6) > Total Deformation

Time [s]	Minimum [mm]	Maximum [mm]	Average [mm]
1.	0.	9.2547e-002	1.2127e-002

FIGURE 6
Model (C4) > Static Structural (C5) > Solution (C6) > Total Deformation > Figure

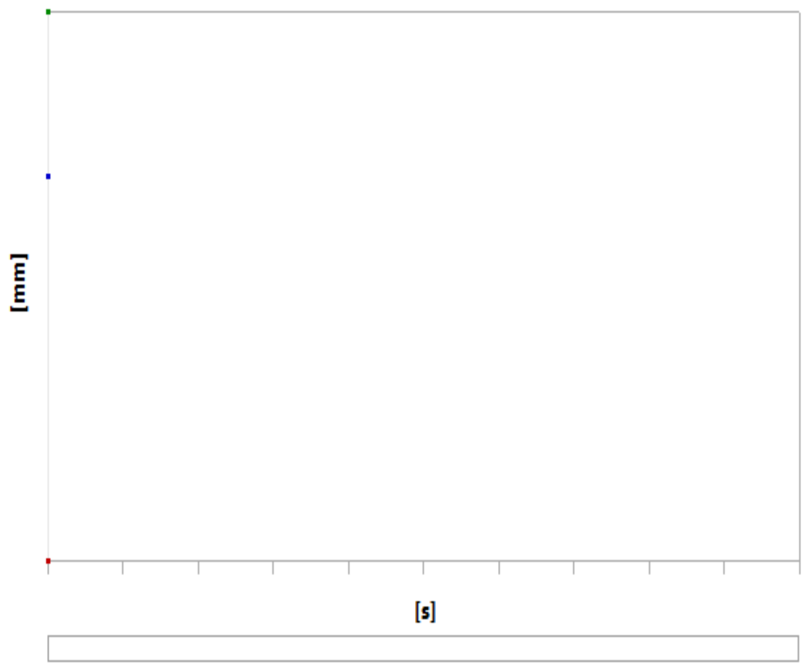

FIGURE 7
Model (C4) > Static Structural (C5) > Solution (C6) > Equivalent Stress

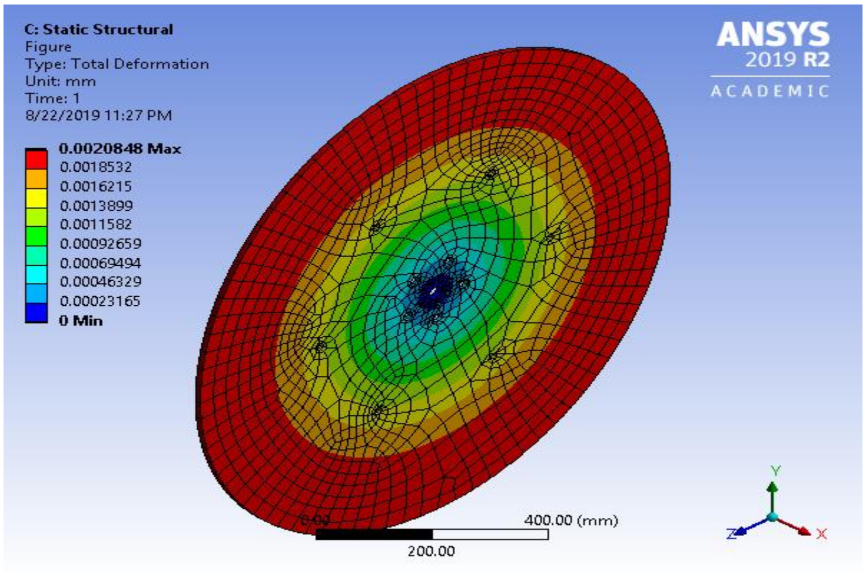

TABLE 16
Model (C4) > Static Structural (C5) > Solution (C6) > Equivalent Stress

Time [s]	Minimum [MPa]	Maximum [MPa]	Average [MPa]
1.	0.11575	25.615	6.0968

FIGURE 8
Model (C4) > Static Structural (C5) > Solution (C6) > Equivalent Stress > Figure

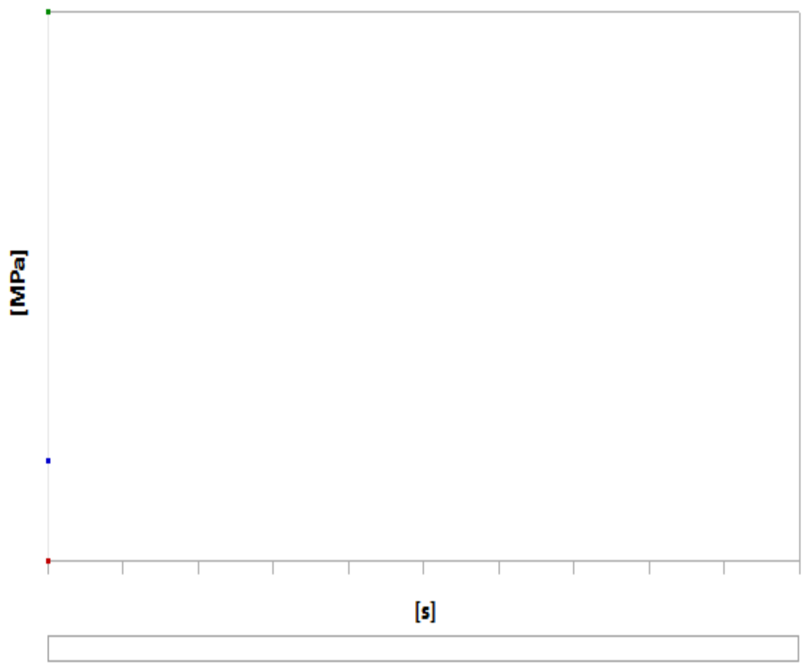

Material Data

Aluminum Alloy

TABLE 17
Aluminum Alloy > Constants

Density	2.77e-006 kg mm^-3
Coefficient of Thermal Expansion	2.3e-005 C^-1
Specific Heat	8.75e+005 mJ kg^-1 C^-1

TABLE 18
Aluminum Alloy > Color

Red	Green	Blue
138	104	46

TABLE 19
Aluminum Alloy > Compressive Ultimate Strength

Compressive Ultimate Strength MPa
0

TABLE 20
Aluminum Alloy > Compressive Yield Strength

Compressive Yield Strength MPa
280

TABLE 21
Aluminum Alloy > Tensile Yield Strength

Tensile Yield Strength MPa
280

TABLE 22
Aluminum Alloy > Tensile Ultimate Strength

Tensile Ultimate Strength MPa
310

TABLE 23
Aluminum Alloy > Isotropic Secant Coefficient of Thermal Expansion

Zero-Thermal-Strain Reference Temperature C
22

TABLE 24
Aluminum Alloy > Isotropic Thermal Conductivity

Thermal Conductivity W mm^-1 C^-1	Temperature C
0.114	-100
0.144	0
0.165	100
0.175	200

TABLE 25
Aluminum Alloy > S-N Curve

Alternating Stress MPa	Cycles	R-Ratio
275.8	1700	-1
241.3	5000	-1
206.8	34000	-1
172.4	1.4e+005	-1
137.9	8.e+005	-1
117.2	2.4e+006	-1
89.63	5.5e+007	-1
82.74	1.e+008	-1
170.6	50000	-0.5
139.6	3.5e+005	-0.5
108.6	3.7e+006	-0.5
87.91	1.4e+007	-0.5
77.57	5.e+007	-0.5
72.39	1.e+008	-0.5
144.8	50000	0
120.7	1.9e+005	0
103.4	1.3e+006	0
93.08	4.4e+006	0

86.18	1.2e+007	0
72.39	1.e+008	0
74.12	3.e+005	0.5
70.67	1.5e+006	0.5
66.36	1.2e+007	0.5
62.05	1.e+008	0.5

TABLE 26
Aluminum Alloy > Isotropic Resistivity

Resistivity ohm mm	Temperature C
2.43e-005	0
2.67e-005	20
3.63e-005	100

TABLE 27
Aluminum Alloy > Isotropic Elasticity

Young's Modulus MPa	Poisson's Ratio	Bulk Modulus MPa	Shear Modulus MPa	Temperature C
71000	0.33	69608	26692	

TABLE 28
Aluminum Alloy > Isotropic Relative Permeability

Relative Permeability
1

Appendix A.13 Ryerson International Hyperloop Team Breakdown

Team Leadership

Mohammed M. **KHAN**
Team Captain, *Grad Student*

Amadeus **COMMISSO**
Operation Lead

Abrar **AHSAN**
Guidance, Navigation & Control Co-Lead

Francis **PICOTTE**
Guidance, Navigation & Control Co-Lead

Adam **GLEESON**
Propulsion Lead

Nathan **PAES**
Propulsion Assistant Lead

Aakash **GOHIL**
Structures Co-Lead

Andrei **MUNTEANU**
Structures Co-Lead

Team Members

Operations (OPS)

Aditya **SALUJA**
Team Account Management

Hitarth **CHUDGAR**
Website Development

Sydney **SCHLUTER**
Social Media Coordinator

Propulsion (PRP)

Abhijeet **ARYAL**
Battery Development

Ashely **ASHOK**
Battery Development

Satchel **FRENCH**
Battery Development

Artin **SARKENZIANS**
LIM Development

Balin **MOHER**
LIM Development

Chirag **TRIVEDI**
LIM Development

Yukei **OYAMA**
LIM Development

Yusef **KHEDR**
LIM Development

Joey **LYON**
PWM Development

Nicholas **PRAYOGO**
MagLev Development

Renee **VETTIVELU**
MagLev Development

Syed **ASAAD**
Propulsion Structures

Guidance, Navigation & Control (GNC)

KRIS **SHARMA**
GNC Member

Kevin **KASA**
GNC Member

Jordan **EPP**
SEI Member

Levi **GREGORASH**
SEI Member

Benjamin **DRYDEN**
Data Acquisition

Thomas **DORS**
VCS Member

Structures (STR)

Amsal **JINDANI**
Braking Member

Musab **ELDALI**
Braking Member, *Grad Student*

Florencia Rios **NICOLAS**
Braking Member

Lior **SAPRIKIN**
Braking Member

Sai **POORSARLA**
Braking Member

Muaz **SALEH**
Vehicle Dynamics

Amin **ISMAIL**
Vehicle Dynamics

Ijaz **QURESHI**
Vehicle Dynamics

Hazzam **NAEEM**
Thermal Management

Niyant **NARAYAN**
Thermal Management

Jordan **VANRIEL**
Thermal Management

Osamah **SOLOMAH**
Pod Chassis

REFERENCES

[1] E. Musk, "Hyperloop Alpha," SpaceX, Hawthorne, 2013.

[2] Hexagon, "HxGN LIVE," 20 June 2019. [Online]. Available: https://hxgnlive.com. [Accessed 20 June 2019].

[3] University of Toronto Institute for Aerospace Studies, "ICASSE 2019," University of Toronto Institute for Aerospace Studies, 1 August 2019. [Online]. Available: http://www.utias.utoronto.ca/icasse-home-copy-conferenceprogram/. [Accessed 5 August 2019].

[4] CBC News, "Toronto to Montreal in 39 minutes? Futuristic people mover zips to next stage," 15 September 2017. [Online]. Available: https://www.cbc.ca/news/canada/ottawa/hyperloop-toronto-ottawa-montreal-route-winner-1.4291893. [Accessed 25 February 2019].

[5] Statistics Canada, "Census Profile, 2016 Census," 1 January 2016. [Online]. Available: http://www12.statcan.gc.ca/census-recensement/2016/dp-pd/prof/details/page.cfm?Lang=E&Geo1=CD&Code1=2466&Geo2=PR&Code2=24&Data=Count&SearchType=Begins&SearchPR=01&B1=All. [Accessed 10 March 2019].

[6] Virgin Hyperloop One, "Route Estimator," 21 September 2018. [Online]. Available: https://hyperloop-one.com/route-estimator/toronto-ca/montral-ca/travel-times. [Accessed 21 September 2018].

[7] S. C. Davis and R. G. Boundy, Transportation Energy Data Book, Oak Ridge: U.S. Department of Energy, 2019.

[8] Hyperloop Transportation Technologies, "Hyperloop Capsule," HyperloopTT, Los Angeles, 2019.

[9] J. C. Chin, J. S. Gray, S. M. Jones and J. J. Berton, "Open-Source Conceptual Sizing Models for the Hyperloop Passenger Pod," American Institue of Aeronautics and Astronautics, Cleveland, 2015.

[10] SpaceX, "SpaceX Hyperloop Test Track and Pod Specifications," SpaceX, Hawthorne, 2018.

[11] Wunderground, "Hawthorne Municipal Airport," Wunderground, 20 November 2018. [Online]. Available: https://www.wunderground.com/weather/KHHR. [Accessed 20 November 2018].

[12] J. Porter, "Elon Musk Promises New Hyperloop Tunnel After Speed Record Broken," 22 July 2019. [Online]. Available:

https://www.theverge.com/2019/7/22/20703423/tum-hyperloop-record-463-kmph-spacex-elon-musk-competition. [Accessed 30 July 2019].

[13] "HFS6 Series Aluminum Extrusions," MiSUMi, 10 June 2019. [Online]. Available: https://us.misumi-ec.com/vona2/detail/110302689160/?HissuCode=HFSP6-5050-2000&PNSearch=HFSP6-5050-2000&searchFlow=results2type&KWSearch=HFSP6-5050-2000. [Accessed 10 June 2019].

[14] "Properties and Selection: Nonferrous Alloys and Special Purpose Materials," in *Metals Handbook*, ASM International, 1998.

[15] H. E. Boyer and T. L. Gall, Metals Handbook, Ohio: American Society for Metals, 1985.

[16] J. M. Holt, C. Y. H. Ed and C. Gibson, Structural Alloys Handbook, West Lafayette: Purdue University, 1996.

[17] "Aluminum Square Tubing," Metal Supermarket, 18 January 2019. [Online]. Available: https://ecommerce.metalsupermarkets.com/MSC-Home.aspx. [Accessed 18 January 2019].

[18] D. J. Peery, "Loads on Fuselage Bulkheads," in *Aircraft Structures*, Mineola, Dover Publications, Inc., 2011, pp. 186-212.

[19] "Mechanical Material Fatigue," Comsol, 21 February 2017. [Online]. Available: https://www.comsol.com/multiphysics/material-fatigue. [Accessed 18 January 2019].

[20] A. Kantrowitz and C. Donaldson, "Preliminary Investigation of Supersonic Diffusers," Langley Memorial Aeronautical Laboratory, Langley Field, 1945.

[21] M. M. J. Opgenoord and P. C. Caplan, "On the Aerodynamic Design of the Hyperloop Concept," AIAA Aviation Forum, Cambridge, 2017.

[22] J. D. Anderson, "Nozzle Flows," in *Fundamentals Of Aerodynamics*, New York, McGraw-Hill, 2001, p. 567.

[23] Hexcel Corporation, "HexTow Carbon Fiber," Hexcel Corporation, 02 March 2018. [Online]. Available: https://www.hexcel.com/user_area/content_media/raw/HexTowSelectorGuide.pdf. [Accessed 22 January 2019].

[24] Aeropoxy, "PR2032 Laminating Resin For Composite Parts," PTM&W Industries Inc., 10 January 2019. [Online]. Available: https://www.aircraftspruce.ca/catalog/pdf/AEROPOXYPR2032TDS.pdf. [Accessed 10 January 2019].

[25] Automation Direct, "Pneumatic Air Cylinders," Automation Direct, 27 December 2018. [Online]. Available: https://www.automationdirect.com/adc/shopping/catalog/pneumatic_compone

nts/pneumatic_air_cylinders/metric_compact_air_cylinders_(h-series)/h50m040md-m. [Accessed 27 December 2018].

[26] First Strike, "HPA Compressed Air Tanks," First Strike, 27 December 2018. [Online]. Available: https://first-strike.ca/first-strike-merc-68-4500-carbon-fibre-hpa-tank/. [Accessed 27 December 2018].

[27] Grainger, "Solenoid Air Control Valves," Grainger, 04 February 2018. [Online]. Available: https://www.grainger.com/product/ARO-1-4-24VDC-4KB40. [Accessed 04 February 2018].

[28] I. Boldea and S. A. Nasar, The Induction Machines Design Handbook, CRC Press, 2009.

[29] J. F. Eastham, "Novel Synchronous Machines: Linear And Disc," *IEE Proceedings B - Electric Power Applications,* vol. 137, no. 1, pp. 49-58, 1990.

[30] M. Poloujadoff, "Linear Induction Machines," *IEEE Spectrum,* vol. 8, no. 2, pp. 72 - 80, 1971.

[31] V. Del Toro, Electric Machines and Power Systems, Englewood Cliffs: Prentice-Hall Inc., 1985.

[32] S. P. Bhamidi, "Design Of A Single Sided Linear Induction Motor (SLIM) Using A User Interactive Computer Program," University of Missouri, Columbia, 2005.

[33] K&J Magnetics Inc., "BX8X8X0 Specification Sheet," K&J Magnetics Inc., 29 July 2010. [Online]. Available: https://www.kjmagnetics.com/specprep.asp?pName=BX8X8X0. [Accessed 4 February 2019].

[34] The Kistler Group, "Aircraft Landing Gear and Brake Testing," The Kistler Group, 18 January 2018. [Online]. Available: https://www.kistler.com/en/applications/sensor-technology/test-measurement/aviation-testing/aircraft-landing-gear-and-brake-testing/. [Accessed 20 June 2019].

[35] Transport Canada, Aeronautical Information Manual, Ottawa: Transport Canada, 2012.

[36] Oriental Motors, "Brushless DC Motor Speed Control System," 20 February 2019. [Online]. Available: https://catalog.orientalmotor.com/item/all-categories/120w-bmu-series-brushless-dc-motors/blm5120hp-30s-bmud120-c2. [Accessed 10 June 2019].

[37] NASA, "Soldered Electrical Connections," 18 January 2001. [Online]. Available: https://nepp.nasa.gov/docuploads/06AA01BA-FC7E-4094-AE829CE371A7B05D/NASA-STD-8739.3.pdf. [Accessed 9 December 2018].

[38] Automation Direct, "Metric Compact Air Cylinders (H-Series)," 15 March 2019. [Online]. Available:

https://cdn.automationdirect.com/static/specs/nitrahseriescyl100mm.pdf. [Accessed 10 June 2019].

[39] I. Boldea, Linear Electric Machines, Drives, and MAGLEVs Handbook, Boca Raton: CRC Press, 2017.

[40] MIT Hyperloop Team, "MIT Hyperloop Final Report," Massachusetts Institute of Technology, Cambridge, 2017.